A Comparative Study on the Effects of Internal VS External Pressure for a Pressure Vessel subjected to Piping Loads at the Shell-to-Nozzle Junction

Ashveer Maharaj

University of KwaZulu-Natal

Durban

This thesis is submitted in fulfillment of the academic requirements for the Degree of Master of Science in Engineering in the School of Mechanical Engineering, University of Natal.

November 2003

Supervisors :

Professor S. Adali

Dr. C. J. von Klemperer

As the candidate's supervisors we have/have not approved this thesis/dissertation for submission

Signed : ....Name : ....Date : ....

Signed : ....Name : ....Date : ....

Acknowledgments

I would like to thank my supervisors Professor S. Adali and Dr. C. J. von Klemperer for their assistance and guidance.

I gratefully acknowledge the assistance given to me by my mentor from SASOL, Mr. Daniel Francis.

I would especially like to thank Mr. John Fogg, of Elgin Engineering, for his help in several aspects of this study.

I would like to thank SASOL Ltd. for a research sponsorship in undertaking this investigation on their behalf.

ii

ABSTRACT

This investigation seeks to perform a comparative study between the combined effects of internal pressure and piping loads versus external pressure and piping loads on a pressure vessel. There are currently several well-known and widely-used procedures for predicting the stress situation and the structural stability of pressure vessels under internal pressure when external piping loads (due to thermal expansion, weight, pressure, etc.) are applied at the nozzles. This project familiarises one with several international pressure vessel design Codes and standards, including ASME (American Society of Mechanical Engineers) pressure vessel code sections and WRC (Welding Research Council) bulletins. It has been found that many vessels are designed to operate under normal or steam-out conditions (in vacuum). The combined effect of the external atmospheric pressure and the piping loads at the nozzle could be catastrophic if not addressed properly – especially when the stability of the structure is a crucial consideration, i.e. when buckling is a concern. The above-mentioned codes and standards do not directly address procedures or provide acceptance criteria for external loads during vacuum conditions.

The approach to the study was, firstly, to investigate the effects of internal pressure and piping loads at the shell-to-nozzle junction. Theoretical stresses were compared with Finite Element results generated using the software package MSC PATRAN. Finite Element Methods provide a more realistic approach to the design of pressure vessels as compared to theoretical methods. It was necessary to determine if the theoretical procedures currently used were adequate in predicting the structural situation of a pressure vessel. Secondly, the buckling effects of vessels subjected to external atmospheric pressure and piping loads were also investigated. Buckling of the shell-to-nozzle region was explored with the aid of Finite Element software. The results gained were used to develop appropriate procedures for the design of vessels under external atmospheric pressure and piping loads. The design is such that it indicates if buckling will occur at the shell-to-nozzle junction. These design procedures form the basis for future exploration in this regard.

CONTENTS

List of figures

List of tables

List of symbols

θ Angle of displacement [°]

β $= 0.875 \dfrac{r_o}{R_m}$

β_r Spring constant

χ Curvature

ε Strain

ϕ_1 $= \dfrac{qr\left(1 - v^2\right)}{ET}$

ϕ_2 $= \dfrac{-N_x\left(1 - v^2\right)}{ET}$

γ Shear Strain for shell and plate theory, $= \dfrac{R_m}{T}$ for WRC 107

α FEM unknown coefficient, $= \dfrac{T^2}{12r^2}$ for buckling of shells

λ $= \dfrac{m\pi r}{l}$

λ_i Eigenvalue

v Poisson's Ratio

σ Stress [MPa]

σ_{yp} Yield Stress [MPa]

σ_x Longitudinal Stress [MPa]

σ_ϕ Circumferential or Hoop Stress [MPa]

σ_r Radial Stress [MPa]

$\sigma_1, \sigma_2, \sigma_3$ Principal Stresses [MPa]

σ_{cr} Critical Buckling Stress [MPa]

σ'_{cr} Reduced Critical Buckling Stress [MPa]

σ_{or} Maximum Compressive out-of-round Stress [MPa]

σ_{UTS} Ultimate Tensile Stress [MPa]

τ Shear Stress [MPa]

δ FEM displacement

Π Total Potential energy

A $= \dfrac{\sigma_{cr}}{E}$ for ASME geometric chart

B	$\dfrac{\sigma_{cr}}{2}$ for ASME material chart
CA	Corrosion Allowance [mm]
D	Flexural Rigidity
D_o	Vessel outer diameter [mm]
DP	Design Pressure [MPa]
e	out-of-roundness value [mm]
E	Young's Modulus [GPa], ASME joint efficiency
F	FEM Applied loading
G	Shear Modulus [GPa]
I_P	Polar moment of inertia for a tube
k_e	FEM element stiffness
K	FEM stiffness matrix
K_G	FEM geometric stiffness
K_d	FEM differential stiffness
K_n, K_b	Membrane and Bending stress concentration factors
l	Length of cylindrical shell [mm]
L	Length of vessel [mm]
L_{cr}	Critical buckling length [mm]
m	Number of lobes in longitudinal direction
M_i	Resultant bending moment per unit length
M_C	WRC 107 Circumferential Moment [Nmm]
M_L	WRC 107 Longitudinal Moment [Nmm]
M_T	WRC 107 Torsional Moment [Nmm]
M_{or}	Maximum bending moment for out-of-roundness
n	Number of lobes in circumferential direction
N_i	Resultant membrane force per unit length
p	Internal or external applied pressure [MPa], FEM lateral load
P	FEM function of position, WRC 107 Radial load [N]
P_{cr}	Critical Buckling Pressure [MPa]
P_{cr}'	Reduced Critical Buckling Pressure [MPa]
q	External radial pressure [MPa]
Q	Resultant Shear Force per unit length
r	Radius [mm]
r_o	Nozzle outer radius [mm]
R_m	Vessel mean radius [mm]
R_o	Vessel outer radius [mm]

R_i Vessel inner radius [mm]

S Combined Stress Intensity [MPa]

S_a Allowable Stress [MPa]

S_m Design Stress Intensity [MPa]

S_y Yield Stress [MPa]

S_T Ultimate Tensile Stress [MPa]

t Plate thickness [mm]

T Vessel thickness [mm]

u, v, w Plate or shell displacements

U_e Total Strain Energy for plate or shell element

W_e Total Potential Energy due to lateral load

z Distance to neutral axis

Chapter 1

PRESSURE VESSELS

1.1 Introduction

Pressure vessels are leak-proof containers. They may be of any shape and range from beverage bottles to the more sophisticated engineering vessels encountered in industrial applications. Familiar examples of pressure vessels for industrial applications will include compressed-air tanks, pipes and heat exchangers. Vessels that have walls that are thin in comparison to their radii and lengths, are classified as shell structures. For the purposes of this study cylindrical vessels with circular cross sections will be considered. Figure 1-1 below shows typical examples of cylindrical pressure vessels found in industry. For industrial vessels, high pressures, extremes of temperatures, and severity of functional performance requirements pose exacting design problems. The term "design" includes not only the calculation of detail dimensions for various components of pressure vessels but also incorporates collectively the following :

- likely modes of damage or failure;
- selection of an appropriate material and its environmental behaviour; and
- stress analyses and the significance of their results.

New concepts in design and selection of appropriate materials challenge the ingenuity of engineers, and the problems that arise from every aspect of pressure vessel design affects both safety and cost-effectiveness.

Figure 1-1 : Typical Cylindrical Pressure Vessels

1

1.2 Design of Pressure Vessels

The ASME VIII, ASME Boiler and Pressure Vessel Code, Div 1 and 2, are used for the design of pressure vessels. It includes various sections which focus on the design of pressure vessel components from nozzles and flanges to supports. It is most commonly used by modern day engineers. The body or shells of vessels are predominantly affected by two important design factors, the design pressure and the design temperature.

1.2.1 Design pressure

Design pressure[18] is the pressure used to determine the minimum required thickness of each vessel shell component and the denoted difference between the internal (design pressure) and external (atmospheric pressure) pressures. The design pressure will include a suitable margin above the operating pressure plus any static head of an operating liquid. The maximum allowable working (operating) pressure is defined by the ASME Code as the maximum gauge pressure permissible at the top of the completed vessel in its operating position at the designated temperature. It is based on the nominal vessel thickness, exclusive of corrosion allowance, and the thickness required for loads other than pressure. In most cases it is very close to the design pressure of the vessels component.

The Code defines the *required thickness* as the minimum vessel wall thickness as computed by the Code formulas, not including a corrosion allowance. The *design thickness* is the minimum required thickness plus corrosion allowance and the *nominal thickness* is the rounded-up design thickness which is used in the actual construction of the vessel for a commercially available material. If the nominal thickness minus corrosion allowance is larger than the required thickness then the design pressure or the corrosion allowance could be increased. For example, excess thickness can be used in nozzle openings in vessels that require added reinforcement. The vessel must be designed to withstand the most severe combination of pressure and temperature under operating conditions.

1.2.2 Design temperature

The design temperature[18] is more of a design environmental condition than a design load. Thermal stresses only occur due to rapid temperature changes or certain temperature gradients, however, the design temperature is needed in the selection of a suitable material. The material used for construction must be able to withstand any temperature effects. Increasing temperatures cause a decrease in strength of most metals, and decreasing temperatures generally

results in materials becoming more brittle. It will be shown that vessel thickness is related to the material strength, which means that dimensional changes could be experienced.

The required Code design temperature should not be less than the mean metal vessel wall temperature expected under operating conditions and computed by standard heat transfer equations or actual measurements. For standard vessels the design temperature is the maximum temperature of the operating fluid plus an added amount for safety, or the minimum temperature of the operating fluid if the vessel is designed for low-temperature service. Various types of pressure vessels have different design temperatures. To ensure the safety of the design of the vessel the appropriate design temperature is crucial.

1.3 Design of thin cylinders – ASME Code

The ASME VIII Div 1 Code[34] indicates that the thickness of cylindrical shells under internal pressure shall not be less than that computed from the following formula.

$$T = \frac{DPR_i}{S_a E - 0.6DP} + CA \qquad (1.1)$$

The above equation indicates that the thickness is related to the material's allowable stress S_a, ASME joint efficiency E (usually = 1), design pressure DP, corrosion allowance CA and the vessel inner radius R_i. Using the above equation if the thickness is calculated as 8.4mm, this value should be rounded-up to obtain the nominal thickness. Standard plate material sizes should be used in the construction of the vessel. In this case the standard nominal thickness would be 10mm. The design of flanges, nozzles, supports, etc can be found in the ASME Code.

Design of nozzles and their reinforcements, found in ASME VIII Div 1, is given in Appendix A. When designing vessels with nozzles, the area of the material removed from the shell, must be adequately reinforced before attaching a nozzle to it. Nozzle thickness is not calculated but is given in a table found in Appendix A. The thickness used for the design, from the table for various nozzle sizes, must be adequate when reinforcement is a concern.

The first stage of the design process requires the dimensional values of the components of the vessel to be calculated. The next stage is to determine the stresses in the vessels due to various loadings. The stresses will indicate whether the vessel will not fail under operating conditions.

Chapter 2

STRESSES IN PRESSURE VESSELS

2.1 Introduction

Pressure vessels used for industrial applications operate under high degrees of pressures, temperatures and various other environmental factors. This means that the operating stresses developed will have to be calculated using various analytical and experimental methods. Stress analysis becomes particularly important when external components are attached to the shell of the vessel.

An example of these components could represent piping attachments in the form of nozzles. The imposed loading on the vessel by these external components can have a great impact on the safety and stability of the vessel. An overall knowledge of the stresses developed by these external attachments is needed to prevent failure of the vessel.

When we consider vessels or shells formed of plates, in which the thickness is small in comparison with the other dimensions, and as such offer little resistance to bending perpendicular to their surface, they are called "membranes" [20]. The stresses calculated by neglecting bending are called "membrane stresses". Membrane stresses are average tensile or compressive stresses acting tangent to the surface of the vessel wall. Membrane stresses includes both direct stresses and shear stresses.

Bending stresses are developed by forces that bend the vessel wall. External loads can cause these stresses. Nozzle piping loads have external forces and moments that cause bending stresses to occur in the vessel. Membrane and bending stresses can be calculated using various theoretical and numerical methods.

2.2   Membrane Stresses in Vessels under Pressure

The membrane stresses in vessels of revolution, including those of complicated geometry, can be evaluated from the equations of statics provided they are loaded in a rotationally symmetrical manner.   The pressure loading should be constant on any plane perpendicular to the axis of rotation O-O indicated in figure 2-1(a, b and c).
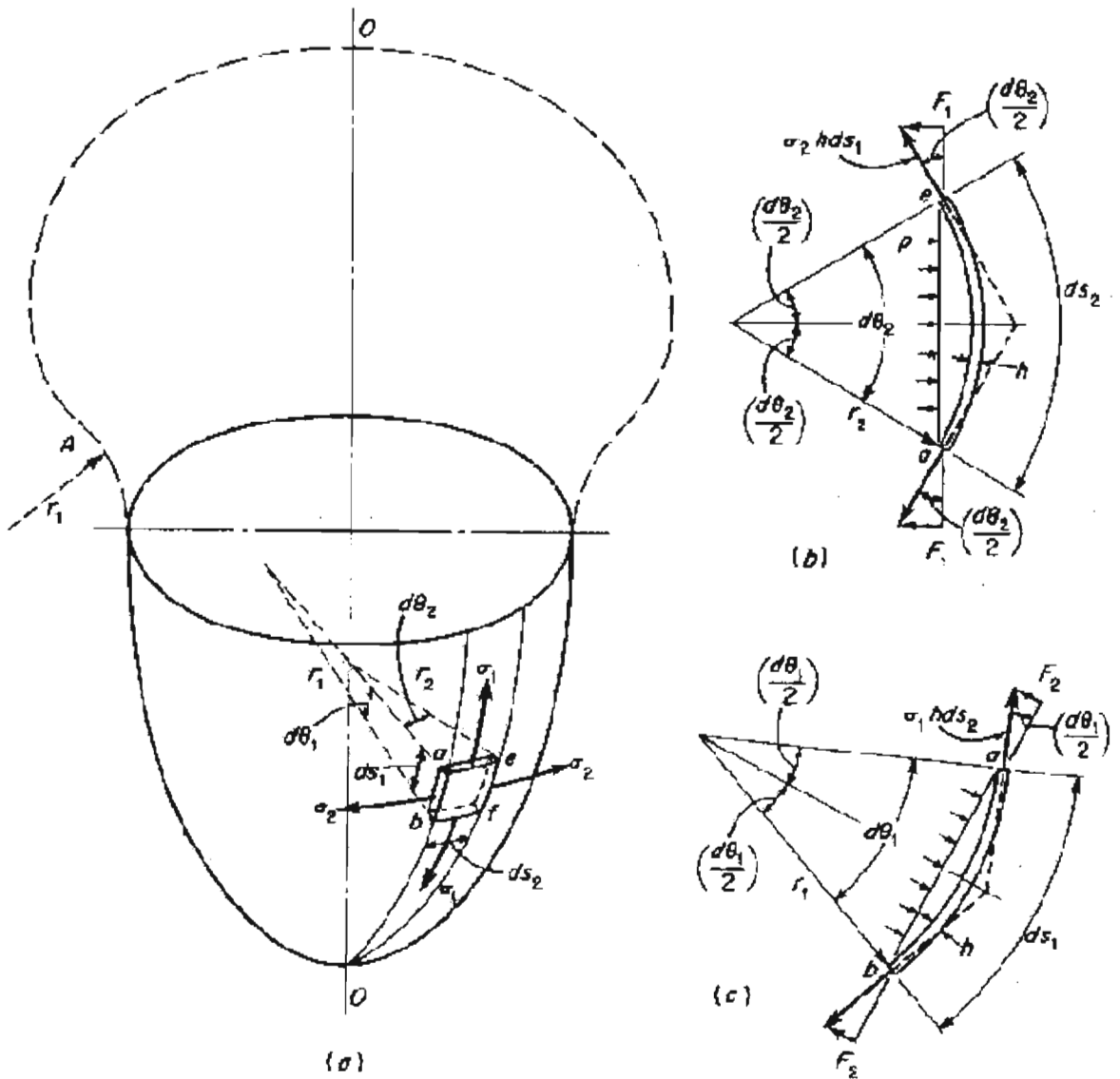
Figure 2-1 :   Membrane stresses in vessel.   Obtained from Harvey[20]

For figure 2-1a; if an element *abef* is cut by two longitudinal sections *ab* and *ef*, as well as two sections normal to the longitudinal sections, *ae* and *bf*, it can be seen that symmetry exists and normal stresses only act on the sides of this element. In the interest of this study the thickness of the shell will be known as *T*, therefore referring to figure 2-1a, the total forces acting on the sides of the elements are respectively $\sigma_1 Tds_2$ and $\sigma_2 Tds_1$. The force $\sigma_2 Tds_1$ has a component in a direction normal to the element indicated in figure 2-1b. This force is given by the following equation :

$$2F_1 = 2\sigma_2 Tds_1 \sin\left(\frac{d\theta_2}{2}\right)$$ (2.1)

and similarly the force $\sigma_1 Tds_2$ has a component in a direction normal to the element indicated in figure 2-1c. This force is given by the following equation :

$$2F_2 = 2\sigma_1 Tds_2 \sin\left(\frac{d\theta_1}{2}\right)$$ (2.2)

The normal pressure force on the element is :

$$P = p\left[2r_1 \sin\left(\frac{d\theta_1}{2}\right)\right]\left[2r_2 \sin\left(\frac{d\theta_2}{2}\right)\right]$$ (2.3)

The above equation is in equilibrium with the sum of the normal membrane component forces $2F_1$ and $2F_2$, hence :

$$2\sigma_1 Tds_2 \sin\left(\frac{d\theta_1}{2}\right) + 2\sigma_2 Tds_1 \sin\left(\frac{d\theta_2}{2}\right) = p\left[2r_1 \sin\left(\frac{d\theta_1}{2}\right)\right]\left[2r_2 \sin\left(\frac{d\theta_2}{2}\right)\right]$$ (2.4)

noting that :

$$\sin\left(\frac{d\theta_1}{2}\right) = \frac{ds_1}{2r_1} \text{ and } \sin\left(\frac{d\theta_2}{2}\right) = \frac{ds_2}{2r_2}$$

$$\frac{\sigma_1}{r_1} + \frac{\sigma_2}{r_2} = \frac{p}{T}$$ (2.5)

For cylindrical vessels under pressure p, where the hoop radius $r_2 = r$ and the longitudinal radius $r_1 = \infty$, each radius is constant through the entire cylinder. Substituting these values in (equation 2.5) gives :

$$\frac{\sigma_1}{\infty} + \frac{\sigma_2}{r} = \frac{p}{T}$$

$$\sigma_2 = \frac{pr}{T}(hoop\ stress) \tag{2.6}$$

Using figure 2-2 below the longitudinal stress can be evaluated by equating the longitudinal forces producing extension to the total pressure force on the cross section of the vessel.
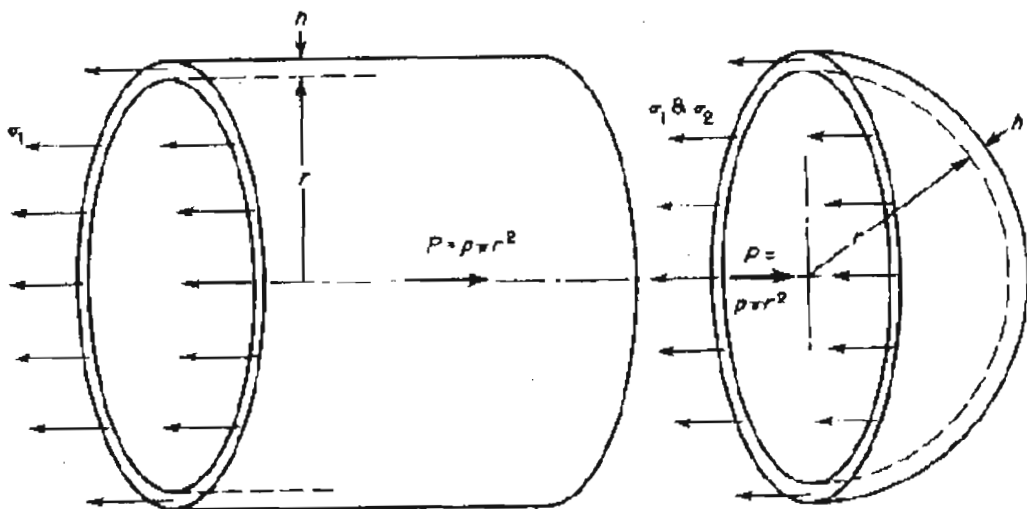
Figure 2-2 : Longitudinal Stress in Cylinder. Obtained from Harvey[20]

$$\sigma_1 2\pi r T = p\pi r^2 \tag{2.7}$$

$$\sigma_1 = \frac{pr}{2T}(longitudinal\ stress) \tag{2.8}$$

7

2.3 Thin Plate theory

In studying pure bending of beams[33], the cross sections of beams rotate with respect to their neutral axes or normal to the deflection. This refers to bending in one perpendicular direction. However, bending in two perpendicular directions occurs in pure bending of plates. Analysis of thin plate theory is thus similar to beam theory. First the bending moments are related to curvature and then the deflection. Consider a plate with no loading indicated by figure 2-3. The components of displacement occurring in the x, y and z directions, are denoted by u, v and w respectively. When lateral loading occurs, the deformation of the *midsurface* at any point (x_a, y_a) is denoted by w. For isotropic, homogenous, elastic thin plates, the following assumptions have to be made.

- Deflections are small compared to thickness of plate.
- The midplane remains unstrained during bending.
- Vertical shear strains and normal strains are negligible, implies no distortion.
- Normal stresses are small compared with other stress components.

The above assumptions are known as *Kirchoff hypotheses*[19].
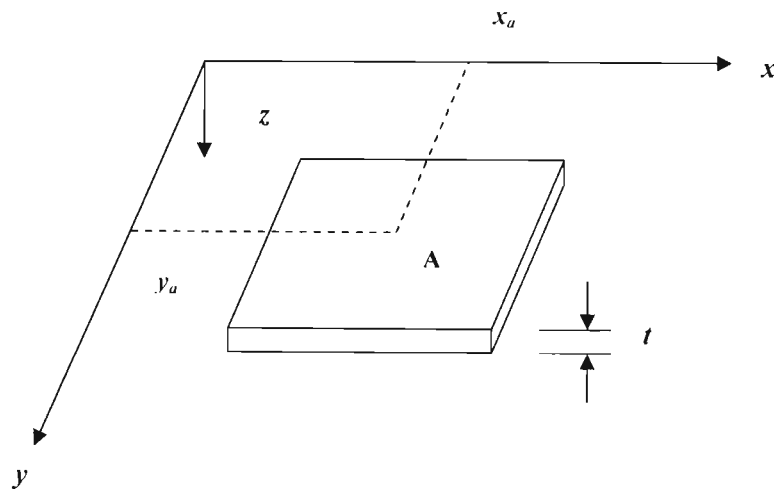
Figure 2-3 : Load-free plate. Reproduced from Ugural[19]

8

Figure 2-4 below shows an element of material cut from a plate subjected to pure bending as in figure 2-5.
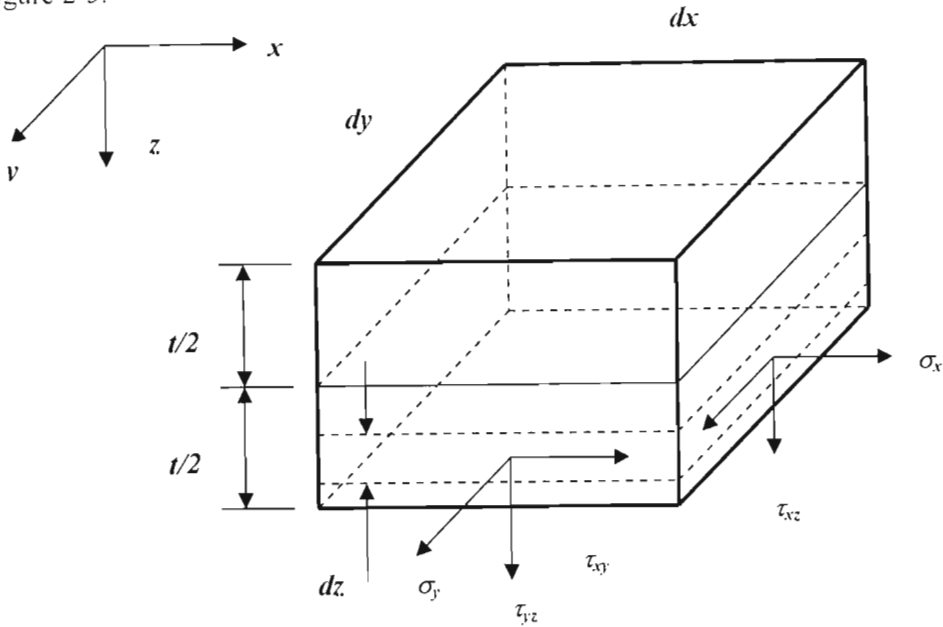
Figure 2-4 : Small plate element. Reproduced from Ugural[19]
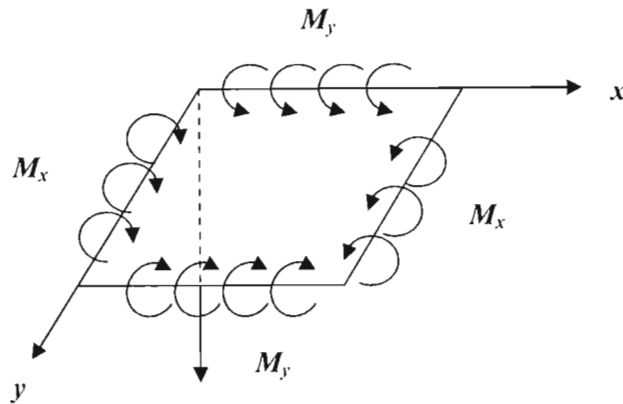
Figure 2-5 : Pure bending of small plate element. Reproduced from Timoshenko[1]

2.3.1 Strain-curvature relationships

The plane shown in figure 2-5 represents the middle of the plate or the neutral surface. The direction of the moments indicate that the plate material above the neutral surface is in compression and the material below the surface is in tension. The moments M_x and M_y per unit length are positive when acting on the middle of the plate. The curvatures of the mid-plane parallel to the xz and yz planes are denoted by $1/r_x$ and $1/r_y$ respectively. The strains at a depth z below the neutral surface in the x and y directions can be determined using figure 2-6 below.
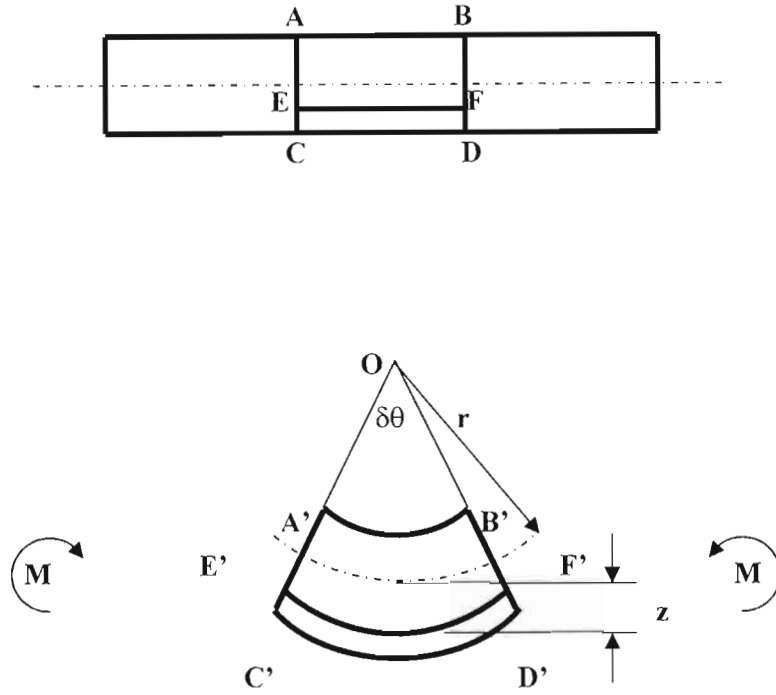
Figure 2-6 : Bending of thin plate. Reproduced from Benham and Crawford[31]

The element *ABCD* deforms to *A'B'C'D'*. The length along the neutral axis is given by $r\delta\theta$. The length of fibre *E'F'* is $(r + z)\delta\theta$. The longitudinal strain for fibre E'F' is the change in length divided by the original length.

$$\varepsilon_x = \frac{(r_x + z)\delta\theta - r_x\delta\theta}{r_x\delta\theta} \tag{2.9}$$

therefore,

$$\varepsilon_x = \frac{z}{r_x} \tag{2.10}$$

and similarly in the *y* direction

$$\varepsilon_y = \frac{z}{r_y} \tag{2.11}$$

Strains can be related to displacements by the following equations.

$$\varepsilon_x = \frac{\partial u}{\partial x} \qquad (2.12)$$

$$\varepsilon_y = \frac{\partial v}{\partial y} \qquad (2.13)$$

$$\gamma_{xy} = \frac{\partial u}{\partial y} + \frac{\partial v}{\partial x} \qquad (2.14)$$

$$\varepsilon_z = \frac{\partial w}{\partial z} = 0 \qquad (2.15)$$

$$\gamma_{xz} = \frac{\partial w}{\partial x} + \frac{\partial u}{\partial z} = 0 \qquad (2.16)$$

$$\gamma_{yz} = \frac{\partial w}{\partial y} + \frac{\partial v}{\partial z} = 0 \qquad (2.17)$$

The strains are determined by the figure below.
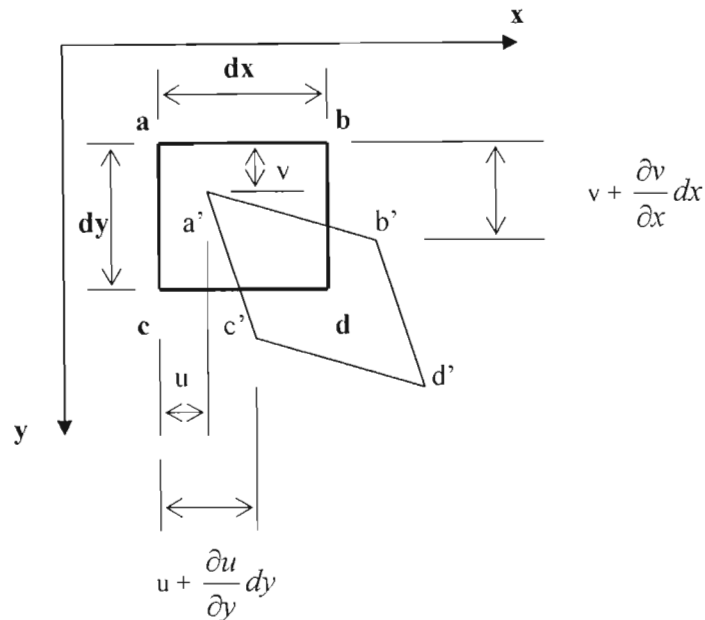
Figure 2-7 : Lamina subjected to shear. Reproduced from Timoshenko[1]

During bending the points *a, b, c,* and *d* undergo small displacements. The components of the displacement at point *a* in the *x* and *y* directions are *u* and *v* respectively. The displacements of

points b and c in the x and y directions are $u + \left(\dfrac{\partial u}{\partial y} \right) dy$ and $v + \left(\dfrac{\partial v}{\partial x} \right) dx$ respectively. Shear strain is the measure of distortion or the change in shape. Therefore, it is the sum of the angles of distortion. The shear strain owing to these displacements is given by equation 2.14. Similarly the above diagram can be used to obtain the remaining shear strains corresponding to their respective directions. Integrating equation 2.15 gives $w = w(x, y)$, and similarly integrating equations 2.16 and 2.17 gives :

$$u = -z \frac{\partial w}{\partial x} \tag{2.18}$$

$$v = -z \frac{\partial w}{\partial y} \tag{2.19}$$

Substituting the above equations into equations 2.12-2.14 gives :

$$\varepsilon_x = -z \frac{\partial^2 w}{\partial x^2} \tag{2.20}$$

$$\varepsilon_y = -z \frac{\partial^2 w}{\partial y^2} \tag{2.21}$$

$$\gamma_{xy} = -2z \frac{\partial^2 w}{\partial x \partial y} \tag{2.22}$$

The curvature of a plane curve is defined as the rate of change of the slope angle of the curve with respect to distance of the curve. Therefore, the partial derivatives of the above equations represent the curvatures. The curvatures given by equations 2.10 and 2.11 are then represented by :

$$\frac{1}{r_x} = -\frac{\partial}{\partial x} \left(\frac{\partial w}{\partial x} \right) = -\frac{\partial^2 w}{\partial x^2} \tag{2.23}$$

$$\frac{1}{r_y} = -\frac{\partial}{\partial y} \left(\frac{\partial w}{\partial y} \right) = -\frac{\partial^2 w}{\partial y^2} \tag{2.24}$$

$$\frac{1}{r_{xy}} = -\frac{\partial}{\partial x} \left(\frac{\partial w}{\partial y} \right) = -\frac{\partial^2 w}{\partial x \partial y} \tag{2.25}$$

2.3.2 Stress Resultants

Stresses and strains are related according to Hooke's Law[33]. The following equations are valid for isotropic homogenous materials.

$$\varepsilon_x = \frac{z}{r_x} = \frac{1}{E}\left[\sigma_x - v\sigma_y\right]$$

$$\varepsilon_y = \frac{z}{r_y} = \frac{1}{E}\left[\sigma_y - v\sigma_y\right] \tag{2.26}$$

$$\gamma_{xy} = \frac{\tau_{xy}}{G}$$

Where $G = \dfrac{E}{2(1+v)}$, the shear modulus. Rearranging the above equations gives.

$$\sigma_x = \frac{E}{1-v^2}\left[\varepsilon_x + v\varepsilon_y\right] = \frac{Ez}{1-\upsilon^2}\left[\frac{1}{r_x} + \frac{v}{r_y}\right]$$

$$\sigma_y = \frac{E}{1-v^2}\left[\varepsilon_y + v\varepsilon_x\right] = \frac{Ez}{1-\upsilon^2}\left[\frac{1}{r_y} + \frac{v}{r_x}\right] \tag{2.27}$$

$$\tau_{xy} = G\gamma_{xy}$$

Introducing equations 2.20 to 2.22 gives the following :

$$\sigma_x = -\frac{Ez}{1-\upsilon^2}\left[\frac{\partial^2 w}{\partial x^2} + v\frac{\partial^2 w}{\partial y^2}\right]$$

$$\sigma_y = -\frac{Ez}{1-\upsilon^2}\left[\frac{\partial^2 w}{\partial y^2} + v\frac{\partial^2 w}{\partial x^2}\right] \tag{2.28}$$

$$\tau_{xy} = -\frac{Ez}{1+v}\frac{\partial^2 w}{\partial x \partial y}$$

The above equations indicate that at the midsurface the stresses vanish as expected on the neutral axis. The stresses also vary linearly over the thickness of the plate.

The stresses distributed over the thickness of the plate can be reduced to the bending moments and twisting moments applied to the plate. In this way the following equations are obtained with the aid of figure 2-4.

$$\int_{-t/2}^{t/2} \sigma_x z \, dy \, dz = M_x dy$$

$$\int_{-t/2}^{t/2} \sigma_y z \, dx \, dz = M_y dx \qquad (2.29)$$

$$\int_{-t/2}^{t/2} \tau_{xy} z \, dz = M_{xy}$$

Substituting equations 2.28 into the above equations and performing the above integrations, the following equations are obtained.

$$M_x = -D\left[\frac{\partial^2 w}{\partial x^2} + v\frac{\partial^2 w}{\partial y^2}\right]$$

$$M_y = -D\left[\frac{\partial^2 w}{\partial y^2} + v\frac{\partial^2 w}{\partial x^2}\right] \qquad (2.30)$$

$$M_{xy} = -D(1-v)\frac{\partial^2 w}{\partial x \partial y}$$

where

$$D = \frac{Et^3}{12(1-v^2)} \qquad (2.31)$$

is known as the *flexural rigidity* of the plate. Finally, substituting equations 2.30 and 2.31 into equations 2.28 gives :

$$\sigma_x = \frac{12M_x z}{t^3} \qquad \sigma_y = \frac{12M_y z}{t^3} \qquad \tau_{xy} = \frac{12M_{xy} z}{t^3} \qquad (2.32)$$

14

2.4 Thin Shell theory

To develop the governing differential equations for the midsurface displacements u, v, and w, which define the kinematics of deformation for a shell, one proceeds as in the case of plates. A small shell element figure 2-8 is considered, which is formed by the intersection of two pairs of adjacent planes perpendicular to the middle surface. The x and y axes are taken as tangents to the point O, and z is perpendicular to the surface. The principal radii of curvatures in the xz and yz planes, are denote by r_x and r_y respectively. The thickness of the shell is denoted by T. To determine the stress resultants σ_x, σ_y, and τ_{xy}, strains developed in the shell have to be obtained.
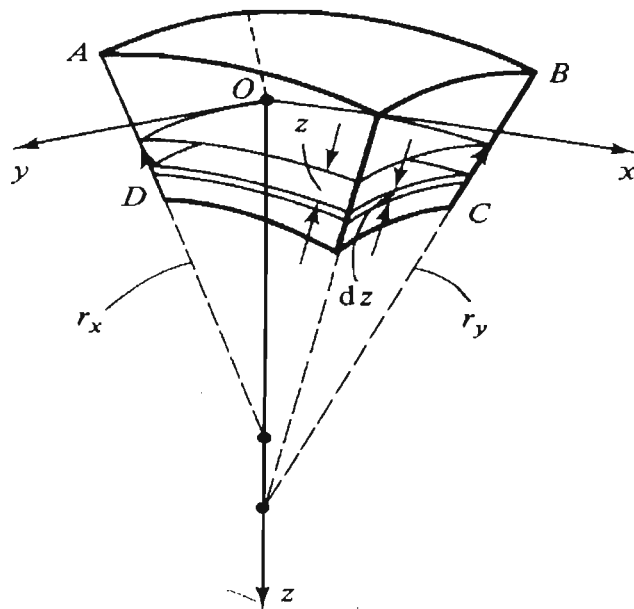
Figure 2-8 : Shell Element. Obtained from Bulson and Allen[17]

In considering bending of the shell, it is assumed that linear elements such as AD and BC, which are perpendicular to the middle surface, remain straight and become perpendicular to the deformed middle surface of the shell. The lateral faces of the element $ABCD$, during bending, rotate only with respect to their lines of intersection with the middle surface. The radii of curvatures after deformation are r'_x and r'_y. However, in addition to rotation, the lateral sides of the element are displaced parallel to themselves as shown in figure 2-9. The corresponding unit elongations of the middle surface in the x and y directions are denoted by ε_1 and ε_2, respectively. The elongation of the middle surface in the x direction is :

$$\varepsilon_x = \frac{l_2 - l_1}{l_1}$$

(2.33)
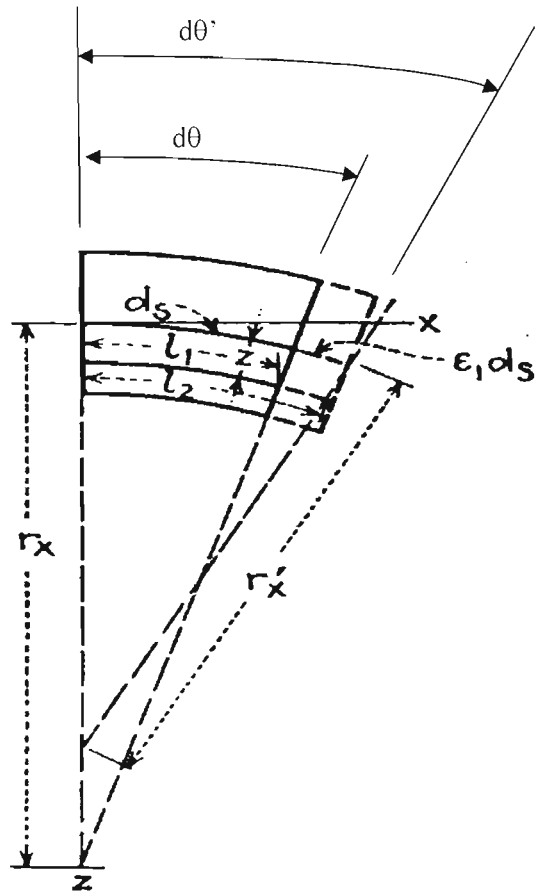
Figure 2-9 : Deformed middle surface. Obtained from Timoshenko[1]

It can be seen that $ds = r_x d\theta$, and $l_1 = d\theta(r_x - z)$, and combining these expressions one obtains :

$$l_1 = ds\left(1 - \frac{z}{r_x}\right) \tag{2.34}$$

Similarly it can be seen that $ds + \varepsilon_1 ds = r_x' \, d\theta'$, and $l_2 = d\theta'(ds - z)$, and combining these expressions one obtains :

$$l_2 = ds(1 + \varepsilon_1)\left(1 - \frac{z}{r_x'}\right) \tag{2.35}$$

16

Substituting the above expressions into equation 2.33 the following equation is obtained :

$$\varepsilon_x = \frac{\varepsilon_1}{1 - \frac{z}{r_x}} - \frac{z}{1 - \frac{z}{r_x}}\left[\frac{1}{(1 - \varepsilon_1)r_x'} - \frac{1}{r_x}\right]$$

(2.36)

The thickness of the shell T, will always be assumed to be small in comparison with the radii of curvatures, therefore z/r_x can be neglected. The effects of ε_1 on the curvature can also be neglected, therefore the above expression is reduced to :

$$\varepsilon_x = \varepsilon_1 - z\left(\frac{1}{r_x'} - \frac{1}{r_x}\right) = \varepsilon_1 - \chi_x z$$

(2.37)

and similarly in the y direction it is reduced to :

$$\varepsilon_y = \varepsilon_2 - z\left(\frac{1}{r_y'} - \frac{1}{r_y}\right) = \varepsilon_2 - \chi_y z$$

(2.38)

The distribution of shear strain is next evaluated. Let γ_{xy0} denote the shear strain of the midsurface. Owing to the rotation of edge BC relative to Oz about the x axis (figure 2-8) and γ_{xy0}, and referring to equation 2.22 for plates, produces :

$$\gamma_{xy} = \gamma_{xy0} - \frac{2z\partial^2 w}{\partial x \partial y} = \gamma_{xy0} - 2z\chi_{xy}$$

(2.39)

Substituting equations 2.37 – 2.39 into equations 2.27, produces :

$$\sigma_x = \frac{E}{1 - v^2}\left[\varepsilon_1 + v\varepsilon_2 - z(\chi_x + v\chi_y)\right]$$

$$\sigma_y = \frac{E}{1 - v^2}\left[\varepsilon_2 + v\varepsilon_1 - z(\chi_y + v\chi_x)\right]$$

(2.40)

$$\tau_{xy} = (\gamma_{xy0} - 2z\chi_{xy})G$$

17

On each side of the element ABCD (figure 2-8) the corresponding forces can be replaced by a normal force applied at the centroid of the side and a bending moment. This is indicated in figure 2-10.
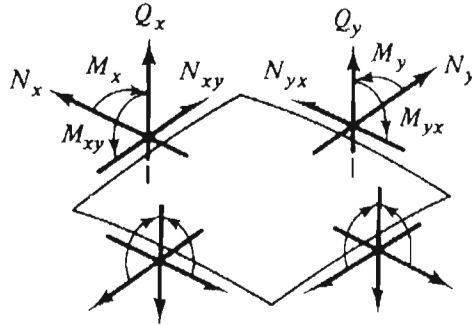
Figure 2-10 : Forces and bending moments on lamina. Obtained from Ugural[19]

Since the thickness of the shell is very small, the lateral sides of the element can be considered as rectangles. The resultant forces will act in the middle surface of the shell. Using the same notations as in plates, for resultant forces and bending moments per unit length, the following are obtained :

$$N_x = \int_{-T/2}^{T/2} \sigma_x dz$$

$$N_y = \int_{-T/2}^{T/2} \sigma_y dz$$

$$N_{xy} = \int_{-T/2}^{T/2} \tau_{xy} dz$$

$$M_x = \int_{-T/2}^{T/2} z\sigma_x dz \qquad (2.41)$$

$$M_y = \int_{-T/2}^{T/2} z\sigma_y dz$$

$$M_{xy} = \int_{-T/2}^{T/2} z\tau_{yx} dz$$

18

Substituting equations 2.40 into 2.41, produces :

$$N_x = \frac{ET}{1-v^2}(\varepsilon_1 + v\varepsilon_2)$$

$$N_y = \frac{ET}{1-v^2}(\varepsilon_2 + v\varepsilon_1)$$

$$N_{xy} = \frac{\gamma_{xy0} Et}{2(1+v)} \tag{2.42}$$

$$M_x = -D(\chi_x + v\chi_y)$$

$$M_y = -D(\chi_y + v\chi_x)$$

$$M_{xy} = -D(1-v)\chi_{xy}$$

Here D defines the *flexural rigidity* of the shell, the same as for plates. The compound stresses in a shell can be expressed in terms of forces and bending moments. Substituting equations 2.42 into 2.40, produces :

$$\sigma_x = \frac{N_x}{T} + \frac{12M_x z}{T^3}$$

$$\sigma_y = \frac{N_y}{T} + \frac{12M_y z}{T^3} \tag{2.43}$$

$$\tau_{xy} = \frac{N_{xy}}{T} + \frac{12M_{xy} z}{T^3}$$

Taking $z = T/2$, the following equations become :

$$\sigma_x = \frac{N_x}{T} + \frac{6M_x}{T^2}$$

$$\sigma_y = \frac{N_y}{T} + \frac{6M_y}{T^2} \tag{2.44}$$

$$\tau_{xy} = \frac{N_{xy}}{T} + \frac{6M_{xy}}{T^2}$$

19

2.5 Stress Theories of Failure

The mechanical properties of structural and pressure vessel materials are determined by simple tensile tests. When a test specimen is subjected to tensile or compressive loading, the allowable or design stress is taken as a fraction of the yield or ultimate stress obtained from the tensile tests. These tensile tests are for uniaxial stress conditions. For pressure vessel design the objective is to determine the allowable stress for a specimen under combined loading. Failure refers to the actual rupture of the material. In ductile materials yielding occurs first. To ensure a safe design, yielding forms the basis of failure theories for these materials. The three most important and widely used failure theories [20] are :

- Maximum Principal Stress Theory
- Maximum Shear Stress Theory or Tresca Criterion
- Maximum Distortion Energy Theory or Von Mises Criterion

2.5.1 Maximum Principal Stress Theory

The Maximum Principal Stress Theory predicts that failure occurs in a stressed body when one of the principal stresses reaches the yield point value in simple tension or compression. For steel, the materials yield strength is the same under tension and compression. The principal or normal stresses for a plate or shell element is shown in figure 2-11.
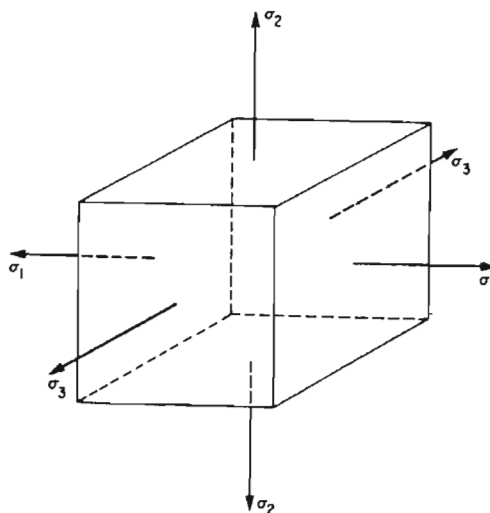
Figure 2-11 : Principal Stresses. Obtained from Harvey[20]

The following equations are obtained

$$|\sigma_1| = \sigma_{yp}$$

$$|\sigma_2| = \sigma_{yp} \tag{2.45}$$

$$|\sigma_3| = \sigma_{yp}$$

for plane stresses $\sigma_3 = 0$, therefore the allowable stresses are taken as the greater of $|\sigma_1|$ and $|\sigma_2|$.

2.5.2   Maximum Shear Stress or Tresca Theory

This theory predicts that failure of a body under combined stresses will occur when the maximum shear stress becomes equal to the maximum shear stress at yield point. The maximum shear stress is equal to half the difference of the maximum and minimum principal stresses. Therefore, the shear stresses are :

$$\tau = \frac{\sigma_1 - \sigma_2}{2}$$

$$\tau = \frac{\sigma_2 - \sigma_3}{2} \tag{2.46}$$

$$\tau = \frac{\sigma_3 - \sigma_1}{2}$$

Likewise, the maximum shear stress in a tensile test is equal to half the normal stress at yielding.

$$\tau = \frac{\sigma_{yp}}{2} \tag{2.47}$$

Equating equation 2.47 with equations 2.46, produces :

$$|\sigma_1 - \sigma_2| = \sigma_{yp}$$

$$|\sigma_2 - \sigma_3| = \sigma_{yp} \tag{2.48}$$

$$|\sigma_3 - \sigma_1| = \sigma_{yp}$$

21

For plane stresses $\sigma_3 = 0$, the above equations are reduced to :

$$\left|\sigma_1 - \sigma_2\right| = \sigma_{yp}$$

$$\left|\sigma_2\right| = \sigma_{yp} \tag{2.49}$$

$$\left|\sigma_1\right| = \sigma_{yp}$$

The allowable stress is taken as the larger of the three values given by equations 2.49.

2.5.3 Distortion Energy or Von Mises Theory

This theory predicts that inelastic action occurs in a body under any combination of stresses, only when the strain energy of distortion (change of shape due to shear stresses) absorbed per unit volume at a point, is equal to the strain energy of distortion absorbed per unit volume at a point in a test specimen stressed to its elastic limit under a tensile test. Using energy theory the following equation is obtained :

$$\left(\sigma_1 - \sigma_2\right)^2 + \left(\sigma_2 - \sigma_3\right)^2 + \left(\sigma_1 - \sigma_3\right)^2 = 2\sigma_{yp}^2 \tag{2.50}$$

In the case of plane stress, $\sigma_3 = 0$, the above equation reduces to :

$$\sigma_1^2 - \sigma_1\sigma_2 + \sigma_2^2 = \sigma_{yp}^2 \tag{2.51}$$

The distortion energy theory corresponds the best with experimental data for steels, however, most design practices and codes employ the maximum shear stress theory. The maximum shear stress or Tresca theory is believed to be the most conservative from all the theories and is the most widely used method of failure for ductile materials. The maximum stress theory corresponds the best with experimental data for brittle materials.

2.6 Finite Element Stress Analysis

The analysis of stress and deformation in an elastic body can be determined by Finite Element Methods (FEM) ([11] and [14]). For this study the finite element software MSC PATRAN[35] was used to perform basic structural analyses for various pressure vessels. Stress analyses were performed using a linear static analysis. Linear static analysis represents the most basic type of analysis. The term *linear* means that the computed stress or deformation is linearly related to the applied load. The term *static* means that the applied loads or forces are not time dependent, or the time variation is insignificant and can be safely ignored. The linear static equation that is used by MSC PATRAN is

$$[K]\{\delta\} = \{F\} \tag{2.52}$$

where K is the stiffness matrix (generated automatically by MSC PATRAN, based on the geometry and material properties), F is the vector of applied loading and δ is the vector of displacements induced by the applied loading. The procedure is to specify the geometry, the material properties, the boundary conditions and applied loading, and to compute the corresponding displacements. The displacements are then used to determine the stresses, strains, etc for the structure being analysed. The applied loading may be applied individually or in combination. Various loading subcases, in which a subcase represents a particular load and boundary condition, can be analysed. Multiple loading subcases provide a means for efficiency, whereby the solution time for subsequent analyses is a small fraction of the solution time of the first.

2.6.1 Energy Methods

Equation 2.52 was developed with the aid of Energy Methods. Energy methods[19] employ the principle of conservation of energy, which state that the strain energy stored in a system is equal to the work done by the applied loads, during the loading process. For a plate or shell element, such as figure 2-10, the stored strain energy is the sum of the work done by the bending moments $M_x dy$ and $M_y dx$, and the twisting moments $M_{xy} dy$ and $M_{yx} dx$. The work done by shearing forces and by the stretching of the middle surface is neglected, which is the same method used in beam theory. The work done by the moments is $\frac{1}{2}$ x (moment) x (angle between

the sides of the element after bending). In the xz plane the angle is $-\left(\partial^2 w/\partial x^2\right)dx$, therefore

the strain energy due to moment $M_x dy$ is $-\frac{1}{2}M_x\dfrac{\partial^2 w}{\partial x^2}dxdy$. The negative sign indicates that

a downward curvature (positive) has a decreasing slope as x increases. The strain energy owing

to $M_y dx$ is computed similarly. For the twisting moments, $M_{xy} dy$ and $M_{yx} dx$, the same

amount of energy is stored by both couples. The angles of the element faces due to twist are

$\left(\partial^2 w/\partial x\partial y\right)dx$ and $\left(\partial^2 w/\partial x\partial y\right)dy$. The total energy due to the twisting moments is

$-M_{xy}\dfrac{\partial^2 w}{\partial x\partial y}dxdy$. The Total Strain Energy for a plate or shell element is :

$$U_e = \frac{1}{2}\iint_A\left(-M_x\frac{\partial^2 w}{\partial x^2}-M_y\frac{\partial^2 w}{\partial y}-2M_{xy}\frac{\partial^2 w}{\partial x\partial y}\right)dxdy \qquad (2.53)$$

The total potential energy stored in a plate or shell under a distributed lateral load $p(x, y)$ is :

$$W_e = \frac{1}{2}\iint_A (pw)dxdy \qquad (2.54)$$

where w is a function of the displacement δ. Therefore, using conservation of energy :

$$U_e = W_e$$

$$\Pi = U_e - W_e = 0 \qquad (2.55)$$

Π is the total potential energy stored in the plate or shell. Substituting equations 2.53 and
2.54 into 2.55, produces :

$$\Pi = \frac{1}{2}\iint_A \left(-M_x \frac{\partial^2 w}{\partial x^2} - M_y \frac{\partial^2 w}{\partial y} - 2M_{xy} \frac{\partial^2 w}{\partial x \partial y} \right) dxdy \; - \frac{1}{2}\iint_A (pw) dxdy = 0 \quad (2.56)$$

$$\Pi = \iint_A \left(-M_x \frac{\partial^2 w}{\partial x^2} - M_y \frac{\partial^2 w}{\partial y} - 2M_{xy} \frac{\partial^2 w}{\partial x \partial y} \right) dxdy \; - \iint_A (pw) dxdy = 0 \quad (2.57)$$

Stress and deformation analyses can be determined using energy methods. Therefore, the Finite Element Method uses equation 2.57.

2.6.2   Finite Element Method

The powerful finite element method[11,14,19] permits the prediction of stress and deflection for a plate or shell, with a degree of ease and precision. In the finite element method, the plate or shell is divided into a finite number of element(triangular or rectangular in shape), connected at points of intersection known as nodes and along specified boundaries. The most commonly used finite element method is the finite displacement approach where the governing set of algebraic equations is expressed in terms of unknown nodal displacements. Consider an individual element of an isotropic plate shown below in figure 2-12 :
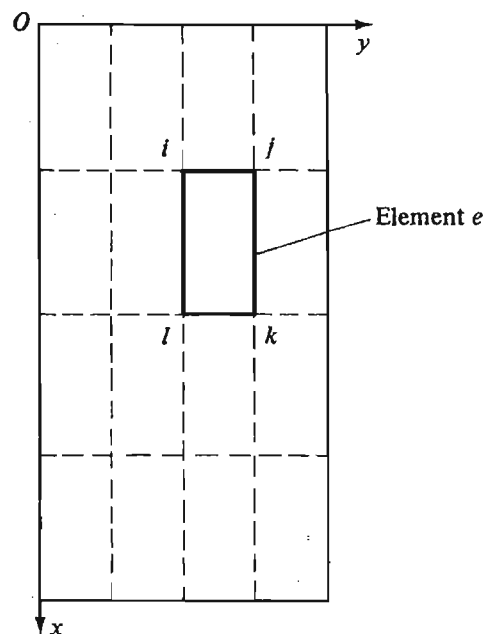
Figure 2-12 : Rectangular Finite Element. Obtained from Bulson and Allen[17]

25

Node i in the above figure has a nodal displacement made up of a deflection and two angular rotations within the element, represented by :

$$\{\delta_i\} = \left\{ \begin{array}{c} w_i \\ \dfrac{\partial w_i}{\partial x} \\ -\dfrac{\partial w_i}{\partial y} \end{array} \right\}$$

(2.58)

where,

$$w(x,y) = \alpha_1 + \alpha_2 x + \alpha_3 y + \alpha_4 x^2 + \alpha_5 xy + \alpha_6 y^2 + \alpha_7 x^3$$
$$+ \alpha_8 x^2 y + \alpha_9 xy^2 + \alpha_{10} y^3 + \alpha_{11} x^3 y + \alpha_{12} xy^3$$

(2.59)

The list of nodal displacements for the four corners is designated by :

$$\{\delta\}_e = \left\{ \begin{array}{c} \delta_i \\ \delta_j \\ \delta_k \\ \delta_l \end{array} \right\}$$

(2.60)

Substituting equations 2.59 into 2.58, we obtain a set of twelve equations in α for equation 2.60 :

$$\{\delta\}_e = [C]\{\alpha\}$$

(2.61)

$$\{\alpha\} = [C]^{-1}\{\delta\}_e$$

(2.62)

26

Substituting equations 2.62 into 2.59, produces :

$$\{w\}_e = [P]\{\delta\}_e \tag{2.63}$$

$\{w\}_e$ is referred to as the displacement function, and the *displacement matrix* is made up of equation 2.63. $[P]$ is a function of position and is often referred to as the shape function. It is determined for a specific element, either triangle or rectangle in shape.

Next, consideration is given to the curvatures and twists at any point in the element, which is represented by :

$$\{\varepsilon\}_e = \begin{Bmatrix} \varepsilon_x \\ \varepsilon_y \\ \gamma_{xy} \end{Bmatrix}_e = \begin{Bmatrix} -\dfrac{\partial^2 w}{\partial x^2} \\ -\dfrac{\partial^2 w}{\partial y^2} \\ -2\dfrac{\partial^2 w}{\partial x \partial y} \end{Bmatrix} \tag{2.64}$$

$\{\varepsilon\}_e$ is referred to as the *generalized strain displacement matrix* (equations 2.20 to 2.22 for a thin plate). Substituting equations 2.59 and 2.62 into 2.64 gives :

$$\{\varepsilon\}_e = [Q][C]^{-1}\{\delta\}_e \tag{2.65}$$

$$\{\varepsilon\}_e = [B]\{\delta\}_e \tag{2.66}$$

Where $[B]$ is determined for a specific element, either triangle or rectangle in shape.

27

The bending and twisting moments M_x, M_y and M_{xy} are related to the curvatures by equations 2.30 and 2.31, which can be written as :

$$\left\{ \begin{matrix} M_x \\ M_y \\ M_{xy} \end{matrix} \right\} = \frac{Et^3}{12(1-v^2)} \begin{bmatrix} 1 & v & 0 \\ v & 1 & 0 \\ 0 & 0 & (1-v)/2 \end{bmatrix} \left\{ \begin{matrix} -\dfrac{\partial^2 w}{\partial x \partial y} \\ -\dfrac{\partial^2 w}{\partial y^2} \\ -2\dfrac{\partial^2 w}{\partial x \partial y} \end{matrix} \right\} \tag{2.67}$$

The above equation is condensed to :

$$\{M\}_e = [D]\{\varepsilon\}_e \tag{2.68}$$

The stresses σ_x, σ_y and τ_{xy} are related to the curvatures by equations 2.28, therefore, a *stress-generalized strain* relationship is obtained :

$$\left\{ \begin{matrix} \sigma_x \\ \sigma_y \\ \tau_{xy} \end{matrix} \right\} = \frac{Et}{2(1-v^2)} \begin{bmatrix} 1 & v & 0 \\ v & 1 & 0 \\ 0 & 0 & (1-v)/2 \end{bmatrix} \left\{ \begin{matrix} -\dfrac{\partial^2 w}{\partial x \partial y} \\ -\dfrac{\partial^2 w}{\partial y^2} \\ -2\dfrac{\partial^2 w}{\partial x \partial y} \end{matrix} \right\} \tag{2.69}$$

The above equation is condensed to :

$$\{\sigma\}_e = [D^*]\{\varepsilon\}_e \tag{2.70}$$

28

According to energy method the variation in the potential energy of the plate shown in figure 2-12, from equation 2.57, is :

$$\Delta\Pi = \sum_{1}^{n} \iint_{A} \left(-M_x \frac{\partial^2 w}{\partial x^2} - M_y \frac{\partial^2 w}{\partial y} - 2M_{xy} \frac{\partial^2 w}{\partial x \partial y} \right) dxdy - \sum_{1}^{n} \iint_{A} (pw)dxdy = 0 \quad (2.71)$$

where n, A and p represent the number of uniform thickness elements comprising the plate, surface area of an element and the lateral load per unit surface area, respectively. The above expression can be rewritten as :

$$\sum_{1}^{n} \iint_{A} \left(\{\Delta\varepsilon\}_e^T \{M\}_e - p\Delta w \right) dxdy = 0 \qquad (2.72)$$

Introducing equations 2.63 and 2.67 into equation 2.72, produces :

$$\sum_{1}^{n} \iint_{A} \{\Delta\delta\}_e^T \left([k]_e \{\delta\}_e - \{F\}_e \right) = 0 \qquad (2.73)$$

The element *stiffness* matrix $[k]_e$ equals :

$$[k]_e = \iint_{A} [B]^T [D][B] dxdy \qquad (2.74)$$

The element *nodal force* matrix $\{F\}_e$, due to transverse load, is :

$$\{F\}_e = \iint_{A} [P]^T p\, dxdy \qquad (2.75)$$

29

For a single element, equation 2.73 can be reduced to :

$$\{\Delta\delta\}_e^T \left([k]_e \{\delta\}_e - \{F\}_e\right) = 0 \qquad (2.76)$$

therefore,

$$[k]_e \{\delta\}_e = \{F\}_e \qquad (2.77)$$

For the entire plate, equation 2.77 becomes 2.78

$$[K]\{\delta\} = \{F\} \qquad (2.78)$$

where

$$[K] = \sum_1^n [k]_e \qquad \{F\} = \sum_1^n \{F\}_e \qquad (2.79)$$

The general procedure for solving plate or shell problems by the finite element method is summarized as follows

- Determine $[k]_e$ from equation 2.74 in terms of the given element properties, and generate $[K] = \sum_1^n [k]_e$.

- Determine $\{F\}_e$ from equation 2.75 in terms of the applied loading, and generate $\{F\} = \sum_1^n \{F\}_e$.

- Determine the nodal displacements by using $\{\delta\} = [K]^{-1}\{F\}$.

The element moments and stresses can be calculated using equation 2.68 and 2.70 respectively.

30

Chapter 3

VESSELS UNDER INTERNAL PRESSURE AND PIPING LOADS

3.1 Introduction

The subject of local stresses in the vicinity of nozzles in pressure vessels has been one of the most researched areas of pressure vessels (see Chao[32]). Several practical approaches to this problem have evolved which allow design engineers to check the adequacy of shell-to-nozzle designs in pressure vessels. The most widely used method for calculating local stresses in vessels due to the combined internal pressure and external nozzle loads, has been detailed in the Welding Research Council (WRC) Bulletin 107[16] published in 1965. In 1989, WRC Bulletin 297[21] was published as a supplement to WRC Bulletin 107.

WRC Bulletin 107 calculates the stresses in the shell at eight points representing the inside and outside surface at the shell-to-nozzle junction due to external loads on the nozzle based on Bijlaard's method. WRC Bulletin 297 covers a wider range of geometric parameters and also calculates at eight points the stresses in the nozzle. Transverse and longitudinal membrane stresses, due to internal pressure, are added to the stresses calculated for external loadings. Design engineers use the WRC 107 method to calculate the local stresses in the shell due to the combined effect of internal pressure and external loads. These stresses are compared with stresses calculated numerically with Finite Element Analysis (FEA) software. The FEA results also indicate the stresses in the nozzle.

However, when evaluating these stresses the effect of the pressure thrust load is overlooked. A pressure thrust load is a load due to the internal pressure acting on the nozzle. The stresses generated by the pressure thrust load are transferred to the shell. WRC Bulletins 107 and 297 calculate the stresses due to the pressure thrust load as membrane stresses induced in the shell acting across the entire cross-section of the shell. The cross-section of the nozzle is much smaller than that of the shell. The equation of stress is :

$$\sigma = \frac{F}{A} \tag{3.1}$$

The above equation indicates that the smaller the area the greater the stress, therefore the stress induced in the shell to the pressure thrust load on the nozzle should be much greater than the membrane stresses calculated by WRC 107 and 297. The reasons for ignoring the effects of the pressure thrust load are :

- The nozzle is reinforced in accordance with ASME Code VIII Div 1 based on the internal design pressure. This has been taken as being sufficient to nullify the effect of nozzle openings, and only the general membrane stresses in the vessel due to internal pressure are calculated and superimposed on those calculated due to external loadings.

- The internal pressure in the nozzle is converted into a radial outward thrust force acting on the nozzle alone and is combined with the nozzle loadings which are used to calculate the local stresses in the nozzle using WRC 107 and 297.

The objective of this study is to determine if the above reasons are justified in ignoring the effects on the shell due to the pressure thrust load acting at the shell-to-nozzle junction.

The ASME Code is used to determine the significance of these stresses. The code gives acceptance criteria for the stresses calculated. If the stresses are within acceptable limits, then the design of the vessel is believed to be safe. The theory of failure used by the ASME Code is the maximum shear stress theory or Tresca criterion. It implies that the maximum shear stress at a point is equal to one half the difference between the algebraically largest and the algebraically smallest of the three principal stresses at the point. To simplify calculations ASME VIII Div 2 uses a stress called *Stress Intensity*. This stress is twice the maximum shear stress thus eliminating the half. Instead of comparing the stress intensity to the maximum shear stress it can now be compared directly to the yield stress or allowable stress of the material. Nozzles are defined by the codes as being *gross structural discontinuities*. They are defined to be sources of stresses and strains that affect large portions of the structure and influence the stress situation of the structures as a whole.

3.2 ASME VIII Div 2 Classification of Stresses

Ductile materials (see Roche[24]) are highly recommended for the construction of pressure vessels. They can withstand excessive plastic deformations. Therefore, computations of stresses are made easier by treating the material as elastic or linear. However, the behaviour of ductile materials is different to that of elastic materials. To use these elastically computed stresses conveniently, these stresses have to be split up into various stress parts. These parts are primary stresses, secondary stresses, peak stresses, etc.

The ASME Code VIII Div 2 gives the following definitions for the stresses occurring in the vessel :

(a) *Primary Stress.* A normal or shear stress developed by an imposed loading which is necessary to satisfy the laws of equilibrium. The basic characteristic of a primary stress is that it is not self-limiting. Mechanical loads cause primary stresses. Primary stresses, which exceed the yield strength, may result in failure or gross distortion of the structure. Primary stresses are divided into two categories : *general* and *local.* A general primary stress in a cylindrical shell is due to internal pressure or live loads.

(b) *Local Primary Membrane Stress.* These membrane stresses arise when pressure, or other mechanical loads, associated with a discontinuity, produce excessive distortion when transferring the loads to other portions of the structure. Conservatism requires that such a membrane stress be classified as a local primary membrane stress even though it has some characteristics of a secondary stress. An example of a local primary membrane stress is the membrane stress in a shell produced by external loads and moments at a nozzle connection.

(c) *Secondary Stress.* Secondary stress is a normal or shear stress developed by the constraint of adjacent parts or by self-constraint of a structure. Secondary stress is 'self-limiting'. Local yielding and minor distortions can cause the stress to occur. An example of a general secondary stress is a thermal stress. Bending stresses developed at gross structural discontinuities, like nozzle connections, are referred to as secondary stresses.

A few definitions have been mentioned. These definitions are most applicable for shell-to-nozzle junctions.

33

The symbols for the stresses mentioned in the definitions are :

- Sum of all General Primary Membrane Stress Components : P_m
- Sum of all Local Primary Membrane Stress Components : P_L
- Sum of all Primary Bending Stress Components : P_b
- Sum of all Secondary Membrane plus Bending Stress Components : Q

The Code classifies the stresses at various locations on a pressure vessel according to the following table:

Vessel Component	Location	Origin of Stress	Type of Stress	Classification
Cylindrical or Spherical Shell	Shell plate remote from discontinuities	Internal pressure	General membrane Gradient through plate thickness	P_m Q
		Axial thermal gradient	Membrane Bending	Q Q
	Junction with head or flange	Internal pressure	Membrane Bending	P_L Q
Any shell or head	Any section across entire vessel	External load or moment, or internal pressure	General membrane averaged across full section. Stress component perpendicular to cross section	P_m
		External load or moment	Bending across full section. Stress component perpendicular to cross section	P_m
	Near nozzle or other opening	External load or moment, or internal pressure	Local membrane Bending Peak (fillet or corner)	P_L Q F
	Any location	Temp. diff, between shell and head	Membrane Bending	Q Q

Table 3-1 : ASME VIII Div 2 Classification of Stresses

The above table from ASME VIII Div 2 indicates that at the shell-to-nozzle junction, the Primary Local Membrane Stresses P_L and the Secondary Bending Stresses Q represent the membrane and bending stresses in the shell respectively. The stresses are produced with the combination of internal pressure and nozzle loads. At the shell-to-nozzle junction there is a transfer of loads from the nozzle to the shell, therefore, the membrane stresses produced at this point, according to the definitions, are local primary membrane stresses. The bending stresses according to the definitions given in the ASME Code are secondary stresses. Peak stresses are stresses that do not cause noticeable distortions and are important in fatigue cases. However, for general static cases they are ignored.

The primary and secondary stresses, or a combination of theses stresses produced by mechanical loads, are divided into *Stress intensities*. For the purpose of this study the three most important *stress intensities* are :

- General Primary Membrane Stress Intensity : P_m
- Local Membrane Stress intensity : P_L
- Primary Plus Secondary Stress Intensity : $P_L + P_b + Q$

3.3 Stress Limits

Stresses calculated theoretically or numerically have to be within the allowable limits given in figure 3-1 obtained from the ASME Code.

Stress Category	Primary			Secondary Membrane plus Bending	Peak
	General Membrane	Local Membrane	Bending		
Description	Average primary stress across solid section. Excludes discontinuities and concentrations. Produced only by mechanical loads.	Average stress across any solid section. Considers discontinuities but not concentrations. Produced only by mechanical loads.	Component of primary stress proportional to distance from centroid of solid section. Excludes discontinuities and concentrations. Produced only by mechanical loads.	Self-equilibrating stress necessary to satisfy continuity of structure. Occurs at structural discontinuities. Can be caused by mechanical load or by differential thermal expansion. Excludes local stress concentrations.	(1) Increment added to primary or secondary stress by a concentration (notch). (2) Certain thermal stresses which may cause fatigue but not distortion of vessel shape.
Symbol	P_m	P_L	P_b	Q	F

Figure 3-1 : ASME VIII Div 2 Stress Categories and Stress Intensity Limits

36

For a vessel subjected to internal pressure and external piping loads, table 3-1 is used to determine the relevant stresses produced, as well as the appropriate stress intensities. The table below summarizes table 3-1 and figure 3-1 for a vessel under internal pressure and nozzle loads.

	Internal Pressure	Internal Pressure + Nozzle Loads	
Type of Stress	General Primary Membrane	Local Primary Membrane and Secondary Bending	
Classification	P_m	P_L and Q	
Stress Intensity	P_m	P_L	$P_L + Q$
Stress Limits	S_m	$1.5S_m$	$3S_m$

Table 3-2 : Appropriate Stress Intensities and Stress Limits

The following diagram represents failure of ductile materials:
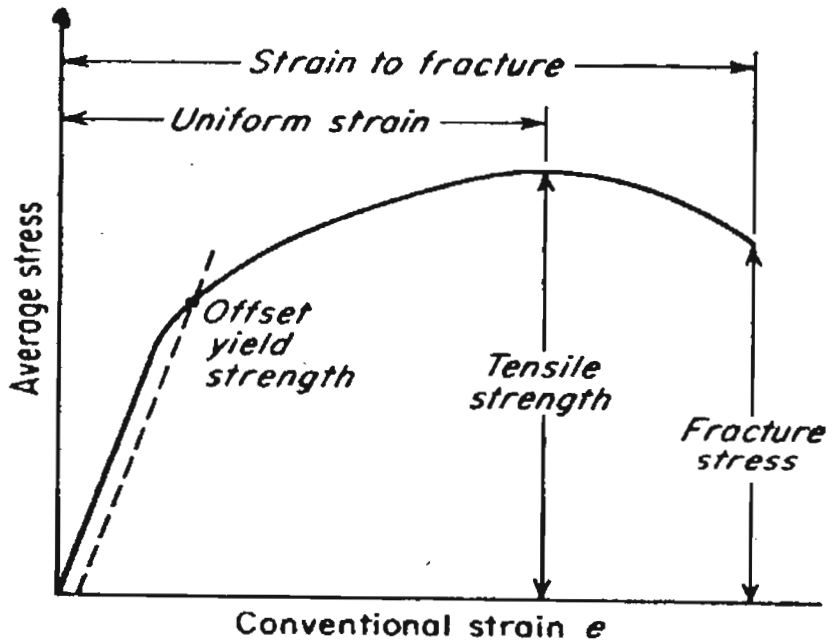
Figure 3-2 : Stress-strain Diagram for typical structural steel under tension. Obtained from Gere and Timoshenko[33]

37

For ductile materials, in figure 3-2, the elastic or linear strain is much smaller than the plastic strain. Therefore, it can be assumed that for pressure vessels, stresses below the yield strength result in negligible strain whereas stresses above the yield strength could result in excessive strains or distortions, which can cause failure.

Designing for stresses below the material's yield strength ensures that negligible or no strains/distortions occur in the material to prevent failure. To prevent severe plastic deformation, which will eventually lead to the structure collapsing, the allowable stress should be the ultimate tensile stress of the material .

The P_L stress intensity includes only local primary membrane stresses. The result of these stresses exceeding the yield strength can cause gross distortion or result in failure of the vessel at the shell-to-nozzle junction. Therefore, the allowable stress limit for the local primary membrane stress intensity should be the yield strength of the material.

The $P_L + Q$ stress intensity includes primary membrane stresses as well as secondary bending stresses. The secondary stresses cause additional distortions to that created by the primary stresses. Substantial unrecoverable deformations may occur. To prevent rupture or ductile bursting the ultimate tensile strength of the material applies to the primary plus secondary stress intensity.

The ASME Code gives the value S_m, and is referred to as the design stress intensity of the material at design temperature. The allowable or design stress of the material S_a is often used instead of S_m. The ASME Code calculates the allowable or design stress as a fraction of the material's yield strength and ultimate tensile strength. The tables showing these relationships can be found in Appendix A. The following summarize these relationships :

$1.5\ S_m$ = Yield Strength (S_y)

$3\ S_m$ = Ultimate Tensile Strength (S_T)

3.4 Calculation of Stress Intensities

The Stress Intensities are calculated using the Maximum Shear Stress theory or Tresca Criterion. For the calculation of the local primary membrane stress intensity P_L, the following procedures need to be followed. The membrane stresses calculated from the combined loadings, which include internal pressure and nozzle loads, have to be divided into four categories. These categories are longitudinal stresses σ_x, transverse (hoop) stresses σ_ϕ, radial stresses σ_r and shear stresses τ. These stresses then need to be converted to three principal stresses representing the longitudinal, transverse and radial directions. These stresses are σ_1, σ_2 and σ_3 respectively. The ASME Code VIII Div 2 calculates three stress differences for a particular location on the vessel.

For the shell-to-nozzle junction the stresses obtained will be transverse stresses σ_ϕ, longitudinal stresses σ_x, radial stresses σ_r and shear stresses τ. At the junction the transverse, longitudinal and shear stresses have to be converted to two principal stresses representing the transverse and longitudinal directions. These stresses σ_2 and σ_1 are mentioned above. The remaining stress component, σ_r, can be represented as a principal stress σ_3. Using the Tresca Criterion the following stress differences are obtained:

$$S_{12} = \sigma_1 - \sigma_2 \tag{3.1}$$

$$S_{23} = \sigma_2 - \sigma_3 \tag{3.2}$$

$$S_{31} = \sigma_3 - \sigma_1 \tag{3.3}$$

The final stress intensity S is the largest absolute value of the three stress differences shown above, for a particular location at the shell-to-nozzle junction. The procedures for deriving the stress intensity is given in ASME VIII Div 2, APPENDIX 4 - *MANDATORY DESIGN BASED ON STRESS ANALYSIS*, ARTICLE 4-1.

For the $P_L + Q$ stress intensity the same procedures mentioned above apply. However the bending stresses calculated have to be included. Again four component stresses have to be calculated and converted to three principal stresses. Using the Tresca Criterion the largest absolute value of the three stress differences (similar to that shown above) is the final stress intensity S. The procedures for deriving the stress intensity are given in ASME VIII Div 2, APPENDIX 5 - *MANDATORY DESIGN BASED ON FATIGUE ANALYSIS*, ARTICLE 5-1.

3.5 WRC Bulletin 107

It has been mentioned that the most common procedures for the computation of stresses in the shell due to the combined effect of internal design pressure and external nozzle loads are given by the Welding Research Council Bulletin 107. The relation between internal membrane forces and internal bending moments are represented by the following equation:

$$\sigma_i = K_n \frac{N_i}{T} \pm K_b \frac{6M_i}{T^2}$$
(3.5)

The above equation takes the form of equations 2.44. The methods for obtaining the membrane forces N_i and bending moments M_i were developed by Professor P. P. Bijlaard[16]. With the use of a shell parameter (γ) and an attachment parameter (β),

$$\gamma = \frac{R_m}{T}$$
(3.6)

$$\beta = 0.875 \frac{r_o}{R_m}$$
(3.7)

Bijlaard was able to develop several nondimensional curves to determine the stresses at the shell-to-nozzle junction.

The membrane stresses due to internal pressure are calculated using the following equations derived from the ASME Code VIII Div 1.

Circumferential (Hoop/Transverse) Stresses :

$$\sigma_\phi = \frac{DP(R_i + 0.6T)}{T} \text{(I.D. Formula)}$$
(3.8)

$$\sigma_\phi = \frac{DP(R_i - 0.4T)}{T} \text{(O.D. Formula)}$$
(3.9)

Longitudinal Stresses :

$$\sigma_x = \frac{DP(R_i + 0.6T)}{2T} \text{ (I.D. Formula)} \tag{3.10}$$

$$\sigma_x = \frac{DP(R_i - 0.4T)}{2T} \text{ (O.D. Formula)} \tag{3.11}$$

The above equations indicate that the greater stresses occur at the inside surface of the shell, since the internal design pressure is applied to the inside surface.

3.5.1 Stresses Resulting from Radial Load, P

3.5.1.1 Circumferential Membrane Stress

Using the parameters γ and β and the nondimensional curves 3C or 4C, values for $\dfrac{N_\phi}{P/R_m}$ are found. The circumferential membrane stress due to the radial load is given by the following equation :

$$\frac{N_\phi}{T} = \left[\frac{N_\phi}{P/R_m}\right] \cdot \left[\frac{P}{R_m T}\right] \tag{3.12}$$

3.5.1.2 Circumferential Bending Stress

Using the parameters γ and β and the nondimensional curves 1C or 2C-1, values for $\dfrac{M_\phi}{P}$ are found. The circumferential bending stress due to the radial load is given by the following equation :

41

$$\frac{6M_\phi}{T^2} = \left[\frac{M_\phi}{P}\right] \cdot \left[\frac{6P}{T^2}\right] \qquad (3.13)$$

3.5.1.3 Longitudinal Membrane Stress

Using the parameters γ and β and the nondimensional curves 3C or 4C, values for $\dfrac{N_x}{P/R_m}$ are found. The longitudinal membrane stress due to the radial load is given by the following equation:

$$\frac{N_x}{T} = \left[\frac{N_x}{P/R_m}\right] \cdot \left[\frac{P}{R_m T}\right] \qquad (3.14)$$

3.5.1.4 Longitudinal Bending Stress

Using the parameters γ and β and the nondimensional curves 1C or 2C-1, values for $\dfrac{M_x}{P}$ are found. The longitudinal bending stress due to the radial load is given by the following equation :

$$\frac{6M_x}{T^2} = \left[\frac{M_x}{P}\right] \cdot \left[\frac{6P}{T^2}\right] \qquad (3.15)$$

3.5.2   Stresses Resulting from Circumferential Moment, M_C

3.5.2.1 Circumferential Membrane Stress

Using the parameters γ and β and the nondimensional curve 3A, values for $\dfrac{N_\phi}{M_C/R_m^2\beta}$ are found. The circumferential membrane stress due to the circumferential moment is given by the following equation :

42

$$\frac{N_\phi}{T} = \left[\frac{N_\phi}{M_C / R_m^2 \beta}\right] \cdot \left[\frac{6M_C}{R_m T^2 \beta}\right] \tag{3.16}$$

3.5.2.2 Circumferential Bending Stress

Using the parameters γ and β and the nondimensional curve 1A, values for $\dfrac{M_\phi}{M_C / R_m \beta}$ are found. The circumferential bending stress due to the circumferential moment is given by the following equation :

$$\frac{6M_\phi}{T^2} = \left[\frac{M_\phi}{M_C / R_m \beta}\right] \cdot \left[\frac{6M_C}{R_m T^2 \beta}\right] \tag{3.17}$$

3.5.2.3 Longitudinal Membrane Stress

Using the parameters γ and β and the nondimensional curve 4A, values for $\dfrac{N_x}{M_C / R_m^2 \beta}$ are found. The longitudinal membrane stress due to the circumferential moment is given by the following equation :

$$\frac{N_x}{T} = \left[\frac{N_x}{M_C / R_m^2 \beta}\right] \cdot \left[\frac{6M_C}{R_m T^2 \beta}\right] \tag{3.18}$$

3.5.2.4 Longitudinal Bending Stress

Using the parameters γ and β and the nondimensional curve 2A, values for $\dfrac{M_x}{M_C / R_m \beta}$ are found. The longitudinal bending stress due to the circumferential moment is given by the following equation :

$$\frac{6M_x}{T^2} = \left[\frac{M_x}{M_C / R_m \beta}\right] \cdot \left[\frac{6M_C}{R_m T^2 \beta}\right] \tag{3.19}$$

43

3.5.3 Stresses Resulting from Longitudinal Moment, M_L

3.5.3.1 Circumferential Membrane Stress

Using the parameters γ and β and the nondimensional curve 3B, values for $\dfrac{N_\phi}{M_L / R_m^2 \beta}$ are found. The circumferential membrane stress due to the circumferential moment is given by the following equation :

$$\frac{N_\phi}{T} = \left[\frac{N_\phi}{M_L / R_m^2 \beta} \right] \cdot \left[\frac{6M_L}{R_m T^2 \beta} \right] \tag{3.20}$$

3.5.3.2 Circumferential Bending Stress

Using the parameters γ and β and the nondimensional curves 1B or 1B-1, values for $\dfrac{M_\phi}{M_L / R_m \beta}$ are found. The circumferential bending stress due to the circumferential moment is given by the following equation :

$$\frac{6M_\phi}{T^2} = \left[\frac{M_\phi}{M_L / R_m \beta} \right] \cdot \left[\frac{6M_L}{R_m T^2 \beta} \right] \tag{3.21}$$

3.5.3.3 Longitudinal Membrane Stress

Using the parameters γ and β and the nondimensional curve 4B, values for $\dfrac{N_x}{M_L / R_m^2 \beta}$ are found. The longitudinal membrane stress due to the circumferential moment is given by the following equation :

$$\frac{N_x}{T} = \left[\frac{N_x}{M_L / R_m^2 \beta} \right] \cdot \left[\frac{6M_L}{R_m T^2 \beta} \right] \tag{3.22}$$

3.5.3.4 Longitudinal Bending Stress

Using the parameters γ and β and the nondimensional curves 2B or 2B-1, values for $\dfrac{M_x}{M_L / R_m \beta}$ are found. The longitudinal bending stress due to the circumferential moment is given by the following equation :

$$\frac{6M_x}{T^2} = \left[\frac{M_x}{M_L / R_m \beta} \right] \cdot \left[\frac{6M_L}{R_m T^2 \beta} \right] \tag{3.23}$$

3.5.4 Stresses Resulting from Torsional Moment, M_T

Torsional moments are assumed to induce shear stresses in the shell. The shear stress due to the torsional moment is :

$$\tau_{\phi x} = \frac{M_T r_o}{I_P} \tag{3.24}$$

The nozzle is assumed to be a tube, therefore, torsional shear stresses for tubes are given by the equation 3.24. I_P for the shell-to-nozzle junction is $2\pi r_o^3 T$. Therefore, substituting this into the above equation we obtain :

$$\tau_{\phi x} = \frac{M_T}{2\pi r_o^2 T} \tag{3.25}$$

3.5.5 Stresses Resulting from Shear Loads, V_C and V_L

Bijlaard predicted that the shear forces transmitted to the shell produced shear membrane stresses (force divided by area). Therefore, shear stresses generated by shear loads for round nozzles are given as :

$$\tau_{x\phi} = \frac{V_C}{\pi r_o T} \tag{3.25}$$

$$\tau_{\phi x} = \frac{V_L}{\pi r_o T} \tag{3.26}$$

3.5.6 Sign Convention

The stresses calculated using the methods given in WRC 107 are either in tension or compression. Tensile stresses are indicated to be positive (+), compressive stresses are indicated to be negative (-). For the shell-to-nozzle junction, there are four points of consideration, indicated in figure 3-3. Figure 3-3 also indicates the directions of the radial and moment loading, which give the sign convention for the stresses resulting from radial and moment loading in table 3-3.
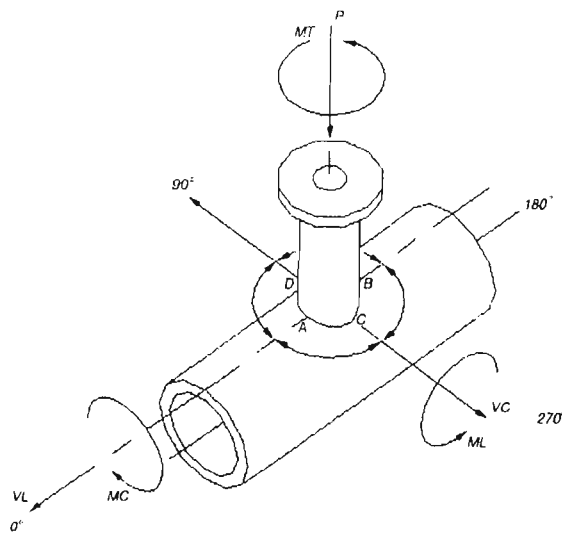
Figure 3-3 : External Loading at shell-to-nozzle junction. Obtained from CodeCalc.

For shear stresses the sign convention is dependent on the direction of the loading. Shear stresses caused by torsional moments are positive. Shear stresses due to V_C are positive at point A and negative at point B, indicated in figure3-3. Shear stresses due to V_L are positive at point D and negative at point C.

46

The table below is used to compute local stresses in cylindrical shells using WRC 107 :

From Fig	Read curves for	Compute absolute values of stress	STRESSES : IF Load is acting in opposite direction, reverse the sign							
			AU	AL	BU	BL	CU	CL	DU	DL
3C or 4C	$\dfrac{N_\phi}{P/R_m}$	$K_n\left[\dfrac{N_\phi}{P/R_m}\right]\cdot\left[\dfrac{P}{R_mT}\right]=$	-	-	-	-	-	-	-	-
1C or 2C-1	$\dfrac{M_\phi}{P}$	$K_b\left[\dfrac{M_\phi}{P}\right]\left[\dfrac{6P}{T^2}\right]=$	-	+	-	+	-	+	-	+
3A	$\dfrac{N_\phi}{M_C/R_m^2\beta}$	$K_n\left[\dfrac{N_\phi}{M_C/R_m^2\beta}\right]\cdot\left[\dfrac{6M_C}{R_mT^2\beta}\right]=$					-	-	+	+
1A	$\dfrac{M_\phi}{M_C/R_m\beta}$	$K_b\left[\dfrac{M_\phi}{M_C/R_m\beta}\right]\cdot\left[\dfrac{6M_C}{R_mT^2\beta}\right]=$					-	+	+	-
3B	$\dfrac{N_\phi}{M_L/R_m^2\beta}$	$K_n\left[\dfrac{N_\phi}{M_L/R_m^2\beta}\right]\cdot\left[\dfrac{6M_L}{R_mT^2\beta}\right]=$	-	-	+	+				
1B or 1B-1	$\dfrac{M_\phi}{M_L/R_m\beta}$	$K_b\left[\dfrac{M_\phi}{M_L/R_m\beta}\right]\cdot\left[\dfrac{6M_L}{R_mT^2\beta}\right]=$	-	+	+	-				

Add algebraically : σ_ϕ

From Fig	Read curves for	Compute absolute values of stress	AU	AL	BU	BL	CU	CL	DU	DL
3C or 4C	$\dfrac{N_x}{P/R_m}$	$K_n\left[\dfrac{N_x}{P/R_m}\right]\cdot\left[\dfrac{P}{R_mT}\right]=$	-	-	-	-	-	-	-	-
1C or 2C	$\dfrac{M_x}{P}$	$K_b\left[\dfrac{M_x}{P}\right]\cdot\left[\dfrac{6P}{T^2}\right]=$	-	+	-	+	-	+	-	+
4A	$\dfrac{N_x}{M_C/R_m^2\beta}$	$K_n\left[\dfrac{N_x}{M_C/R_m^2\beta}\right]\cdot\left[\dfrac{6M_C}{R_mT^2\beta}\right]=$					-	-	+	+
2A	$\dfrac{M_x}{M_C/R_m\beta}$	$K_b\left[\dfrac{M_x}{M_C/R_m\beta}\right]\cdot\left[\dfrac{6M_C}{R_mT^2\beta}\right]=$					-	+	+	-
4B	$\dfrac{N_x}{M_L/R_m^2\beta}$	$K_n\left[\dfrac{N_x}{M_L/R_m^2\beta}\right]\cdot\left[\dfrac{6M_L}{R_mT^2\beta}\right]=$	-	-	+	+				
2B or 2B-1	$\dfrac{M_x}{M_L/R_m\beta}$	$K_b\left[\dfrac{M_x}{M_L/R_m\beta}\right]\cdot\left[\dfrac{6M_L}{R_mT^2\beta}\right]=$	-	+	+	-				

Add algebraically : σ_x

Shear Stresses due to torsion, M_T	$\tau_{\phi x}=\dfrac{M_T}{2\pi r_o^2 T}$	+	+	+	+	+	+	+	+
Shear Stress due to load, V_C	$\tau_{x\phi}=\dfrac{V_C}{\pi r_o T}$	+	+	-	-				
Shear Stresses due to load, V_L	$\tau_{\phi x}=\dfrac{V_L}{\pi r_o T}$					-	-	+	+

Add algebraically : τ

Table 3-3 : WRC Bulletin 107 Computation Sheet for Local Stresses in Cylindrical Shells

47

3.5.7 Stress Intensities

The final Combined Stress Intensity S is calculated using the Tresca Criterion. This stress intensity is equal to the $P_L + Q$ stress intensity. The stresses are computed for eight points at the shell-to-nozzle junction. The algebraic sums of all circumferential stresses at these points are indicated by σ_ϕ and the algebraic sum of all the longitudinal stresses at these points are indicated by σ_x. The circumferential, longitudinal and shear stresses are computed on the same plane, therefore, these stresses need to be converted to principal stresses. The principal stress equation is given by:

$$\sigma_1, \sigma_2 = \frac{\sigma_x + \sigma_\phi}{2} \pm \frac{\sqrt{(\sigma_x - \sigma_\phi)^2 + 4\tau^2}}{2} \qquad (3.27)$$

The ASME Code indicates that the combined stress intensity S is given by the largest absolute magnitude of three stress differences, equations 3.2 to 3.4. Radial stresses are not computed therefore the radial principal stresses can be assumed to be zero. Therefore equations 3.2 to 3.4 become :

$$S_{12} = \sigma_1 - \sigma_2 \qquad (3.28)$$

$$S_{23} = \sigma_2 \qquad (3.29)$$

$$S_{13} = \sigma_1 \qquad (3.30)$$

Using equations 3.27 to 3.30, the following WRC 107 rules apply :

1. When $\tau \neq 0$, $S =$ the absolute largest magnitude of either

$$S = \frac{1}{2}\left[\sigma_x - \sigma_\phi \pm \sqrt{(\sigma_x - \sigma_\phi)^2 + 4\tau^2} \right] \ or \ \sqrt{(\sigma_x - \sigma_\phi)^2 + 4\tau^2}$$

2. When $\tau = 0$, $S =$ the absolute largest magnitude of either

$$S = \sigma_x, \sigma_\phi \ or \ (\sigma_x - \sigma_\phi)$$

3.6 Numerical Results

The theoretical stresses for vessels under the combined loading of internal pressure and nozzle piping loads, were calculated using the methods described in WRC Bulletin 107. The WRC 107 equations and nondimensional curves are programmed into a software called Codecalc. The vessels are loaded according to the WRC 107 convention, shown in figure 3-3 above. The WRC 107 format of the results, presented by Codecalc, is shown below :

DESIGN

Internal Design pressure(DP)	2.51MPa
Design Temperature	150degrees C
Vessel Material	SA - 516Grade 70
Nozzle Material	SA - 106Grade B

CYLINDRICAL SHELL

Vessel Inner Diameter(DV)	570mm
Vessel Thickness(TV)	14mm
Corrosion Allowance(CAS)	3mm
Vessel Allowable Stress(Sm)	137.9MPa

NOZZLE (6 inch)

Nozzle Outer Diameter(DN)	168.275mm
Nozzle Thickness(TN)	10.97mm
Corrosion Allowance(CAN)	3mm
Nozzle Alowable Stress(SNm)	117.9MPa

Nozzle Loads WRC 107 Sign Convention (SASOL LOADS)

Radial Load(P)	-9450N
Circumferential Shear(VC)	0N
Longitudinal Shear(VL)	0N
Circumferential Moment(MC)	4350000Nmm
Longitudinal Moment(ML)	6300000Nmm
Torsional Moment(MT)	0Nmm

GEOMETRIC PARAMETERS WRC 107

$Rm = (DV+TV-CAS)/2$	290.50mm
$T=TV-CAS$	11.00mm
$ro=DN/2$	84.14mm
$GAMMA=Rm/T$	26.41
$BETA=0.875*ro/Rm$	0.253

Dimensionless loads from WRC 107 Figure

(PHI - circumferential, x - longitudinal)

Figure		Gamma	Beta	VALUE
4C	N(PHI)/(P/Rm)	26.41	0.253	**3.562**

2C1	M(PHI)/P	26.41	0.253	0.031
3A	N(PHI)/(MC/(Rm^2*BETA))	26.41	0.253	1.129
1A	M(PHI)/(MC/(Rm*BETA))	26.41	0.253	0.079
3B	N(PHI)/(ML/(Rm^2*BETA))	26.41	0.253	2.628
1B	M(PHI)/(ML/(Rm*BETA))	26.41	0.253	0.024
3C	N(x)/(P/Rm)	26.41	0.253	2.202
1C1	M(x)/P	26.41	0.253	0.06
4A	N(x)/(MC/(Rm^2*BETA))	26.41	0.253	2.069
2A	M(x)/(MC/(Rm*BETA))	26.41	0.253	0.036
4B	N(x)/(ML/(Rm^2*BETA))	26.41	0.253	1.09
2B	M(x)/(ML/(Rm*BETA))	26.41	0.253	0.039

POINTS C & D

3C	N(PHI)/(P/Rm)	26.41	0.253	2.202
1C	M(PHI)/P	26.41	0.253	0.06
1B1	M(PHI)/(ML/(Rm*BETA))	26.41	0.253	0.024
4C	N(x)/(P/Rm)	26.41	0.253	3.562
2C	M(x)/P	26.41	0.253	0.031
2B1	M(x)/(ML/(Rm*BETA))	26.41	0.253	0.042

STRESS CONCENTRATION FACTORS Kn=1, Kb=1

STRESS VALUES MPa - NOZZLE TO SHELL JUNCTION								
	AU	AL	BU	BL	CU	CL	DU	DL
CM(DP)	63.7	66.2	63.7	66.2	63.7	66.2	63.7	66.2
CM(P)	10.5	10.5	10.5	10.5	6.5	6.5	6.5	6.5
CB(P)	14.5	-14.5	14.5	-14.5	28.1	-28.1	28.1	-28.1
CM(MC)	0.0	0.0	0.0	0.0	-20.9	-20.9	20.9	20.9
CB(MC)	0.0	0.0	0.0	0.0	-231.5	231.5	231.5	-231.5
CM(ML)	-70.4	-70.4	70.4	70.4	0.0	0.0	0.0	0.0
CB(ML)	-101.8	101.8	101.8	-101.8	0.0	0.0	0.0	0.0
S(PHI)	*-83.5*	*93.7*	*261.0*	*30.7*	*-154.0*	*255.2*	*350.7*	*-166.0*
LM(DP)	31.8	31.8	31.8	31.8	31.8	31.8	31.8	31.8
LM(P)	6.5	6.5	6.5	6.5	10.5	10.5	10.5	10.5
LB(P)	28.1	-28.1	28.1	-28.1	14.5	-14.5	14.5	-14.5
LM(MC)	0.0	0.0	0.0	0.0	-38.3	-38.3	38.3	38.3
LB(MC)	0.0	0.0	0.0	0.0	-105.5	105.5	105.5	-105.5
LM(ML)	-29.2	-29.2	29.2	29.2	0.0	0.0	0.0	0.0
LB(ML)	-165.5	165.5	165.5	-165.5	0.0	0.0	0.0	0.0
S(x)	*-128.2*	*146.5*	*261.2*	*-126.1*	*-86.8*	*95.1*	*200.6*	*-39.4*
SHEAR(MT)	0.0	0.0	0.0	0.0	0.0	0.0	0.0	0.0
SHEAR(VC)	0.0	0.0	0.0	0.0	0.0	0.0	0.0	0.0
SHEAR(VL)	0.0	0.0	0.0	0.0	0.0	0.0	0.0	0.0
τ	*0.0*	*0.0*	*0.0*	*0.0*	*0.0*	*0.0*	*0.0*	*0.0*
S(PL + Q)	*128.2*	*146.5*	*261.2*	*156.8*	*154.0*	*255.2*	*350.7*	*166.0*

Figure 3-4 : Codecalc Computation Sheet for Local Stresses in Cylindrical Shells

The finite element results were calculated using Model A, shown below :

Isometric View

Figure 3-5 : Finite Element Model A

Model A was constructed as close as possible (considering [15], [23] and [27]) to the actual geometry of a vessel with a nozzle attachment. Shell elements or 4-noded quadrilateral elements were used to mesh the model. MSC PATRAN has a node limit of 6000 nodes, therefore, vessels using Model A were meshed as close to 6000 nodes as possible to generate an appropriate fine mesh. No welds have been modelled for the nozzle connection to the shell, to ensure more conservative results for external loads and more realistic pressure stresses. The material of the shell is SA 516 Grade 70 (carbon steel) and the nozzle material is SA 106 Grade B (carbon steel). Their properties can be found in Appendix A. An elastic modulus of 200GPa and a Poisson's ratio of 0.3 were used.

The two types of nozzle loadings, SASOL Loads and Foster Wheeler Loads, can also be found in Appendix A. Model A is validated by comparing theoretical results with FEM values. The primary membrane stress, generated by internal pressure, is calculated theoretically, remote from the shell-to-nozzle junction, and compared with the finite element stress. The objective is to reach at least a 5% model convergence. To verify the model's convergence the following vessels were analysed. Vessels with different diameters were chosen.

Vessel	Inner Diameter (mm)	Thickness (mm)	Corrosion Allowance	Design Pressure (MPa)	Design Temperature (degrees Celsius)	Nozzle (inch)	Nozzle Loading
1	570	14	3	2.51	150	6"	SASOL
2	570	10	3	1.03	160	2"	FW
3	700	8	-	0.24	60	4"	FW
4	760	10	3	1.02	60	4"	FW
5	760	8	-	0.24	60	10"	FW
6	800	8	-	1.13	140	4"	FW
7	840	8	-	0.21	65	10"	FW
8	1080	13	3	1.05	160	10"	FW
9	1200	16	3	2.51	150	12"	SASOL
10	1260	16	3	2.51	205	2"	FW
11	1270	13	3	1.03	160	8"	FW
12	1410	8	-	0.2	80	14"	FW
13	1420	16	-	1.46	150	10"	SASOL
14	1710	8	-	0.26	125	4"	FW
15	2450	12	-	0.26	75	16"	FW

*FW – Foster Wheeler

Table 3-4 : Vessels used to verify convergence

The following results were achieved :
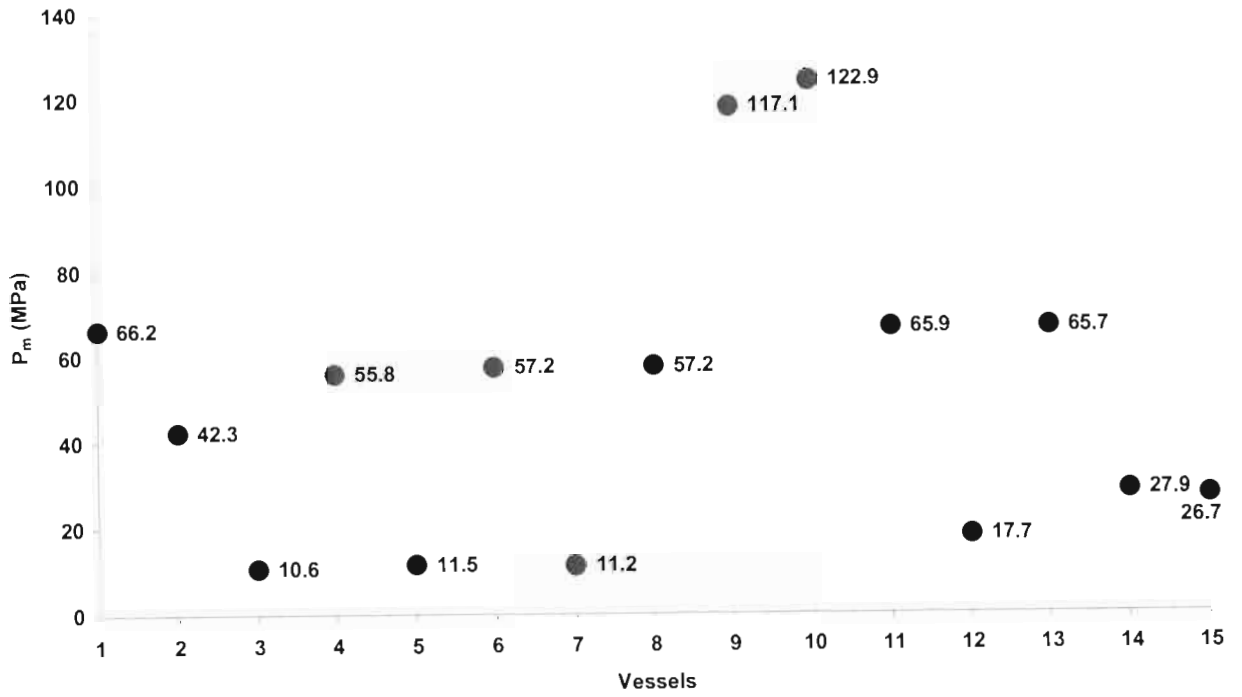
Figure 3-6 : Theoretical General Primary Membrane Stress P_m
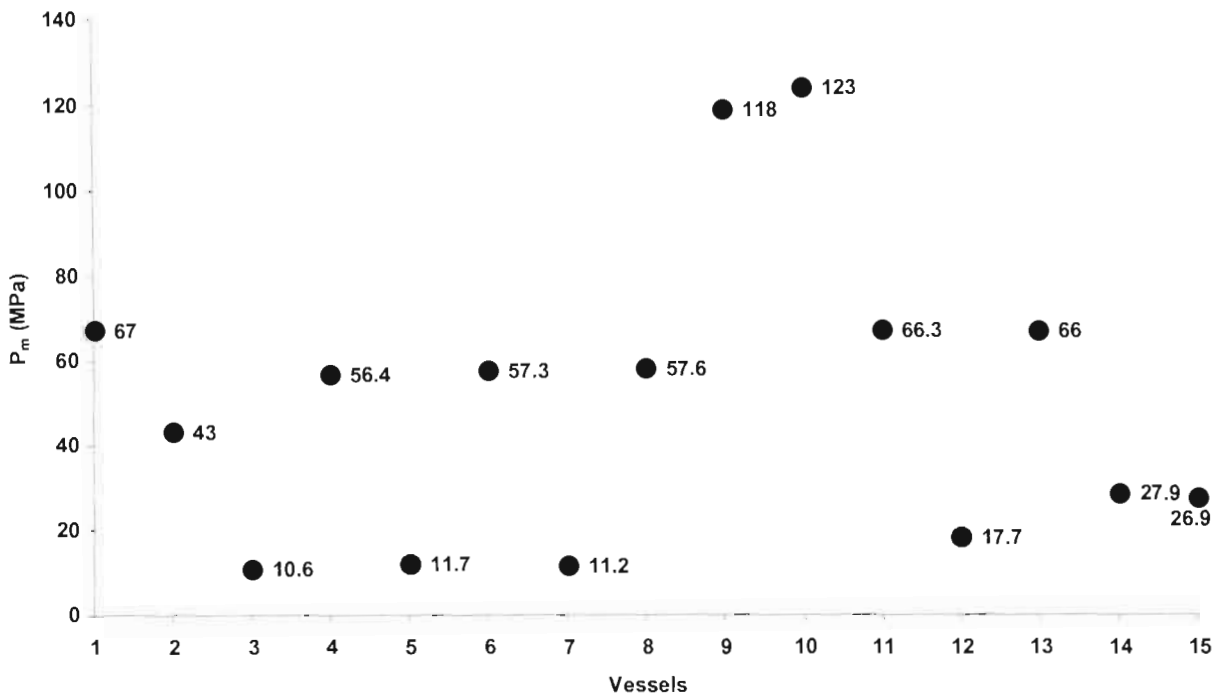
Figure 3-7 : FEM General Primary Membrane Stress P_m
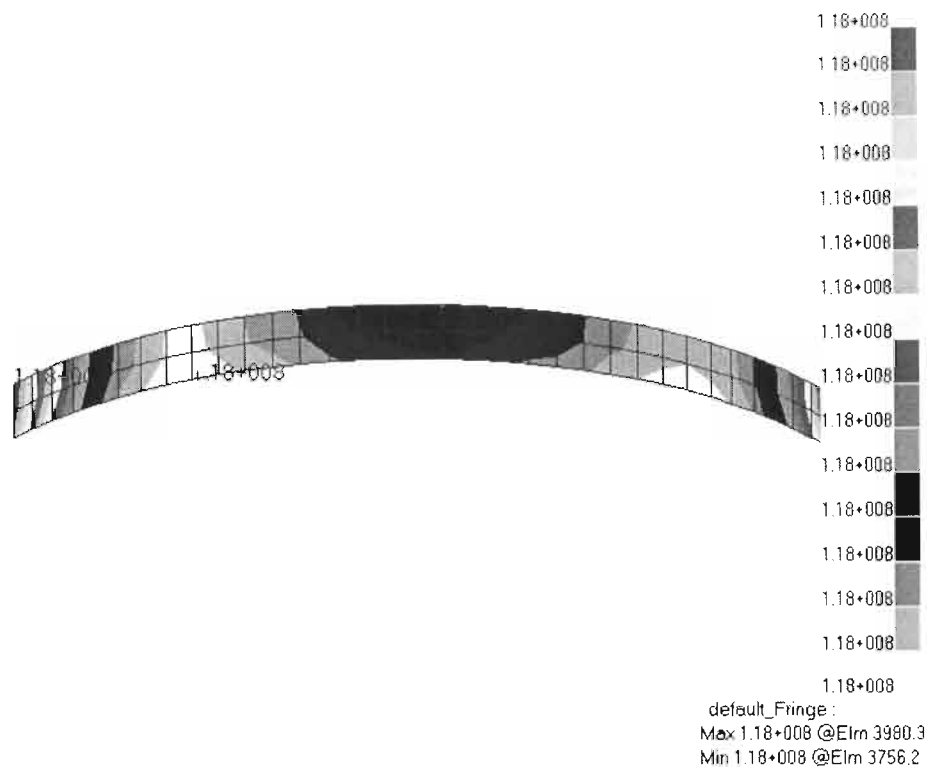
Figure 3-8 : FEM general membrane stress for Vessel 9

Figure 3-8 is an example of a stress analysis, using Model A to determine the general membrane stress for vessel 9.
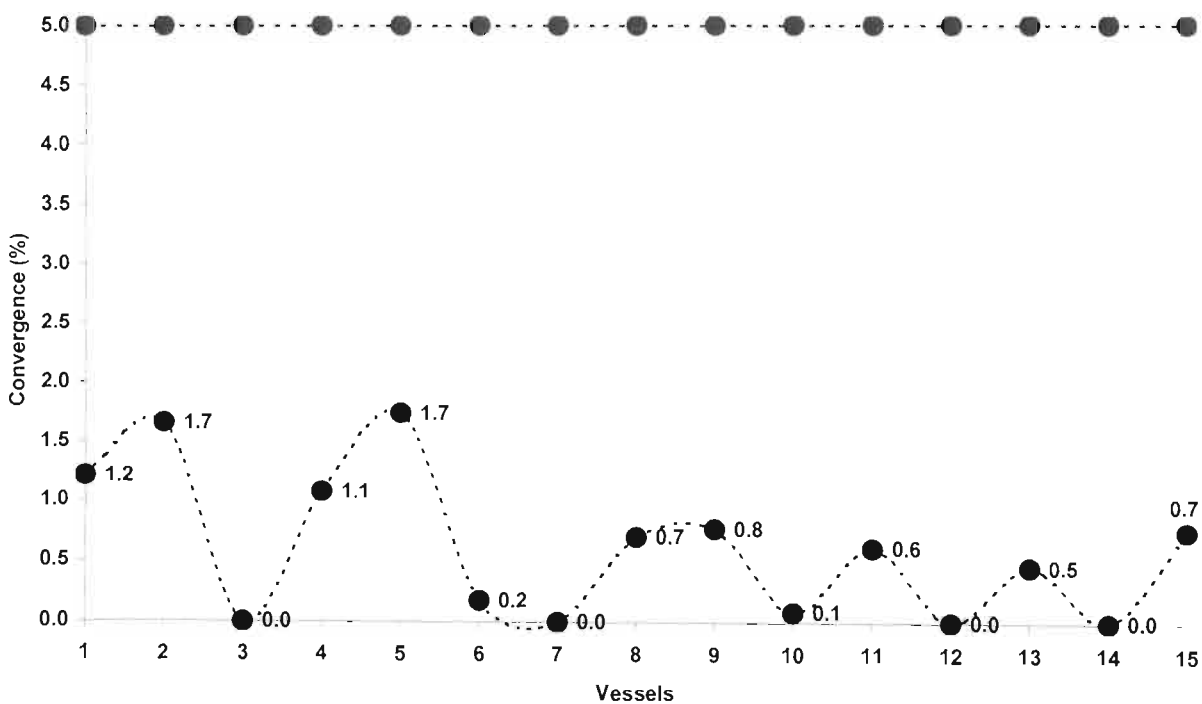
Figure 3-9 : Convergence between Theoretical and FEM results

Figure 3-9 indicates that FEM analyses using Model A are within the 5% model convergence. FEM results accurately coincide with theoretical results. The FEM combined stress intensity, S, was determined for each of the vessels and compared with the theoretical results. The results achieved were :
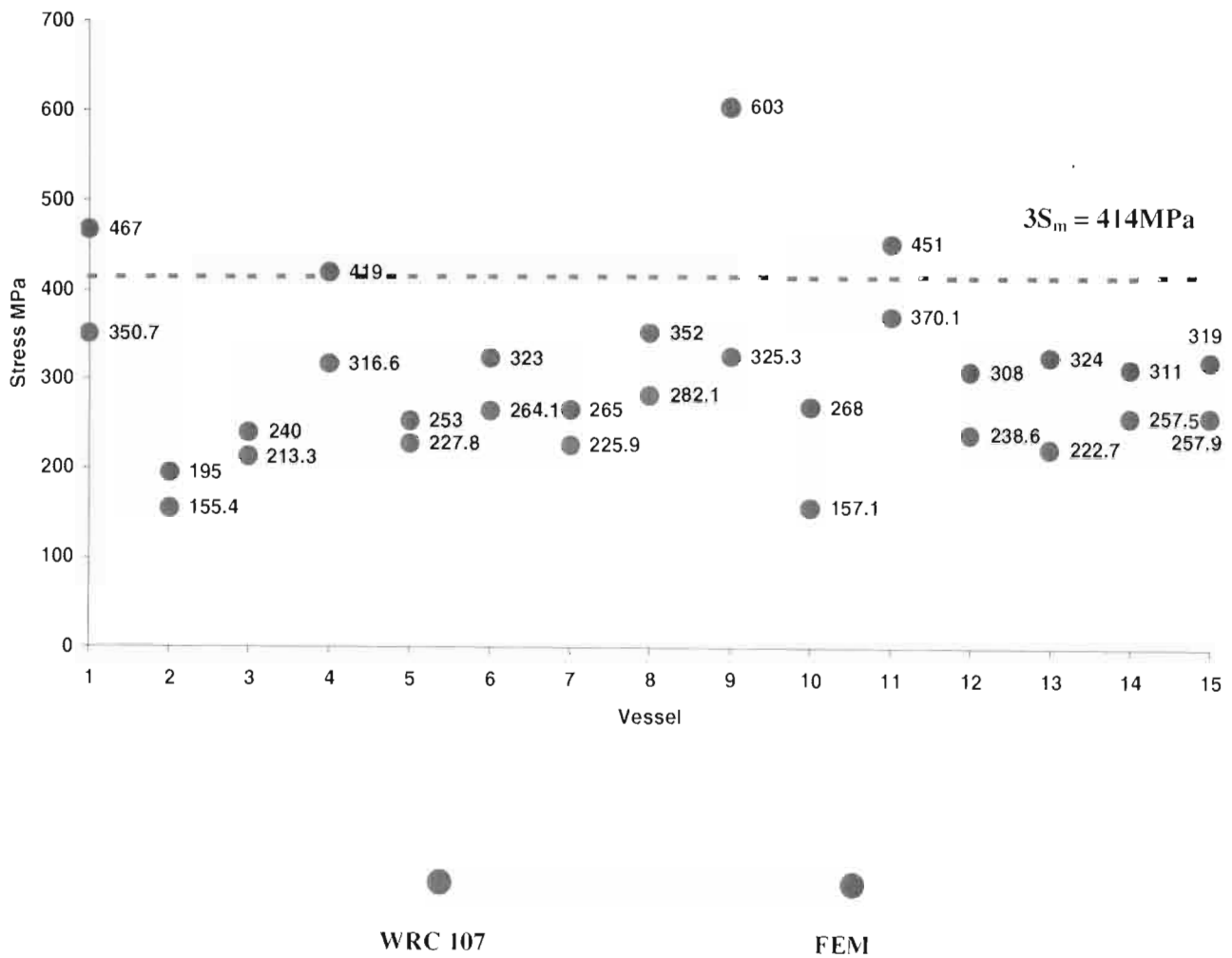
Figure 3-10 : Comparison between FEM and Theoretical (WRC 107) Combined Stress Intensities S

An example of a stress analysis, using Model A to determine the combined stress intensity, is shown below.
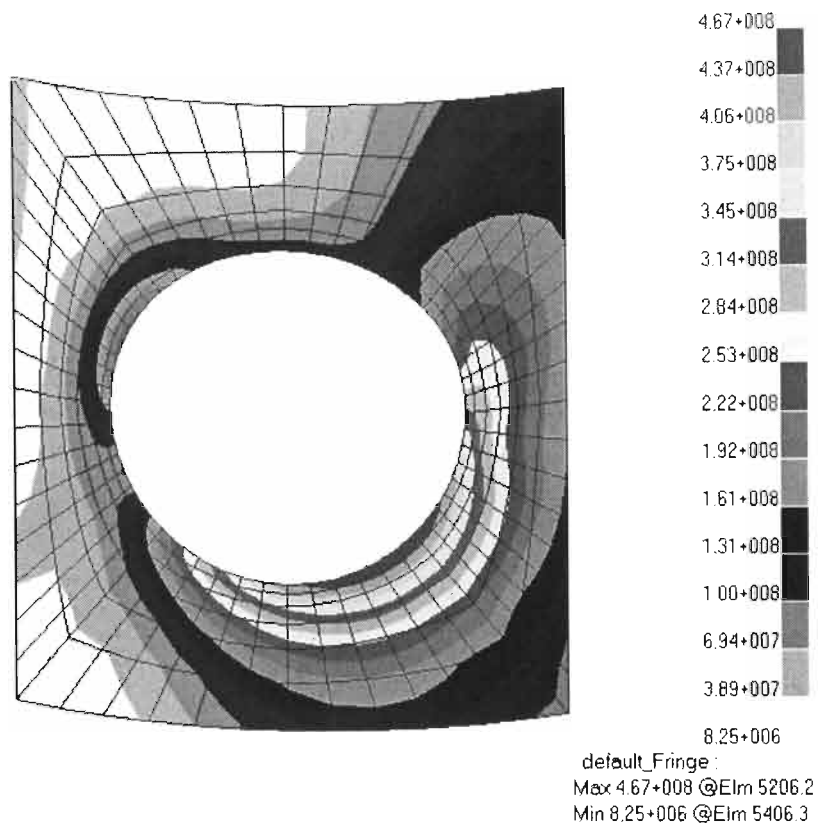
Figure 3-11 : FEM Combined Stress Intensity for Vessel 1 using Model A

For vessel 1, the theoretical S was calculated to be 350.7MPa. The FEM value of 467MPa is much greater, due to the internal pressure thrust load developed at the shell-to-nozzle junction. The effects of the internal pressure thrust load were investigated. First, a set of vessels was analysed with an internal pressure of 0.26MPa and, thereafter, a second set of vessels, identical to the first set, was analysed with an increased internal pressure of 1.05MPa. The vessels analysed are shown below :

Vessel	Inner Diameter (mm)	Thickness (mm)	Corrosion Allowance (mm)	Design Pressure (MPa)	Design Temperature (degrees Celsius)	Nozzle (inch)	Nozzle Loading
16	1990	14	-	0.26	150	2"	SASOL
17	1990	14	-	0.26	150	4"	SASOL
18	1990	14	-	0.26	150	8"	SASOL
19	1990	14	-	0.26	150	12"	SASOL
20	1990	14	-	0.26	150	16"	SASOL

Table 3-5 : Vessels analysed with an internal pressure of 0.26MPa

Vessel	Inner Diameter (mm)	Thickness (mm)	Corrosion Allowance (mm)	Design Pressure (MPa)	Design Temperature (degrees Celsius)	Nozzle (inch)	Nozzle Loading
21	1990	14	-	1.05	150	2"	SASOL
22	1990	14	-	1.05	150	4"	SASOL
23	1990	14	-	1.05	150	8"	SASOL
24	1990	14	-	1.05	150	12"	SASOL
25	1990	14	-	1.05	150	16"	SASOL

Table 3-6 : Vessels analysed with an internal pressure of 1.05MPa

Stress analyses for the above vessels were generated. The vessels were first subjected to internal pressure alone. For tables 3-5 and 3-6 the following results were achieved :
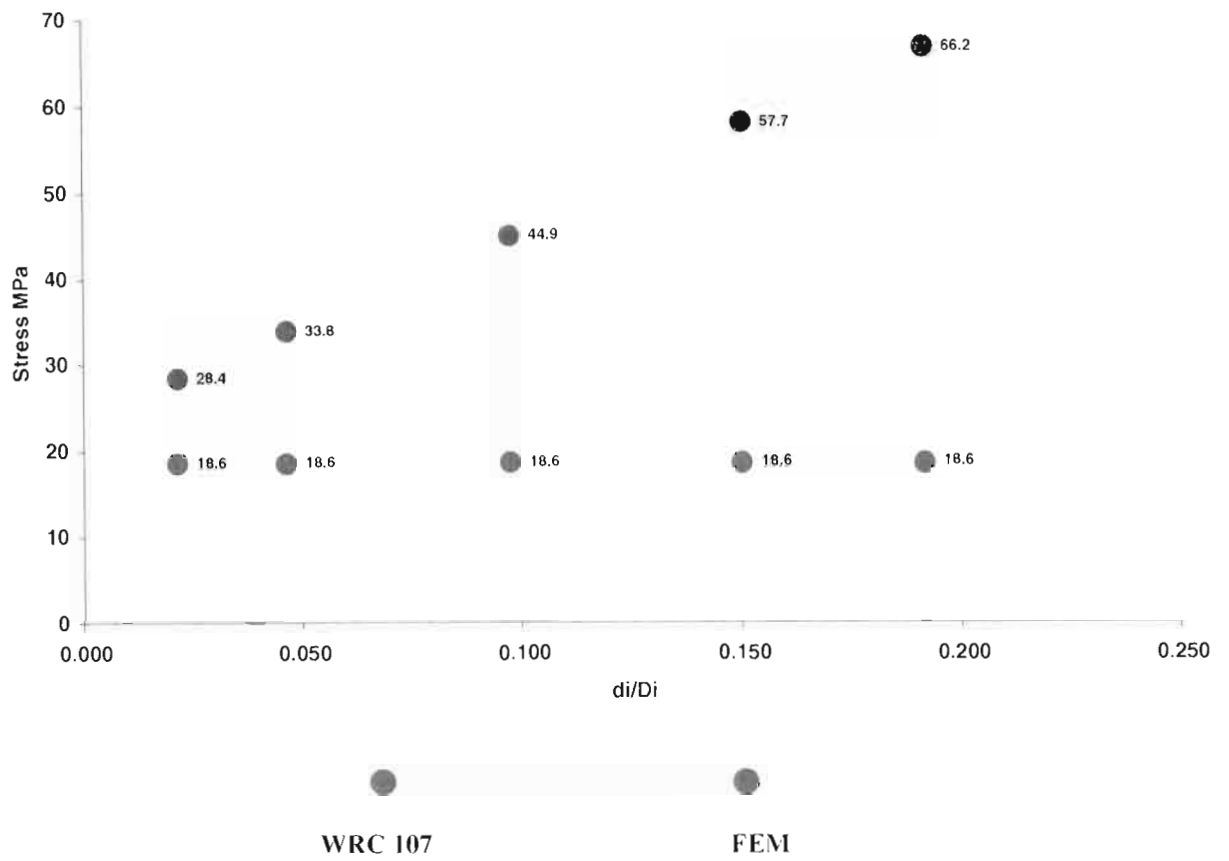
Figure 3-12 : FEM and Theoretical (WRC 107) stresses for vessels subjected to internal pressure 0.26MPa
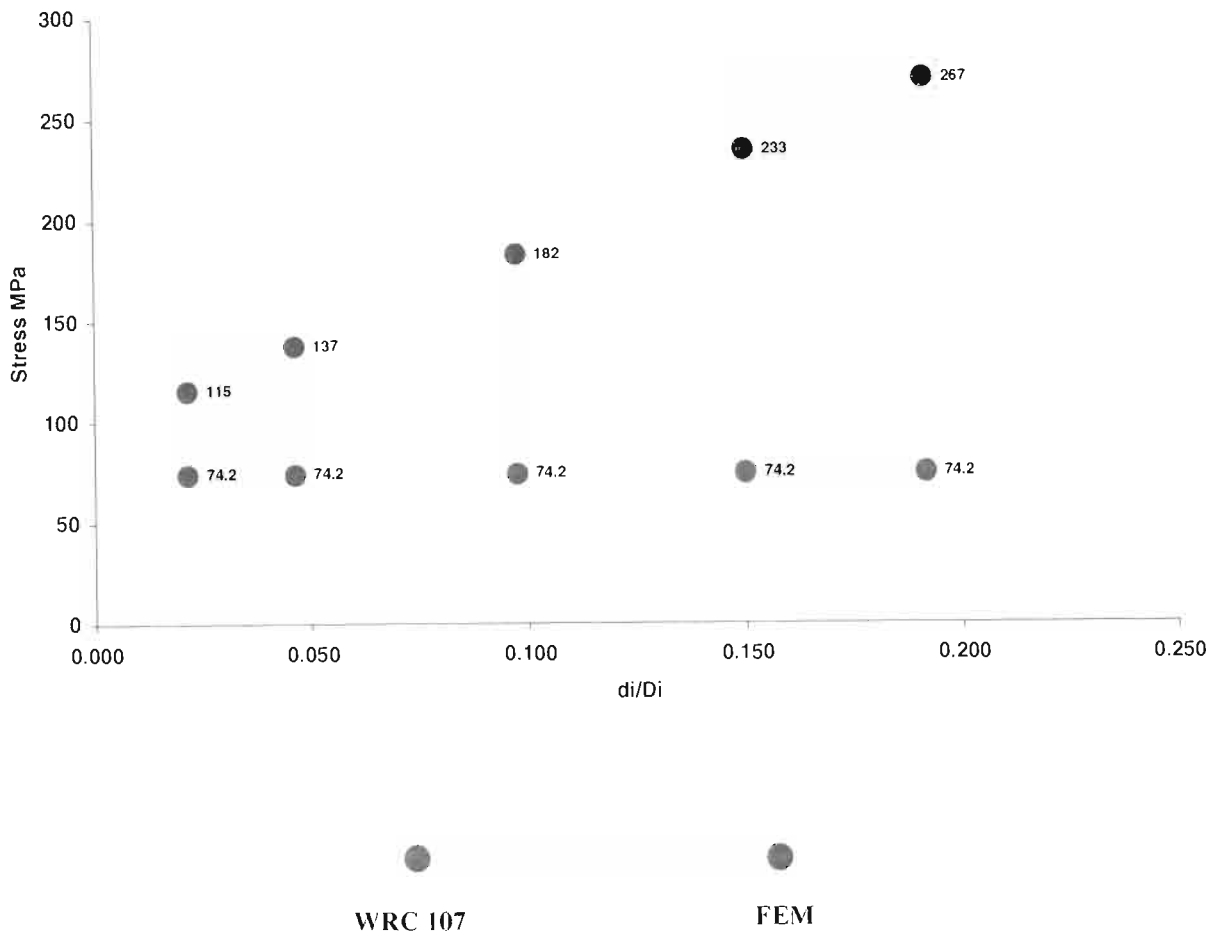
Figure 3-13 : FEM and Theoretical (WRC 107) stresses for vessels subjected to internal
pressure 1.05MPa

It can be observed from figures 3-12 and 3-13 that the FEM stresses due to internal pressure
alone do not coincide with the theoretical WRC 107 values. The stresses according to FEM are
much higher than the theoretical values. This clearly illustrates the effect of the internal
pressure thrust load that occurs at the shell-to-nozzle junction. The type of nozzle is also an
important consideration. An increase in the size of the nozzle also increases the stress at the
shell-to-nozzle junction. Figure 3-13 indicates that an increase in the internal pressure produces
a much greater stress at the shell-to-nozzle junction, and this stress can be quite severe if the
size of the nozzle is increased. Figures 3-14 and 3-15 are FEM stress analyses showing an
increase in the stress, as the internal pressure is increased from 0.26MPa to 1.05MPa, for
identical vessels 16 and 21.
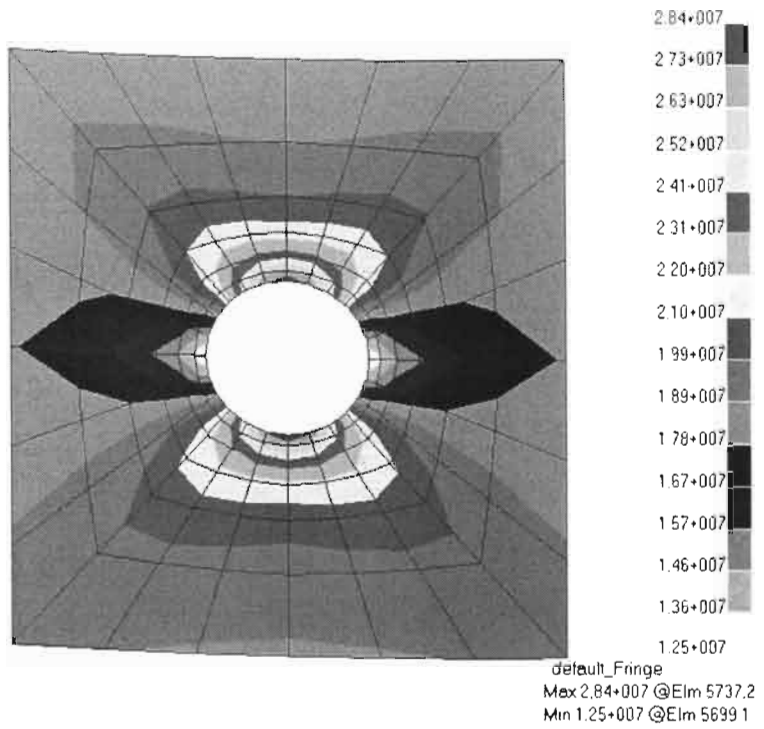
Figure 3-14 : FEM Stress analysis for Vessel 16 (internal pressure 0.26MPa)
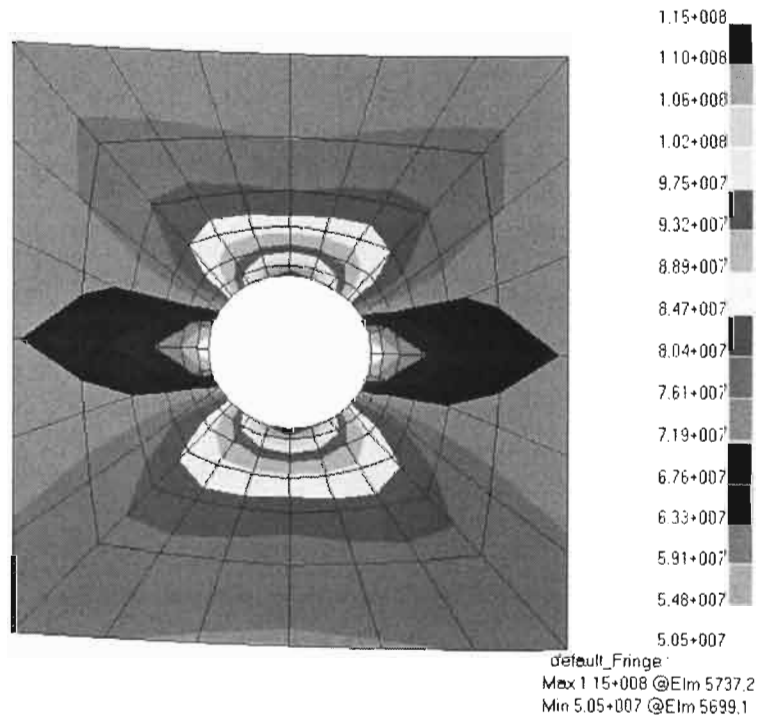
Figure 3-15 : FEM Stress analysis for Vessel 21 (internal pressure 1.05MPa)

Further FEM Stress analyses for vessels 16 to 25, under internal pressure alone, can be found in Appendix B.

The vessels were also analysed with only the external nozzle loads being applied. The following results were achieved :
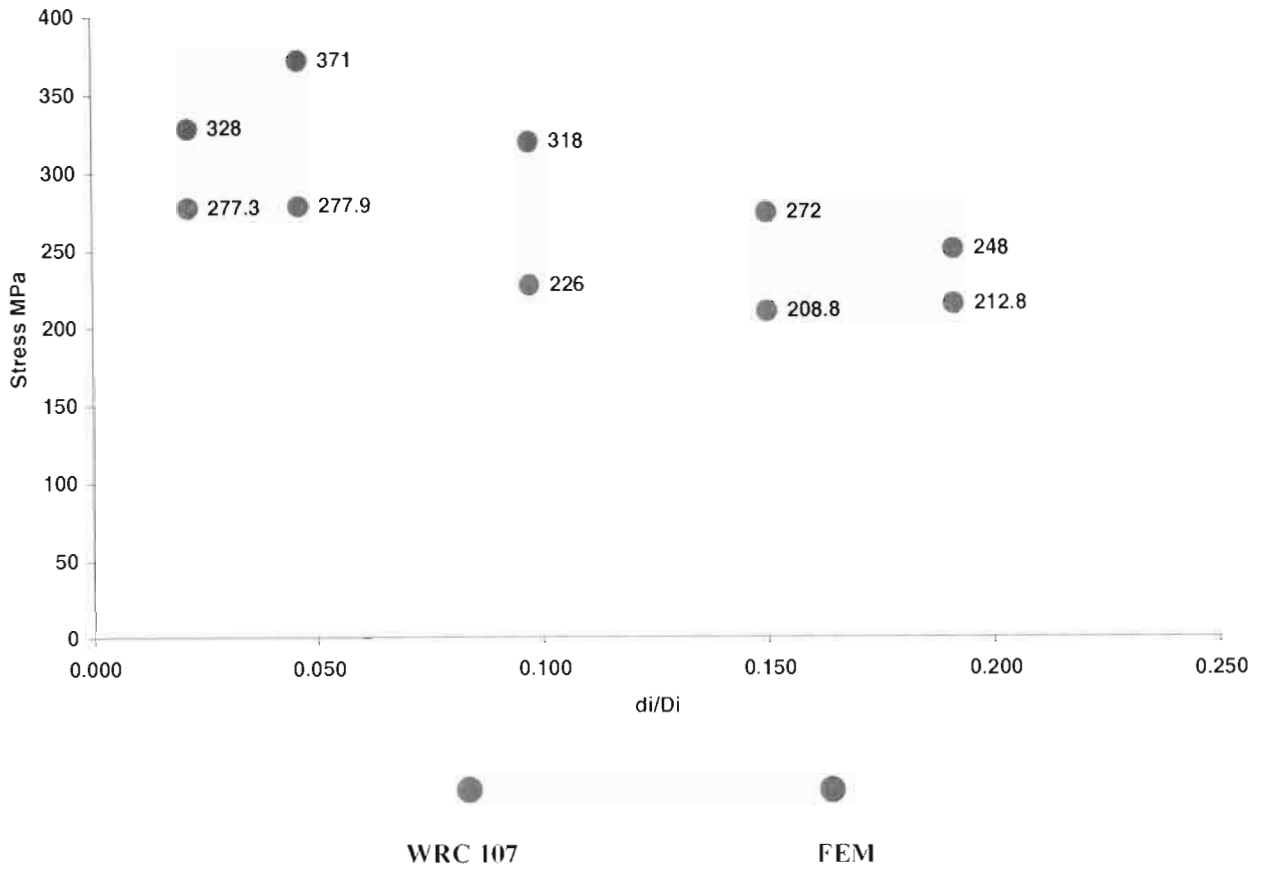
Figure 3-16 : FEM and Theoretical stresses for vessels 16 to 20 (identical to vessels 21 to 25) subjected to external nozzle loads

Figure 3-17 below shows the FEM stress analysis for vessel 16 under external nozzle loads alone.
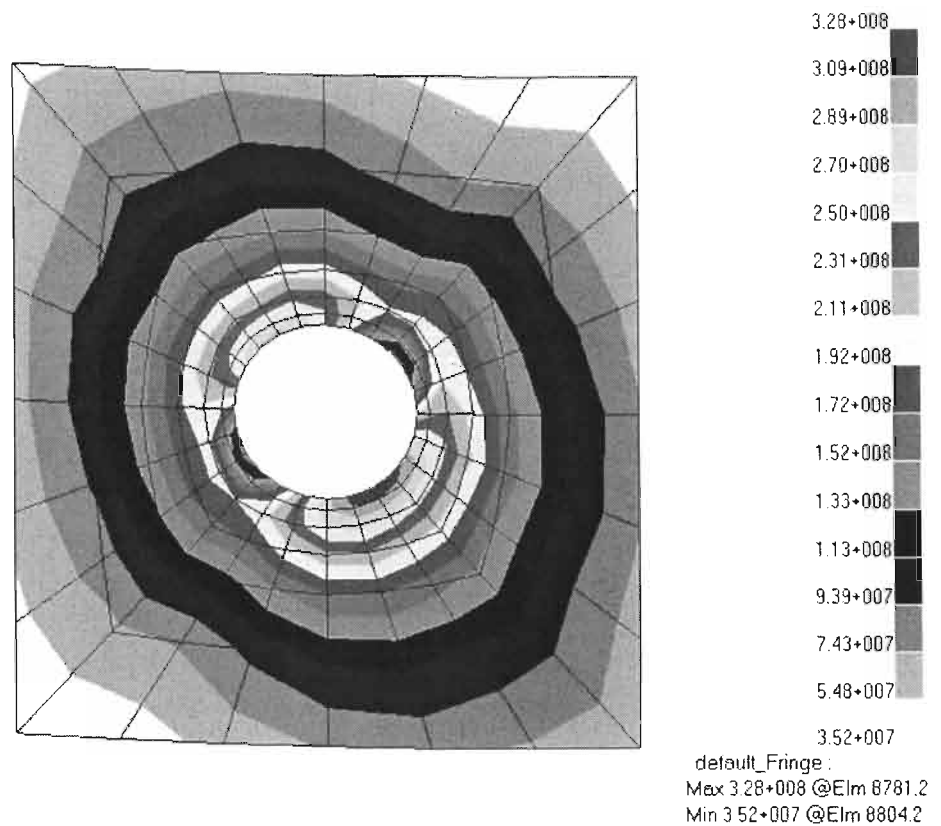
Figure 3-17 : FEM Stress analysis for vessel 16 subjected to external nozzle loads

It can be observed from figure 3-17 that the stresses induced in the shell, due to external nozzle loads, are not at a maximum at the points A, B, C and D, shown in figure 3-3. WRC 107 calculates stresses for points A, B, C and D only. The results indicate that greater stresses can occur in regions between points A, B, C and D. Further FEM stress analyses for vessels 16 to 25, subjected to external nozzle loads, can be found in Appendix B.

The internal pressure thrust load and the greater stresses between points *A, B, C* and *D*, due to external nozzle loads, affect the combined stress intensity *S*, as the results below indicate.
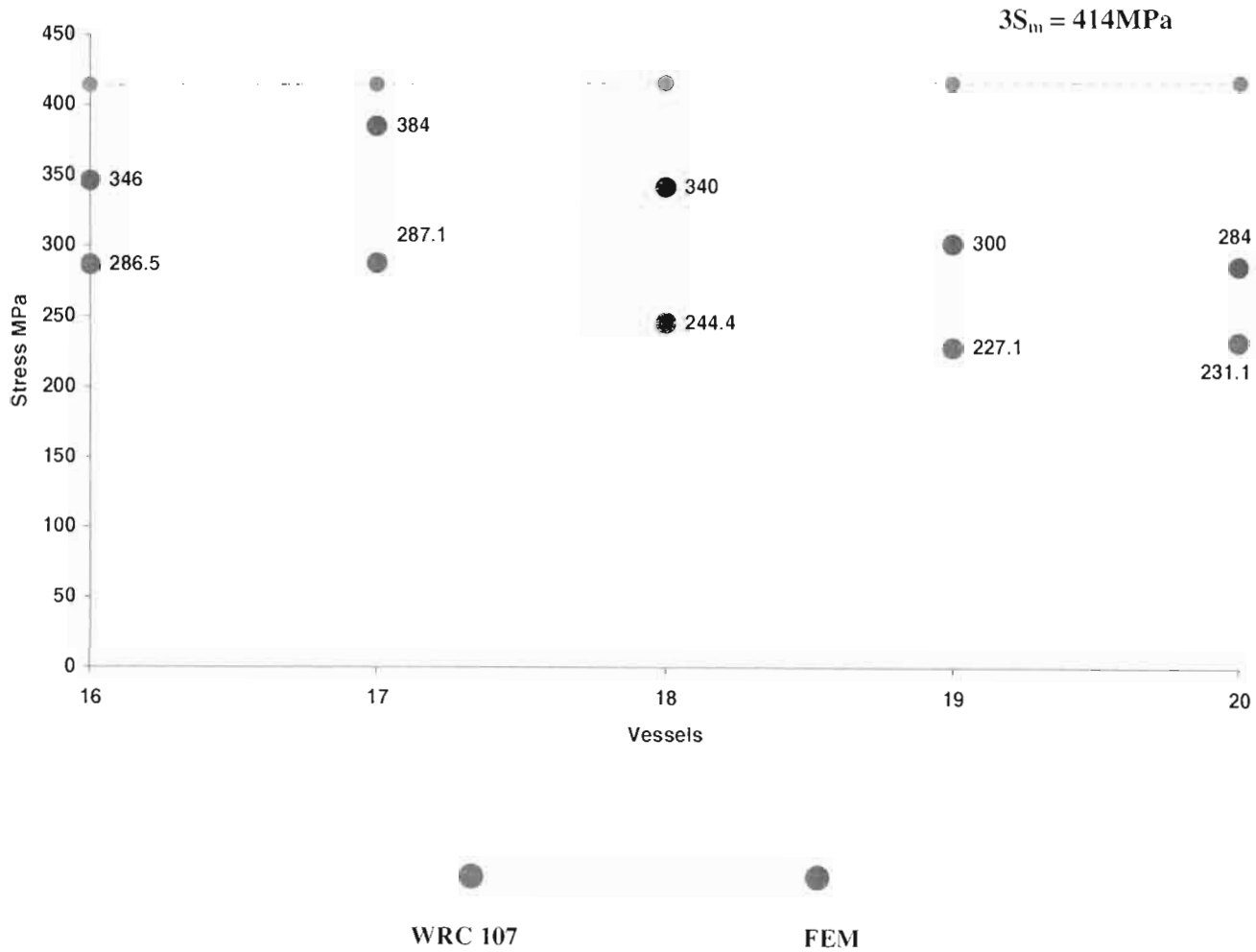
Figure 3-18 : FEM and Theoretical (WRC 107) Combined Stress Intensity *S* for vessels subjected to 0.26MPa internal pressure and nozzle loads
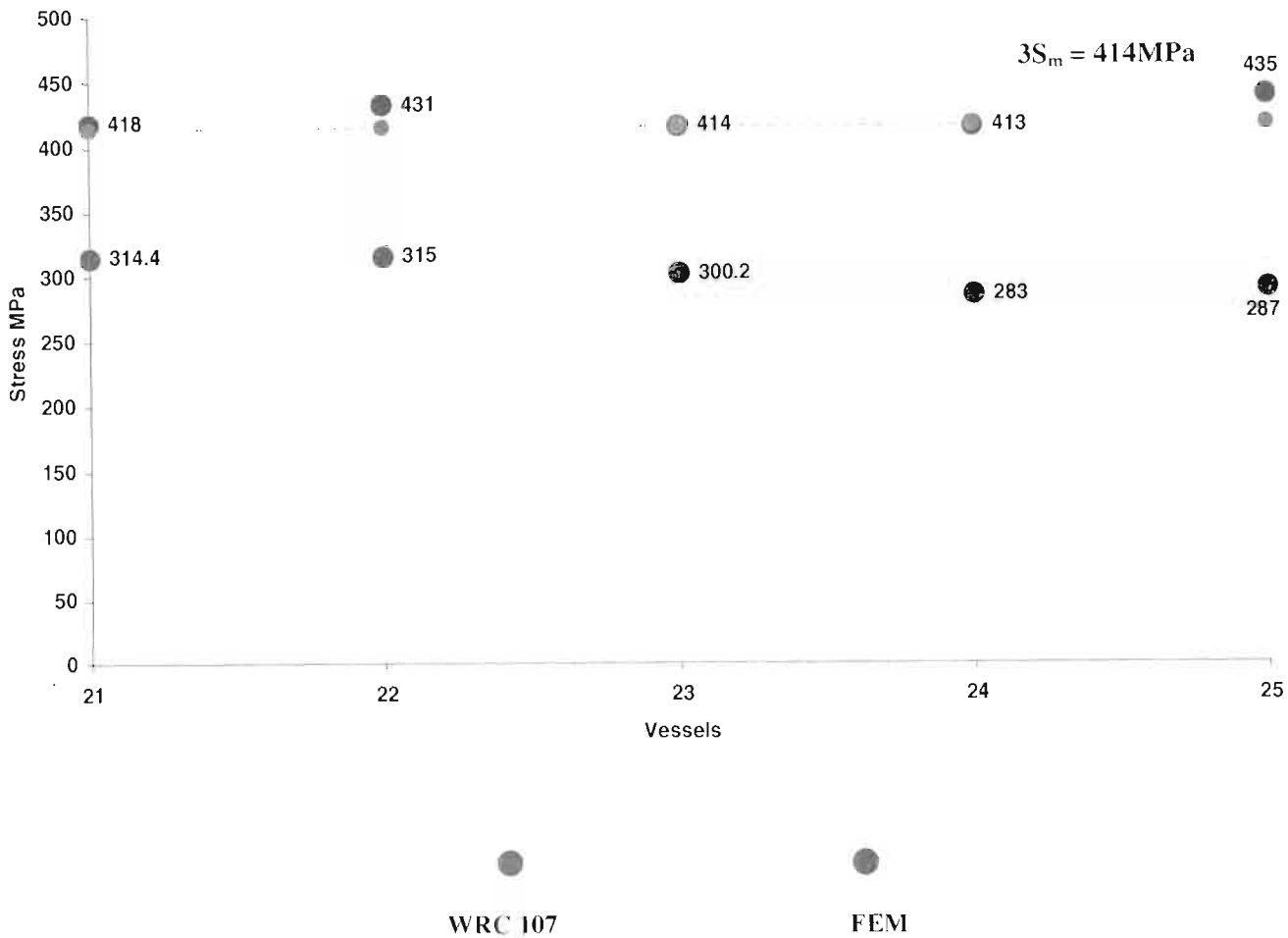
Figure 3-19 : FEM and Theoretical (WRC 107) Combined Stress Intensity *S* for vessels subjected to 1.05MPa internal pressure and nozzle loads

Figure 3-18 shows that the stresses are close to the allowable limit of 414MPa. Figure 3-19 shows that for some vessels the allowable limit of 414MPa is exceeded, whereas, the theoretical or WRC 107 stresses are well within the allowable limit. The FEM results of figure 3-19, thus, indicate that the internal pressure thrust load and greater external nozzle loads stresses can increase the stresses at the shell-to-nozzle junction. Failure, by exceeding the allowable limit given by ASME VIII Div 2, can occur. Below are FEM stress analyses for identical vessels 16 and 21, subjected to both internal pressure and nozzle loads.
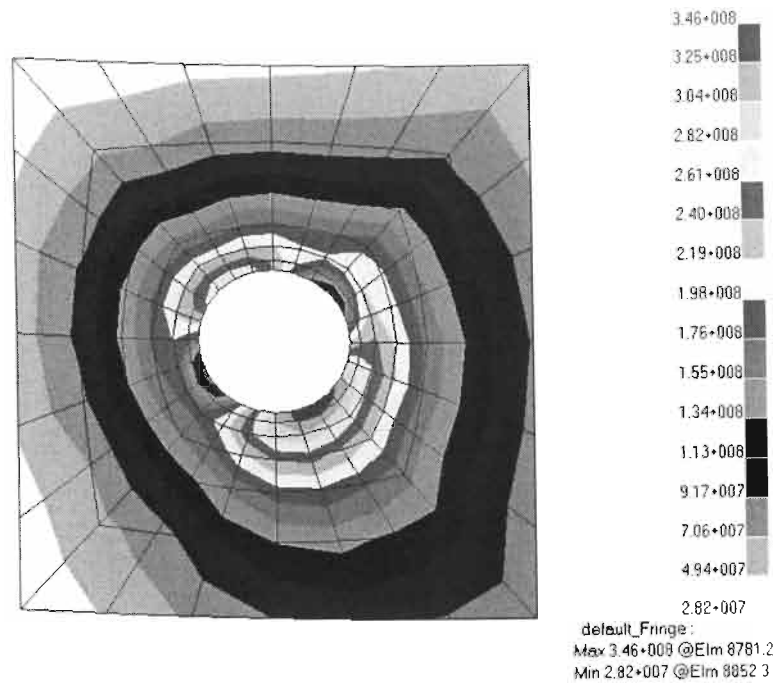
Figure 3-20 : FEM Stress analysis for Vessel 16 subjected to 0.26MPa internal pressure and nozzle loads
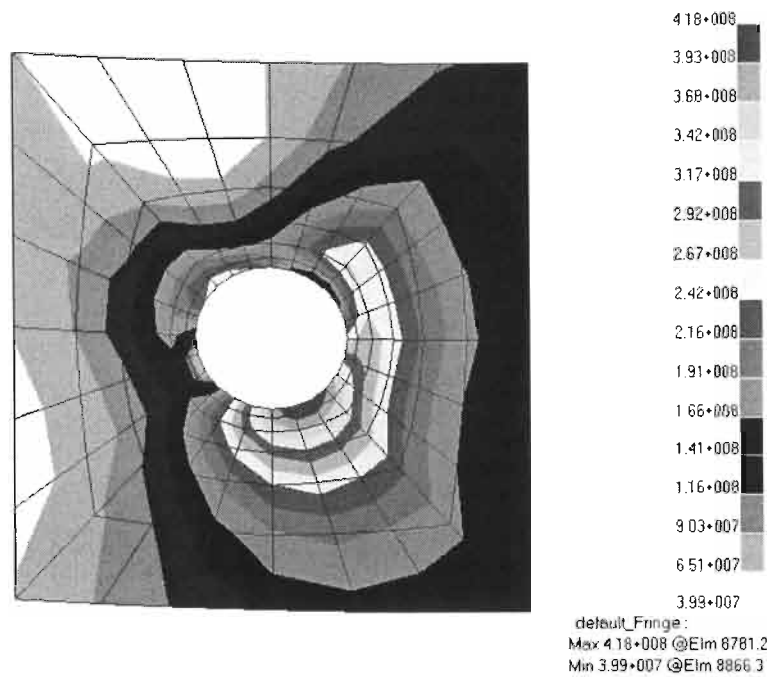
Figure 3-21 : FEM Stress analysis for Vessel 21 subjected to 1.05MPa internal pressure and nozzle loads

Further FEM stress analyses for vessels 16 to 25, subjected to the combined loading of internal pressure and external nozzle loads, can be found in Appendix B.

3.6 Compensation Pads

Compensation pads are used to reduce the stresses in the shell-to-nozzle junction. Pads are used if the combined stress intensity S exceeds the allowable limit. Another method to reduce the stresses in the shell, would be to increase the thickness of the shell. Since the shell-to-nozzle junction is the most highly stressed area, as compared to the rest of the shell, compensation pads can be used to increase the thickness of the shell at the shell-to-nozzle junction, as shown in figure 3-22 below. The increased thickness results in an increased rigidity for the shell-to-nozzle area. The shell-to-nozzle junction is much stronger and the stresses induced in the shell, due to the combined effect of internal pressure and external nozzle loads, are much lower.
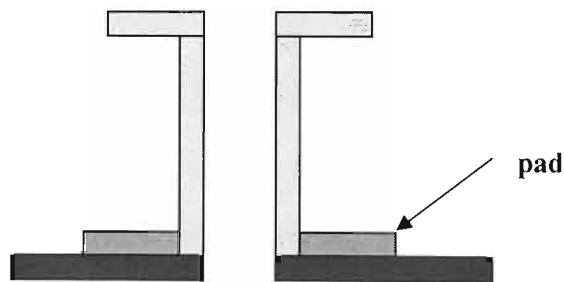
Figure 3-22 : Shell-to-nozzle junction with Compensation Pad. Reproduced from WRC 107[16]

Consider Vessel 1 given in table 3-4. The WRC 107 combined stress intensity for vessel 1 is given in figure 3-10 as 350.7MPa. Using a compensation pad, WRC 107 calculates the following :

DESIGN
Internal Design pressure(DP)	2.51 MPA
Design Temperature	150 DEGREES C
Vessel Material	SA - 516 Grade70
Nozzle Material	SA - 106 Grade B

CYLINDRICAL SHELL
Vessel Inner Diameter(DS)	570 mm
Vessel Thickness(TS)	14 mm
Corrosion Allowance(CA)	3 mm
Vessel Allowable Stress(Sm)	137.9 MPa
Compensation Pad Diameter(CPD)	290 mm
Compensation Pad Thickness(CPT)	14 mm

NOZZLE (6 inch)
Nozzle Outer Diameter(DN)	168.3 mm
Nozzle Thickness(TN)	10.97 mm
Corrosion Allowance(CA)	3 mm
Nozzle Alowable Stress(SNm)	117.9 MPa

Nozzle Loads WRC 107 Sign Convention (SASOL LOADS)
Radial Load(P)	-9450 N
Circumferential Shear(VC)	0 N
Longitudinal Shear(VL)	0 N
Circumferential Moment(MC)	4350000 Nmm
Longitudinal Moment(ML)	6300000 Nmm
Torsional Moment(MT)	0 Nmm

GEOMETRIC PARAMETERS WRC 107
Rm1 = (DS+TS+CPT-CA)/2	297.50 mm
T1=TV+CPT-CA	25.00 mm
ro1=DN/2	84.15 mm
GAMMA1=Rm1/T1	11.90
BETA1=0.875*ro1/Rm1	0.248
Rm2 = (DS+TS-CA)/2	290.50 mm
T2=TV-CA	11.00 mm
ro2=CPD/2	145.00 mm
GAMMA2=Rm2/T2	26.41
BETA2=0.875*ro2/Rm2	0.437

Dimensionless loads from WRC 107	(PHI - circumferential, **x** - longitudinal)						
Figure		Gamma1	Beta1	Gamma2	Beta2	VALUE	VALUE
4C	N(PHI)/(P/Rm)	11.90	0.248	26.41	0.437	**1.923**	**2.502**
2C1	M(PHI)/P	11.90	0.248	26.41	0.437	**0.059**	**0.012**
3A	N(PHI)/(MC/(Rm^2*BETA))	11.90	0.248	26.41	0.437	**0.443**	**0.864**
1A	M(PHI)/(MC/(Rm*BETA))	11.90	0.248	26.41	0.437	**0.09**	**0.066**
3B	N(PHI)/(ML/(Rm^2*BETA))	11.90	0.248	26.41	0.437	**1.388**	**1.519**

67

1B	M(PHI)/(ML/(Rm*BETA))	11.90	0.248	26.41	0.437	**0.037**	**0.011**
3C	N(x)/(P/Rm)	11.90	0.248	26.41	0.437	**1.53**	**1.142**
1C1	M(x)/P	11.90	0.248	26.41	0.437	**0.089**	**0.026**
4A	N(x)/(MC/(Rm^2*BETA))	11.90	0.248	26.41	0.437	**0.769**	**2.645**
2A	M(x)/(MC/(Rm*BETA))	11.90	0.248	26.41	0.437	**0.049**	**0.028**
4B	N(x)/(ML/(Rm^2*BETA))	11.90	0.248	26.41	0.437	**0.439**	**0.816**
2B	M(x)/(ML/(Rm*BETA))	11.90	0.248	26.41	0.437	**0.061**	**0.017**

POINTS C & D

3C	N(PHI)/(P/Rm)	11.90	0.248	26.41	0.437	**1.53**	**1.142**
1C	M(PHI)/P	11.90	0.248	26.41	0.437	**0.086**	**0.06**
1B1	M(PHI)/(ML/(Rm*BETA))	11.90	0.248	26.41	0.437	**0.038**	**0.012**
4C	N(x)/(P/Rm)	11.90	0.248	26.41	0.437	**1.923**	**2.502**
2C	M(x)/P	11.90	0.248	26.41	0.437	**0.058**	**0.03**
2B1	M(x)/(ML/(Rm*BETA))	11.90	0.248	26.41	0.437	**0.061**	**0.024**

STRESS CONCENTRATION FACTORS Kn=1, Kb=1

STRESS VALUES Mpa - NOZZLE TO PAD JUNCTION								
	AU	**AL**	**BU**	**BL**	**CU**	**CL**	**DU**	**DL**
CM(DP)	27.5	30.0	27.5	30.0	27.5	30.0	27.5	30.0
CM(P)	2.4	2.4	2.4	2.4	1.9	1.9	1.9	1.9
CB(P)	5.4	-5.4	5.4	-5.4	7.8	-7.8	7.8	-7.8
CM(MC)	0.0	0.0	0.0	0.0	-3.5	-3.5	3.5	3.5
CB(MC)	0.0	0.0	0.0	0.0	-51.0	51.0	51.0	-51.0
CM(ML)	-16.0	-16.0	16.0	16.0	0.0	0.0	0.0	0.0
CB(ML)	-30.4	30.4	30.4	-30.4	0.0	0.0	0.0	0.0
S(PHI)	*-11.1*	*41.5*	*81.6*	*12.6*	*-17.4*	*71.6*	*91.8*	*-23.4*
LM(DP)	13.7	13.7	13.7	13.7	13.7	13.7	13.7	13.7
LM(P)	1.9	1.9	1.9	1.9	2.4	2.4	2.4	2.4
LB(P)	8.1	-8.1	8.1	-8.1	5.3	-5.3	5.3	-5.3
LM(MC)	0.0	0.0	0.0	0.0	-6.1	-6.1	6.1	6.1
LB(MC)	0.0	0.0	0.0	0.0	-27.8	27.8	27.8	-27.8
LM(ML)	-5.1	-5.1	5.1	5.1	0.0	0.0	0.0	0.0
LB(ML)	-50.1	50.1	50.1	-50.1	0.0	0.0	0.0	0.0
S(x)	*-31.4*	*52.7*	*78.9*	*-37.5*	*-12.5*	*32.6*	*55.3*	*-10.8*
SHEAR(MT)	0.0	0.0	0.0	0.0	0.0	0.0	0.0	0.0
SHEAR(VC)	0.0	0.0	0.0	0.0	0.0	0.0	0.0	0.0
SHEAR(VL)	0.0	0.0	0.0	0.0	0.0	0.0	0.0	0.0
τ	*0.0*	*0.0*	*0.0*	*0.0*	*0.0*	*0.0*	*0.0*	*0.0*
S(1)	*11.1*	*41.5*	*81.6*	*12.6*	*17.4*	*71.6*	*91.8*	*23.4*
S(2)	*31.4*	*52.7*	*78.9*	*37.5*	*12.5*	*32.6*	*55.3*	*10.8*
S(1)-S(2)	*20.3*	*11.2*	*2.7*	*50.1*	*4.9*	*39.0*	*36.4*	*12.6*
S(PL + Q)	**31.4**	**52.7**	**81.6**	**50.1**	**17.4**	**71.6**	**91.8**	**23.4**

68

STRESS VALUES Mpa - PAD TO SHELL JUNCTION								
	AU	AL	BU	BL	CU	CL	DU	DL
CM(DP)	63.7	66.2	63.7	66.2	63.7	66.2	63.7	66.2
CM(P)	7.4	7.4	7.4	7.4	3.4	3.4	3.4	3.4
CB(P)	5.6	-5.6	5.6	-5.6	28.1	-28.1	28.1	-28.1
CM(MC)	0.0	0.0	0.0	0.0	-9.3	-9.3	9.3	9.3
CB(MC)	0.0	0.0	0.0	0.0	-112.2	112.2	112.2	-112.2
CM(ML)	-23.6	-23.6	23.6	23.6	0.0	0.0	0.0	0.0
CB(ML)	-27.1	27.1	27.1	-27.1	0.0	0.0	0.0	0.0
S(PHI)	**26.0**	**71.5**	**127.4**	**64.5**	**-26.3**	**144.4**	**216.7**	**-61.5**
LM(DP)	31.8	31.8	31.8	31.8	31.8	31.8	31.8	31.8
LM(P)	3.4	3.4	3.4	3.4	7.4	7.4	7.4	7.4
LB(P)	12.2	-12.2	12.2	-12.2	14.1	-14.1	14.1	-14.1
LM(MC)	0.0	0.0	0.0	0.0	-28.4	-28.4	28.4	28.4
LB(MC)	0.0	0.0	0.0	0.0	-47.6	47.6	47.6	-47.6
LM(ML)	-12.7	-12.7	12.7	12.7	0.0	0.0	0.0	0.0
LB(ML)	-41.9	41.9	41.9	-41.9	0.0	0.0	0.0	0.0
S(x)	**-7.1**	**52.2**	**101.9**	**-6.1**	**-22.7**	**44.4**	**129.3**	**6.0**
SHEAR(MT)	0.0	0.0	0.0	0.0	0.0	0.0	0.0	0.0
SHEAR(VC)	0.0	0.0	0.0	0.0	0.0	0.0	0.0	0.0
SHEAR(VL)	0.0	0.0	0.0	0.0	0.0	0.0	0.0	0.0
τ	**0.0**	**0.0**	**0.0**	**0.0**	**0.0**	**0.0**	**0.0**	**0.0**
S(1)	26.0	71.5	127.4	64.5	26.3	144.4	216.7	61.5
S(2)	7.1	52.2	101.9	6.1	22.7	44.4	129.3	6.0
S(1)-S(2)	33.2	19.2	25.5	70.6	3.6	100.0	87.4	67.4
S(PL + Q)	**33.2**	**71.5**	**127.4**	**70.6**	**26.3**	**144.4**	**216.7**	**67.4**

Figure 3-23 : Codecalc Computation Sheet including Compensation Pad

The initial FEM combined stress intensity for Vessel 1, as shown in figure 3-11, is 467MPa. After modifying Model A, to include a compensation pad, the following FEM stresses were achieved :

9.24+007
8.86+007
8.47+007
8.09+007
7.71+007
7.32+007
6.94+007
6.56+007
6.17+007
5.79+007
5.41+007
5.03+007
4.64+007
4.26+007
3.88+007
3.49+007

default_Fringe :
Max 9.24+007 @Elm 4462.2
Min 3.49+007 @Elm 4017.1

Figure 3-24 : Vessel 1 with Compensation Pad subjected to internal pressure alone

1.90+008
1.77+008
1.65+008
1.52+008
1.40+008
1.27+008
1.15+008
1.02+008
8.95+007
7.69+007
6.44+007
5.18+007
3.93+007
2.67+007
1.42+007
1.66+006

default_Fringe :
Max 1.90+008 @Elm 4060.3
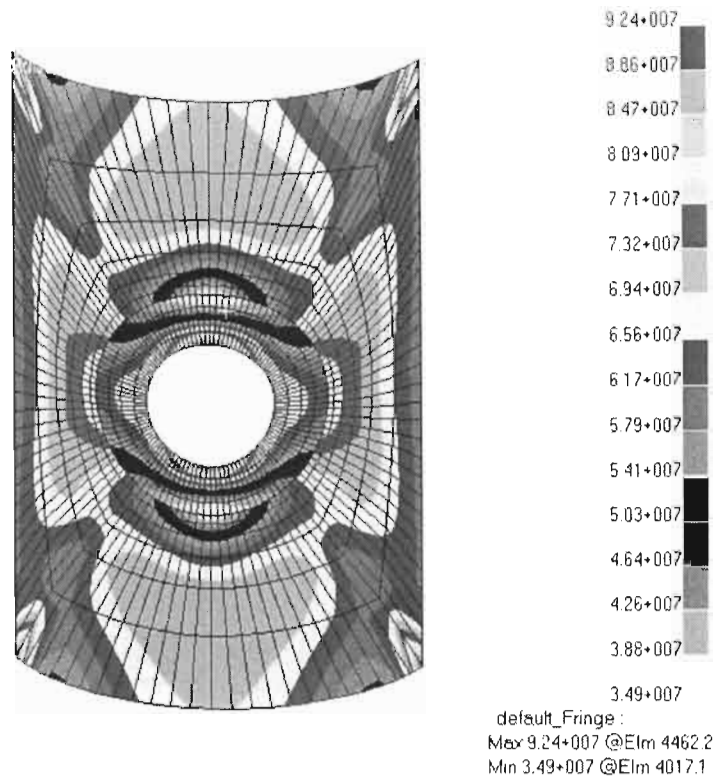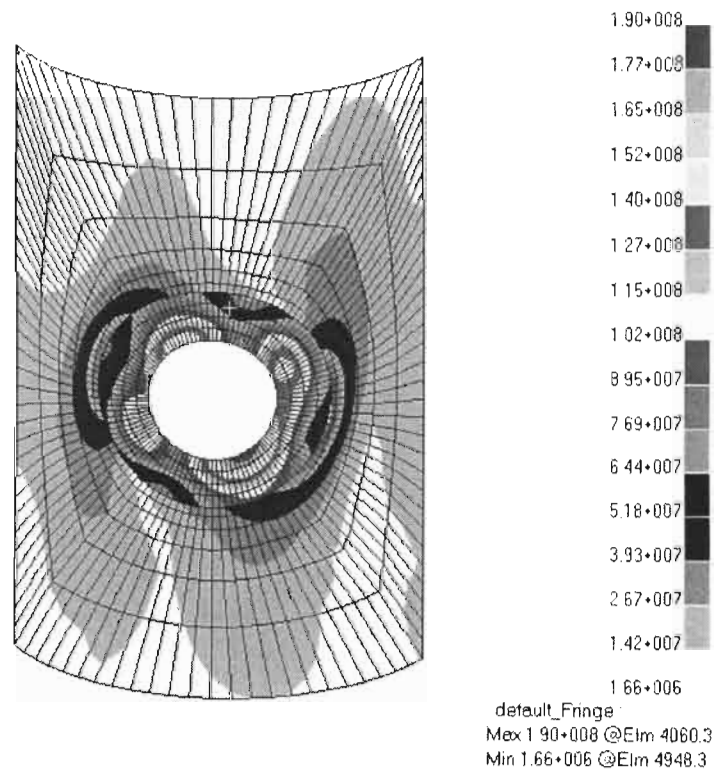Min 1.66+006 @Elm 4948.3

Figure 3-25 : Vessel 1 with Compensation Pad subjected to external nozzle loads alone

70
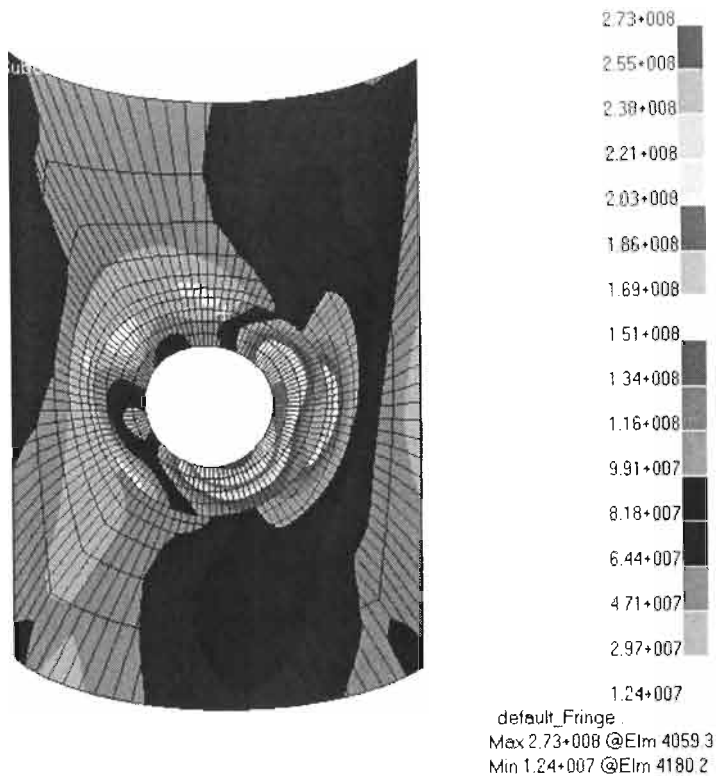
Figure 3-26 : Vessel 1 with Compensation Pad subjected to both internal pressure
and external nozzle loads

The FEM stresses do not coincide with the WRC 107 stresses. WRC 107 calculates the maximum combined stress intensity to be located at the pad-to-shell junction. However, the FEM results, according to figure 3-26, indicate that the maximum stress occurs at the pad-to-nozzle junction. This is due to the high stresses induced by the internal pressure thrust load, see figure 3-24, and the higher stresses created by the external nozzle loads, figure 3-25. The combined stress intensity has been reduced from 467MPa to 273MPa. This indicates that compensation pads are useful in reducing high stresses that exist at the shell-to-nozzle junction.

Chapter 4

THEORY OF BUCKLING

4.1 Theory of Stability

Load-carrying structures fail in a variety of ways. A type of failure, which is of concern for the purposes of this study, is buckling. To illustrate the fundamental concepts of buckling and stability, we need to study the *idealized structure* shown in figure 4-1 below :
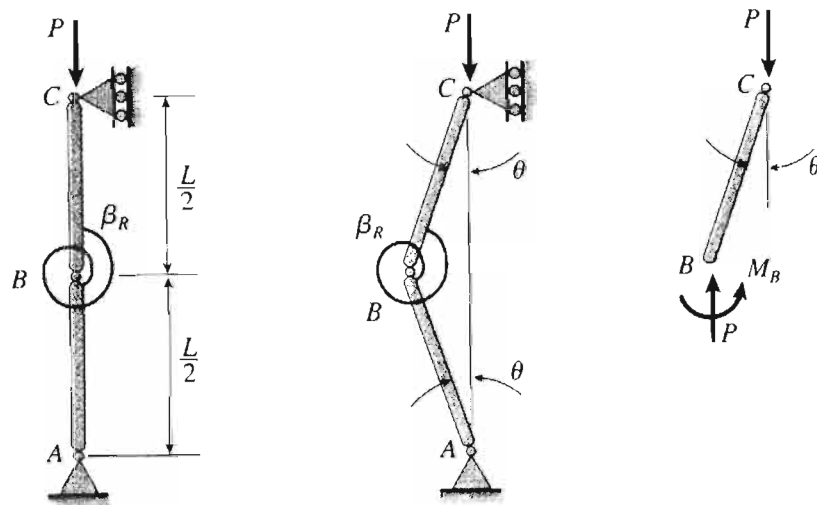

Figure 4-1 : Buckling of an Idealized Structure. Obtained from Gere and Timoshenko[33]

The structure represents two bars, *AB* and *BC*, each of length L/2. They are joined by a pin connection at point *B* and held in a vertical position by a rotational spring with a spring constant of β_R. An axial compressive load *P* is applied and is vertically aligned along the longitudinal axis of the bars. Initially the spring is unstressed and the bars are in direct compression. Suppose the structure is disturbed by some external force that causes point *B* to deflect a small distance laterally. The two bars rotate through small angles θ about points *A* and *C*, respectively. A *restoring moment* develops in the spring, which tends to return the bars to their original straight positions. At the same time the axial force acts to increase the lateral deflection, thereby acting opposite to the moment. If the axial force *P* is relatively small, the restoring moment is the more dominant force and will return the structure to its original position. Under these conditions the structure is said to be stable. However, if the axial force *P*

is greater than the restoring moment, point B will continue to deflect and the bars will rotate through larger and larger angles until the structure will eventually collapse. This failure is referred to as buckling and the structure is deemed unstable.

The restoring moment M_B is equal to the rotation stiffness β_R times the angle of rotation 2θ of the spring:

$$M_B = 2\beta_R\theta \qquad (4.1)$$

The lateral displacement of point B is $\theta L/2$. We thus obtain the following equation of equilibrium:

$$M_B - P\left(\frac{\theta L}{2}\right) = 0 \qquad (4.2)$$

Substituting equation 4.1 into 4.2 gives:

$$2\beta_R\theta - P\left(\frac{\theta L}{2}\right) = 0 \qquad (4.3)$$

To ensure that the structure is stable, we obtain a critical load (for axial load P) from the above equation:

$$P_{cr} = \frac{4\beta_R}{L} \qquad (4.4)$$

The following conditions are developed:

- If $P < P_{cr}$, the structure is stable (no buckling).
- If $P > P_{cr}$, the structure is unstable (buckling occurs).

When the axial load is less that the critical load ($0 < P < P_{cr}$), the structure is in equilibrium when it is perfectly straight ($\theta = 0$). If a disturbance occurs, the structure will return to its original position and the equilibrium is deemed stable. When $P > P_{cr}$, the structure is still in equilibrium when $\theta = 0$ (no moment in spring, structure in direct compression), but the equilibrium cannot be maintained and is deemed unstable. The slightest disturbance will cause the structure to buckle. When the axial load equals the critical load, the structure is still in equilibrium for any value of θ. The structure is neither stable nor unstable. This condition is referred to as neutral equilibrium. The equilibrium conditions are shown in figure 4-2 below, representing the graph of axial load P against the angle of rotation θ.
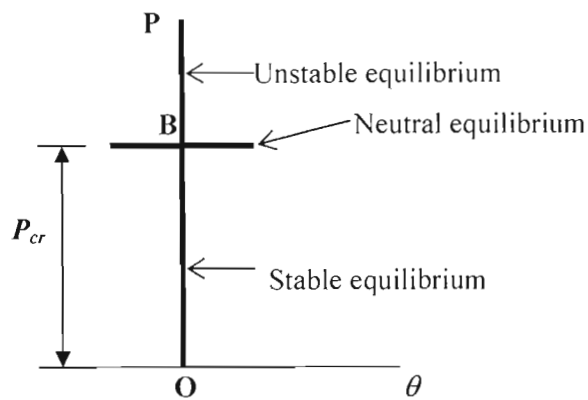
73

Figure 4-2 : Equilibrium diagram for idealized structure. Reproduced from Gere and Timoshenko[33]

The two heavy lines, one vertical and one horizontal, represent the equilibrium conditions. Point *B* is called the bifurcation point (see Fung and Sechler[12]). The neutral condition extends to the left and right of the vertical axis because the angle θ may be clockwise or counterclockwise. The angle is assumed small, therefore, the line extends a short distance. This assumption is valid since θ is small when the structure first departs from its vertical position and buckling begins. Thin-walled shells[8] are subjected to compressive forces in extensive areas. The question arises as to whether the equilibrium of such shells is stable. A shell carrying a certain load or basic load produces basic stresses and basic displacements. The equilibrium is disturbed by imposing a small additional deformation, by some external force. The equilibrium is stable if the external force is removed and the disturbance (a system of additional stresses and displacements occurring spontaneously) vanishes. When the basic load is increased, a less external force is needed to produce the same disturbance until a certain disturbance becomes possible without any external force. The equilibrium and this point is deemed neutral. The smallest value which the basic load must assume to reach neutral equilibrium is the critical load or buckling load. When the critical or buckling load is exceeded, the equilibrium becomes unstable and any disturbance can cause the shell to buckle or, perhaps, eventually collapse. To find the critical load we formulate the differential equations for the disturbed equilibrium without an external disturbing load. These equations also include new terms for the additional stresses caused by the disturbing load. Since the disturbance is assumed to be very small, these new terms must be of the same order of magnitude. These terms indicate that the basic load is now acting on a slightly deformed element. Since the conditions of equilibrium are satisfied, and Hooke's Law expresses stresses in terms of displacements, we obtain homogenous linear differential equations for the displacements *u*, *v* and *w* (shell theory).

4.2 Buckling of Shells

4.2.1 Differential Equations of Equilibrium

Deformation of a cylindrical shell is defined by the displacements u, v and w. This is illustrated in figure 4-3 below :
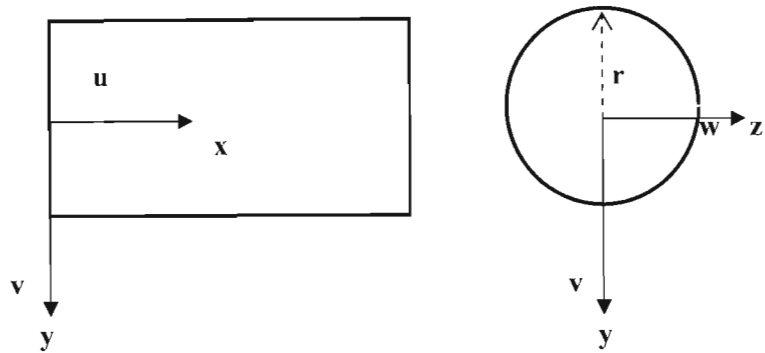
Figure 4-3 : Cylindrical Shell showing displacements. Reproduced from Timoshenko[1]

The figure above shows that the displacements in the x, y and z directions are denoted by u, v and w respectively. Differential equations for these displacements are needed to examine the behaviour of cylindrical shells under the combined loading of radial and axial external pressures. By considering the equilibrium of an element of a cylindrical shell, figure 4-4, it is possible to determine relationships between edge moments, shear forces and edge forces. Figure 4-4 is shown below :

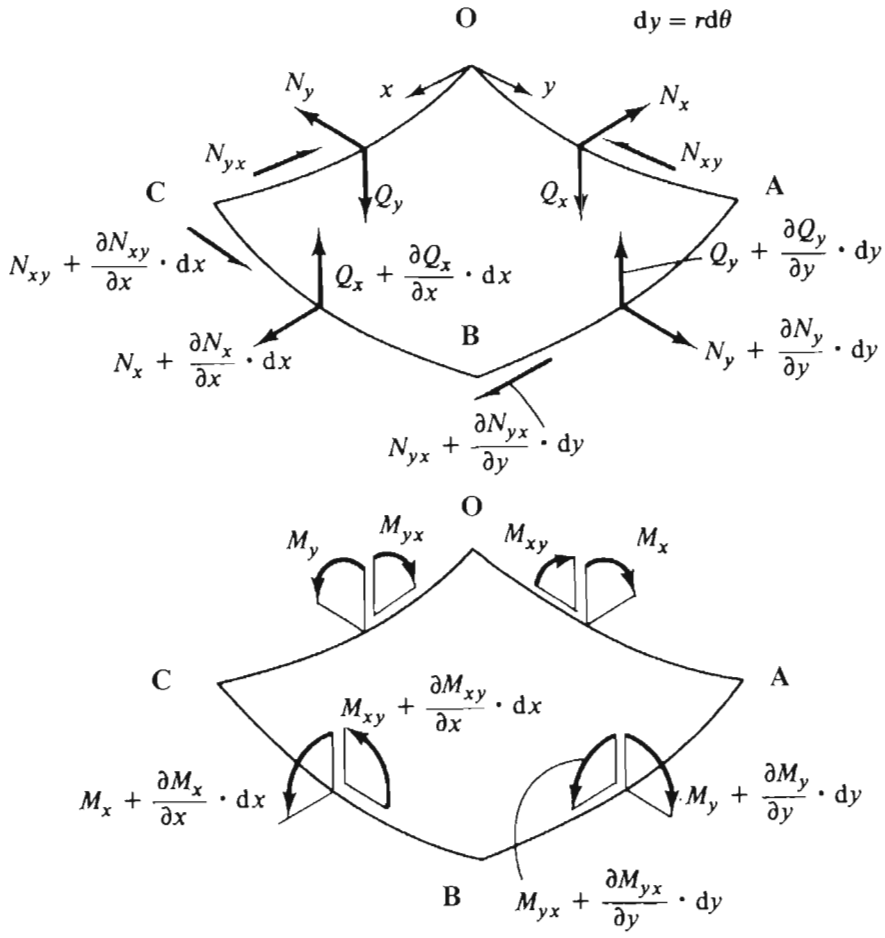**Figure 4-4 : Element of Cylindrical Shell. Obtained from Bulson and Allen[17]**

Before deformation, the axes x, y and z are tangent to the element in the longitudinal direction, tangent to the element in the circumferential direction and normal to the middle surface of the shell respectively. After deformation, which is assumed to be very small, these directions are altered slightly. The z axis is now normal to the deformed middle surface of the shell, the x axis is tangent to the deformed element in the longitudinal direction and the y axis is perpendicular to the xz plane. The directions of the resultant forces will also be changed slightly and these changes must be considered in writing the equations of equilibrium of the element OABC.

Firstly, the angular displacements of sides BC and AB with respect to sides OA and OC of the element has to be established. The rotation of side BC with respect to side OA can be resolved into three components with respect to the x, y and z axes. Rotation of the sides OA and BC with respect to the x axis is due to displacements v and w. Since the displacement v represents the motion of the sides OA and BC in the circumferential directions (see figure 4-4) and r is the

76

radius of the middle surface of the cylinder, the corresponding rotation of the side *OA*, with respect to the *x* axis, is *v/a* and that of the side BC is :

$$\frac{1}{r}\left(v + \frac{\partial v}{\partial x}dx\right) \qquad (4.5)$$

Thus, owing to displacement *v*, the relative angular motion of *BC* with respect to *OA* about the *x* axis is :

$$\frac{1}{r}\frac{\partial v}{\partial x}dx \qquad (4.6)$$

Owing to displacement *w*, the side *OA* rotates with respect to the *x* axis by the angle $\partial w/(r\partial \theta)$, and the side *BC* by the angle :

$$\frac{\partial w}{r\partial \theta} + \frac{\partial}{\partial x}\frac{\partial w}{r\partial \theta}dx \qquad (4.7)$$

Thus, because of displacement *w*, the relative angular displacement is :

$$\frac{\partial}{\partial x}\frac{\partial w}{r\partial \theta}dx \qquad (4.8)$$

Combining equations 4.6 and 4.8, the relative angular displacement of the side *BC* with respect to the side *OA* about the *x* axis is :

$$\frac{1}{r}\left(\frac{\partial v}{\partial x} + \frac{\partial^2 w}{\partial x \partial \theta}\right)dx \qquad (4.9)$$

The rotation of side *BC* with respect to side *OA* about the *y* axis is due to bending of the axial (longitudinal) plane and is equal to (sign convention is determined using the right-hand rule) :

$$-\frac{\partial^2 w}{\partial x^2}dx \qquad (4.10)$$

77

The rotation of side BC with respect to side OA about the z axis is due to bending of the tangential (circumferential) plane and is equal to :

$$\frac{\partial^2 v}{\partial x^2}dx \tag{4.11}$$

The last three expressions, equations 4.9 – 4.11, give the three components of rotation of side BC with respect to side OA.

The corresponding formulas for the angular displacement of the side AB with respect to OC has to be established. Due to the curvature of the cylindrical shell, the initial angle between the axial sides of element $OABC$ is $d\theta$. However, because of displacements v and w, this angle will change. The rotation of the axial side OC with respect to the x axis can be expressed as :

$$\frac{v}{r}+\frac{\partial w}{r\partial\theta} \tag{4.12}$$

The corresponding rotation of axial side AB being :

$$\frac{v}{r}+\frac{\partial w}{r\partial\theta}+\frac{\partial}{\partial\theta}\left(\frac{v}{r}+\frac{\partial w}{r\partial\theta}\right)d\theta \tag{4.13}$$

The initial angle is changed to :

$$d\theta+d\theta\left(\frac{\partial v}{r\partial\theta}+\frac{\partial^2 w}{r\partial\theta^2}\right) \tag{4.14}$$

To calculate the angle of rotation of side AB with respect to side OC about the y axis, one needs to determine the expression for twist. It is observed that after deformation the element rotates about the y axis through an angle of $-\partial w/\partial x$ and with respect to the z axis through an angle of $\partial v/\partial x$. If one considers an element a distance $rd\theta$ from the first one, it is observed that its rotation about the y axis, corresponding to displacement w, is :

$$-\frac{\partial w}{\partial x}-\frac{\partial^2 w}{\partial\theta\partial x}d\theta \tag{4.15}$$

Rotation of the same element in the plane tangent to the shell is :

$$\frac{\partial v}{\partial x} + \frac{\partial(\partial v / \partial x)}{\partial \theta} d\theta \qquad (4.16)$$

The latter rotation has a component with respect to the y axis and is equal to :

$$-\frac{\partial v}{\partial x} d\theta \qquad (4.17)$$

Therefore, the angular displacement of side AB with side OC about the y axis is given using equations 4.15 and 4.17, and is equal to :

$$-\left(\frac{\partial^2 w}{\partial \theta \partial x} + \frac{\partial v}{\partial x}\right) d\theta \qquad (4.18)$$

Rotation of side AB with respect to OC about the z axis is due to displacements v and w. Owing to displacement v, the angle of rotation of side OC is $\partial v / \partial x$ and that of side AB is given by equation 4.16. The relative angular displacement is :

$$\frac{\partial^2 v}{\partial \theta \partial x} d\theta \qquad (4.19)$$

Due to displacement w, the side AB rotates in the axial plane by the angle $\partial w / \partial x$. The component of this rotation with respect to the z axis is :

$$-\frac{\partial w}{\partial x} d\theta \qquad (4.20)$$

Combining equations 4.19 and 4.20, the relative angular displacement about the z axis of the side AB with respect to the side OC is obtained.

$$\left(\frac{\partial^2 v}{\partial \theta \partial x} - \frac{\partial w}{\partial x}\right) d\theta \qquad (4.21)$$

79

Having the formulas for the angles, the three equations of equilibrium of element $OABC$ can be obtained. This is achieved by projecting all the forces onto the x, y and z axes. The x component of those forces parallel to the resultant forces N_x and N_{yx} are :

$$\frac{\partial N_x}{\partial x} dx r d\theta$$

$$\frac{\partial N_{yx}}{\partial \theta} d\theta dx$$

(4.22)

Due to the angle of rotation, equation 4.21, the forces parallel to N_y give a component in the x direction :

$$-N_y \left(\frac{\partial^2 v}{\partial \theta \partial x} - \frac{\partial w}{\partial x} \right) d\theta dx$$

(4.23)

Due to the rotation given in equation 4.11, the forces parallel to the resultant forces N_{xy} have a x component of :

$$-N_{xy} \frac{\partial^2 v}{\partial x^2} dx r d\theta$$

(4.24)

Finally, due to the expressions of the angles given in equations 4.10 and 4.18, the forces parallel to Q_x and Q_y gives x components of :

$$-Q_x \frac{\partial^2 w}{\partial x^2} dx r d\theta - Q_y \left(\frac{\partial^2 w}{\partial \theta \partial x} + \frac{\partial v}{\partial x} \right) d\theta dx$$

(4.25)

The expressions for the projections in the x direction, calculated above, are combined, as well as expressions for the y and z directions. For radial pressure a normal pressure intensity of q is used with zero projections on the x and y axes. After simplification, the three differential equations of equilibrium for displacements u, v and w are, repectively :

80

$$r\frac{\partial N_x}{\partial x} + \frac{\partial N_{yx}}{\partial \theta} - rQ_x\frac{\partial^2 w}{\partial x^2} - rN_{xy}\frac{\partial^2 v}{\partial x^2} - Q_y\left(\frac{\partial v}{\partial x} + \frac{\partial^2 w}{\partial x\partial \theta}\right) - N_y\left(\frac{\partial^2 v}{\partial x\partial \theta} - \frac{\partial w}{\partial x}\right) = 0$$

$$\frac{\partial N_y}{\partial \theta} + r\frac{\partial N_{yx}}{\partial x} + rN_x\frac{\partial^2 v}{\partial x^2} - Q_x\left(\frac{\partial v}{\partial x} + \frac{\partial^2 w}{\partial x\partial \theta}\right) +$$
$$N_{yx}\left(\frac{\partial^2 v}{\partial x\partial \theta} - \frac{\partial w}{\partial x}\right) - Q_y\left(1 + \frac{\partial v}{r\partial \theta} + \frac{\partial^2 w}{r\partial \theta^2}\right) = 0 \tag{4.26}$$

$$r\frac{\partial Q_x}{\partial x} + \frac{\partial Q_y}{\partial \theta} + N_{xy}\left(\frac{\partial v}{\partial x} + \frac{\partial^2 w}{\partial x\partial \theta}\right) + rN_x\frac{\partial^2 w}{\partial x^2} + N_y\left(1 + \frac{\partial v}{r\partial \theta} + \frac{\partial^2 w}{r\partial \theta^2}\right) + N_{yx}\left(\frac{\partial v}{\partial x} + \frac{\partial^2 w}{\partial x\partial \theta}\right) + qr = 0$$

The above equations relate edge forces to shear forces. Similarly we can obtain equilibrium equations that relate edge moments to shear forces. We obtain three equations of moments with respect to the x, y and z axes (figure 4-4). Again, we take into consideration the small angular displacements of the sides BC and AB with respect to OA and OC respectively. The three equilibrium equations are :

$$r\frac{\partial M_{xy}}{\partial x} - \frac{\partial M_y}{\partial \theta} - rM_x\frac{\partial^2 v}{\partial x^2} - M_{yx}\left(\frac{\partial^2 v}{\partial x\partial \theta} - \frac{\partial w}{\partial x}\right) + rQ_y = 0$$

$$\frac{\partial M_{yx}}{\partial \theta} + r\frac{\partial M_x}{\partial x} + rM_{xy}\frac{\partial^2 v}{\partial x^2} - M_y\left(\frac{\partial^2 v}{\partial x\partial \theta} - \frac{\partial w}{\partial x}\right) - rQ_x = 0 \tag{4.27}$$

$$M_x\left(\frac{\partial v}{\partial x} + \frac{\partial^2 w}{\partial x\partial \theta}\right) + rM_{xy}\frac{\partial^2 w}{\partial x^2} + M_{yx}\left(1 + \frac{\partial v}{r\partial \theta} + \frac{\partial^2 w}{r\partial \theta^2}\right) - M_y\left(\frac{\partial v}{\partial x} + \frac{\partial^2 w}{\partial x\partial \theta}\right) + r\left(N_{xy} - N_{yx}\right) = 0$$

Substituting Q_x and Q_y from equation 4.27 into equation 4.26, three equations containing the resultant forces N_x, N_y and N_{xy} and the moments M_x, M_y and M_{xy} are obtained. Using equation 2.42 we can express all these quantities in terms of three strain components ε_1, ε_2 and γ_{xy} of the middle surface and the three curvature changes χ_x, χ_y and χ_{xy}, as :

$$\varepsilon_1 = \frac{\partial u}{\partial x}$$

$$\varepsilon_2 = \frac{\partial v}{r\partial\theta} - \frac{w}{r}$$

$$\gamma_{xy} = \frac{\partial u}{r\partial\theta} + \frac{\partial v}{\partial x} \qquad (4.28)$$

$$\chi_x = \frac{\partial^2 w}{\partial x^2}$$

$$\chi_y = \frac{1}{r^2}\left(\frac{\partial v}{\partial\theta} + \frac{\partial^2 w}{\partial\theta^2}\right)$$

$$\chi_{xy} = \frac{1}{r}\left(\frac{\partial v}{\partial x} + \frac{\partial^2 w}{\partial x\partial\theta}\right)$$

Equations 4.26 and 4.27 represent the differential equations of equilibrium for the three displacements u, v and w.

4.2.2 Cylindrical Shells under External Axial and Radial Pressure

Using the differential equations of equilibrium, the critical buckling strength of a cylindrical shell can be determined under the combined loading of external axial and radial pressure. Initially, shells subjected to external axial pressure will be considered. For shells under external axial pressure we assume that all resultant forces, except N_x, are very small. The products of these forces with the derivatives of the displacements u, v and w, which are also small, are neglected. Thus, equations 4.26 become :

$$r\frac{\partial N_x}{\partial x} + \frac{\partial N_{yx}}{\partial \theta} = 0$$

$$\frac{\partial N_y}{\partial \theta} + r\frac{\partial N_{yx}}{\partial x} + rN_x\frac{\partial^2 v}{\partial x^2} - Q_y = 0 \qquad (4.29)$$

$$r\frac{\partial Q_x}{\partial x} + \frac{\partial Q_y}{\partial \theta} + rN_x\frac{\partial^2 w}{\partial x^2} + N_y = 0$$

For equations 4.27, we neglect the products of moment and derivatives of the displacements u, v and w. The equations become :

$$Q_x = \frac{\partial M_x}{\partial x} + \frac{\partial M_{yx}}{r\partial \theta}$$

$$\qquad (4.30)$$

$$Q_y = \frac{\partial M_y}{r\partial \theta} - \frac{\partial M_{xy}}{\partial x}$$

Substituting equations 4.30 into equations 4.29 the three equations of equilibrium for buckling of an axially compressed cylindrical shell becomes :

$$r\frac{\partial N_x}{\partial x} + \frac{\partial N_{yx}}{\partial \theta} = 0$$

$$\frac{\partial N_y}{\partial \theta} + r\frac{\partial N_{yx}}{\partial x} + rN_x\frac{\partial^2 v}{\partial x^2} + \frac{\partial M_{xy}}{\partial x} - \frac{\partial M_y}{r\partial \theta} = 0 \qquad (4.31)$$

$$rN_x\frac{\partial^2 w}{\partial x^2} + N_y + r\frac{\partial^2 M_x}{\partial x^2} + \frac{\partial^2 M_{yx}}{\partial x\partial \theta} + \frac{\partial^2 M_y}{r\partial \theta^2} - \frac{\partial^2 M_{xy}}{\partial x\partial \theta} = 0$$

The resultant forces and moments are expressed using equations 2.42. Substituting equations 4.28 into 2.42 produces :

$$N_x = \frac{ET}{1-v^2}\left(\frac{\partial u}{\partial x} + v\left(\frac{\partial v}{r\partial \theta} - \frac{w}{r}\right)\right)$$

$$N_y = \frac{ET}{1-v^2}\left(\left(\frac{\partial v}{r\partial \theta} - \frac{w}{r}\right) + v\frac{\partial u}{\partial x}\right)$$

$$N_{xy} = \frac{ET}{2(1+v)}\left(\frac{\partial u}{r\partial \theta} + \frac{\partial v}{\partial x}\right) = N_{yx} \qquad (4.32)$$

$$M_x = -\frac{ET^3}{12(1-v^2)}\left(\frac{\partial^2 w}{\partial x^2} + \frac{v}{r^2}\left(\frac{\partial v}{\partial \theta} + \frac{\partial^2 w}{\partial \theta^2}\right)\right)$$

$$M_y = -\frac{ET^3}{12(1-v^2)}\left(\frac{1}{r^2}\left(\frac{\partial v}{\partial \theta} + \frac{\partial^2 w}{\partial \theta^2}\right) + \frac{v\partial^2 w}{\partial x^2}\right)$$

$$M_{xy} = -\frac{ET^3}{12(1-v^2)}(1-v)\frac{1}{r}\left(\frac{\partial v}{\partial x} + \frac{\partial^2 w}{\partial x\partial \theta}\right) = -M_{yx}$$

and substituting equations 4.32 into 4.31, finally produces :

$$\frac{\partial^2 u}{\partial x^2} + \frac{1+\nu}{2r}\frac{\partial^2 v}{\partial x \partial \theta} - \frac{\nu}{r}\frac{\partial w}{\partial x} + \frac{1-\nu}{2}\frac{\partial^2 u}{r^2 \partial \theta^2} = 0$$

$$\frac{1+\nu}{2}\frac{\partial^2 u}{\partial x \partial \theta} + \frac{r(1-\nu)}{2}\frac{\partial^2 v}{\partial x^2} + \frac{\partial^2 v}{r \partial \theta^2} - \frac{\partial w}{r \partial \theta}$$
$$+ \frac{T^2}{12r^2}\left[\frac{\partial^2 v}{r \partial \theta^2} + \frac{\partial^3 w}{r \partial \theta^3} + r\frac{\partial^3 w}{\partial x^2 \partial \theta} + r(1-\nu)\frac{\partial^2 v}{\partial x^2}\right] - \frac{N_x r(1-\nu^2)}{ET}\frac{\partial^2 v}{\partial x^2} = 0 \qquad (4.33)$$

$$-\frac{N_x r(1-\nu^2)}{ET}\frac{\partial^2 w}{\partial x^2} + \nu\frac{\partial u}{\partial x} + \frac{\partial v}{r \partial \theta} - \frac{w}{r}$$
$$- \frac{T^2}{12r^2}\left[\frac{\partial^3 v}{r \partial \theta^3} + (2-\nu)r\frac{\partial^3 v}{\partial x^2 \partial \theta} + r^3\frac{\partial^4 w}{\partial x^4} + \frac{\partial^4 w}{r \partial \theta^4} + 2r\frac{\partial^4 w}{\partial x^2 \partial \theta^2}\right] = 0$$

Equations 4.33 represent the differential equations of equilibrium for a cylindrical shell compressed under axial pressure. One also needs to consider a cylindrical shell compressed laterally under radial pressure. For this condition, the differential equations of equilibrium are determined and the following assumptions are made. Firstly, all resultant forces, except N_y, are small, and the products of these with the derivatives of displacements u, v and w can be neglected. All bending and twisting moments are small, and the products of these with the derivatives of displacements can be neglected as well. Substituting the above conditions into equations 4.26 and 4.27 produces :

$$r\frac{\partial N_x}{\partial x}+\frac{\partial N_{yx}}{\partial \theta}-N_y\left(\frac{\partial^2 v}{\partial x\partial\theta}-\frac{\partial w}{\partial x}\right)=0$$

$$\frac{\partial N_y}{\partial\theta}+r\frac{\partial N_{xy}}{\partial x}-Q_y=0 \tag{4.34}$$

$$r\frac{\partial Q_x}{\partial x}+\frac{\partial Q_y}{\partial\theta}+N_y\left(1+\frac{\partial v}{r\partial\theta}+\frac{\partial^2 w}{r\partial\theta^2}\right)+qr=0$$

$$Q_x=\frac{\partial M_x}{\partial x}+\frac{\partial M_{yx}}{r\partial\theta}$$

$$\tag{4.35}$$

$$Q_y=\frac{\partial M_y}{r\partial\theta}-\frac{\partial M_{xy}}{\partial x}$$

Substituting equations 4.35 into 4.34, produces :

$$r\frac{\partial N_x}{\partial x}+\frac{\partial N_{yx}}{\partial\theta}-N_y\left(\frac{\partial^2 v}{\partial x\partial\theta}-\frac{\partial w}{\partial x}\right)=0$$

$$\frac{\partial N_y}{\partial\theta}+r\frac{\partial N_{xy}}{\partial x}-\frac{\partial M_y}{r\partial\theta}+\frac{\partial M_{xy}}{\partial x}=0 \tag{4.36}$$

$$\frac{\partial^2 M_{yx}}{\partial x\partial\theta}+\frac{r\partial^2 M_x}{\partial x^2}+\frac{\partial^2 M_y}{r\partial\theta^2}-\frac{\partial^2 M_{xy}}{\partial x\partial\theta}+N_y\left(1+\frac{\partial v}{r\partial\theta}+\frac{\partial^2 w}{r\partial\theta^2}\right)+qr=0$$

Due to the action of uniform external radial pressure, the following assumption is made. The circular cylindrical shell remains circular and only undergoes compression in the circumferential direction, so that N_x, M_x, M_y, $M_{xy}=0$ and

$$N_y=-qr+N_y^{'} \tag{4.37}$$

$N_y{}'$ is a small change in the resultant force $-qr$. With the stretching of the middle surface of the shell during buckling, $N_y(1+\varepsilon_1)$ and $q(1+\varepsilon_1)$ $(1+\varepsilon_2)$ are used for N_y and q respectively in the second and third equations of equations 4.36. Since, $\varepsilon_1 = \dfrac{\partial u}{\partial x}$ and $\varepsilon_2 = \dfrac{\partial v}{r\partial \theta} - \dfrac{w}{r}$, and substituting equation 4.37 into equations 4.36, produces :

$$r\frac{\partial N_x}{\partial x} + \frac{\partial N_{yx}}{\partial \theta} + qr\left(\frac{\partial^2 v}{\partial x\partial \theta} - \frac{\partial w}{\partial x}\right) = 0$$

$$\frac{\partial N_y{}'}{\partial \theta} + r\frac{\partial N_{xy}}{\partial x} - \frac{\partial M_y}{r\partial \theta} + \frac{\partial M_{xy}}{\partial x} = 0 \qquad (4.38)$$

$$\frac{\partial^2 M_{yx}}{\partial x\partial \theta} + \frac{r\partial^2 M_x}{\partial x^2} + \frac{\partial^2 M_y}{r\partial \theta^2} - \frac{\partial^2 M_{xy}}{\partial x\partial \theta} + N_y{}' - q\left(w + \frac{\partial^2 w}{\partial \theta^2}\right) = 0$$

Substituting equations 4.32 into equations 4.38, produces :

$$r^2\frac{\partial^2 u}{\partial x^2} + \frac{1+v}{2}\frac{r\partial^2 v}{\partial x\partial \theta} - vr\frac{\partial w}{\partial x} + \frac{qr^2(1-v^2)}{ET}\left(\frac{\partial^2 v}{\partial x\partial \theta} - \frac{\partial w}{\partial x}\right) + \frac{1-v}{2}\frac{\partial^2 u}{\partial \theta^2} = 0$$

$$\frac{1+v}{2}\frac{r\partial^2 u}{\partial x\partial \theta} + \frac{r^2(1-v)}{2}\frac{\partial^2 v}{\partial x^2} + \frac{\partial^2 v}{\partial \theta^2} - \frac{\partial w}{\partial \theta}$$
$$+ \frac{T^2}{12r^2}\left[\frac{\partial^2 v}{\partial \theta^2} + \frac{\partial^3 w}{\partial \theta^3} + r^2\frac{\partial^3 w}{\partial x^2\partial \theta} + r^2(1-v)\frac{\partial^2 v}{\partial x^2}\right] = 0 \qquad (4.39)$$

$$rv\frac{\partial u}{\partial x} + \frac{\partial v}{\partial \theta} - w - \frac{T^2}{12r^2}\left[\frac{\partial^3 v}{\partial \theta^3} + (2-v)r^2\frac{\partial^3 v}{\partial x^2\partial \theta} + r^4\frac{\partial^4 w}{\partial x^4} + \frac{\partial^4 w}{\partial \theta^4} + 2r^2\frac{\partial^4 w}{\partial x^2\partial \theta^2}\right]$$
$$= \frac{qr(1-v^2)}{ET}\left(w + \frac{\partial^2 w}{\partial \theta^2}\right)$$

The differential equations of equilibrium for a cylindrical shell compressed both axially and laterally under uniform external pressure can be determined. Using the notations :

$$\frac{qr\left(1-v^2\right)}{ET} = \phi_1$$

$$\frac{N_x\left(1-v^2\right)}{ET} = -\phi_2 \qquad (4.40)$$

$$\frac{T^2}{12r^2} = \alpha$$

equations 4.33 and 4.39 are combined to obtain the following three equations :

$$r^2\frac{\partial^2 u}{\partial x^2} + \frac{1+v}{2}\frac{r\partial^2 v}{\partial x\partial\theta} - vr\frac{\partial w}{\partial x} + r\phi_1\left(\frac{\partial^2 v}{\partial x\partial\theta} - \frac{\partial w}{\partial x}\right) + \frac{1-v}{2}\frac{\partial^2 u}{\partial\theta^2} = 0$$

$$\frac{1+v}{2}\frac{r\partial^2 u}{\partial x\partial\theta} + \frac{r^2\left(1-v\right)}{2}\frac{\partial^2 v}{\partial x^2} + \frac{\partial^2 v}{\partial\theta^2} - \frac{\partial w}{\partial\theta}$$
$$+ \alpha\left[\frac{\partial^2 v}{\partial\theta^2} + \frac{\partial^3 w}{\partial\theta^3} + r^2\frac{\partial^3 w}{\partial x^2\partial\theta} + r^2\left(1-v\right)\frac{\partial^2 v}{\partial x^2}\right] - r^2\phi_2\frac{\partial^2 v}{\partial x^2} = 0 \qquad (4.41)$$

$$rv\frac{\partial u}{\partial x} + \frac{\partial v}{\partial\theta} - w - \alpha\left[\frac{\partial^3 v}{\partial\theta^3} + \left(2-v\right)r^2\frac{\partial^3 v}{\partial x^2\partial\theta} + r^4\frac{\partial^4 w}{\partial x^4} + \frac{\partial^4 w}{\partial\theta^4} + 2r^2\frac{\partial^4 w}{\partial x^2\partial\theta^2}\right]$$
$$= \phi_1\left(w + \frac{\partial^2 w}{\partial\theta^2}\right) + \phi_2 r^2\frac{\partial^2 w}{\partial x^2}$$

88

The edges are assumed to be simply supported $w = 0$ and $\dfrac{\partial^2 w}{\partial x^2} = 0$. The general solutions of the displacement u, v and w for a cylindrical shell compressed both axially and laterally are represented below (r – radius of shell, l – length of shell) :

$$u = A \sin n\theta \cos \frac{m\pi x}{l}$$

$$v = B \cos n\theta \sin \frac{m\pi x}{l} \qquad (4.42)$$

$$w = C \sin n\theta \sin \frac{m\pi x}{l}$$

The above equations indicate that during buckling the shell buckles into m half-waves in the longitudinal direction and $2n$ half-waves in the circumferential direction. Substituting equations 4.42 into 4.41, three homogeneous linear equations are obtained for A, B and C. The equation for calculating the critical buckling pressure is determined by equating the determinant of these equations to zero. After simplification, the equation derived from equating the determinant to zero is :

$$C_1 + C_2 \alpha = C_3 \phi_1 + C_4 \phi_2 \qquad (4.43)$$

where

$$C_1 = (1 - v^2)\lambda^4$$

$$C_2 = (\lambda^2 + n^2)^4 - 2[v\lambda^6 + 3\lambda^4 n^2 + (4 - v)\lambda^2 n^4 + n^6] + 2(2 - v)\lambda^2 n^2 + n^4$$

$$C_3 = n^2(\lambda^2 + n^2)^2 - (3\lambda^2 n^2 + n^4)$$

$$C_4 = \lambda^2(\lambda^2 + n^2)^2 + \lambda^2 n^2$$

and $\qquad \alpha = \dfrac{T^2}{12r^2} \qquad \lambda = \dfrac{m\pi r}{l} \qquad (4.44)$

The buckling condition contains four unknowns i.e. The dimensionless loads ϕ_1 and ϕ_2 and the modal parameters n and λ. It is known that n must be an integer $(0,1,2,...)$ and λ must be an integer multiple $(1,2,3,...)$ of $\dfrac{\pi r}{l}$. Equation 4.43 represents a linear relationship between quantities ϕ_1 and ϕ_2. If one keeps m constant and give to n the values 2, 3, 4,..., a system of straight lines is obtained as shown in figure 4-5 below.
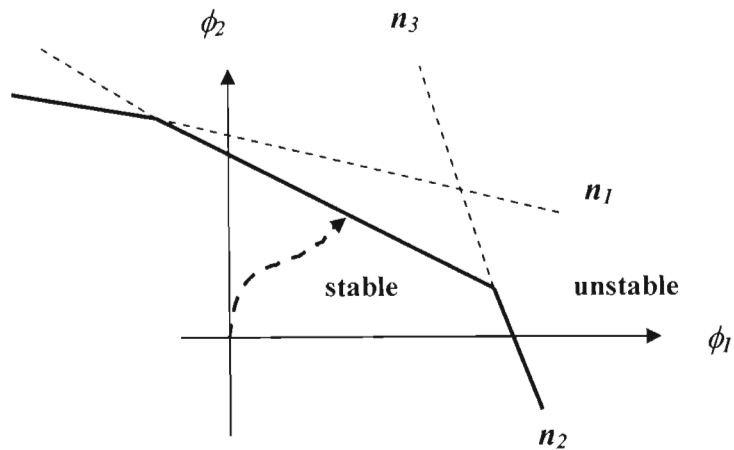

Figure 4-5 : Stable and Unstable regions in the ϕ_1 and ϕ_2 plane. Reproduced from Flugge [8]

The origin $\phi_1 = \phi_2 = 0$ represents the unloaded shell. When a load is applied, the path shown in figure 4-5 by the dotted line is followed. The cylindrical shell is in stable equilibrium if it does not meet any of the curves. When one curve is reached the equilibrium becomes neutral. The region enclosed by the envelope of the curves is stable, however the region outside the envelope is regarded unstable. Taking the points of intersection of these curves with the horizontal axis ($\phi_2 = 0$) we obtain the critical values of ϕ_1 when lateral pressure acts alone. In the case of lateral pressure acting alone, the buckled shape has only one half-wave length in the axial direction $m = 1$, and the critical pressure increases as λ increases and the length of the shell decreases. Taking the points of intersection of the same curves with the vertical axis ($\phi_1 = 0$) we obtain the critical values of ϕ_2 when axial pressure acts alone. For any given value of the ratio ϕ_1 / ϕ_2 one draws through the origin a straight line with slope ϕ_1 / ϕ_2. The points of intersection of this line with the polygons generated by the curves determine the corresponding critical values of ϕ_1 and ϕ_2. It is observed that axial pressure causes the critical value of the lateral pressure to decrease and lateral pressure causes the critical value of the axial pressure to

90

decrease.   The most common case is that of a cylindrical shell with closed ends under uniform external pressure. This case indicates that $\phi_2 = \frac{1}{2}\phi_1$. Assuming that the shell is thin and in keeping only the principal terms of equation 4.43, the critical buckling pressure for a cylindrical shell under external axial and radial pressure, is obtained :

$$q_{cr} = \frac{ET}{r}\frac{1}{n^2 + \frac{1}{2}\left(\pi r / l\right)^2}\left\{\frac{1}{[n^2\left(l / \pi r\right)^2 + 1]^2} + \frac{T^2}{12r^2\left(1 - v^2\right)}\left[n^2 + \left(\frac{\pi r}{l}\right)^2\right]^2\right\}$$ (4.45)

The above equation was derived by R von Mises in 1929[2].

4.3 Finite Element Buckling Analysis

In a linear static analysis a structure is assumed to be in a state of stable equilibrium. When the load is removed the structure returns to its original undeformed position. However, buckling occurs due to the structure continuing to deform without any increase in the applied loading. The structure has become unstable. Various FEM packages or MSC PATRAN have developed elastic or linear buckling analysis, to determine the buckling load for a particular structure. The analysis assumes that there is no yielding of the structure and the direction of the applied loading does not change.

The elastic buckling analysis creates a differential stiffness, in addition to the system stiffness matrix, and includes the higher-order strain displacement relationships that are functions of the geometry, element type and applied loads. The differential stiffness represents a linear approximation of reducing the stiffness matrix for a compressive load and increasing the stiffness matrix for a tensile load.

In a buckling analysis eigenvalues (see Walker[37] and Dahlgren[41]) are solved. These eigenvalues represent scale factors that are multiplied to the applied load to produce the critical buckling load. In general, the lowest buckling load is of interest, since the structure will fail before reaching any higher-order buckling loads. Therefore only the smallest eigenvalue needs to be calculated. The buckling equation used by MSC PATRAN is (Equation 4.46 was also derived by energy methods) :

$$\left| K + \lambda_i K_d \right| = 0 \qquad (4.46)$$

K is the system stiffness matrix, K_d is the differential stiffness matrix, generated automatically by MSC PATRAN, and λ_i are the eigenvalues to be computed. Once the eigenvalues are found, the buckling load is solved for

$$F_{cr} = \lambda_i F_a \qquad (4.47)$$

where F_{cr} is the critical buckling load and F_a is the applied load.

92

4.3.1   Stability and Energy Methods

The stability of a structure can be determined with the aid of energy methods. Consider the three cases of equilibrium of the ball shown in figure 4-5 below :
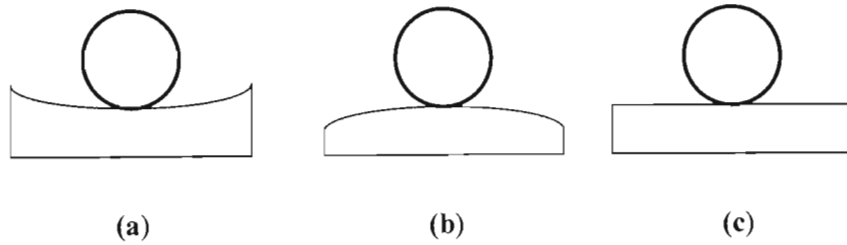

(a)   (b)   (c)

Figure 4-6 : Ball in stable, unstable and neutral equilibrium. Obtained from Timoshenko [1]

In figure 4-5(a) the surface is a concave spherical surface or shaped like a dish. The equilibrium is stable since the ball will always return to its position of equilibrium or low point when disturbed. In figure 4-5(b) the surface is a convex spherical surface or shaped like a dome. The equilibrium is unstable because if the ball is disturbed, it will roll away and not return to its position of equilibrium. In figure 4-5(c) the surface is perfectly flat, therefore, the ball is in neutral equilibrium and remains wherever it is placed. The type of equilibrium can be ascertained by considering the energy of the system. In the first case, figure 4-5(a), any displacement of the ball from its position of equilibrium will raise its center of gravity. Therefore, the potential energy of the system is increased. In the second case, figure 4-5(b), any displacement of the ball from its position of equilibrium will lower its center of gravity and the potential energy of the system will decrease. The third case, figure 4-5(c), there is no change in the ball's center of gravity, therefore, the potential energy of the system remains unchanged. It can be concluded that for stable equilibrium the potential energy of the system is a minimum (concave) and for unstable equilibrium the potential energy of the system is a maximum (convex). To obtain stable equilibrium, the potential energy of the system must be minimized with respect to the system's deflection :

$$\frac{\partial \Pi}{\partial \delta} = 0$$

(4.48)

93

4.3.2   Finite Element Method

Consider the individual element of an isotropic plate shown in figure 2-12. It has been discussed that the total strain energy for the element[17] is :

$$\Delta U_e = \frac{1}{2} \{\Delta \delta\}_e^T [k]_e \{\delta\}_e \qquad (4.49)$$

This can be derived from equations 2.53 and 2.73. For the entire plate the above equation becomes :

$$\Delta U = \frac{1}{2} \{\Delta \delta\}^T [K]\{\delta\} \qquad (4.50)$$

The element is now loaded with an external compressive stress σ. The compressive stress can be divided into stresses in the axial (longitudinal), σ_x, and radial (circumferential), σ_y, directions. Using similar methods for calculating the total strain energy for the plate[17] element, the work done by the compressive stress is given by :

$$\Delta W = \frac{1}{2} \{\Delta \delta\}^T [K_G]\{\delta\} \qquad (4.51)$$

K_G is referred to as the *geometric* stiffness matrix. It is so called because the terms representative of instability effects are geometric in nature. The total potential energy of the plate is :

$$\Delta \Pi = \frac{1}{2} \{\Delta \delta\}^T \big[[K] + [K_G] \big]\{\delta\} \qquad (4.52)$$

94

The above equation can be rewritten as :

$$\frac{\Delta \Pi}{\Delta \delta} = \frac{1}{2} \left[\left[K \right] + \left[K_G \right] \right] \{ \delta \}$$ (4.53)

and using equation 4.48 one obtains :

$$\frac{\partial \Pi}{\partial \delta} = \left[\left[K \right] + \left[K_G \right] \right] \{ \delta \} = 0$$ (4.54)

The objective is to determine the critical buckling load, F_{cr}. K_G contains the terms related to the applied compressive load, therefore the above equation can be written as :

$$\left[\left[K \right] + F_{cr} \left[\bar{K}_d \right] \right] \{ \delta \} = 0$$ (4.55)

Substituting equation 4.47, produces :

$$\left[\left[K \right] + \lambda_i F_a \left[\bar{K}_d \right] \right] \{ \delta \} = 0$$ (4.56)

$$\left[\left[K \right] + \lambda_i \left[K_d \right] \right] \{ \delta \} = 0$$ (4.57)

Since the deflections are not equal to zero, the above equation has a nontrivial solution. This is in the form of an eigenvalue problem, therefore, the eigenvalues are determined by finding the determinant of $\left[\left[K \right] + \lambda_i \left[K_d \right] \right]$ and equating it to zero (equation 4.46). The lowest eigenvalue is determined to produce the lowest critical buckling load using equation 4.47. Any applied load, greater than the critical buckling load, makes the plate or shell structure unstable. Therefore, failure due to buckling occurs.

95

Chapter 5

VESSELS UNDER EXTERNAL PRESSURE AND PIPING LOADS

5.1 Design of Pressure Vessels Under External Pressure

5.1.1 Literature Survey

For thin-walled vessels, buckling (see Ross[26]) over an extensive region must be considered. Presently, pressure vessels are designed to withstand failure due to buckling by determining a critical load. Pressure vessels with loads greater than that of the critical value will give rise to much larger and permanent deformations. As a result, buckling is said to occur and complete collapse of the vessel will result.

For vacuum operations, buckling or elastic instability occurs due to the imposition of an external force or pressure. A cylindrical vessel subjected to external pressure alone has a circumferential compressive stress equal to twice the longitudinal compressive stress. This larger circumferential compressive stress results in the vessel collapsing due buckling or elastic instability.

Long, thin cylinders will buckle at stresses below the yield point of the material being used. This can be best understood by a comparison with a rod. A rod in tension can carry a load even after the yield point of the material is reached, while a rod in compression might bend and not be able to carry an increased load at stresses below the yield point. This implies that a long thin vessel will collapse at very low stresses under external pressure.

The degree of stability of a vessel under external pressure depends on its length, thickness and diameter. Therefore, pressure vessels can be divided into three categories:

- Short Vessels : The vessel collapses near the yield point of the material. The influence of length on the vessel is negligible.

- Vessels of Intermediate Length : The vessel collapses by unstable buckling. The collapsing pressure depends on the t/D ratio and L/D ratio; t – thickness, D – diameter, L – length.

- Long Vessels : The shell collapses by unstable buckling. The collapsing pressure depends principally on the t/D ratio.

For this study, vessels with intermediate length will be used where the collapsing pressure depends all three factors : thickness, diameter and length.

Several formulas have been developed for the computation of the buckling pressure of vessels under external pressure. The first and most accurate formulas were derived by R von Mises in 1929 (formula 4.45) . His formula for the buckling pressure of a vessel subjected to external axial and radial pressure, related to the vessel's outer diameter, is shown below :

$$ P_{cr} = \left\{ \frac{1}{3}\left[n^2 + \left(\frac{\pi D_o}{2L}\right)^2 \right]^2 \frac{2E}{1-v^2}\left(\frac{T}{D_o}\right)^3 + \frac{2E\dfrac{T}{D_o}}{\left[n^2\left(\dfrac{2L}{\pi D_o}\right)^2 + 1 \right]^2} \right\} \frac{1}{n^2 + \dfrac{1}{2}\left(\dfrac{\pi D_o}{2L}\right)^2} \qquad (5.1) $$

The values of n, the number of circumferential waves or lobes (figure5-1), which makes this expression a minimum, is taken from figure 5-2.

n waves
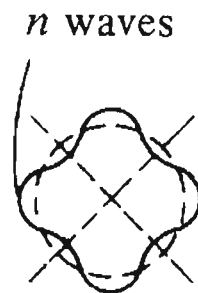
Figure 5-1 : Buckled Cylinder. Obtained from Bulson and Allen[17]

97
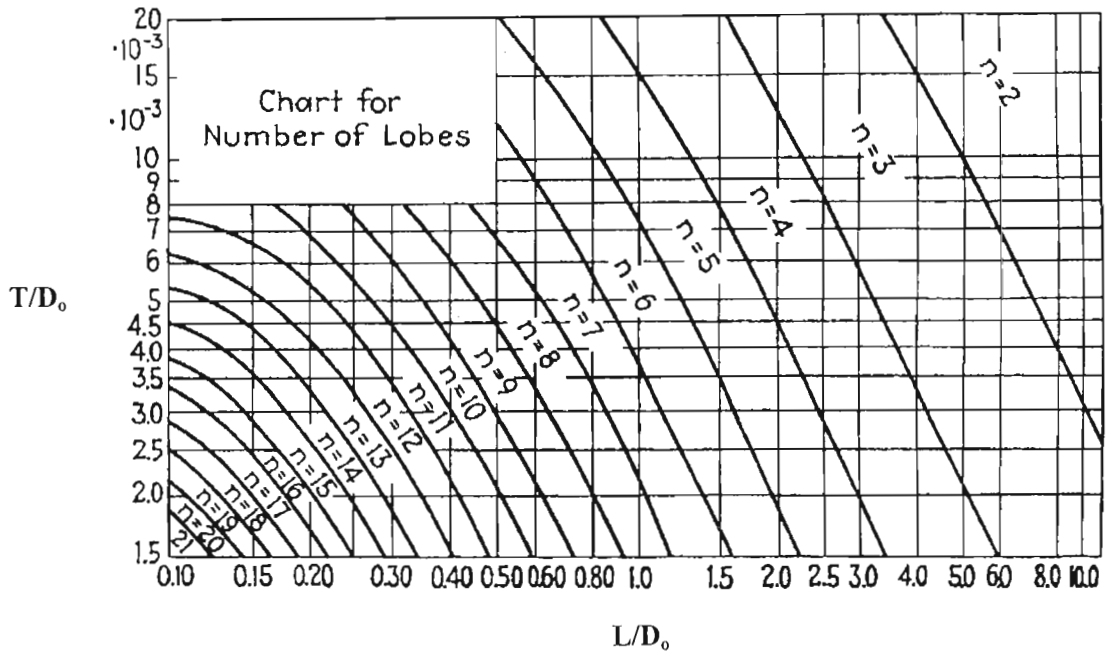
Figure 5-2 : Chart for number of lobes n. Obtained from Timoshenko[1]

For long vessels equation 5.1 is reduced to :

$$P_{cr} = \frac{2E}{3(1-v^2)}(n^2-1)\left(\frac{T}{D_o}\right)^3 \qquad (5.2)$$

Southwell[2] later developed the following equation for vessels under radial pressure alone :

$$P_{cr} = \frac{1}{3}(n^2-1)\frac{2E}{1-v^2}\left(\frac{T}{D_o}\right)^3 + \frac{2E\dfrac{T}{D_o}}{(n^2-1)n^4\left(\dfrac{2L}{\pi D_o}\right)^4} \qquad (5.3)$$

Using the above equation, he later developed an approximate formula, independent of n :

98

$$P_{cr} = \frac{8\sqrt{6}\pi}{27} \cdot \frac{E}{\left(1 - v^2\right)^{3/4}} \cdot \frac{\left(\dfrac{T}{D_o}\right)^{5/2}}{L / D_o} \tag{5.4}$$

The buckling pressures were restricted for vessels of $L < L_{cr}$. The critical length of a vessel is the minimum length beyond which the resistance of the vessel to collapse, due to external pressure, is independent of the length. Southwell derived the following formula :

$$L_{cr} = \frac{4\sqrt{6}\pi}{27} \cdot \sqrt[4]{1 - v^2} \cdot D_o \sqrt{\frac{T}{D_o}} \tag{5.5}$$

Taking $v = 0.3$, for carbon steel, the above equation reduces to :

$$L_{cr} = 1.1 D_o \sqrt{\frac{T}{D_o}} \tag{5.6}$$

Southwell's formula is differentiable. Thus an equation for n could be developed. The value for n to be used in the formulas is the integral value which makes the buckling pressure a minimum. An approximate value could be obtained from the following :

$$n = \sqrt[4]{\frac{\dfrac{3}{4}\pi^2 \left(1 - v^2\right)^{1/2}}{\left(L / D_o\right)^2 \left(T / D_o\right)}} \tag{5.7}$$

99

In 1934, at the U.S. Experimental Model Basin, Windenburg and Trilling[9] derived an approximate formula to equation 5.1, independent of n, to determine the critical buckling pressure for a vessel under external axial and radial pressure :

$$P_{cr} = \frac{2.42E}{\left(1-v^2\right)^{3/4}} \frac{\left(\dfrac{T}{D_o}\right)^{5/2}}{\dfrac{L}{D_o} - 0.45\left(\dfrac{T}{D_o}\right)^{1/2}}$$

(5.8)

Taking $v = 0.3$, for carbon steel, and ignoring the second term in the denominator since it has no discernible effect, one obtains :

$$P_{cr} = \frac{2.6E\left(\dfrac{T}{D_o}\right)^{5/2}}{\dfrac{L}{D_o}}$$

(5.9)

The above equation's results deviates about one percent from equation 5.1. On account of this formula's simplicity it is recommended for the design of vessels shorter than the critical length. The ASME Code incorporated this formula to create their procedures for the design of pressure vessels for external pressure.

100

ASME DESIGN CRITERIA

Long Cylinders

If the length of the vessels is greater than the critical length then the collapsing pressure is given by equation 5.2. The critical length is determined by equation 5.6. The buckling mode $n = 2$, makes equation 5.2 a minimum. Therefore, substituting $n = 2$ into equation 5.2 gives :

$$P_{cr} = \frac{2E}{\left(1 - v^2\right)}\left(\frac{T}{D_o}\right)^3 \tag{5.10}$$

Short Cylinders

In these vessels failure is by plastic yielding at the yield strength of the material. The influence of the length of the vessel is negligible. The critical pressure is given by the following :

$$P_{cr} = \frac{2\sigma_{yp}T}{D_o} \tag{5.11}$$

Intermediate Length Vessels

The collapsing pressure for vessels, whose lengths are less than the critical length, is given by Windenburg and Trilling's equation 5.9.

For the design of pressure vessels under external pressure the ASME VIII Code developed the *Geometric Chart* and the *Material Chart*. The geometric chart values for strain were developed using the following strain equation :

$$\varepsilon = \frac{\sigma_{cr}}{E} \qquad (5.12)$$

where $\sigma_{cr} = \dfrac{P_{cr} D_o}{2T}$ (hoop stress equation). For long cylinders equation 5.10 is used to obtain :

$$\varepsilon = \frac{\sigma_{cr}}{E} = 1.1 \left(\frac{T}{D_o} \right)^2 \qquad (5.13)$$

For intermediate length cylinders one uses equation 5.9 and obtain :

$$\varepsilon = \frac{\sigma_{cr}}{E} = \frac{1.3 \left(\dfrac{T}{D_o} \right)^{1.5}}{\dfrac{L}{D_o}} \qquad (5.14)$$

The strain produced is represented in the *Geometric Chart* by the factor A. The *Geometric Chart* is represented by figure 5-3 below :
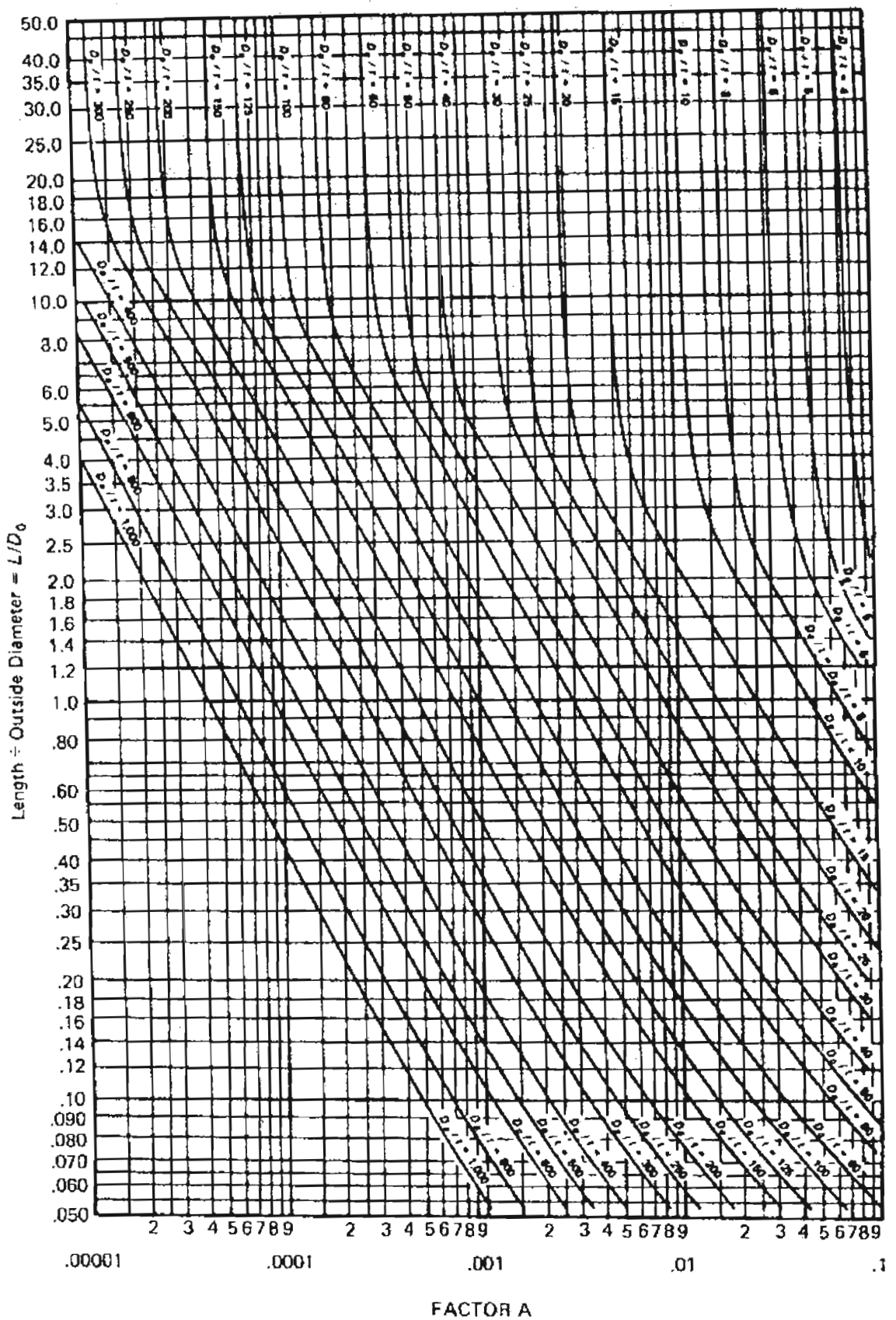
Figure 5-3 : Geometric Chart for Cylindrical Vessels under External Pressure. Obtained from Harvey[20]

The *Material Chart* is used to determine the external allowable pressure, and is basically made up of stress-strain curves for the material at various design temperatures. Factor A mentioned above is plotted against factor B :

$$B = \frac{\sigma_{cr}}{2} \qquad\qquad (5.15)$$

The *Material Chart* is shown in figure 5-4 below :

FACTOR A
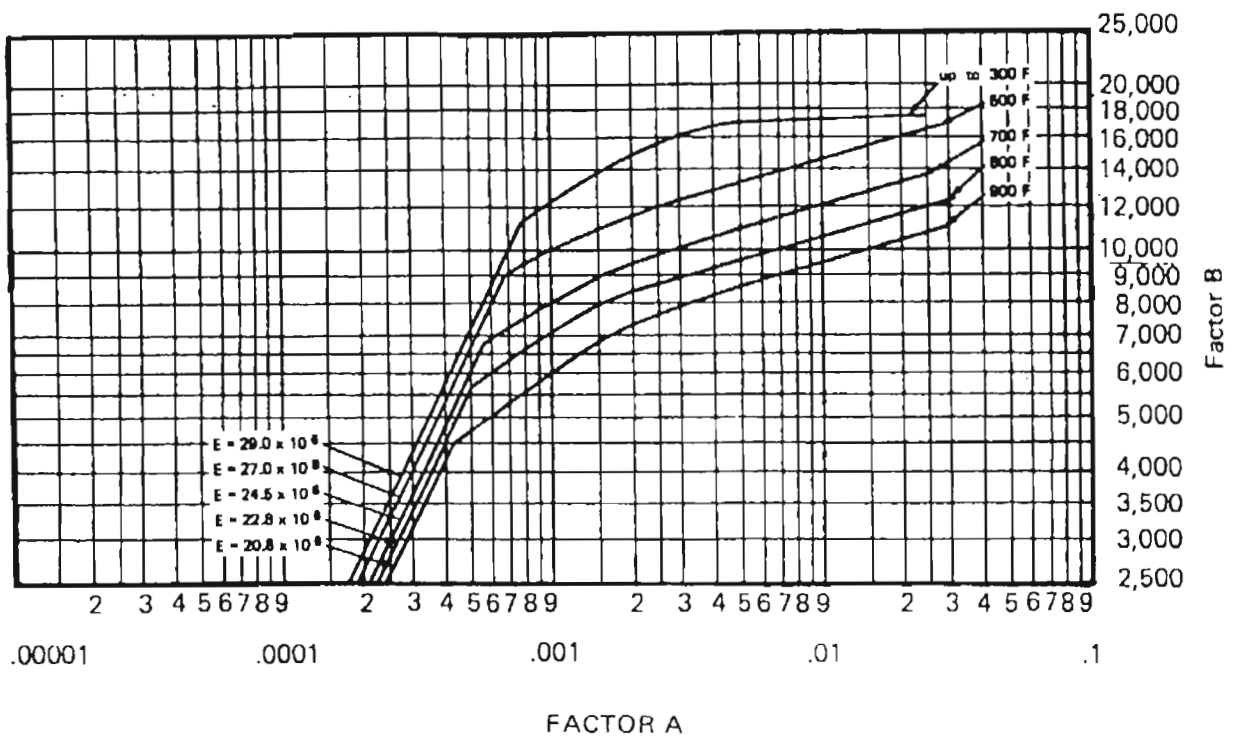
Figure 5-4 : Material Chart for Cylindrical Vessels under External Pressure. Obtained from Harvey[20]

The procedure used by the ASME Code is as follows :

- Determine the L/D_o and T/D_o ratios.
- Using these ratios use the *Geometric Chart* to determine factor A.
- Using the *Material Chart* and factor A, determine factor B for the appropriate design temperature.

104

The ASME Code uses a safety factor of 3 for the allowable external pressure, therefore :

$$P_a = \frac{P_{cr}}{3} = \frac{2\sigma_{cr}T}{3D_o} = \frac{4B}{3D_o/T} \qquad (5.16)$$

For a perfect circular, cylindrical vessel the collapsing pressure can be determined with the above equation. For vacuum conditions the external pressure is mainly atmospheric pressure[26]. If the applied or atmospheric pressure is less than the above allowable pressure, the vessel is safe under buckling. If the applied pressure is greater than the allowable pressure, the vessel will collapse under buckling. The thickness of the vessel can then be increased to raise the allowable pressure, thereby ensuring that the applied load is lower and the vessel will not buckle under external pressure.

5.1.2   Numerical Results

For this study, typical medium and large diameter vessels have been chosen. The vessels subjected to external atmospheric pressure are shown below

Vessel	Outer Diameter (mm)	Thickness (mm)	Corrosion Allowance (mm)	Length (mm)	External Pressure (MPa)
1	2800	8	-	2000	0.1
2	2800	10	-	2000	0.1
3	2800	12	-	2000	0.1
4	2800	14	-	2000	0.1
5	2800	16	-	2000	0.1
6	2800	20	-	2000	0.1
7	1200	8	-	2000	0.1
8	1200	10	-	2000	0.1
9	1200	12	-	2000	0.1
10	1200	14	-	2000	0.1
11	1200	16	-	2000	0.1
12	1200	20	-	2000	0.1

Table 5-1 : Vessels under External Pressure

Theoretical buckling pressures are calculated using the equations given above. The ASME Code procedures for designing pressure vessels under external pressure, are also programmed into the CodeCalc software. The CodeCalc format for the results can be found in Appendix C. The FEM model, Model B, for analyzing the above vessels under external pressure, is shown below

Isometric View

Figure 5-5 : FEM Model B

Shell elements or 4-noded quadrilateral elements were used to mesh the model. MSC PATRAN has a node limit of 6000 nodes, therefore, vessels using Model B were meshed[2] as close to 6000 nodes as possible to generate an appropriate fine mesh. The material of the shell is SA 516 Grade 70 (carbon steel). An elastic modulus of 200GPa and a poisson's ratio of 0.3 were used.

106

Theoretical critical buckling pressures and FEM values were generated. The results are shown below
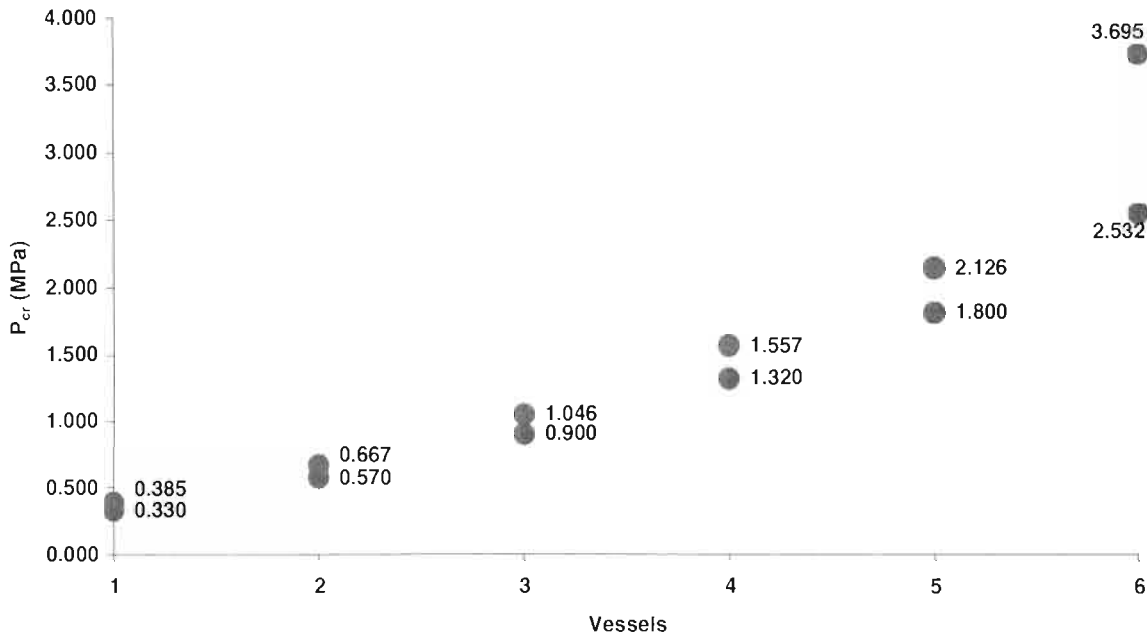
Figure 5-6 : Comparison of ASME and FEM Critical Buckling Pressures
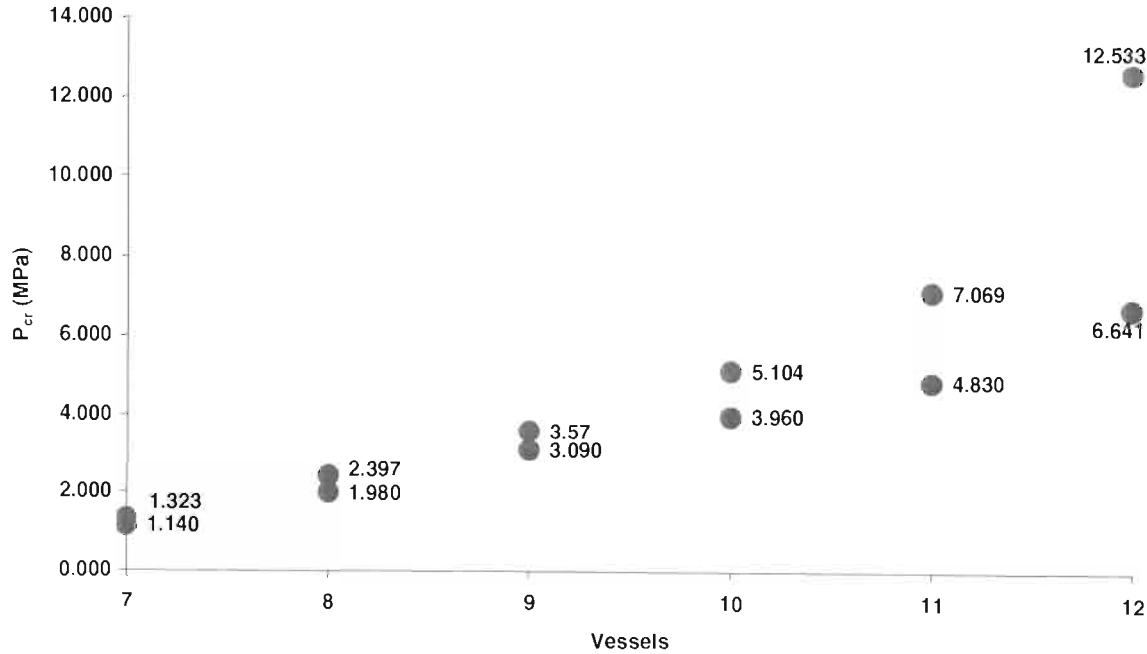
Figure 5-7 : Comparison of ASME and FEM Critical Buckling Pressures
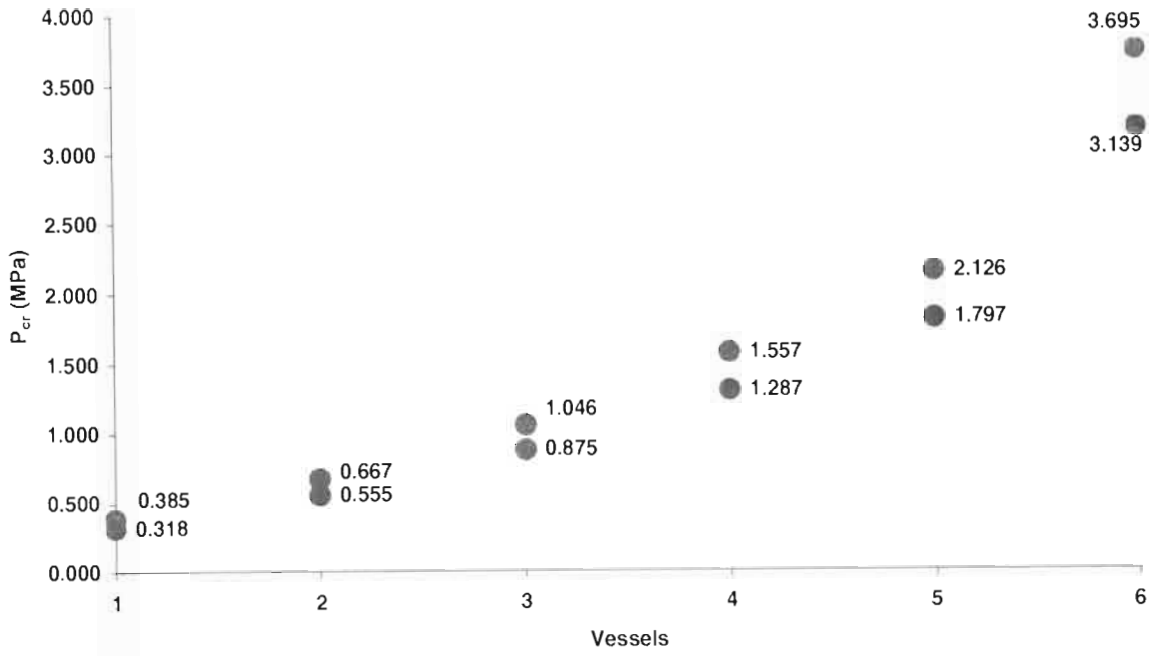
Figure 5-8 : Comparison of Windenburg & Trilling and FEM Critical Buckling Pressures
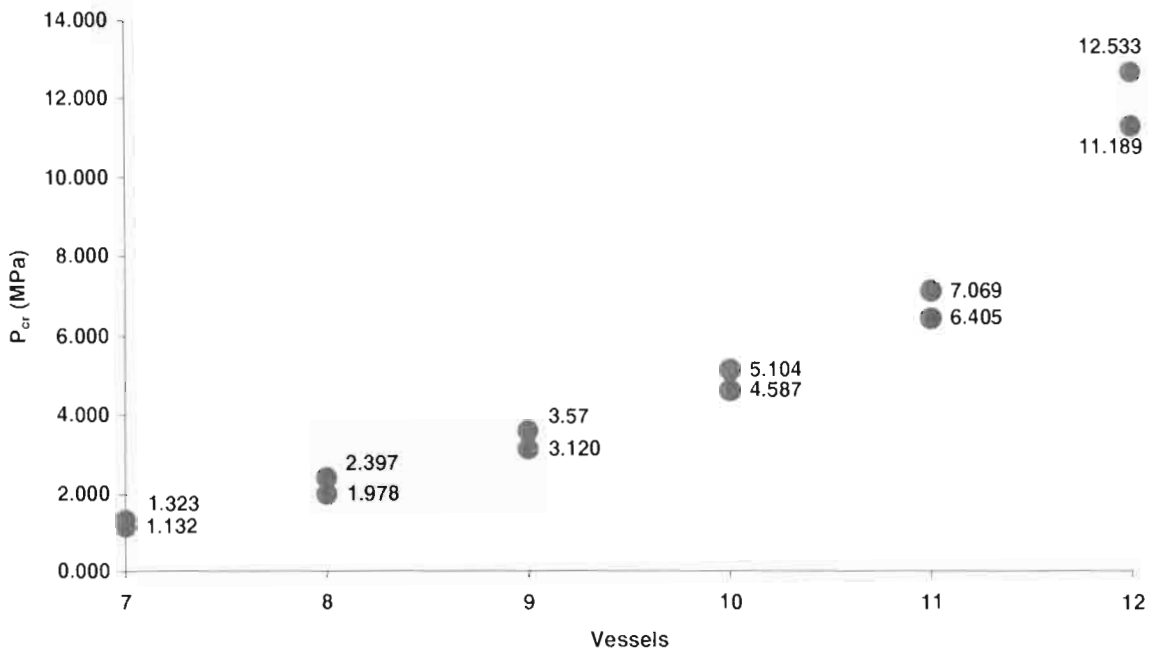
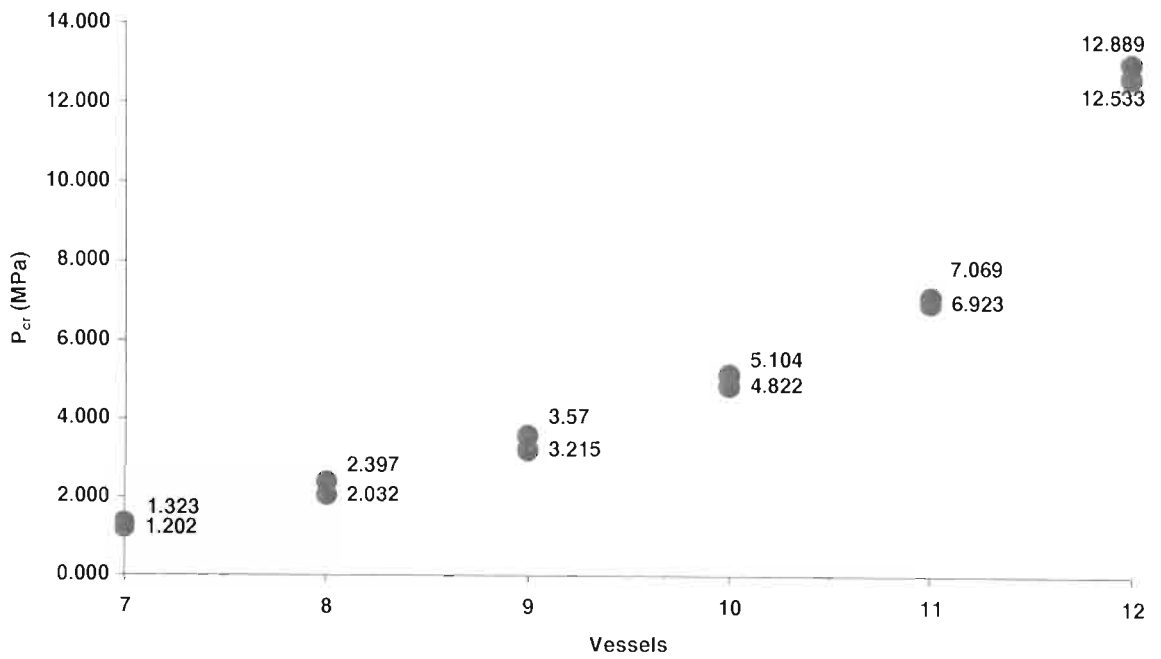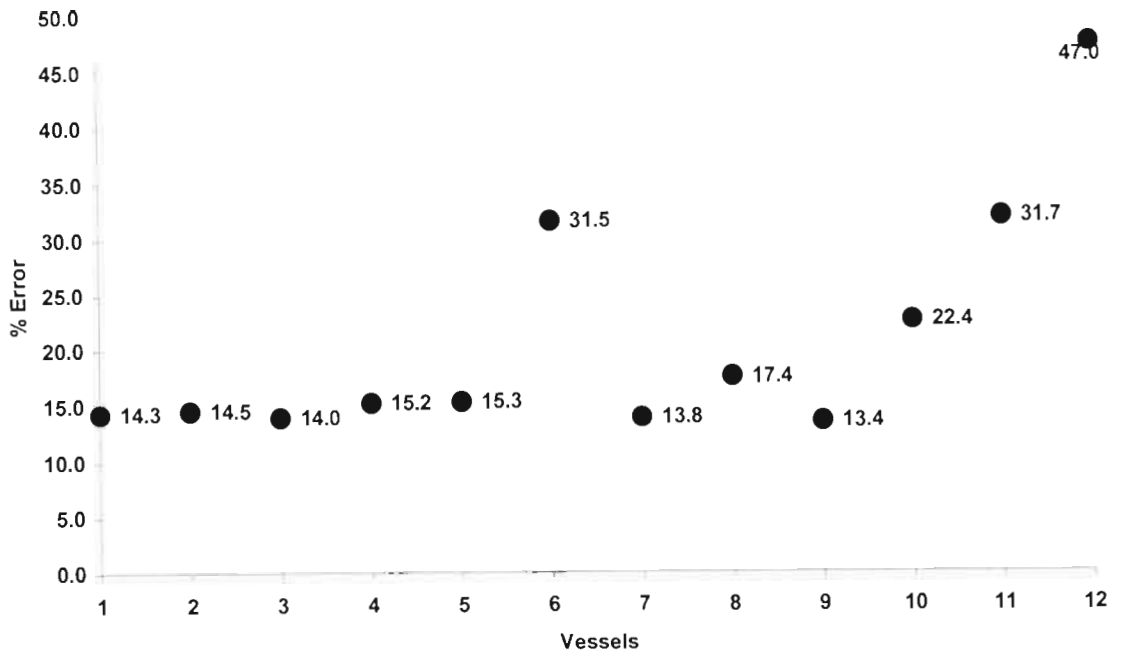Figure 5-9 : Comparison of Windenburg & Trilling and FEM Critical Buckling Pressures

ASME   FEM

108
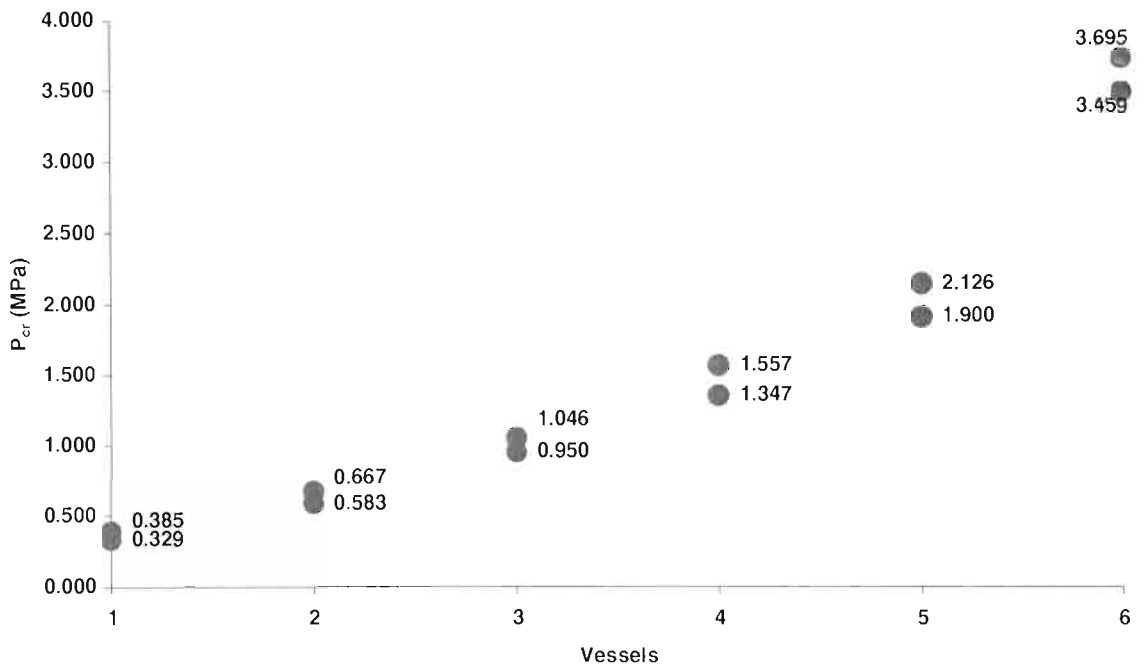
Figure 5-10 : Comparison of R Von Mises and FEM Critical Buckling Pressures

Figure 5-11 : Comparison of R Von Mises and FEM Critical Buckling Pressures

ASME   FEM

Figure 5-12 : Percentage errors between ASME and FEM Critical Buckling Pressures
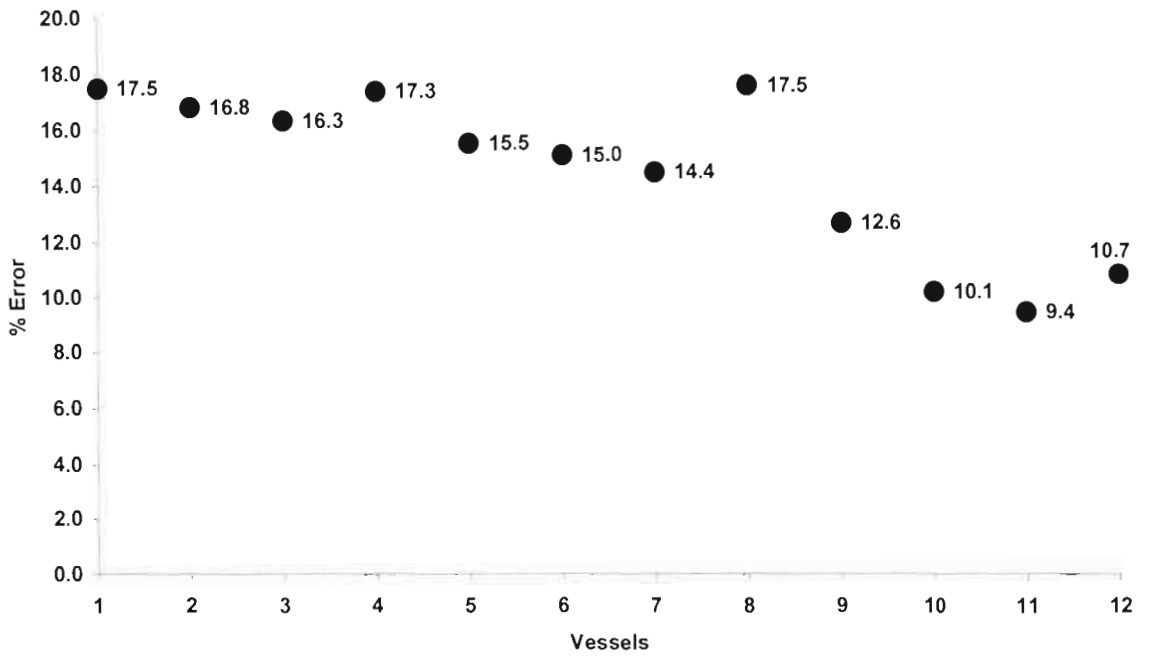
Figure 5-13 : Percentage errors between Windenburg & Trilling and FEM Critical Buckling Pressures
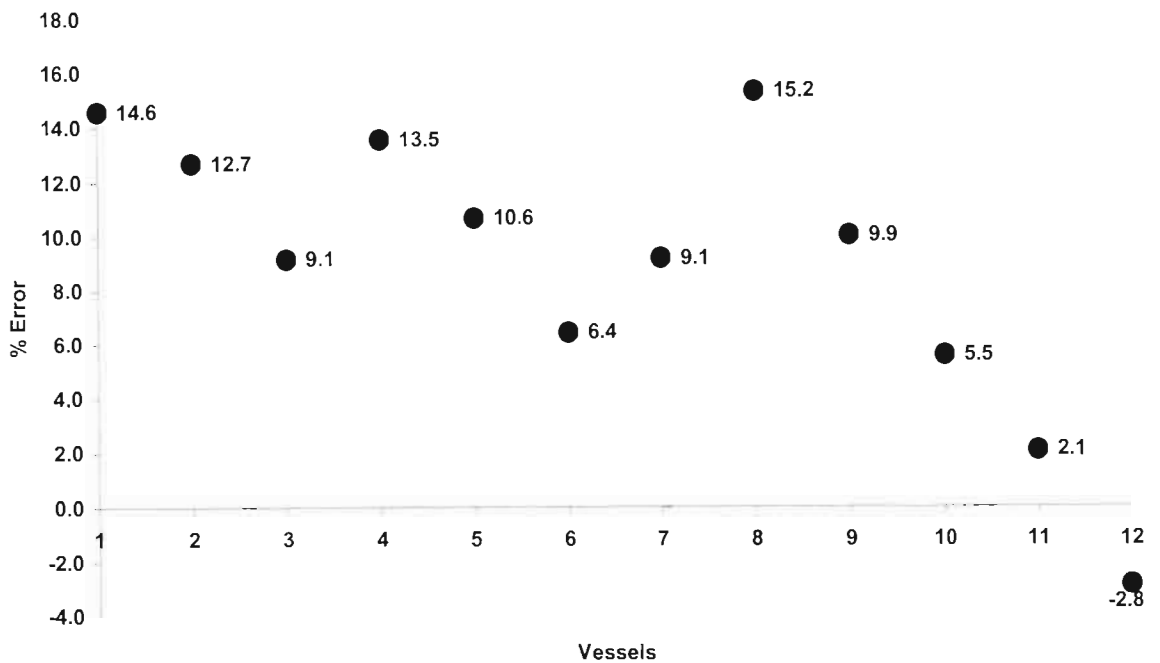
Figure 5-14 : Precentage errors between R Von Mises and FEM Critical Buckling Pressures

The results indicate that the FEM and Von Mises critical buckling pressures coincide the best. The ASME critical buckling pressures differ due the safety factor of 80% that exists in the material chart, which is needed to determine the factor B. To verify Model B, analyses to determine the theoretical and FEM number of lobes of buckling n were made. The following results were obtained :

Vessel	n (Figure 5-2)	n (equation 5.7)	n FEM
1	8	8	9
2	8	8	8
3	8	8	8
4	7	7	8
5	7	7	7
6	7	7	7
7	4	4	5
8	4	4	5
9	4	4	4
10	4	4	4
11	4	4	4
12	4	4	4

Table 5-2 : Comparison between Theoretical and FEM lobes of buckling n
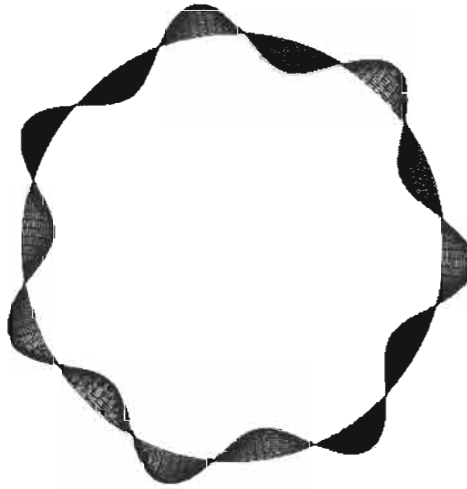
Top View

Figure 5-15 : FEM Buckling pattern for Vessel 7

The number of lobes of buckling n coincides with the theoretical values, thereby verifying Model B. The FEM results can be found in Appendix C.

5.2 Design of Pressure Vessels under External Pressure and Piping Loads

The shell-to-nozzle region is a localized area and nozzle loads are regarded as local loads being applied to this region. Therefore, the combination of external pressure and nozzle loads will result in local buckling (see [20], [38] and [39]) occurring at the shell-to-nozzle junction. This can be illustrated in the figure below
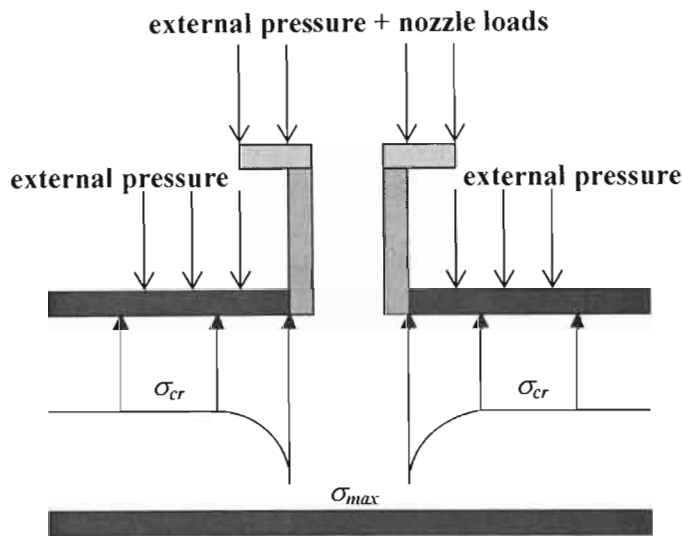

Figure 5-16 : Local Stresses exceeding Critical Buckling Stress. Reproduced from Harvey[20]

It has been discussed that, to prevent buckling from occurring, stresses should be less than the critical buckling stress σ_{cr}. However, at the shell-to-nozzle junction, nozzle loads create local stresses that can exceed the critical buckling stress, as shown in figure 5-16 above. Since the critical buckling stress is exceeded, local buckling will occur. Nozzle loads also cause deviations or deformations[9] to occur around this highly stressed region. At the shell-to-nozzle junction the cross-section of the shell is not circular. With the added deviations it can be assumed that this will have the same effect on the stability of a vessel as does a vessel with geometric imperfections. The collapse pressure of cylindrical vessels subjected to external pressure is dependent on the final fabricated shape. Imperfections or out-of-roundness in cylindrical vessels reduce the ability of these vessels to withstand buckling (see [4], [5], [6], [10], [28] and [40]) i.e. out-of-roundness (deflections caused by nozzle loads) at the shell-to-nozzle junction, reduces the buckling strength of the vessel. With the inclusion of geometric imperfections, figure 5-16 resembles figure 5-17 below.
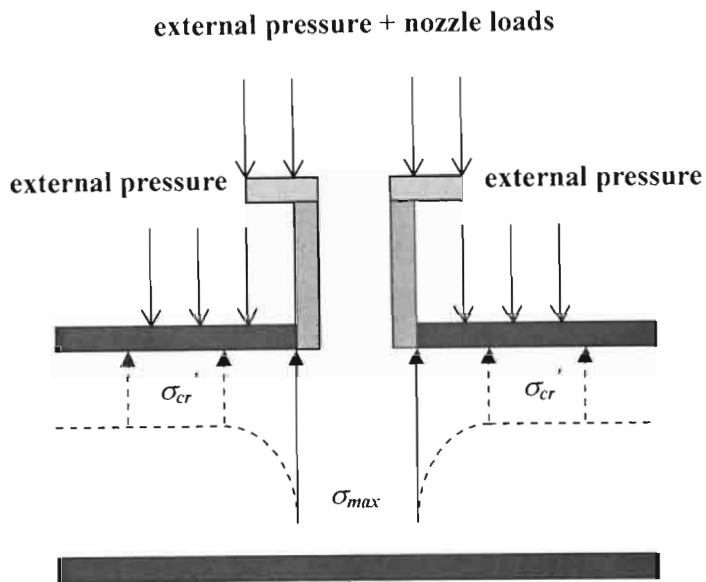
113

external pressure + nozzle loads

Figure 5-17 : Local Stresses exceeding reduced Critical Buckling Stress

Stresses at the shell-to-nozzle junction, shown in figure 5-17 above, are much greater than the reduced buckling strength σ_{cr}, thus rendering the vessel more unstable. For the design of pressure vessels under the combined loading of external pressure and nozzle loads, the reduced critical buckling stress, at the shell-to-nozzle junction, needs to be calculated. Local stresses at this region should be within the reduced critical buckling stress to prevent failure of the vessel due to buckling.

5.2.1   Vessels with Geometric Imperfections

It has been discussed that the collapse pressure of cylindrical vessels subjected to external pressure is dependent on the final fabricated shape. Imperfections or out-of-roundness in cylindrical vessels reduce the strength of these vessels to withstand buckling. The out-of-roundness results in increased stress concentrations. This means that the stresses in the vessel are much greater than the allowable stress for the vessel to withstand buckling. Out-of-roundness after fabrication represents vessels of elliptical shape, dented vessels or vessels with flat spots. Since nozzle loads cause deviations in the shell and stress concentrations at the shell-to-nozzle junction, a relationship between out-of-roundness and nozzle loads was developed.

114

M Holt[3] developed the following equation for the buckling pressure of a vessel with an initial out-of-roundness :

$$P_{cr}^{'} = \cfrac{2\sigma_{UTS}\cfrac{T}{D_o}}{1+\cfrac{4A}{T}\cfrac{E\left[n^2-1+v\left(\cfrac{\pi D_o}{2L}\right)^2\right]}{\left(1-v^2\right)\left(P_{cr}-P_{cr}^{'}\right)}\left(\cfrac{T}{D_o}\right)^3}$$

(5.17)

The above equation calculates the critical buckling pressure for a vessel in its buckled state. Holt's equation is a rational approach to the design of an imperfect vessel under external pressure. However, the calculation of the buckling pressure is less straightforward. The German Code[9] developed a much simplified equation shown below :

$$P_{cr}^{'} = \cfrac{2\sigma_{yp}\cfrac{T}{D_o}}{1+\cfrac{1.5\left(\cfrac{4A}{D_o}\times100\right)\left(1-0.2D_o/L\right)}{100\cfrac{T}{D_o}}}$$

(5.18)

The German Code calculates the reduced critical buckling pressure to be a certain fraction of the critical buckling pressure calculated for a perfect cylindrical vessel. The equations above use out-of-round values A. ASME VIII Div 2 contains manufacturing tolerances when out-of-roundness becomes a consideration. For external pressure the maximum deviation from true circular form must not exceed 1% of the inner/outer diameter of the vessel. If an opening exists, then 2% of the inner diameter of the opening must not be exceeded. The ASME Code also calculates out-of-roundness values e given by the figure below
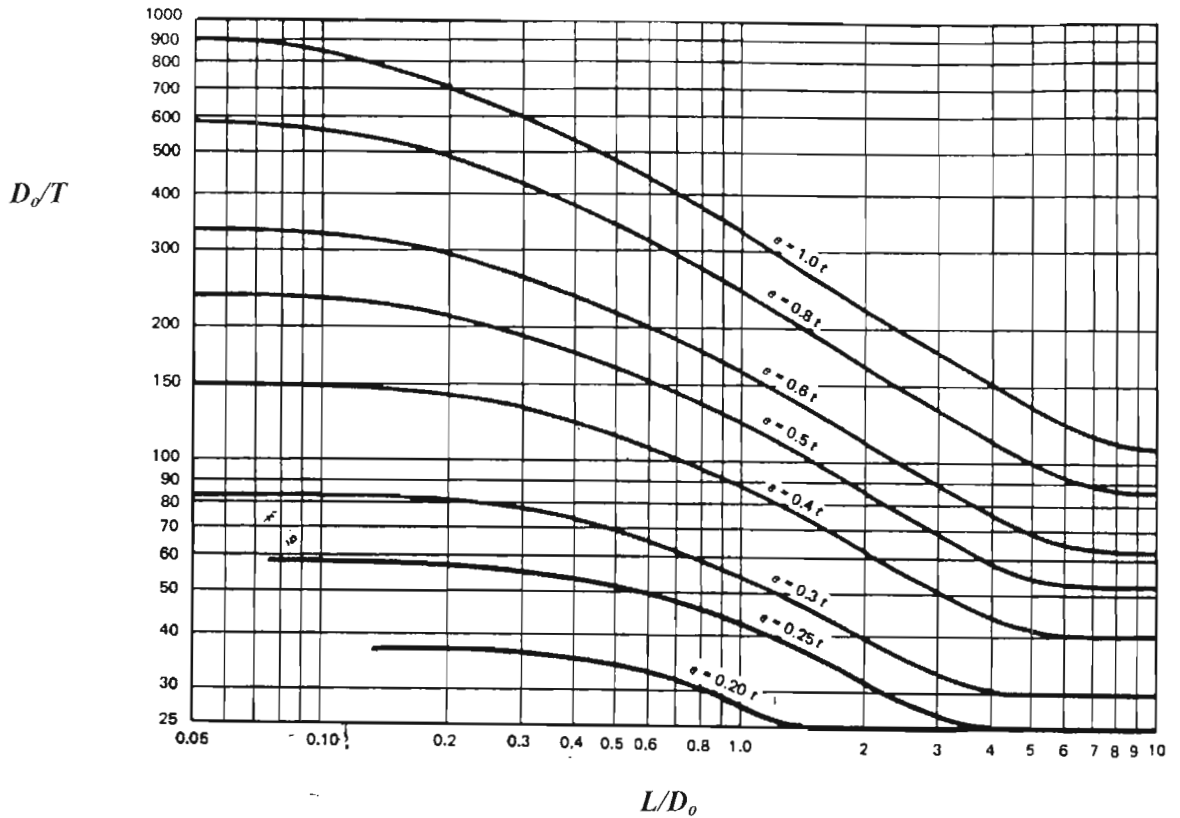
115

Figure 5-18 : ASME maximum permissible deviation from a circular form *e* for vessels Under external pressure. Obtained from ASME VIII[34]

The out-of-round values given by figure 5-18 can be used by equations 5.17 and 5.18. However, the values do not reflect the variation in deflections caused by different nozzle loads. The out-of-round value *e* may be much greater than the actual deflection caused by the nozzle, thereby giving a much lower critical buckling pressure. Therefore, more accurate out-of-roundness values related to nozzle loads were developed. Equation 5.17 was derived on the assumption that the initial out-of-roundness is similar in form to the assumed buckling mode shape. This is not the case for vessels under external pressure and external piping loads. A relationship between nozzle loads and the more acceptable equation 5.18 was developed. In developing this relationship it was understood that nozzle loads increase the local stresses at the shell-to-nozzle junction. Geometric imperfections at localised areas also increase stress concentrations. Therefore, stresses caused by out-of-roundness and stresses developed by nozzle loads were related. S Timoshenko[7] developed an equation to determine the stress caused due to out-of-roundness in the shell when subjected to external pressure. He studied the effects of cylinders and tubes with initial non-circularity subjected to external pressure and developed a theory around this. The most common form of non-circularity is that of an

116

elliptical or oval shape. Using this, the deviation caused by non-circularity could be shown in the following formula :

$$w_1 = w_o \cos 2\phi \qquad (5.19)$$

w_o is the maximum initial radial deviation, which is considered small in comparison with the vessel radius. This is shown in the figure below
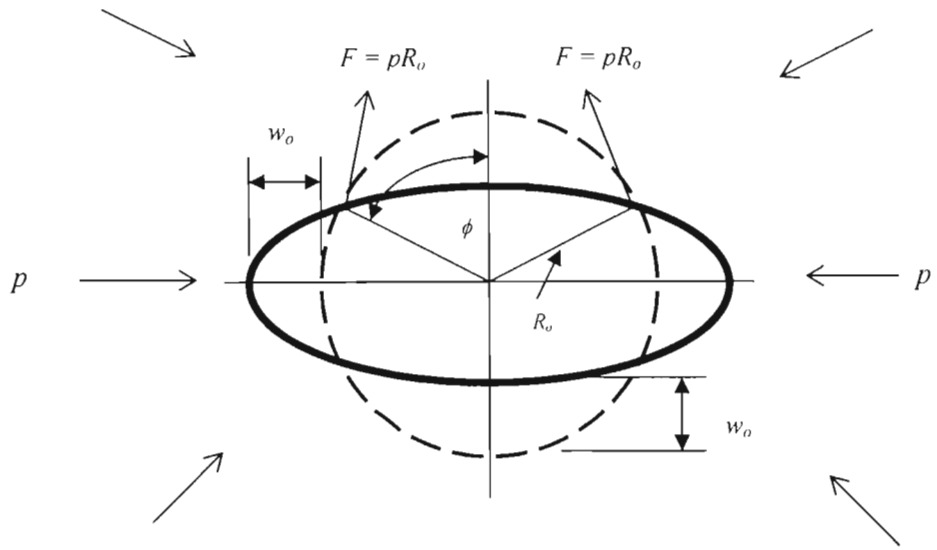

Figure 5-19 : Shell with Initial Ellipticity under External Pressure. Reproduced from Harvey[20]

When an external pressure is applied, an additional radial displacement w_2 will occur. Timoshenko determined that the deflection caused by external pressure is given by the following higher order deferential equation :

$$\frac{d^2 w_2}{d\phi^2} + w_2 = -\frac{R_o^2 M}{D} \qquad (5.20)$$

To determine the bending moment M in the shell, consider a strip in the circumferential direction of unit width. The bending moment at any cross section is equal to the compressive force F multiplied by the total radial deviation $w_1 + w_2$ at this cross section, or

117

$$M = pR_o\left(w_2 + w_o \cos 2\phi\right) \tag{5.21}$$

Substituting this into equation 5.20 and rearranging gives :

$$\frac{d^2 w_2}{d\phi^2} + w_2\left(1 + \frac{pR_o^3}{D}\right) = -\frac{pR_o^3 w_o \cos 2\phi}{D} \tag{5.22}$$

The solution to the above equation is :

$$w_2 = \frac{-w_o pR_o^3 \cos 2\phi}{pr_o^3 - 3D} \tag{5.23}$$

The critical buckling pressure for figure 5-19 is obtained by substituting $n = 2$ into equation 5.2. One obtains :

$$P_{cr} = \frac{2E}{\left(1 - v^2\right)}\left(\frac{T}{D_o}\right)^3 \tag{5.24}$$

Since D is the flexural rigidity, we substitute equation 5.24 into 5.23 and obtain :

$$w_2 = \frac{w_o p \cos 2\phi}{P_{cr} - p} \tag{5.25}$$

Substituting equation 5.25 into equation 5.21 and taking the bending moment to be maximum at points $\phi = 0$ and $\phi = \pi$, one obtains :

118

$$M_{or} = \frac{p w_o R_o}{1 - \left(\frac{p}{P_{cr}}\right)}$$

(5.26)

The compressive stress is obtained by converting M_{or} to a stress :

$$\sigma_{or} = \frac{6 M_{or}}{T^2} = \frac{6}{T^2} \cdot \frac{p R_o w_o}{1 - \left(\frac{p}{P_{cr}}\right)}$$

(5.27)

$$\sigma_{or} = \frac{3}{T^2} \cdot \frac{p D_o w_o}{1 - \left(\frac{p}{P_{cr}}\right)}$$

Equation 5.27 (obtained from Jawad and Farr[22]) gives the compressive stress induced in an out-of-round cylindrical shell subjected to external pressure. The total compressive stress will be equal to the sum of the stress given by equations 5.27 and the compressive stress calculated using equation 2.6 for the external applied pressure.

5.2.2 Numerical Results

The theoretical and FEM numerical results are based on the models given in table 5-1. These vessels were also analyzed with nozzle loads. The 4", 8", 12", 16", 20" and 24" inch nozzles were used for each of the twelve vessels given in table 5-1. SASOL piping loads, found in Appendix A, were used for each of the six nozzles. The orientation of these loads are given in figure 3-4. For vessels with piping loads under external atmospheric pressure, the radial load is in the same direction as the external pressure. The table below gives the ASME VIII Div 2 results for vessels 1-12.

Vessel	ASME P_{cr} MPa	ASME σ_{cr} MPa
1	0.330	56.5
2	0.570	79.0
3	0.900	103.8
4	1.320	130.8
5	1.800	156.2
6	2.532	177.3
7	1.140	84.9
8	1.980	118.6
9	3.090	154.6
10	3.960	169.5
11	4.830	181.5
12	6.641	199.3

Table 5-3 : ASME VIII Div 2 Critical Buckling Pressures and Stresses for vessels 1-12

FEM stress analyses were performed on Vessel 5 to determine the stress at the shell-to-nozzle junction under the combined loading of external atmospheric pressure and nozzle piping loads. These stresses are compared with the ASME critical buckling stress given in table 5-3 above. The results obtained are

The chart shows:
- Y-axis: Stress (MPa) ranging from 0.0 to 300.0
- X-axis: Nozzles (inches) ranging from 4 to 24
- Data points: 263 (at 4), 271 (at 8), 245 (at 12), 231 (at 16), 218 (at 20), 182 (at 24)
- $\sigma_{cr} = 156.2\text{MPa}$ (dashed horizontal line)
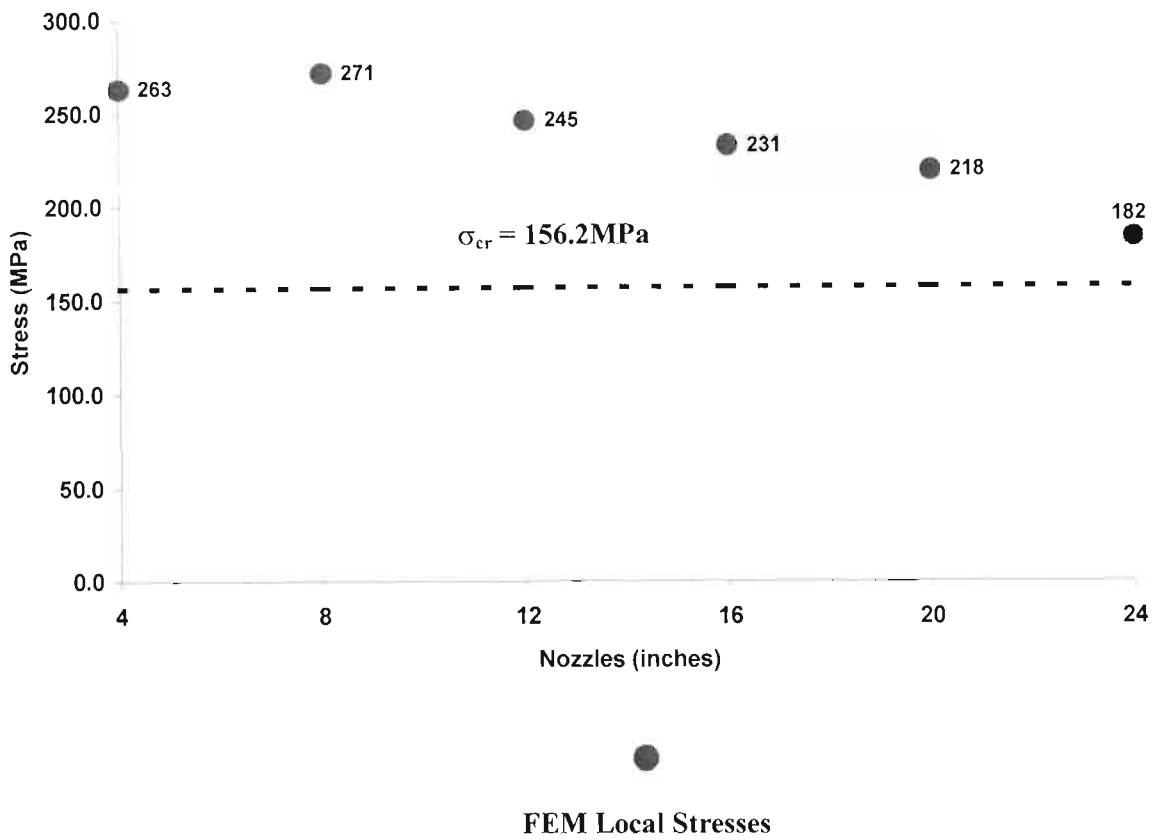
FEM Local Stresses

Figure 5-20 : FEM Local Stresses compared to ASME Critical Buckling Stress for Vessel 5

Figure 5-20 shows that the local stresses at the shell-to-nozzle junction exceed the critical buckling stress, ensuring local buckling to occur. Further FEM analyses were performed on Vessels 1-12 and a 24" nozzle was used. The results obtained are
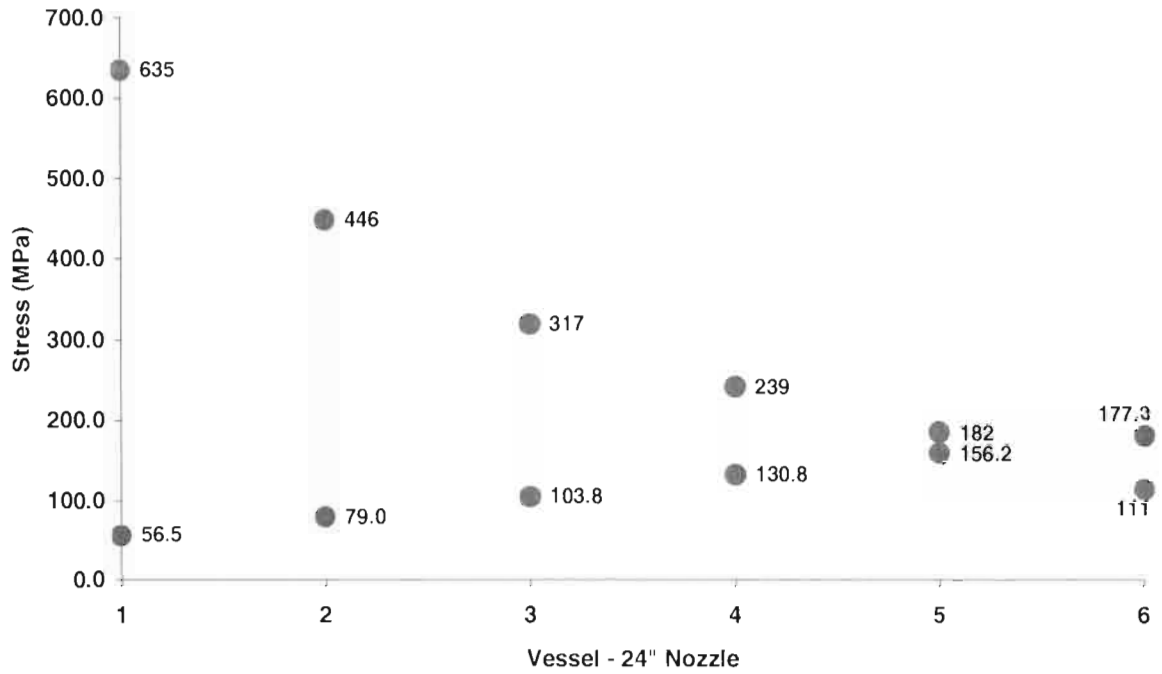
Figure 5-21 : FEM Local Stresses compared to ASME Critical Buckling Stress
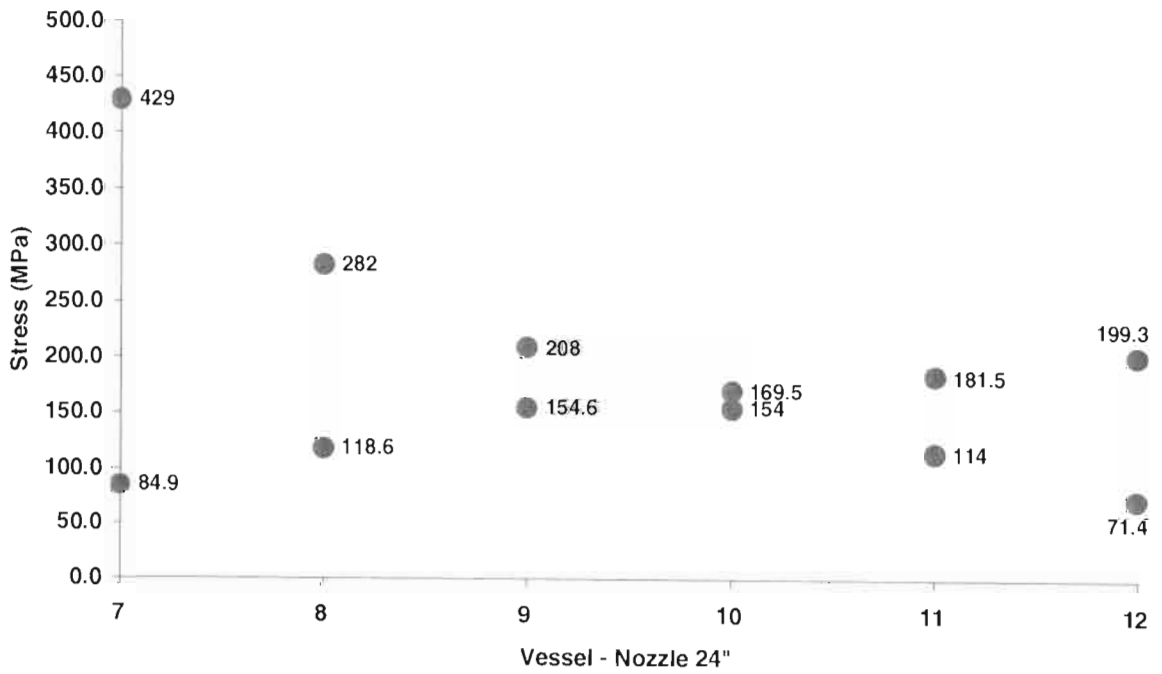
Figure 5-22 : FEM Local Stresses compared to ASME Critical Buckling Stress

FEM Local Stresses   ASME σ_{cr}

122
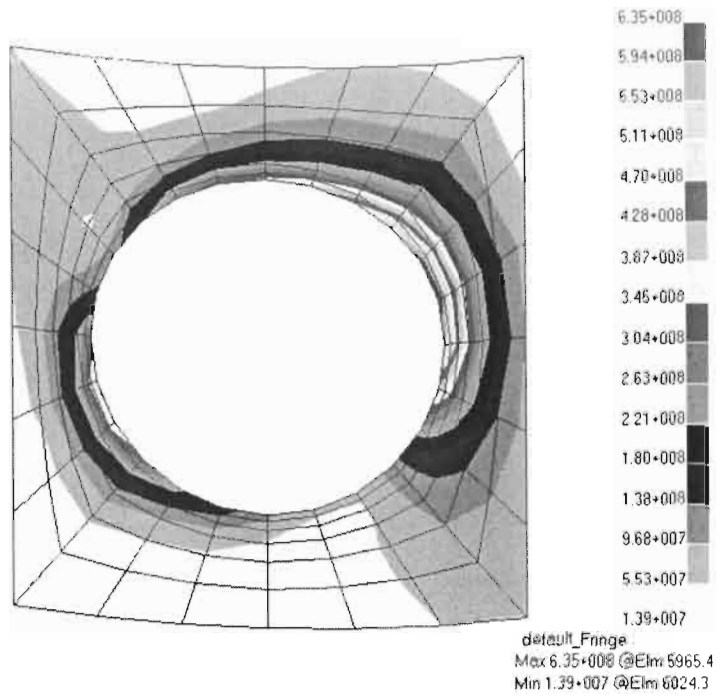
Figure 5-23 : FEM Stress Analysis for Vessel 1 under external pressure and 24" nozzle piping loads
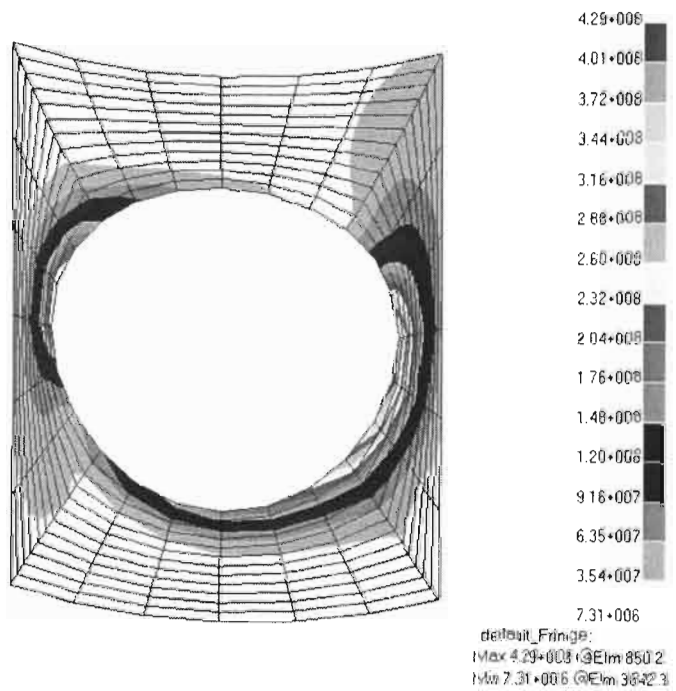
Figure 5-24 : FEM Stress Analysis for Vessel 7 under external pressure and 24" nozzle piping loads

For Vessels 1-12, subjected to external pressure and piping loads for a 24" nozzle, the results indicate that for some vessels the critical buckling stress is exceeded. However, the objective is to achieve results as for vessels 6, 10, 11 and 12, where the local stresses are much lower than the critical buckling stress to prevent local buckling from occurring. All FEM stress results can be found in Appendix C. It has been discussed that local buckling becomes more severe due to the fact that the critical buckling strength of the vessel is reduced to the deviation created at the shell-to-nozzle junction. The effects of deviations created by nozzle loads have been investigated. The figure below show deflections caused by external pressure and a 24" nozzle for vessels 1 to 6 at the shell-to-nozzle junction.
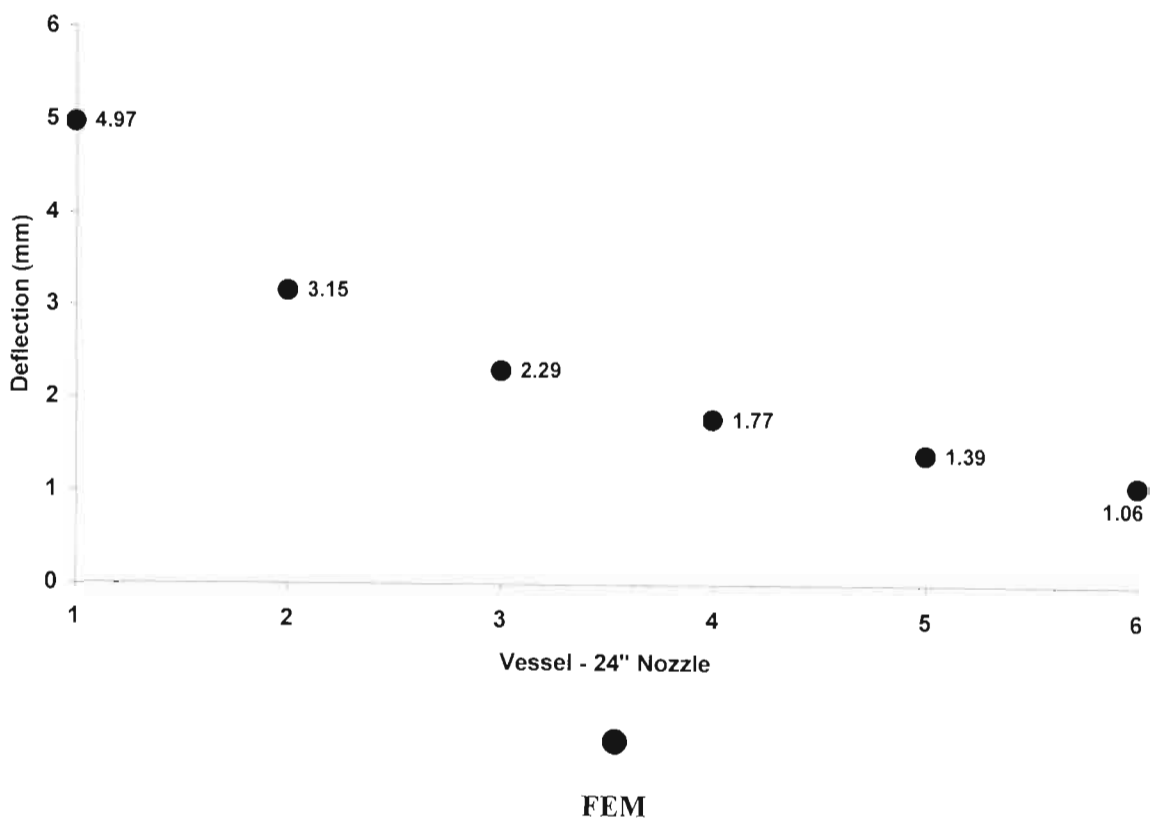
Figure 5-25 : Maximum FEM Deflection for Vessels 1 to 6 under external pressure and 24" nozzle loads at shell-to-nozzle junction

An appropriate FEM Model, Model C shown below, was developed to determine the effects of nozzle piping loads on the critical buckling pressure for vessels 1-12 subjected to atmospheric pressure and piping loads for 4", 8", 12", 16", 20" and 24" nozzles.
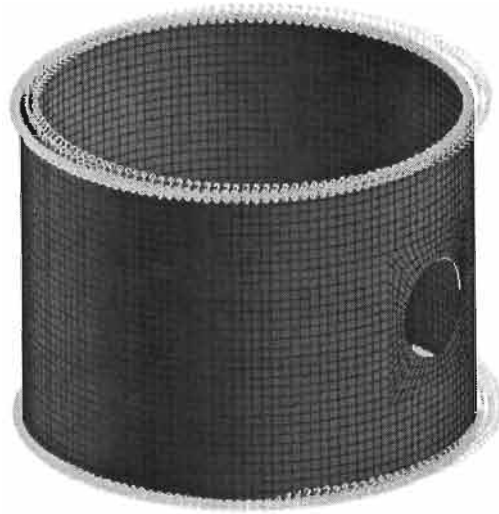
Isometric View

Figure 5-26 : FEM Model C

Shell elements or 4-noded quadrilateral elements were used to mesh the model. Model C was meshed as close as possible to 6000 nodes to generate an appropriate fine mesh. Identical material properties to Model A and B were used. The circular region removed from the shell, shown in Model C, represents the shell-to-nozzle junction. The appropriate nozzle loads were applied to this region. Out-of-roundness represents a model with geometric imperfections. For this type of model, where large displacements occur, a geometric nonlinear analysis (see [29] and [39]) is advised. A nonlinear solution involves a series of incremental solutions. The load is applied in increments and during each increment a solution is predicted. Convergence occurs when each solution is achieved. If a solution does not converge, then it indicates that equilibrium is unstable and buckling will occur due to nonlinearity. A nonlinear analysis was performed on Vessel 1 for a 4" nozzle and convergence was reached for each of the load increments. Model C does not represent a model with severe geometric imperfections, therefore, the linear eigenvalue buckling analysis, described in Chapter 4, was used. Vessels 6 and 12 were analyzed with the six nozzles, mentioned earlier, and the FEM results obtained are
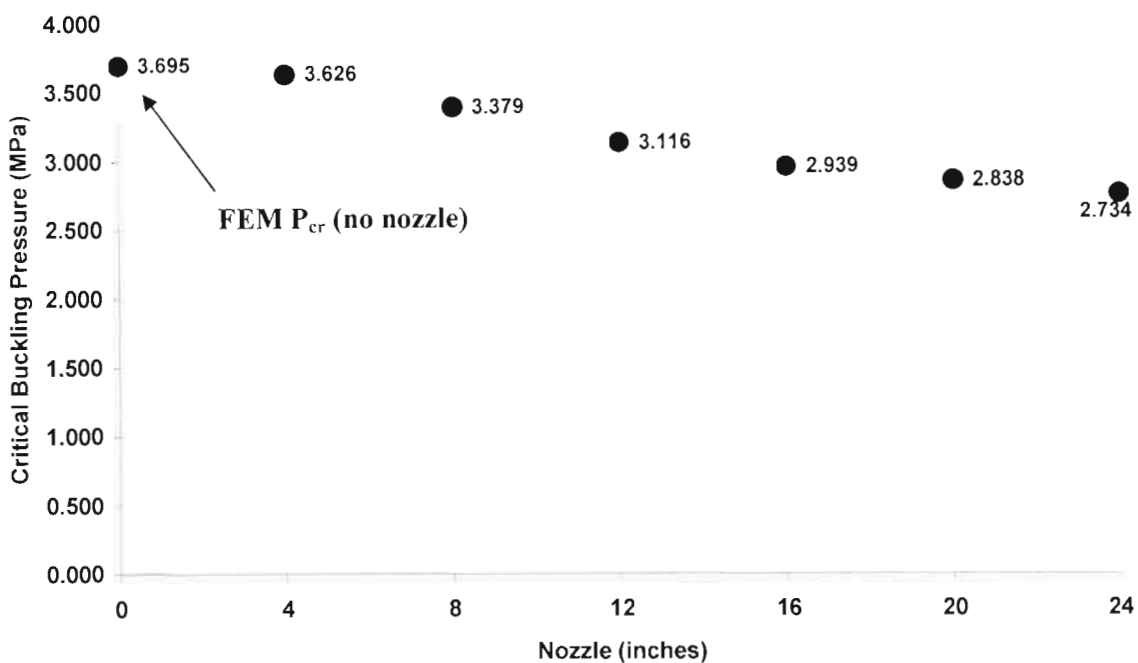
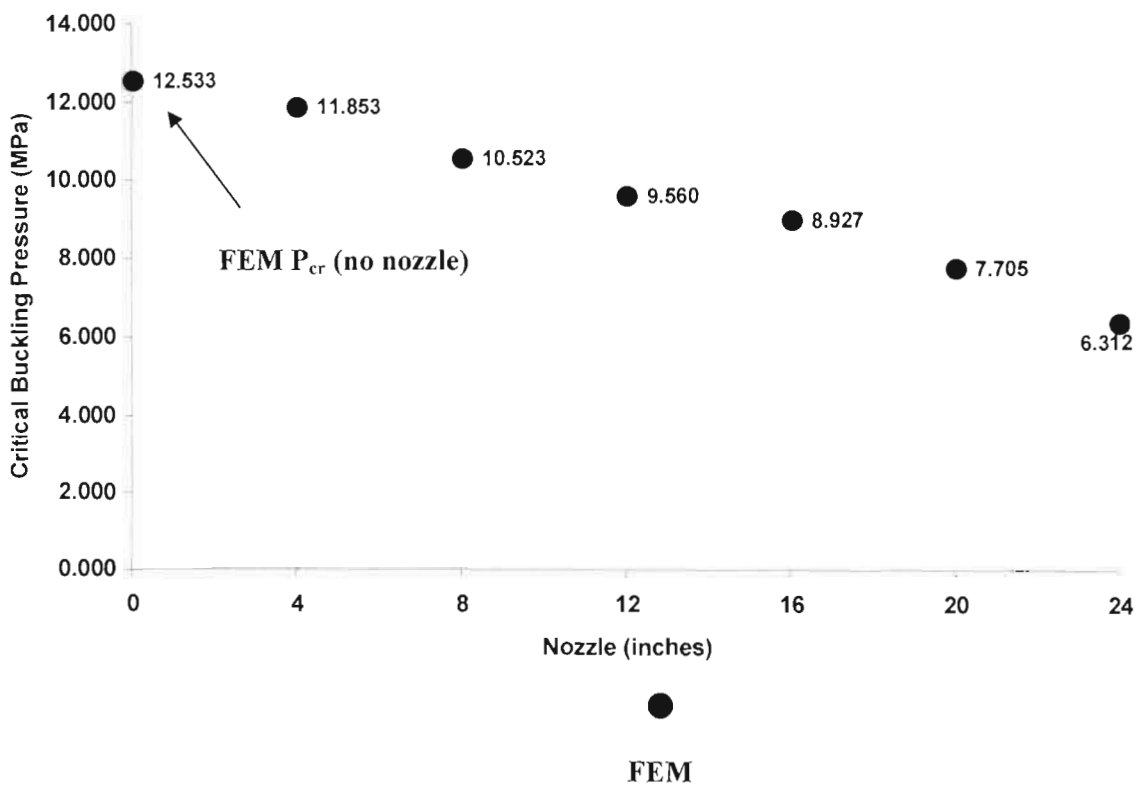**Figure 5-27 : Reduction in Critical Buckling Pressure for Vessel 6 due to nozzle loads**

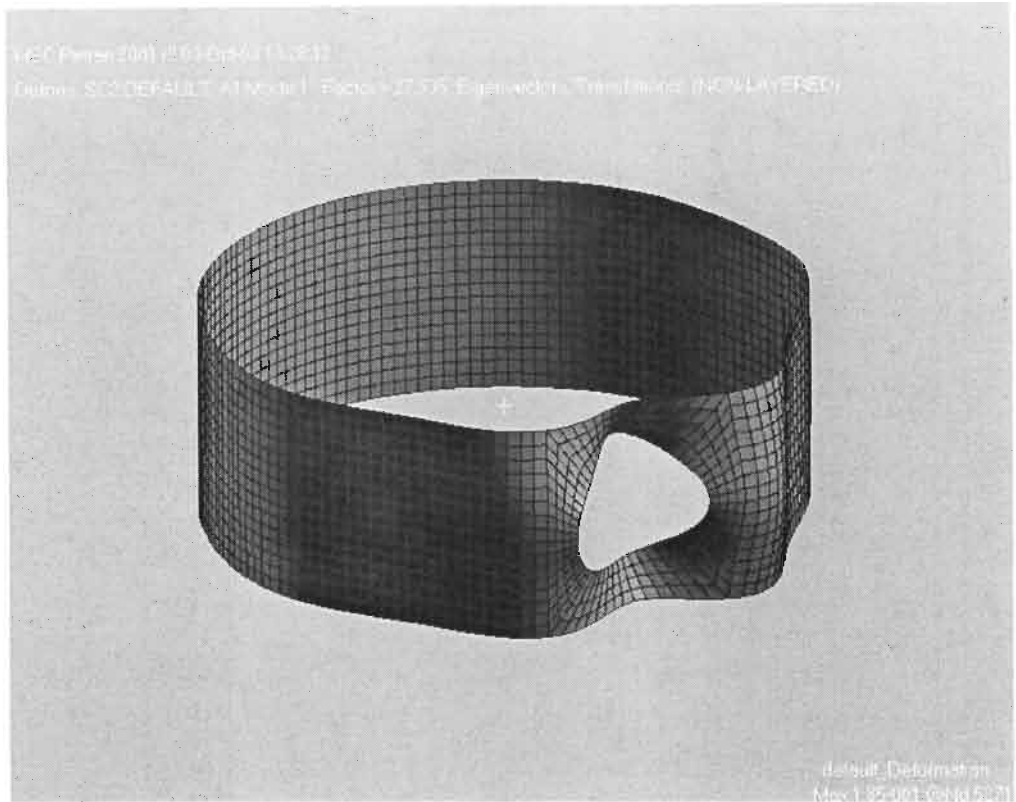**Figure 5-28 : Reduction in Critical Buckling Pressure for Vessel 12 due to nozzle loads**

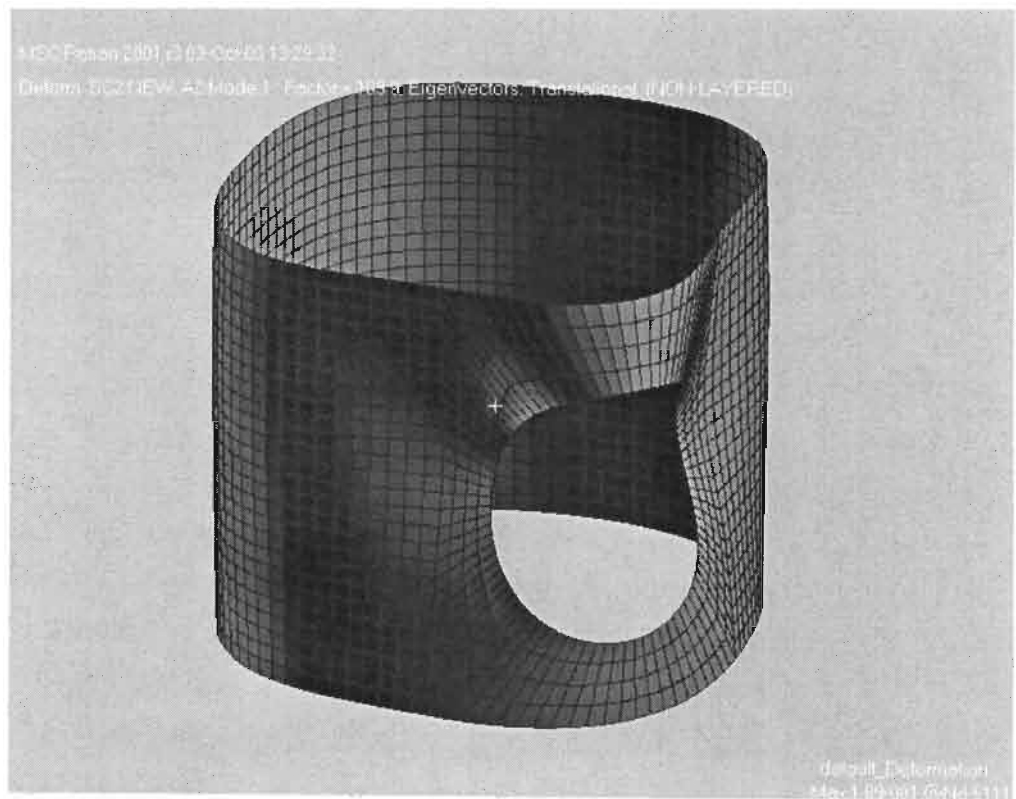Figure 5-29 : FEM Buckled Vessel 6 under external pressure and 24" nozzle loads

Figure 5-30 : FEM Buckled Vessel 12 under external pressure and 24" nozzle loads

127

FEM buckling analyses for vessel 6 and 12 under external pressure and nozzle loads can be found in Appendix D. The results indicate that the reduction in critical buckling pressure for vessels under external atmospheric pressure and nozzle piping loads can be obtained by using FEM. The buckled patterns given in figures 5-29 and 5-30 are different to the buckled patterns for the perfect cylindrical vessels. With the inclusion of nozzle loads, vessels buckle at much lower modes than those predicted without nozzle loads. The reduction of the critical buckling pressure results in local stresses being much greater at the shell-to-nozzle junction and severe local buckling can occur. This is indicated in the figures below
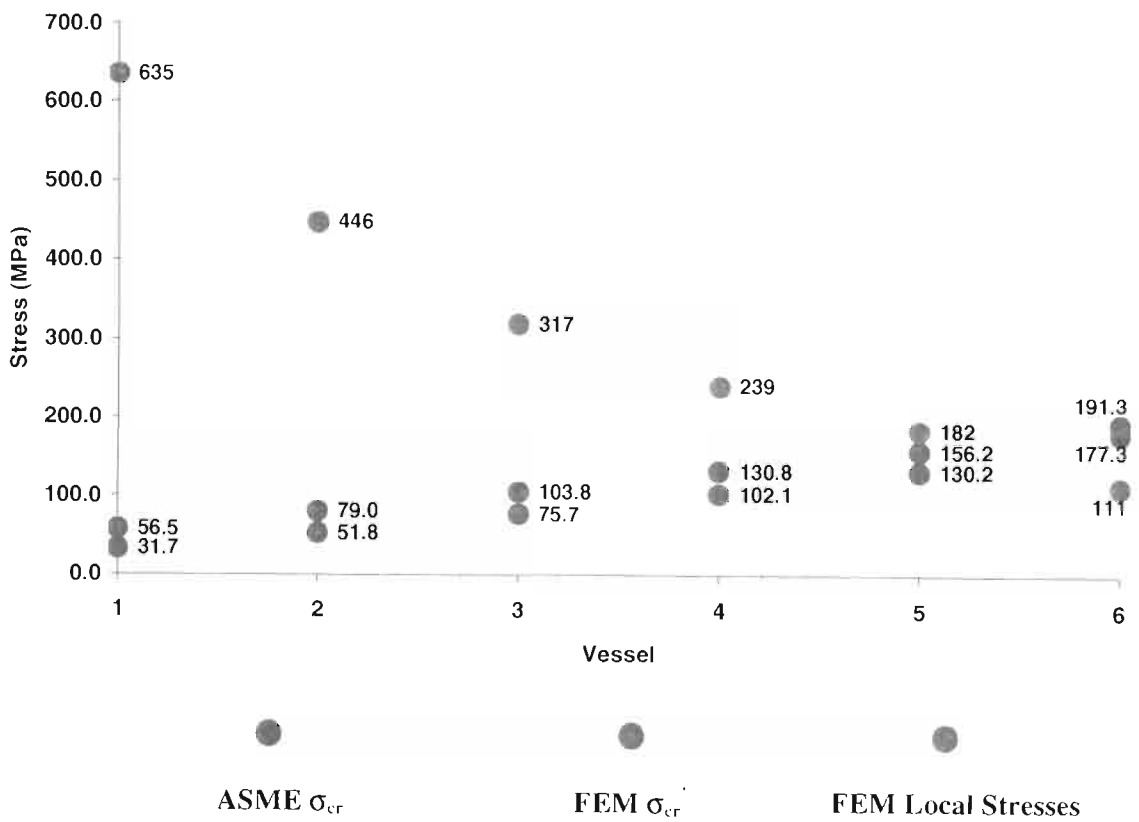

Figure 5-31 : Comparison between Local Stresses and Critical Buckling Stresses for Vessels 1 – 6 under external pressure and 24" nozzle piping loads
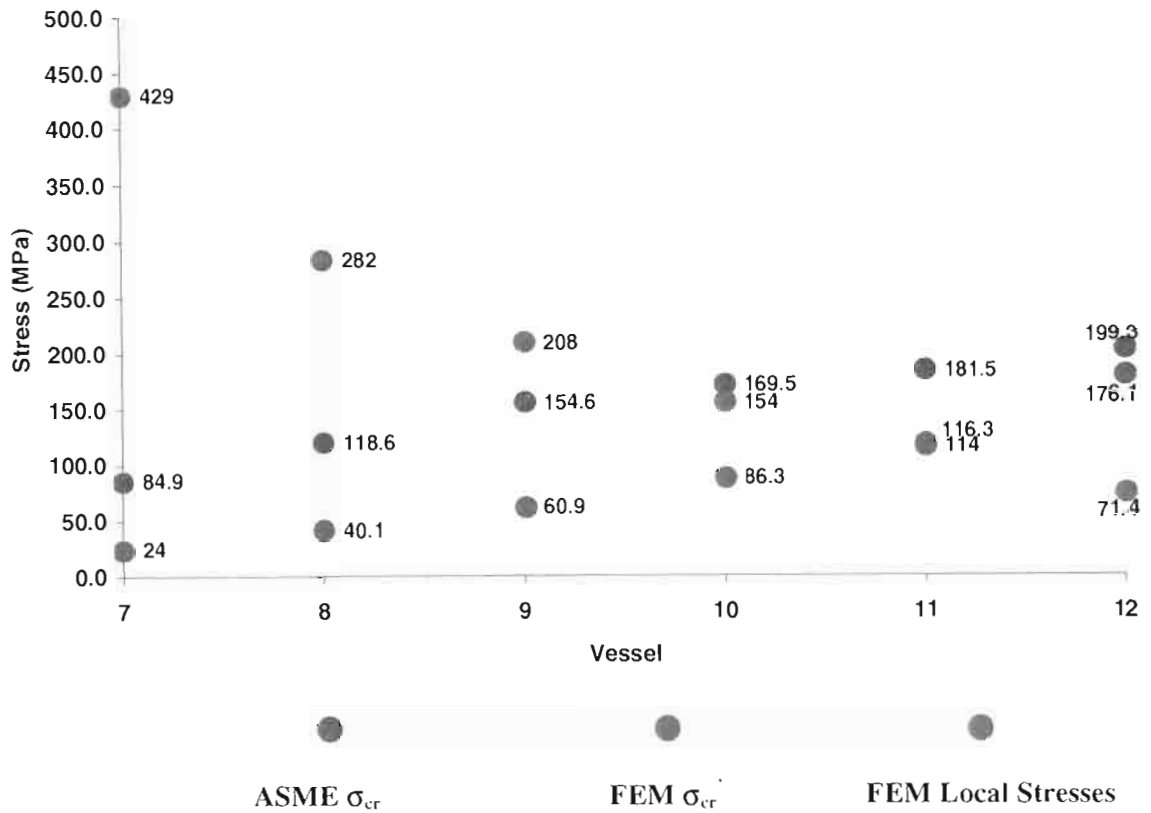
Figure 5-32 : Comparison between Local Stresses and Critical Buckling Stresses for Vessels 7 – 12 under external pressure and 24" nozzle piping loads

The objective for the design of vessels under external pressure and nozzle piping loads will be to determine the reduced critical buckling stress and ensure that local stresses at the shell-to-nozzle junction are lower than the buckling stress. Results for vessels 6 and 12 give the FEM local stresses to be much lower than both the ASME critical buckling stress and the FEM reduced critical buckling stress. This is ideal in ensuring that local buckling will not occur at the shell-to-nozzle junction. It has been shown that the reduction in the critical buckling stress can be determined by FEM methods. However, for this study, a theoretical procedure was developed for the design of pressure vessels under atmospheric pressure and nozzle piping loads. The theoretical procedures relate local stresses caused by nozzle loads alone to of out-of-round stresses generated using equation 5.27. WRC 107 can calculate the local stresses which can be used to determine the equivalent out-of-round stress. It should be noted that this stress is not the actual reduced critical buckling stress of the vessel. An out-of-round value can be determined from the out-of-round stress. This out-of-round value can be used in the out-of-roundness equation. equation 5.17. to determine the reduced critical buckling pressure. The reduced critical buckling pressure can be converted to a stress and must be compared with the more accurate FEM local stresses to determine if local buckling occurs at the shell-to-nozzle

junction. Lets consider vessels 1 to 12 subjected to atmospheric pressure and 24" nozzle piping loads. Using the reduced critical buckling pressures, generated using FEM, these values were substituted into equation 5.17. Out-of-round values were calculated and substituted into equation 5.27. For equation 5.27 the value of P_{cr} was also taken from equation 5.9. Out-of-round stresses σ_{or} were generated and a relationship, between these values and the WRC 107 maximum local compressive stresses, under nozzle loads alone, was determined. The relationship is shown in the table and figure below

Vessel	1	2	3	4	5	6	7	8	9	10	11	12
WRC 107 (MPa)	595.2	394.7	278.2	207.4	165.2	111.3	577.9	375.4	264.2	198	154.1	101.3
σ_{or} (MPa)	341.2	100.1	39.0	25.0	12.5	4.4	239.9	94.5	38.4	17.9	9.3	3.0

Table 5-4 : WRC 107 Local Stresses and Out-of-round Stresses for vessels 1 – 12 under external pressure and 24" nozzle piping loads
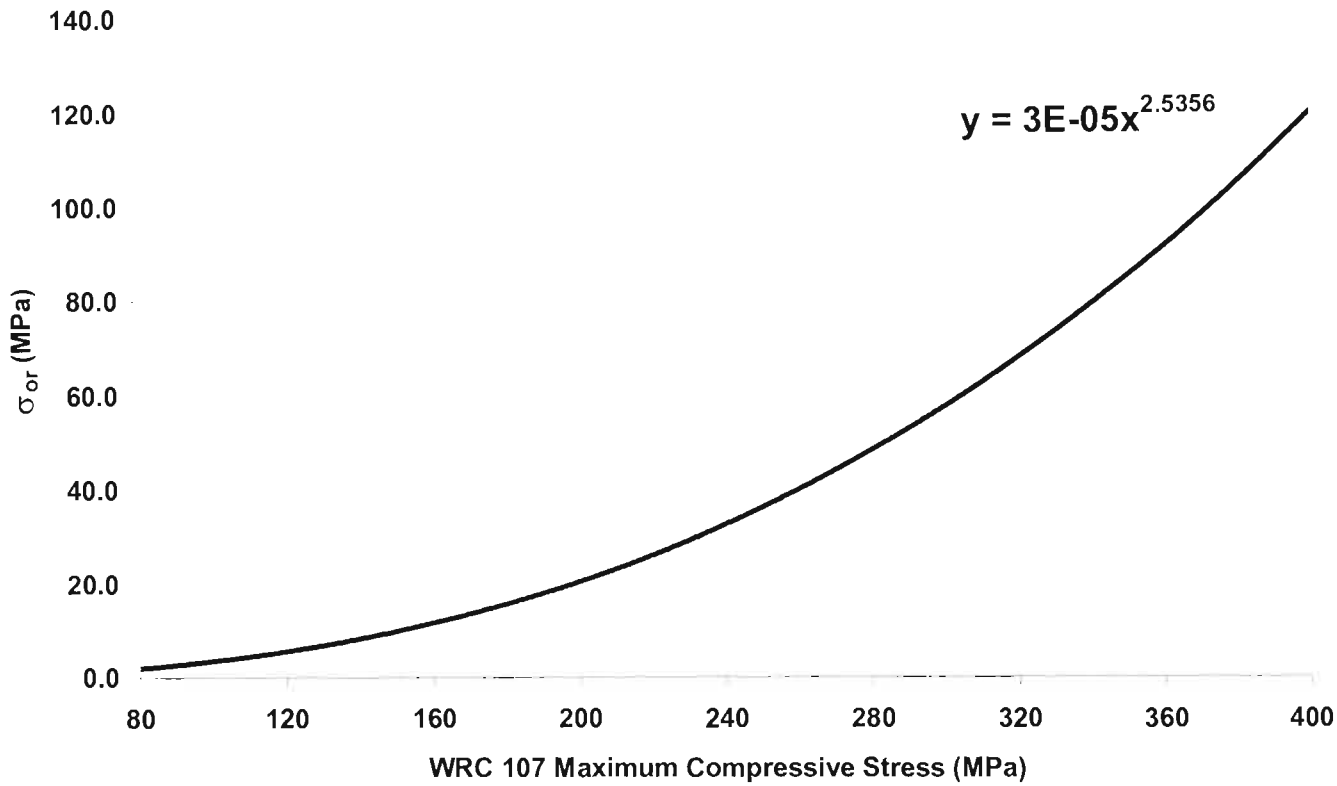
Figure 5-33 : Relationship between WRC 107 Local Stresses and Out-of-round Stresses for vessels 1 – 12 under external pressure and 24" nozzle piping loads

Further relationships for the remaining nozzles can be found in Appendix D. The table below gives values obtained from the relationships and should be used for the design of vessels under atmospheric pressure and nozzle piping loads.

WRC 107	σ_{or}					
	4	8	12	16	20	24
80	0.1	0.2	0.7	0.9	1.3	2.0
90	0.1	0.3	1.0	1.3	1.8	2.7
100	0.2	0.4	1.3	1.7	2.4	3.5
110	0.3	0.5	1.7	2.2	3.1	4.5
120	0.4	0.7	2.1	2.9	3.9	5.6
130	0.5	0.8	2.7	3.6	4.9	6.9
140	0.6	1.0	3.3	4.4	5.9	8.3
150	0.8	1.3	4.0	5.3	7.1	9.9
160	1.0	1.6	4.7	6.4	8.5	11.6
170	1.2	1.9	5.6	7.6	10.0	13.6
180	1.5	2.2	6.5	8.9	11.7	15.7
190	1.8	2.6	7.6	10.4	13.5	18.0
200	2.2	3.0	8.7	12.0	15.5	20.5
210	2.5	3.5	10.0	13.8	17.7	23.2
220	3.0	4.0	11.4	15.7	20.0	26.1
230	3.5	4.6	12.8	17.8	22.5	29.2
240	4.0	5.2	14.4	20.1	25.3	32.5
250	4.6	5.9	16.2	22.5	28.2	36.1
260	5.3	6.7	18.0	25.1	31.4	39.9
270	6.0	7.4	20.0	27.9	34.7	43.9
280	6.8	8.3	22.1	31.0	38.3	48.1
290	7.7	9.2	24.3	34.2	42.1	52.6
300	8.6	10.2	26.7	37.6	46.1	57.3
310	9.6	11.3	29.2	41.2	50.3	62.3
320	10.7	12.4	31.9	45.1	54.8	67.5
330	11.9	13.6	34.7	49.2	59.5	73.0
340	13.2	14.8	37.7	53.5	64.5	78.7
350	14.5	16.2	40.8	58.0	69.7	84.7
360	16.0	17.6	44.1	62.8	75.2	91.0
370	17.6	19.1	47.6	67.8	81.0	97.5
380	19.3	20.7	51.2	73.1	87.0	104.3
390	21.0	22.4	55.0	78.7	93.3	111.4
400	22.9	24.1	59.0	84.5	99.9	118.8

Table 5-5 : Out-of-round Stresses for various nozzles

The reduced critical buckling stress can be determined using the computation sheet given below

Design of Pressure Vessels under External Pressure and Nozzle Piping Loads

: user fill in

ASME VIII Div 1 : UG-28

Do =	2800 mm
t =	20 mm
CA =	0 mm
L =	2000 mm
E =	200000 MPa
n =	7

Critical Buckling Pressure Pcr =   **3.139 MPa**

Nozzle

Nozzle :   **24** inch

Calculation of Buckling Stress σ_{cr}'

σ_{UTS} =	**483 MPa**
WRC 107 =	**111.3 MPa**
Out of Roundness Stress =	**4.5 MPa**
A =	2.075 mm

σ_{cr}' =   **165.7 MPa**   **Holt**

Figure 5-34 : Computation Sheet for determining the reduced Critical Buckling Stress

Appendix E shows results for two vessels (Vessels 1 and 3 shown in Chapter 3) subjected to external pressure and nozzle piping loads. The reduced critical buckling stress is calculated for both vessels using table 5-5 and the computation sheet shown above.

Chapter 6

DISCUSSION

6.1 Design of Pressure Vessels

The objective of this study was to investigate the effects of both internal and external pressure on a pressure vessel subjected to external piping loads at the nozzle. The study required an understanding of the design procedures for pressure vessels. The ASME VIII Divisions 1 and 2 Code contains the most widely used procedures for the design of pressure vessels and various other components. The ASME Code is accurate and effective in calculating detailed dimensions of pressure vessel shells, and even components like nozzles, flanges and supports. The Code also contains properties for the vast range of materials used in the design of pressure vessels. However, stress calculations for the nozzle attachments, and their corresponding loads, are not given by the ASME Code. The Code contains allowable limits for the stresses calculated using the procedures given in the Welding Research Bulletins 107 and 297. These allowable limits are based on the materials yield and ultimate tensile stresses.

6.2 Design of Pressure Vessels under Internal Pressure and Piping Loads

This study investigates the use of the WRC Bulletins and compares stresses calculated theoretically with stresses determined by Finite Element Models generated using MSC PATRAN. Finite Element Analysis is believed to provide a more realistic approach with regards to the design of pressure vessels. The Finite Element Models were validated by obtaining convergence for values of the general primary membrane stress P_m (figure 3-7 and figure 3-8), to be within 5% (figure 3-9). These stresses are due to internal pressure alone and are determined by accurate theoretical equations. The difference between the theoretical and FEM values of P_m are considerably small (uncertainties range from 0% to 1.7%). However, greater uncertainties arise when local stresses are generated at the shell-to-nozzle junction.

By analysing various vessels, it was determined that FEM stresses, due to the combined loading of internal pressure and piping loads, are much greater than stresses calculated theoretically using WRC 107 (figure 3-10). Two factors are responsible for the marked differences between the FEM and theoretical results. The first factor concerns the pressure thrust load, created by the internal pressure, on the nozzle. This pressure thrust load increases the local stresses at the

shell-to-nozzle junction and becomes more severe if larger diameter nozzles are used. High internal pressures ranging from 1MPa to about 5MPa can create extremely large pressure thrust loads, thus, drastically increasing the stress concentration at the shell-to-nozzle junction (figure 3-12 and figure 3-13). For example, the theoretical stress obtained for Vessel 25 was 74.2MPa and the FEM stress, which includes the pressure thrust load, was 267MPa. Theoretically, WRC 368[36] was developed to determine the stresses caused by the pressure thrust load. However, the location and orientation of these stresses are not determined, thereby, limiting their use in conjunction with WRC 107. The FEM results indicated that the local stresses generated due to piping loads at the nozzle can be much greater at locations different from those given in WRC 107 (figure 3-17). As a result of these two factors the FEM local stresses due to the combined loading of piping loads at the nozzle and internal pressure, proved to be more accurate. FEM provides more accurate locations of these stresses and being more conservative, the results ensure the design of much safer pressure vessels (see [13], [25] and [30]). Apart from MSC PATRAN there are pressure vessel FEM software packages like PV-Elite/CodeCalc, NOZPRO, etc, that solely calculate local stresses and deformations at the shell-to-nozzle junction as well as stresses generated by other components. The development of these software packages have proven useful in determining the stress situations of pressure vessels. MSC PATRAN is a more powerful and accurate Finite Element software, therefore, it was used for this investigation. When local stresses in the shell exceed the allowable limits given by ASME VIII Div 2, it has been shown that increasing the shell thickness or the use of compensation pads can be useful.

6.3 Design of Pressure Vessels under External Pressure and Piping Loads

When designing vessels under external atmospheric pressure buckling becomes a crucial consideration. Buckling can occur at stresses well below the yield or ultimate tensile stress of the material, therefore, it is important to design a vessel that can withstand the effects of buckling. The effects of buckling on pressure vessels, subjected to external atmospheric pressure alone, have been investigated. Typical large to medium diameter vessels used in industry were chosen. The design for these vessels involves determining a critical buckling pressure P_{cr}. This critical buckling pressure must be greater than the applied external pressure and stresses generated by the applied external pressure must be within the critical buckling stress σ_{cr} calculated from P_{cr}. Various expressions and procedures to determine the critical buckling pressure have been investigated. These range from the early works of R Von Mises, later modified by Windenburg and Trilling, to the more recent procedures given in the ASME VIII Div 1 and 2 code. The study shows that the procedures found in the ASME code are closely related to the equations developed by Von Mises and Windenburg and Trilling. The

ASME Code uses two important charts, Geometric and Material, to determine the critical buckling pressure and stress.

As part of the study, a second FEM model, Model B, was developed to correlate the theoretical critical buckling pressures with FEM values. The results coincided quite well for the pressures given by Windenburg and Trilling and Von Mises (figures 5-8 to 5-11). The ASME code critical buckling pressures (figure 5-6 and 5-7) differed for some vessels due to the safety factor of 80% included in the Material Chart. The ASME procedures calculates the critical buckling stress or factor B to be within the elastic region of the material. Designing within the elastic region gives a much lower critical buckling stress and from this a much lower critical buckling pressure. MSC PATRAN has a node limit of 6000 nodes, therefore, a model with a much finer mesh would have generated more accurate results. However, the FEM model was validated by comparing FEM modes of buckling (number of lobes n) with the modes of buckling determined by the theoretical methods. The results coincided well, and, for vessels under external atmospheric pressure and piping loads, a third model (Model C) similar to Model B was also developed as part of this investigation.

There are currently no accepted procedures for the design of pressure vessels under the combined loading of external atmospheric pressure and piping loads. The objective of this study is to develop appropriate procedures for the design of these vessels and this was achieved in the following manner. Firstly, local loads cause local buckling to occur in the shell. The shell-to-nozzle junction, being a localized region, will have local stresses much greater than the critical buckling stress of the vessel (figure 5-20). For Vessel 5, the FEM local stress, for a 24" nozzle and atmospheric pressure, of 182MPa was greater than the ASME critical buckling stress of 156.2MPa. Secondly, the piping loads at the nozzle create deformations in the shell (figure 5-25), which reduce the critical buckling pressure. This study investigates the effects of these two factors. The vessels were subjected to various piping loads and atmospheric pressure. The FEM local stresses, generated at the shell-to-nozzle-junction, for some vessels were much greater than the critical buckling stresses calculated using the ASME Code procedures (figure 5-21 and figure 5-22). A FEM model, Model C, was used to analyze the buckling effects of various piping loads for the vessels. The 24" nozzle is typically the largest size nozzle used in industry. The FEM results showed a reduction in the critical buckling pressure as the piping loads were increased. For example, the FEM critical buckling pressure for Vessel 6 was determined to be 3.695MPa and this value was reduced to 2.734MPa as a result of applying piping loads for a 24" nozzle. It was also observed that these vessels buckled at a much lower mode than that predicted for the vessels under external atmospheric pressure only (figure 5-29 and figure 5-30). The reduction in the critical buckling pressure reduces the critical buckling

136

stress, thereby, causing the local stresses at the shell-to-nozzle junction to be much greater (figure 5-31 and 5-32). The results also indicated that by increasing the thickness of these vessels, the local stresses are reduced and can be lower than the reduced critical buckling stress. This is ideal to prevent local buckling from occurring. Using a 24" nozzle the FEM local stress, for Vessel 12, was determined to be 71.4MPa and this was much lower than the FEM reduced critical buckling stress of 176.1MPa.

Since piping loads at the nozzle reduce the critical buckling pressure, it was investigated that this has the same effect as that of vessels with geometric imperfections or out-of-roundness. There are currently equations for determining the reduced critical buckling pressures for imperfect or out-of-round vessels. The objective was to relate out-of-round theory to that of piping loads at the nozzle. Timoshenko[7] developed an equation for determining the increased compressive stress due to out-of-roundness in a cylinder. It is understood that both geometric imperfections and piping loads increase stress concentrations, therefore, Timoshenko's equation was related to maximum compressive stresses generated using WRC 107 for vessels under piping loads. The objective is to calculate an appropriate out-of-round value that can be used in an out-of-round equation to determine the reduced critical buckling pressure. In Appendix E, two random vessels were analyzed using the theoretical procedures developed. The theoretical reduced critical buckling pressures coincide quite well with the FEM values. To prevent local buckling from occurring, the local stresses generated at the shell-to-nozzle junction must be less than the reduced critical buckling stress calculated using the computation sheet given in Chapter 5, figure 5-33.

If local stresses are greater than the reduced critical buckling stress, the study showed that increasing the thickness of the shell will reduce the local stresses. Theoretically, reducing the length of the shells or using stiffening rings can increase the buckling strength of the vessel.

Chapter 7

CONCLUSION

A comparative study between the effects of internal pressure versus external pressure when combined with piping loads at the shell-to-nozzle junction of a pressure vessel has been undertaken. Various numerical models were analyzed theoretically as well as analytically using the Finite Element software, MSC PATRAN. For vessels under internal pressure and piping loads at the nozzle, the following conclusions were made :

1. The pressure thrust load created by the internal pressure increases the local stresses at the shell-to-nozzle junction.
2. Higher stresses may exist in locations that differ from those given in WRC 107.
3. The allowable limits given by the ASME Code are acceptable since they are related to the material properties of the vessel.
4. More accurate and conservative FEM stresses should be used, instead of WRC 107, when designing vessels under internal pressure and piping loads.

Extensive research with regard to the design of pressure vessels under external atmospheric pressure and piping loads was undertaken. Procedures for determining the reduced critical buckling pressure of a vessel under external atmospheric pressure and piping loads have been developed with the aid of finite element methods. The design should :

1. Determine σ_{cr}' using the computation sheet, figure 5-33 and table 5-5.
2. Determine the local stresses at the shell-to-nozzle junction, taking FEM values to be more accurate and conservative.
3. Compare the local stresses with σ_{cr}'. Redesign if local buckling occurs.

The effects of stiffening rings has not been explored in this study. For future study, the effects of stiffening rings and compensation pads could be a consideration in the design of vessels under external atmospheric pressure and piping loads at the nozzle. The FEM results are understood to represent a more realistic approach to the design of pressure vessels. It would be useful to correlate the theoretical results obtained with actual experimental data in a further exploration of this topic. Appendix F contains a paper, based on this study, to be submitted to the International Journal of Pressure Vessels and Piping.

Appendix A

Nozzle Reinforcement

GENERAL NOTE:
Includes consideration of these areas if
$S_n/S_v < 1.0$ (both sides of C)

2.5t or 2.5$t_n + t_e$
Use smaller value

h, 2.5t, 2.5t_i
Use smallest value

See UG-40
for limits of
reinforcement

d or $R_n + t_n + t$
Use larger value

d or $R_n + t_n + t$
Use larger value

For nozzle wall inserted through the vessel wall ——|—— For nozzle wall abutting the vessel wall
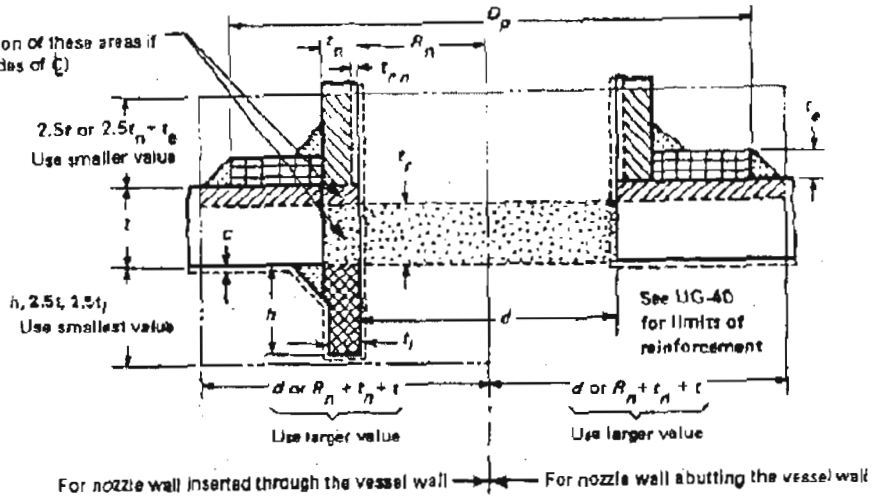
Without Reinforcing Element

$A = d\,t_r\,F + 2t_n\,t_r\,F(1 - f_{r1})$ — Area required

$A_1\begin{cases} = d(E_1 t - Ft_r) - 2t_n\,(E_1 t - Ft_r)\,(1 - f_{r1}) \\ = 2(t + t_n)(E_1 t - Ft_r) - 2t_n(E_1 t - Ft_r)(1 - f_{r1}) \end{cases}$ — Area available in shell; use larger value

$A_2\begin{cases} = 5(t_n - t_{rn})\,f_{r2}\,t \\ = 5(t_n - t_{rn})\,f_{r2}\,t_n \end{cases}$ — Area available in nozzle projecting outward; use smaller value

$A_3\begin{cases} = 5t\,t_i\,f_{r2} \\ = 5t_i\,h\,f_{r2} \\ = 2h\,t_i\,f_{r2} \end{cases}$ — Area available in inward nozzle; use smallest value

$A_{41} = $ outward nozzle weld $= (\text{leg})^2 f_{r2}$ — Area available in outward weld

$A_{43} = $ inward nozzle weld $= (\text{leg})^2 f_{r2}$ — Area available in inward weld

If $A_1 + A_2 + A_3 + A_{41} + A_{43} \geq A$ — Opening is adequately reinforced

If $A_1 + A_2 + A_3 + A_{41} + A_{43} < A$ — Opening is not adequately reinforced so reinforcing elements must be added and/or thicknesses must be increased

With Reinforcing Element Added

$A = $ same as A, above — Area required

$A_1 = $ same as A_1, above — Area available

$A_2\begin{cases} = 5(t_n - t_{rn})f_{r2}t \\ = 2(t_n - t_{rn})\,(2.5t_n + t_e)\,f_{r2} \end{cases}$ — Area available in nozzle projecting outward; use smaller area

$A_3 = $ same as A_3, above — Area available in inward nozzle

$A_{41} = $ outward nozzle weld $= (\text{leg})^2 f_{r3}$ — Area available in outward weld

$A_{42} = $ outer element weld $= (\text{leg})^2 f_{r4}$ — Area available in outer weld

$A_{43} = $ inward nozzle weld $= (\text{leg})^2 f_{r2}$ — Area available in inward weld

$A_5 = (D_p - d - 2t_n)\,t_e\,f_{r4}$ [Note (1)] — Area available in element

$A_1 + A_2 + A_3 + A_{41} + A_{42} + A_{43} + A_5 \geq A$ — Opening is adequately reinforced

NOTE:
(1) This formula is applicable for a rectangular cross-sectional element that falls within the limits of reinforcement.

ASME VIII Div 1 Fig. UG-37.1 NOMENCLATURE AND FORMULAS FOR REINFORCED OPENINGS

REPRODUCED TABLE OF SELECTIVE PIPE SCHEDULES AND WALL THICKNESSES

Imperial Nom. Size	Imperial Outside Diameter	Metric Outside Diameter		Std wall	Sch XS	Sch 160
1.500	1.900	48.260	ins	0.145	0.200	0.281
			mm	3.68	5.08	7.14
2.000	2.375	60.325	ins	0.154	0.218	0.344
			mm	3.91	5.54	8.74
2.500	2.875	73.025	ins	0.203	0.276	0.375
			mm	5.16	7.01	9.53
3.000	3.500	88.900	ins	0.216	0.300	0.438
			mm	5.49	7.62	11.13
4.000	4.500	114.300	ins	0.237	0.337	0.531
			mm	6.02	8.56	13.49
5.000	5.563	141.300	ins	0.258	0.375	0.625
			mm	6.55	9.53	15.88
6.000	6.625	168.275	ins	0.280	0.432	0.719
			mm	7.11	10.97	18.26
8.000	8.625	219.075	ins	0.322	0.500	0.906
			mm	8.18	12.70	23.01
10.000	10.750	273.050	ins	0.365	0.500	1.125
			mm	9.27	12.70	28.58
12.000	12.750	323.850	ins	0.375	0.500	1.312
			mm	9.53	12.70	33.33
14.000	14.000	355.600	ins	0.375	0.500	1.406
			mm	9.53	12.70	35.71
16.000	16.000	406.400	ins	0.375	0.500	1.594
			mm	9.53	12.70	40.49
18.000	18.000	457.200	ins	0.375	0.500	1.781
			mm	9.53	12.70	45.24
20.000	20.000	508.000	ins	0.375	0.500	1.969
			mm	9.53	12.70	50.01
22.000	22.000	558.800	ins	0.375	0.500	2.125
			mm	9.53	12.70	53.98
24.000	24.000	609.600	ins	0.375	0.500	2.344
			mm	9.53	12.70	59.54

TABLE 1-100

CRITERIA FOR ESTABLISHING ALLOWABLE STRESS VALUES FOR TABLES 1A AND 1B

Product/ Material	Below Room Temperature		Room Temperature and Above			
	Tensile Strength	Yield Strength	Tensile Strength		Yield Strength	
Wrought or cast ferrous and nonferrous	$\dfrac{S_T}{3.5}$	$\frac{2}{3}S_y$	$\dfrac{S_T}{3.5}$	$\dfrac{1.1}{3.5}S_T R_T$	$\frac{2}{3}S_y$	$\frac{2}{3}S_y R_y$ or $0.9S_y R_y$ [*Note*(1)]
Welded pipe or tube, ferrous and nonferrous	$\dfrac{0.85}{3.5}S_T$	$\frac{2}{3}\times 0.85S_y$	$\dfrac{0.85S_T}{3.5}$	$\dfrac{(1.1\times 0.85)}{3.5}S_T R_T$	$\frac{2}{3}\times 0.85S_y$	$\frac{2}{3}\times 0.85S_y R_y$ or $0.9\times 0.85S_y R_y$ [*Note*(1)]

TABLE 2-100(a)

CRITERIA FOR ESTABLISHING DESIGN STRESS INTENSITY VALUES FOR TABLES 2A AND 2B

Product/Material	Tensile Strength		Yield Strength	
Wrought or cast ferrous and nonferrous	$\frac{1}{3}S_T$	$\dfrac{1.1}{3}S_T R_T$	$\frac{2}{3}S_y$	$\frac{2}{3}S_y R_y$ or $0.9S_y R_y$ [*Note*(1)]
Welded pipe or tube, ferrous and nonferrous	$\dfrac{0.85S_T}{3.5}$	$\dfrac{(1.1\times 0.85)}{3}S_T R_T$	$\dfrac{0.85}{1.5}S_y$	$\dfrac{0.85}{1.5}S_y R_y$ or $0.9\times 0.85S_y R_y$ [*Note*(1)]

MATERIAL PROPERTIES :

SA 516 GRADE 70 : S_a = 137.9MPa

SA 106 GRADE B : S_a = 117.9MPa
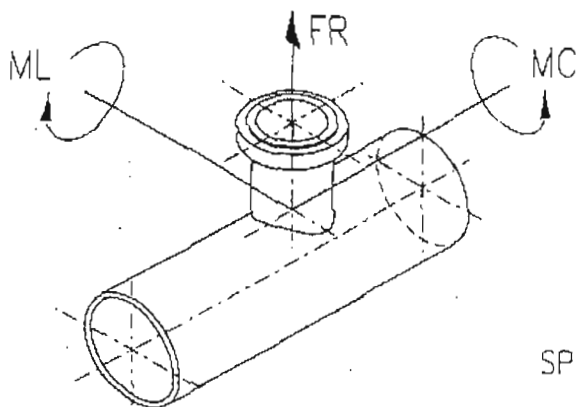
LEGEND:-

NPS & DN :- NOMINAL DIAMETER OF NOZZLE
FR :- RADIAL LOAD (N)
ML :- LONGITUDINAL MOMENT (Nm)
MC :- TANGENTIAL MOMENT (Nm)

ELLIPTICAL HEADS,
TORISPHERICAL HEADS,
SPHERICAL SHELLS & HEADS

$$M_{max.} = \sqrt{ML^2 + MC^2}$$

NPS	DN	FR (N)	ML (Nm)	MC (Nm)
2"	50	3150	2100	1450
3"	80	5040	3360	2320
4"	100	6300	4200	2900
6"	150	9450	6300	4350
8"	200	12600	8400	5800
10"	250	15750	10500	7250
12"	300	18900	12600	8700
14"	350	22050	14700	10150
16"	400	25200	16800	11600
18"	450	28350	18900	13050
20"	500	31500	21000	14500
24"	600	35500	24800	16900
28"	700	39500	28500	19300
32"	800	43500	32400	21700
36"	900	47500	36200	24100
40"	1000	51500	40000	26500
48"	1200	59500	47600	31300
✳ WRC 107 EQUIVALENT		−P (N)	M2 (Nm)	M1 (Nm)

✳ WRC SYMBOLOGY SHOWN FOR INFORMATION

Seq Sub
SASOL 0259 01

NOTE:-

1. FOR NOZZLE LOAD REQUIREMENTS ON PRESSURE VESSELS
OTHER THAN SHELL & TUBE HEAT EXCHANGERS SEE STDD-4039A

SASOL

No	DESCRIPTION OF REVISIONS	DRAWN	APPR.	DATE
01				
CHARGE No: SH31A		DIMENSIONS IN mm U.O.S.		
CAD FILE No.	...\SH31\STDD\4039B-MC.DGN			

NOZZLE LOAD REQUIREMENTS
FOR HEAT EXCHANGERS

SASOL DRG.No. STDD-4039B | REV | 01 | SHT 1/1

Foster Wheeler Piping Loads

HEAT EXCHANGER GROUP

GENERAL REQUIREMENTS
FOR HEAT EXCHANGERS

FOSTER WHEELER
ENGINEERING STANDARD

25722-21A1

PAGE 15 OF 16
REV 01
DSN 542

13.0 HEAT EXCHANGER NOZZLE LOADS AND MOMENTS /02\

HEAT EXCHANGER NOZZLE LOADS AND MOMENTS. (TO BE USED AS A BASIS FOR PIPING DESIGN)											
LOADS AND MOMENTS (F-KN, M-KNM) (APPLIED AT NOZZLE TO CYLINDER INTERSECTION)											
PIPE N.B.	FLANGE RATING										
INCHES	150#		300#		600#		900#		1500#		2500#	
	Fxyz	Mxyz	Fxyz	Mxyz	Fxyz	Mxyz	Fxyz	Mxyz	Fxyz	Mxyz	Fxyz	Mxyz
2	1.0	0.2	1.0	0.2	1.2	0.3	1.5	0.3	1.8	0.4	2.0	0.5
3	1.5	0.6	1.5	0.6	2.0	0.8	2.2	1.0	2.5	1.2	3.0	1.5
4	3.0	1.0	3.0	1.2	3.5	1.5	3.5	1.7	4.0	2.0	4.5	2.6
6	5.0	2.5	5.0	3.0	6.5	3.0	5.5	3.3	6.0	3.5	8.0	4.0
8	8.0	5.0	8.0	6.0	9.0	7.0	9.0	9.0	11.0	11.0	13.0	13.0
10	10.0	7.0	10.0	8.0	12.0	10.0	12.0	12.0	4.0	14.0	16.0	16.0
12	12.0	8.0	12.0	9.0	14.0	12.0	14.0	14.0	16.0	16.0	18.0	18.0
14	14.0	9.0	14.0	10.0	18.0	14.0	16.0	16.0	18.0	18.0	20.0	20.0
16	16.0	10.0	16.0	12.0	18.0	16.0	18.0	18.0	20.0	20.0	22.0	22.0
18	18.0	12.0	18.0	14.0	20.0	18.0	22.0	22.0	24.0	24.0	26.0	26.0
20	20.0	14.0	20.0	16.0	22.0	20.0	24.0	24.0	26.0	26.0	28.0	28.0
24	24.0	20.0	24.0	20.0	26.0	24.0	28.0	28.0	30.0	30.0	34.0	34.0

26   26   22
28   28   26   + VE RADIAL LOADS 'PUSH'

NOTES

1. The tabulated loads and moments at the nozzle to cylinder intersection are the minimum which the Heat Exchanger design must accommodate, except as noted in 2, 3, and 4 below.

2. For High Alloy Heat Exchangers (excluding alloy clad) designed for temperatures between -100°C and +250°C the loads and moments may be reduced to a minimum of 50% of the tabulated values.

3. For Carbon Steel and Low Alloy Heat Exchangers designed for temperatures between -50°C and +250°C the loads and moments may be reduced to a minimum of 75% of the tabulated values.

4. In exceptional cases (e.g. where application of the tabulated loads increases the shell/channel barrel thickness) the loads may be reduced further by agreement with Purchaser. Normally the minimum loads are, 50%, for CS and low alloy, or 25%, for high alloy equipment, of the tabulated values.

Appendix B

FEM Stress Plots for Vessels 16-25 under internal pressure alone (0.26 and 1.05MPa)
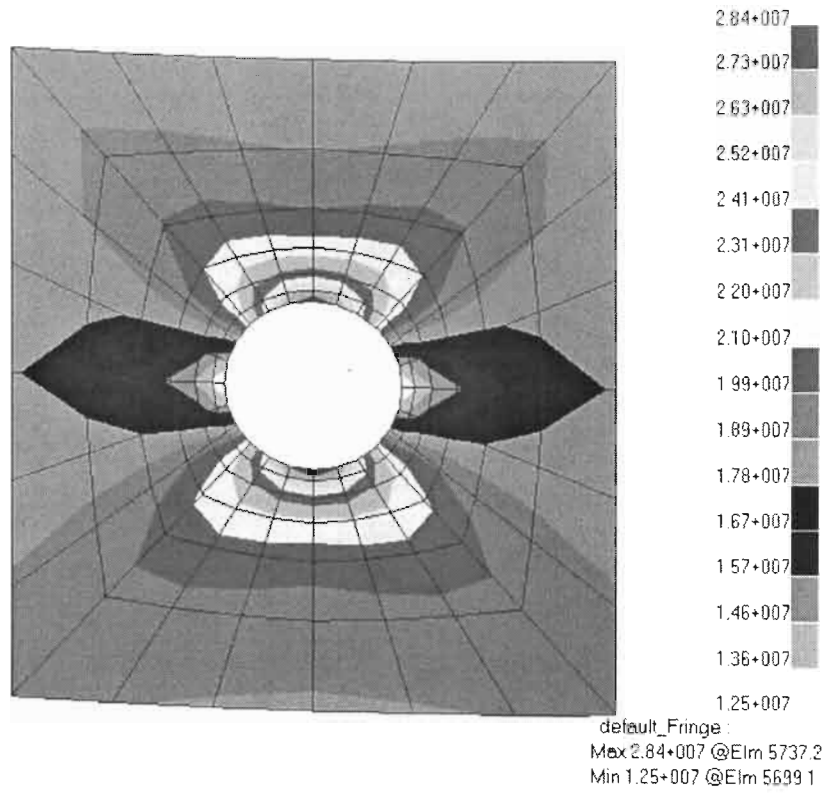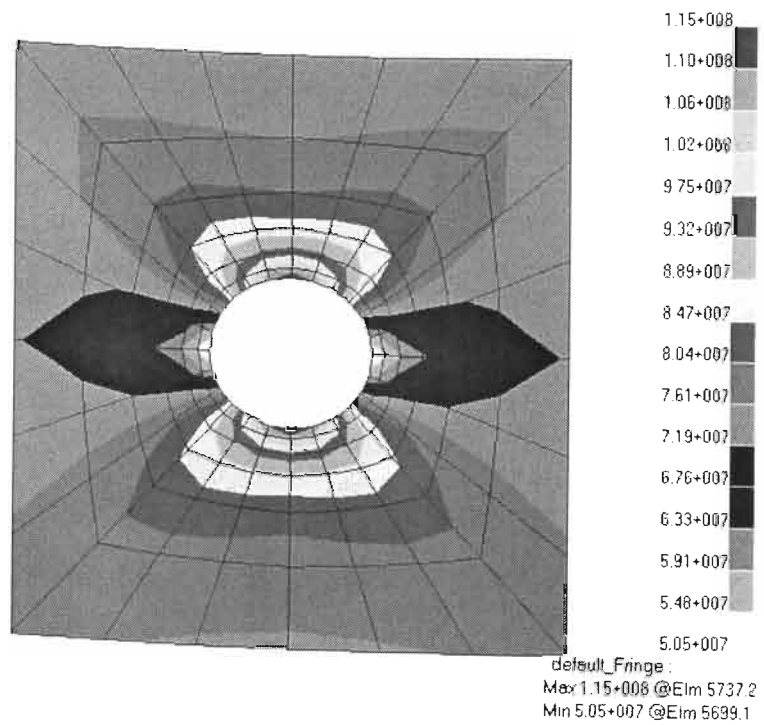
default_Fringe :
Max 2.84+007 @Elm 5737.2
Min 1.25+007 @Elm 5699.1

Vessel 16 – Internal pressure 0.26MPa

default_Fringe :
Max 1.15+008 @Elm 5737.2
Min 5.05+007 @Elm 5699.1

Vessel 21 – Internal Pressure 1.05MPa

3.38+007	
3.24+007	
3.10+007	
2.96+007	
2.82+007	
2.68+007	
2.54+007	
2.40+007	
2.26+007	
2.12+007	
1.98+007	
1.84+007	
1.70+007	
1.56+007	
1.42+007	
1.28+007	
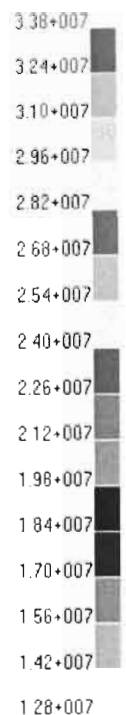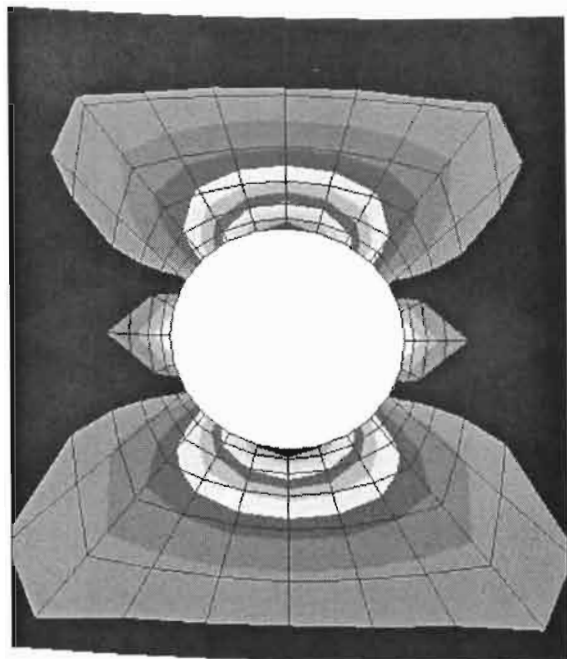
default_Fringe
Max 3.38+007 @Elm 5983.2
Min 1.28+007 @Elm 5945.1

Vessel 17 – Internal Pressure 0.26MPa

1.37+008	
1.31+008	
1.25+008	
1.20+008	
1.14+008	
1.08+008	
1.03+008	
9.71+007	
9.14+007	
8.58+007	
8.01+007	
7.45+007	
6.88+007	
6.32+007	
5.75+007	
5.19+007	
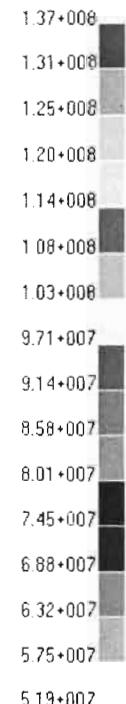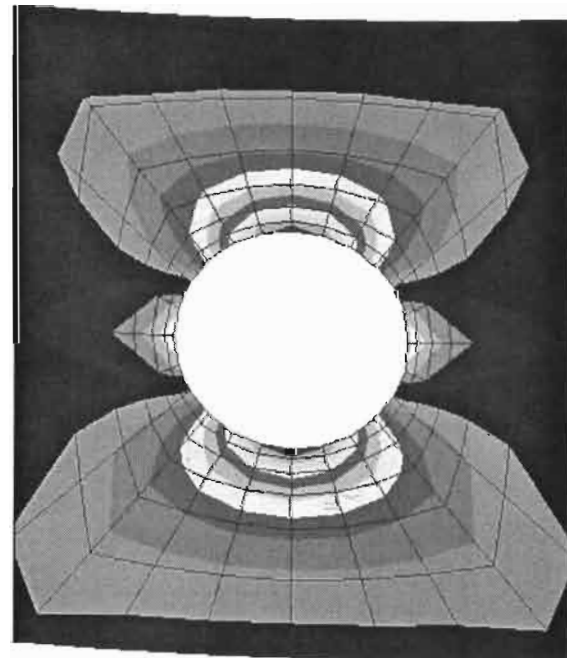
default_Fringe :
Max 1.37+008 @Elm 5983.2
Min 5.19+007 @Elm 5945.1

Vessel 22 – Internal Pressure 1.05MPa

147
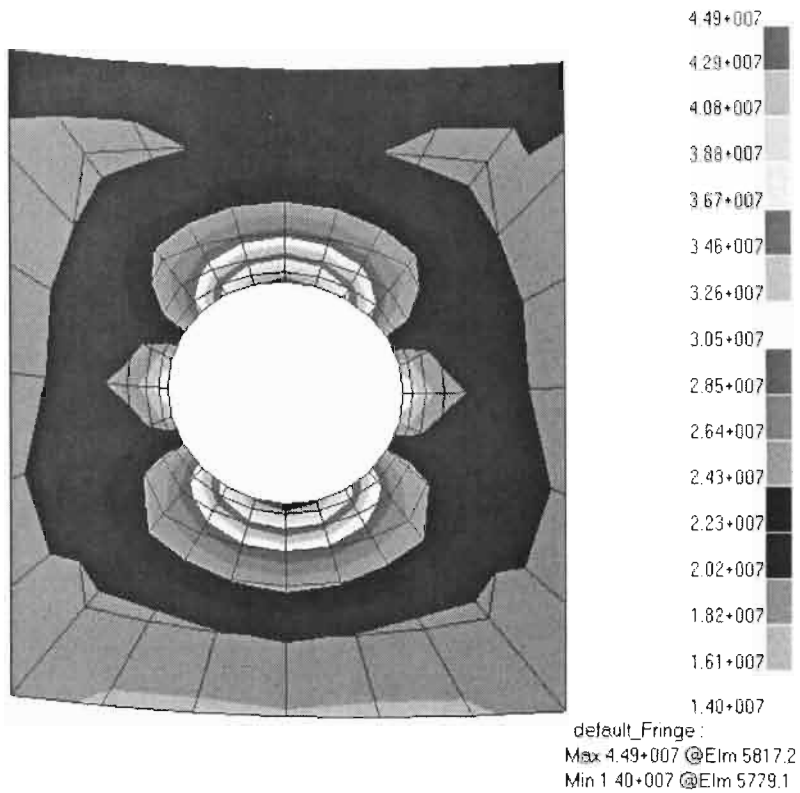
Vessel 18 – Internal Pressure 0.26MPa
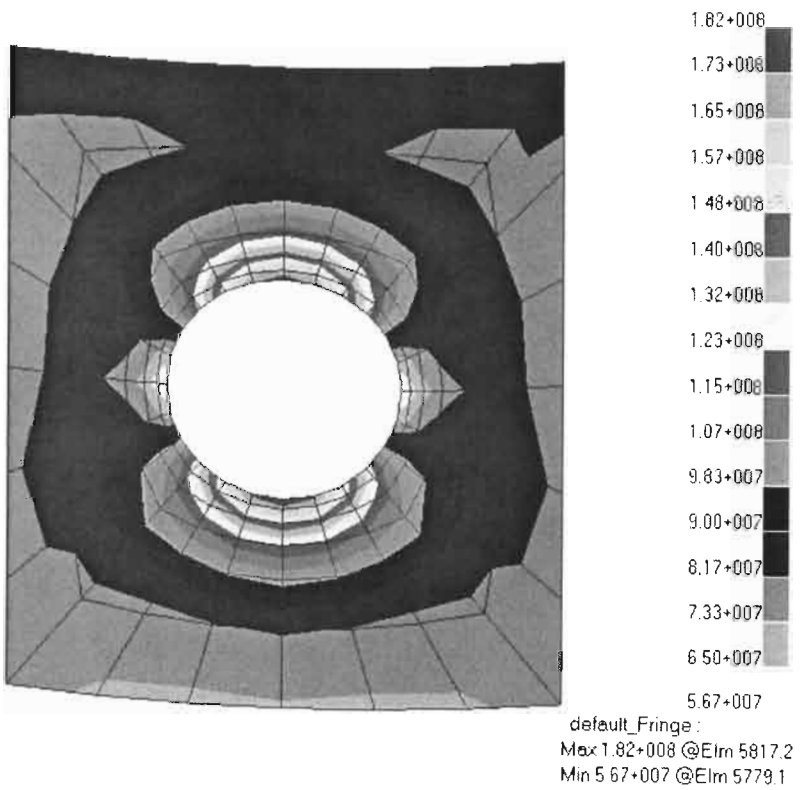
Vessel 23 – Internal Pressure 1.05MPa

148
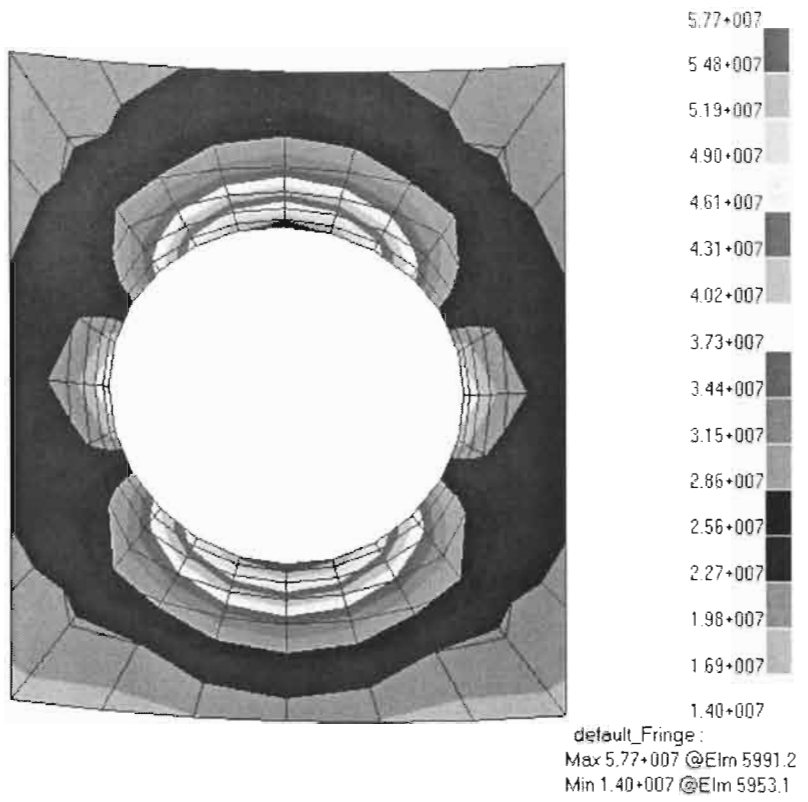
Vessel 19 – Internal Pressure 0.26MPa
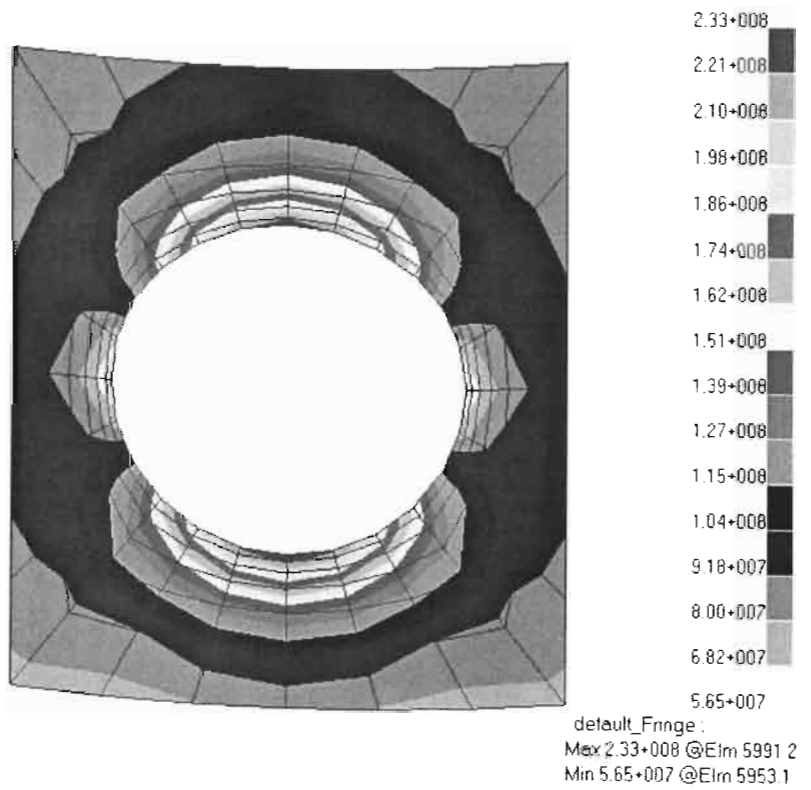
Vessel 24 – Internal Pressure 1.05MPa
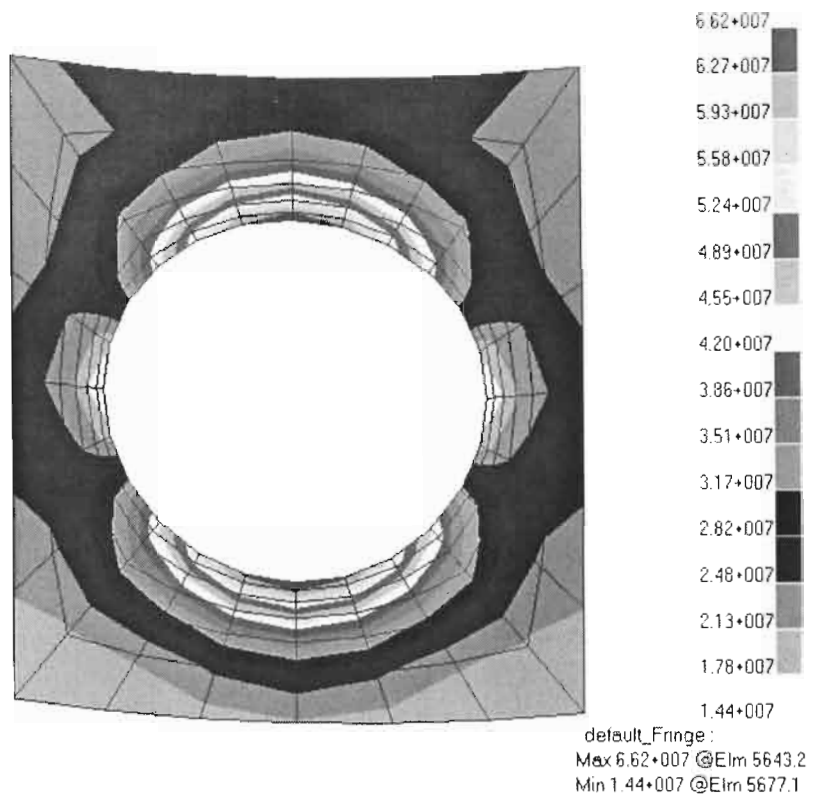
Vessel 20 – Internal Pressure 0.26MPa
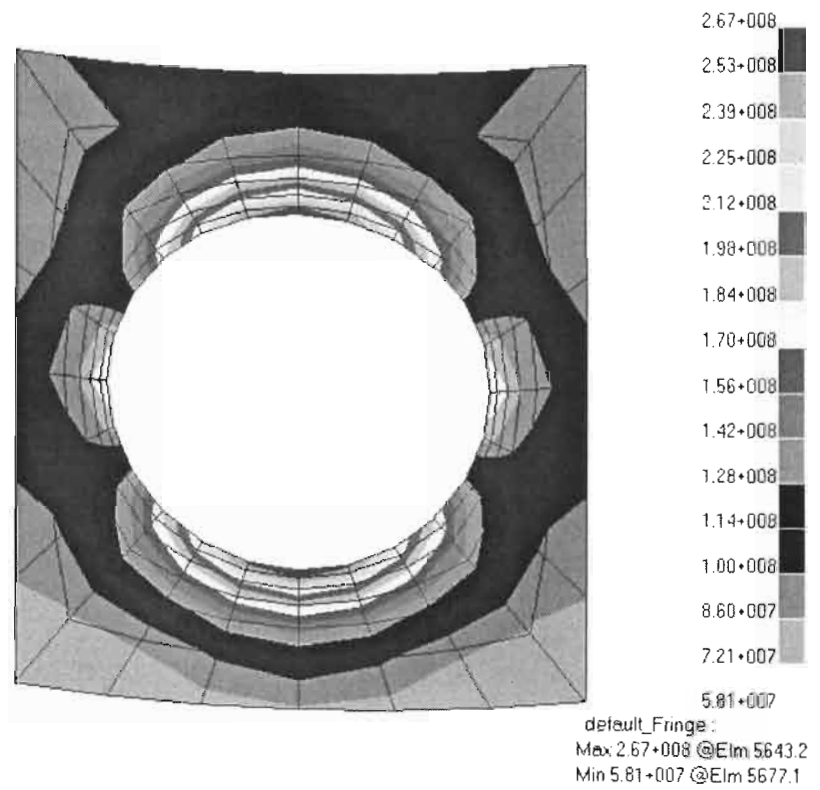
Vessel 25 – Internal Pressure 1.05MPa

FEM Stress Plots for Vessels 16-25 under piping loads alone (SASOL)

	3.28+008
	3.09+008
	2.89+008
	2.70+008
	2.50+008
	2.31+008
	2.11+008
	1.92+008
	1.72+008
	1.52+008
	1.33+008
	1.13+008
	9.39+007
	7.43+007
	5.48+007
	3.52+007

default_Fringe :
Max 3.28+008 @Elm 8781.2
Min 3.52+007 @Elm 8804.2
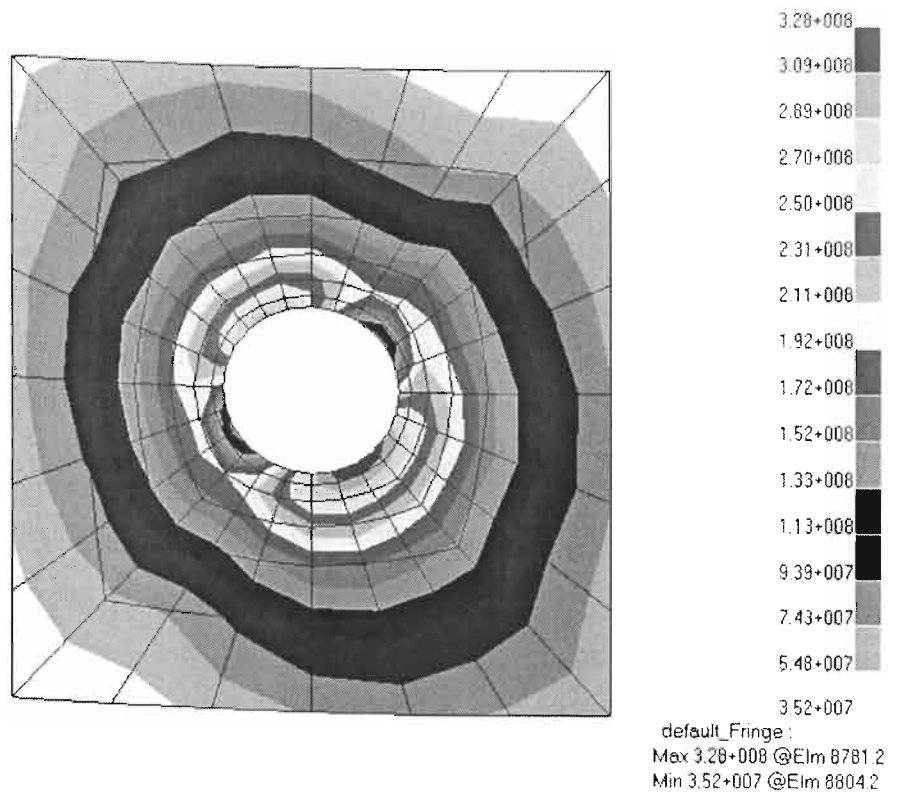
Vessels 16 and 21 – SASOL Nozzle Loads only

	3.71+008
	3.48+008
	3.25+008
	3.02+008
	2.79+008
	2.56+008
	2.34+008
	2.11+008
	1.88+008
	1.65+008
	1.42+008
	1.19+008
	9.64+007
	7.36+007
	5.07+007
	2.79+007

default_Fringe :
Max 3.71+008 @Elm 5577.2
Min 2.79+007 @Elm 5616.2
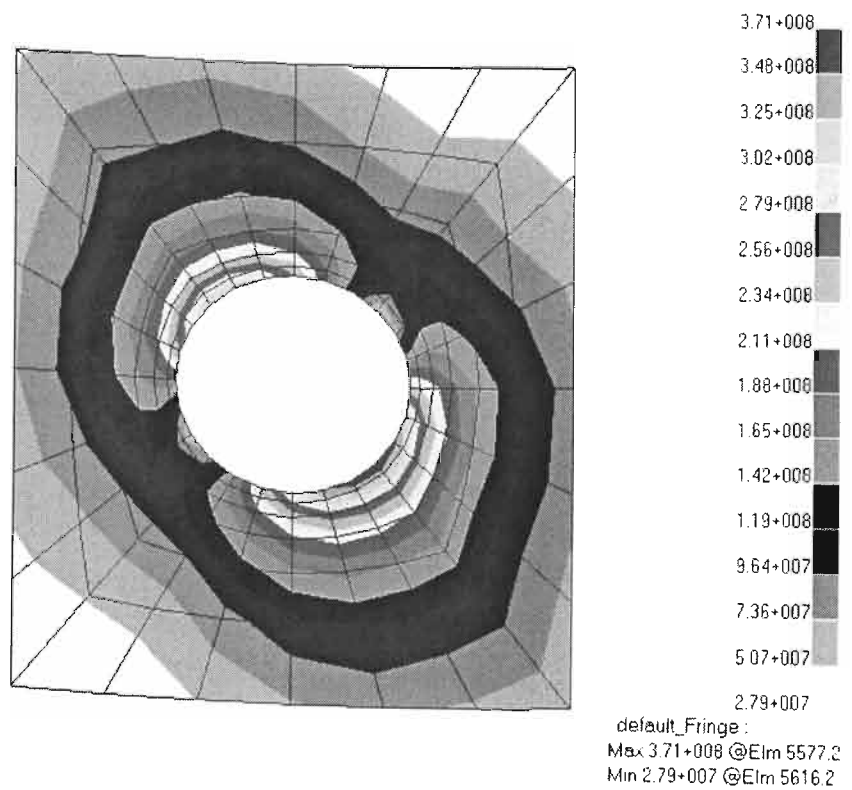
Vessels 17 and 22 – SASOL Nozzle Loads only

151
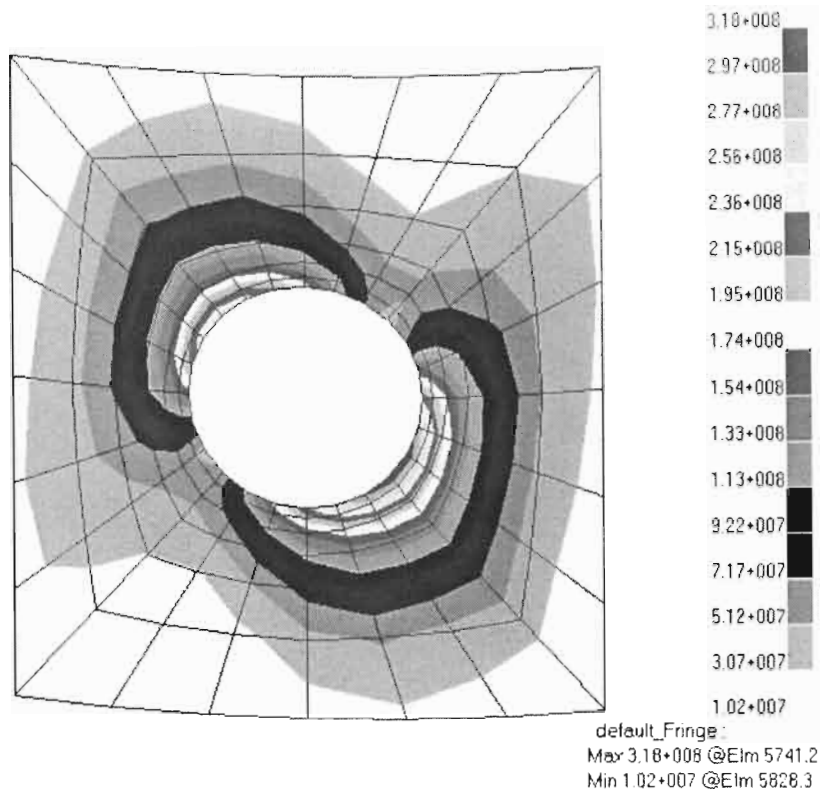
Vessels 18 and 23 – SASOL Nozzle Loads only
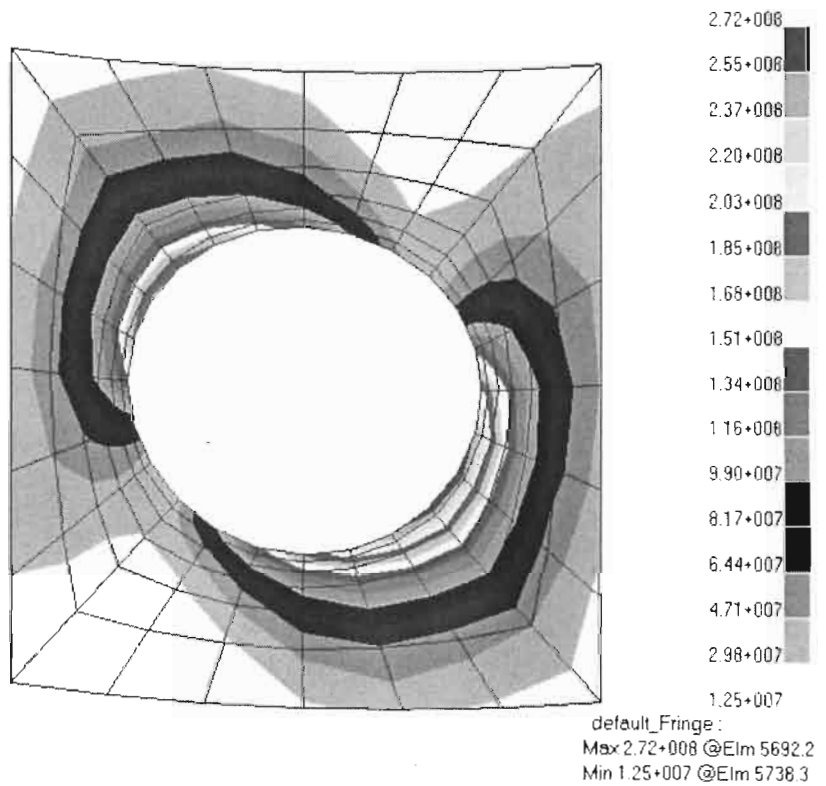
Vessels 19 and 24 – SASOL Nozzle Loads only

default_Fringe :
Max 2.48+008 @Elm 5644.2
Min 1.23+007 @Elm 5684.3
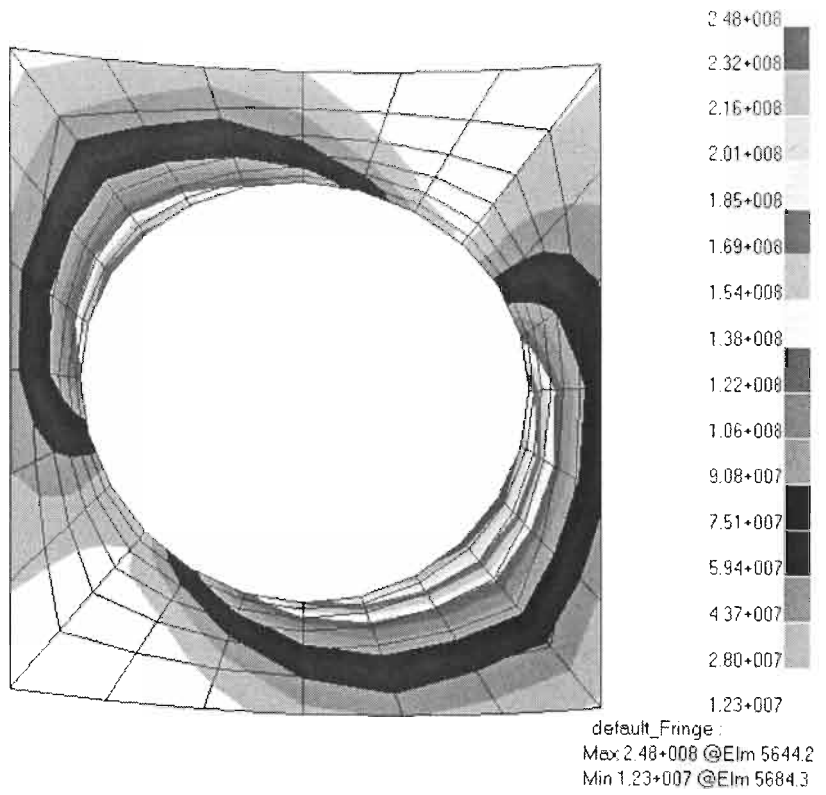
Vessels 20 and 25 – SASOL Nozzle Loads only

FEM Stress Plots for Vessels 16-25 under combined loading of internal pressure and piping loads
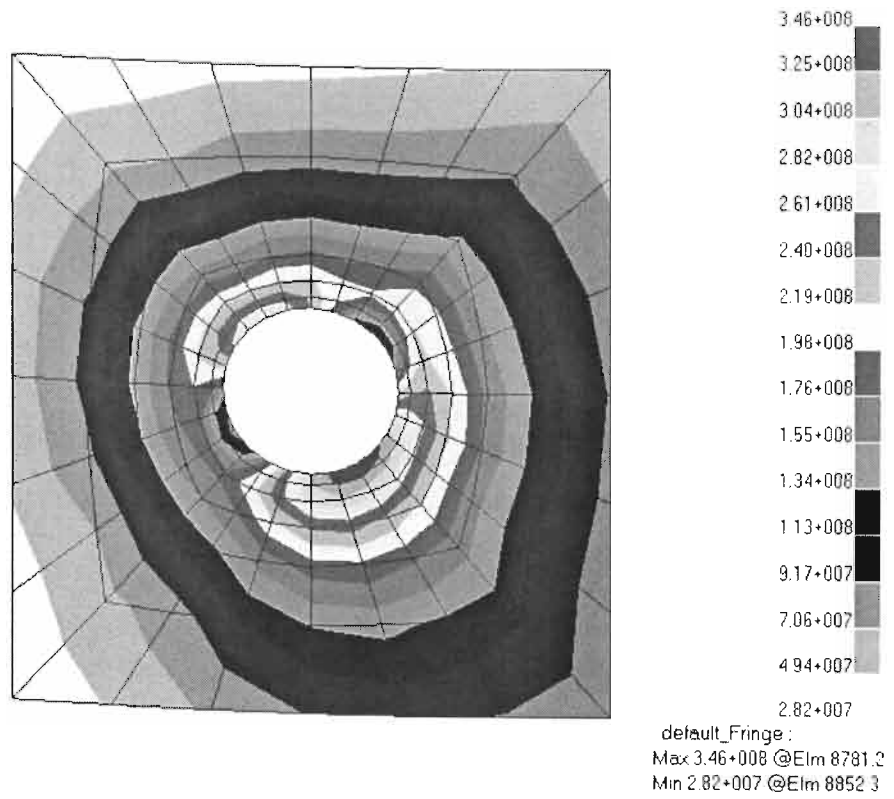
Vessel 16 – Combined Stress Intensity _S_
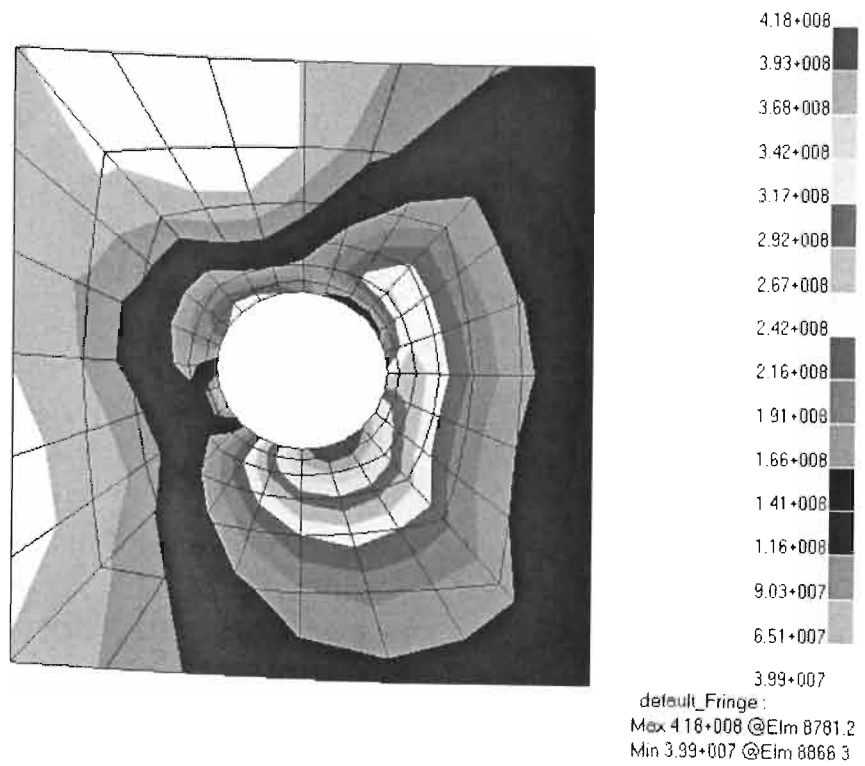
Vessel 21 – Combined Stress Intensity _S_
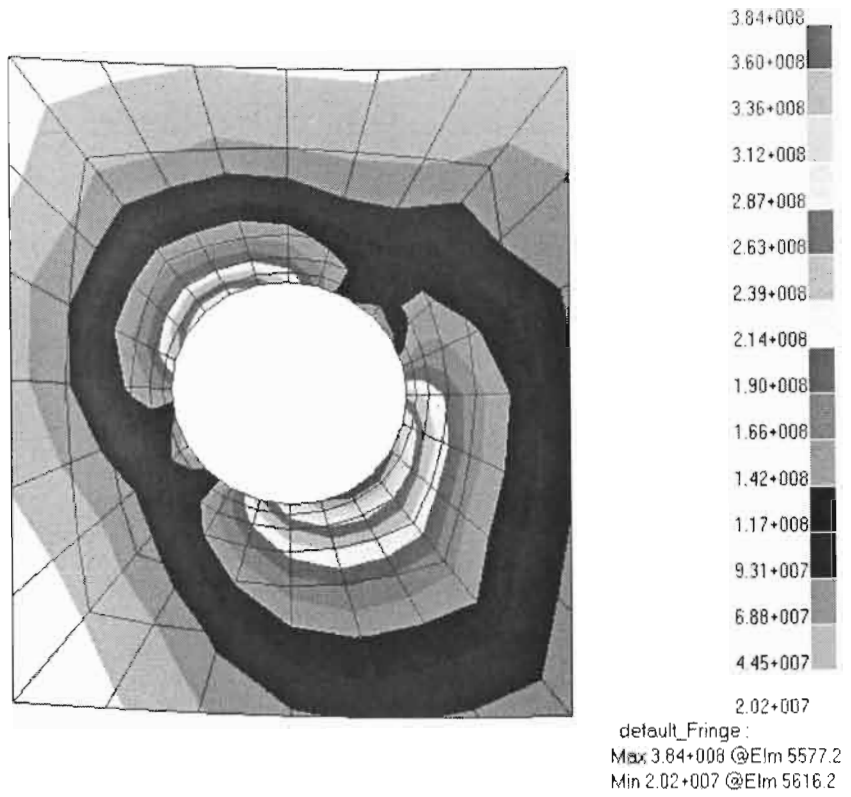
Vessel 17 – Combined Stress Intensity S
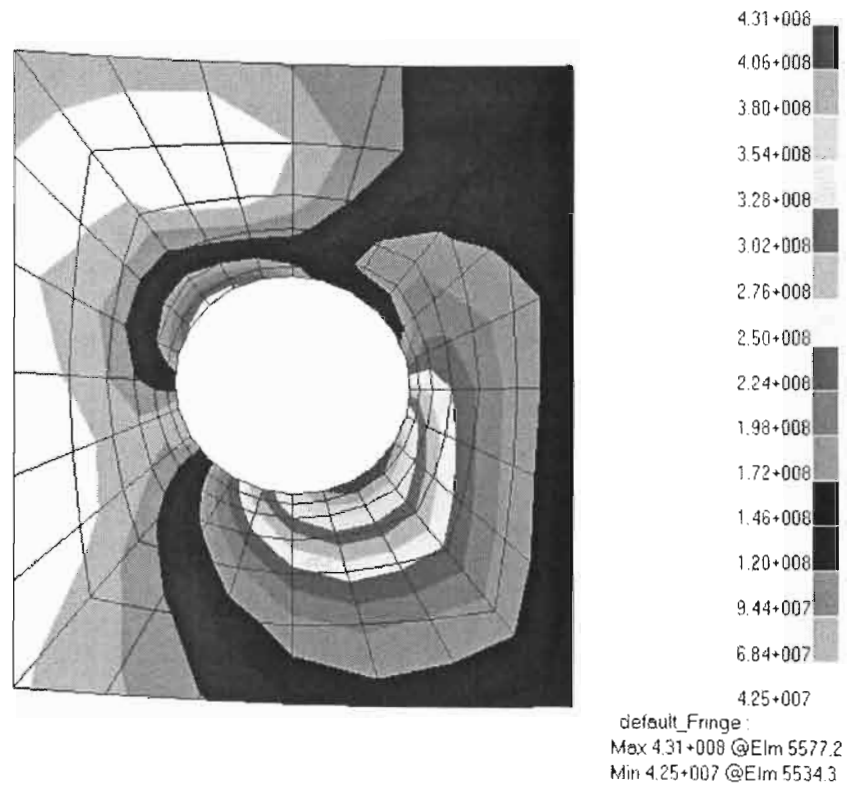
Vessel 22 – Combined Stress Intensity S

default_Fringe :
Max 3.40+008 @Elm 5741.2
Min 9.83+006 @Elm 5779.2
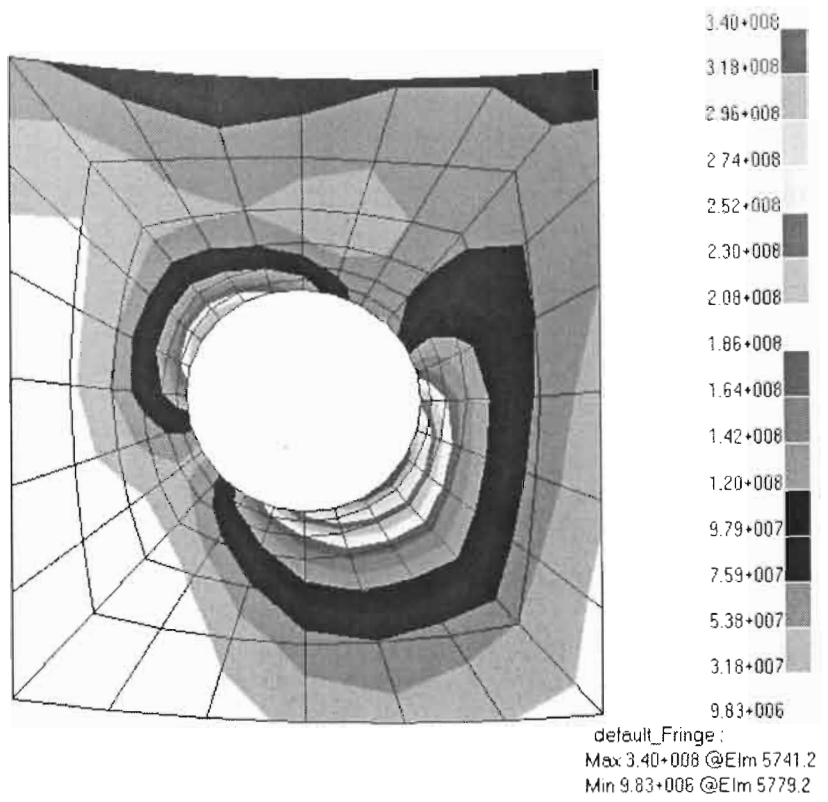
Vessel 18 – Combined Stress Intensity *S*

default_Fringe :
Max 4.14+008 @Elm 5741.2
Min 3.91+007 @Elm 5796.3
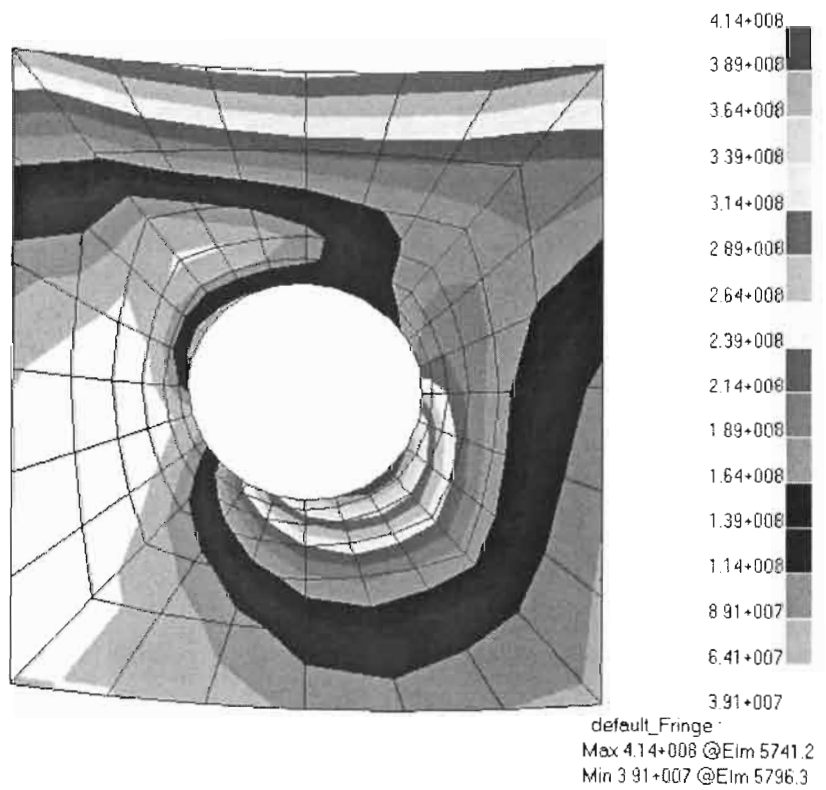
Vessel 23 – Combined Stress Intensity *S*

default_Fringe :
Max 3.00+008 @Elm 5693.2
Min 1.07+007 @Elm 5731.2
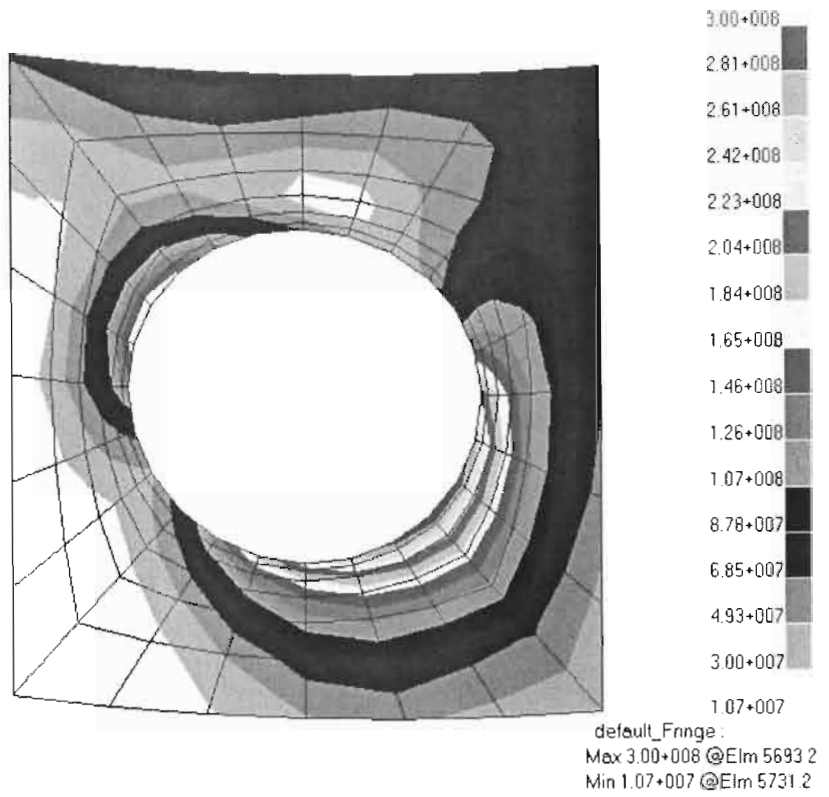
Vessel 19 – Combined Stress Intensity S

default_Fringe :
Max 4.13+008 @Elm 5709.2
Min 4.60+007 @Elm 5748.2
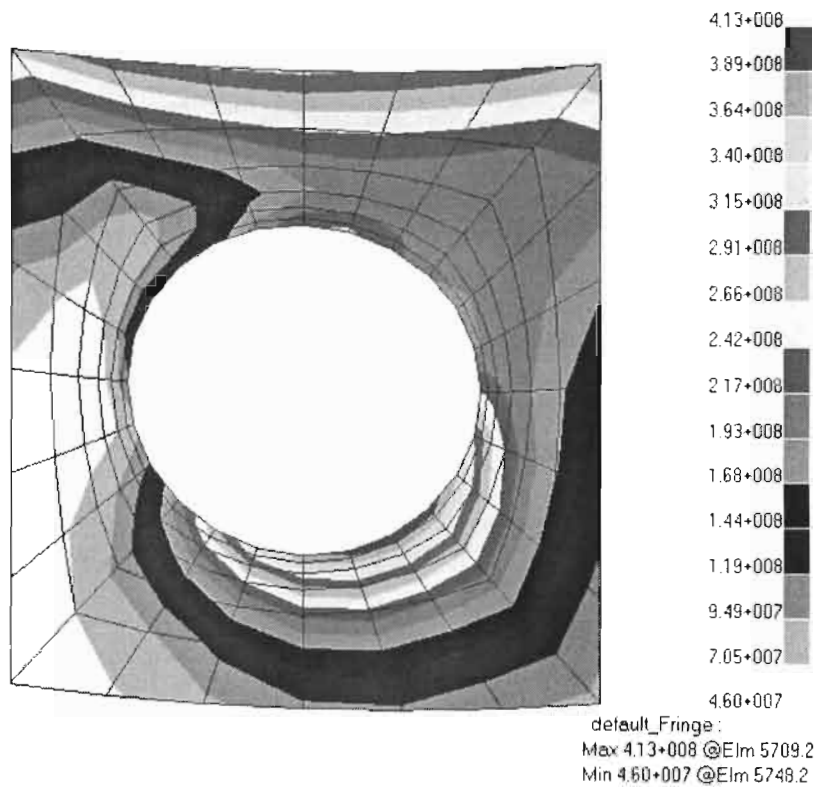
Vessel 24 – Combined Stress Intensity S

157
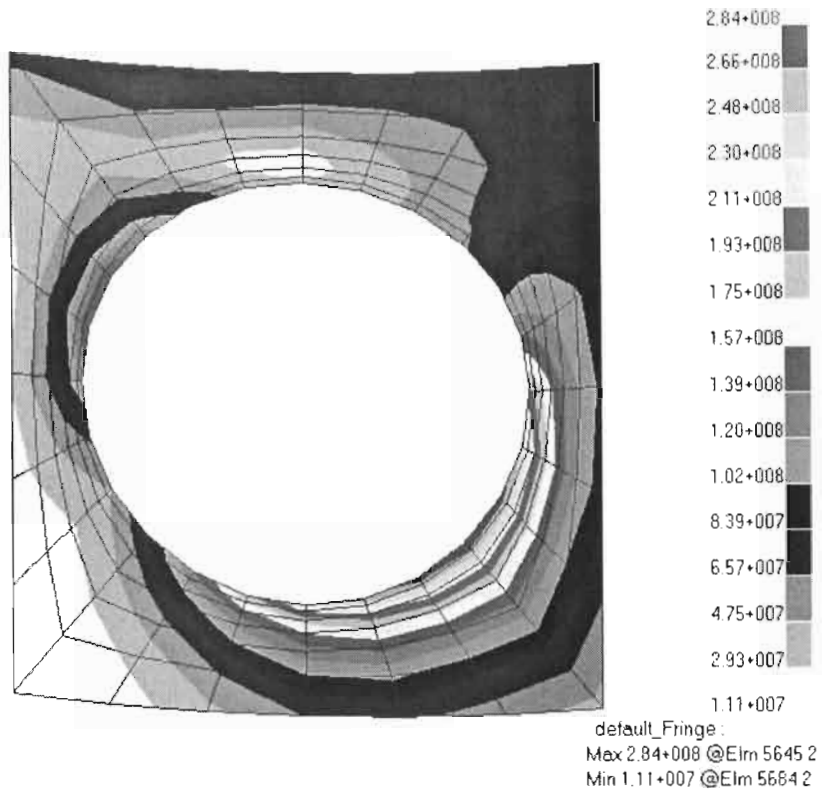
Vessel 20 – Combined Stress Intensity S
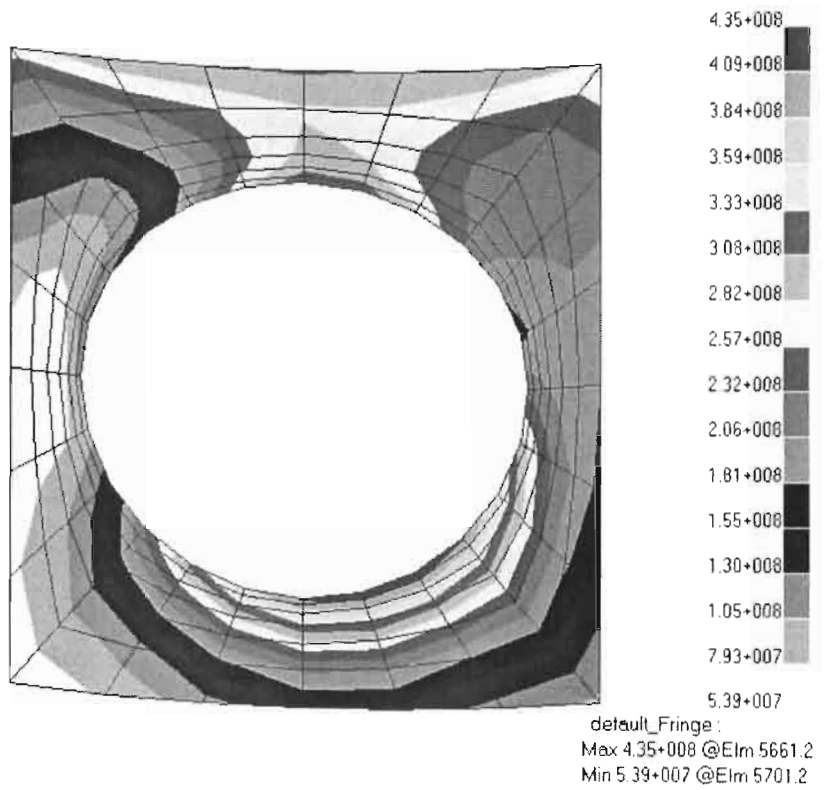
Vessel 25 – Combined Stress Intensity S

158

Appendix C

Numerical Results for Vessels under External Pressure										
Vessels	Do (mm)	T (mm)	CA (mm)	L (mm)	n	E (GPa)	Pcr(W&T) (MPa)	Pcr(ASME) (MPa)	Pcr Von Mises (MPa)	Pcr FEM (MPa)
1	2800	8	-	2000	8	200	0.318	0.330	0.329	0.385
2	2800	10	-	2000	8	200	0.555	0.570	0.583	0.667
3	2800	12	-	2000	8	200	0.875	0.900	0.950	1.046
4	2800	14	-	2000	7	200	1.287	1.320	1.347	1.557
5	2800	16	-	2000	7	200	1.797	1.800	1.900	2.126
6	2800	20	-	2000	7	200	3.139	2.532	3.459	3.695
7	1200	8	-	2000	4	200	1.132	1.140	1.202	1.323
8	1200	10	-	2000	4	200	1.978	1.980	2.032	2.397
9	1200	12	-	2000	4	200	3.120	3.090	3.215	3.570
10	1200	14	-	2000	4	200	4.587	3.960	4.822	5.104
11	1200	16	-	2000	4	200	6.405	4.830	6.923	7.069
12	1200	20	-	2000	4	200	11.189	6.641	12.889	12.533

Codecalc external pressure computation sheet

Input Echo, Component   1,   Description: ext1

User Entered Minimum Design Metal Temperature		21.00 C
Design External Pressure	PEXT	0.10 N./sq.mm.
Temperature for External Pressure		37.78 C
External Pressure Chart Name	CS-2	
Include Hydrostatic Head Components	NO	
Material Specification (Not Normalized)	SA-516 70	
Allowable Stress At Temperature	S	137.90 N./mm²
Allowable Stress At Ambient	SA	137.90 N./mm²
Curve Name for Chart UCS 66	B	
Joint efficiency for Shell Joint	E	1.00
Design Length of Section	L	2000.0000 mm.
Outside Diameter of Cylindrical Shell	D	2800.0000 mm.
Minimum Thickness of Pipe or Plate	T	8.0000 mm.
Corrosion Allowance	CA	0.0000 mm.

Type of Element: Cylindrical Shell

EXTERNAL PRESSURE RESULTS, SHELL NUMBER   1, Desc.: ext1
ASME Code, Section VIII, Division 1, 1998, A-99

External Pressure Chart CS-2 at		148.90 C
Elastic Modulus for Material		199955.00 N./sq.mm.

Results for Max. Allowable External Pressure (Emawp):

Corroded Thickness of Shell	TCA	8.0000 mm.
Outside Diameter of Shell	OD	2800.0000 mm.
Design Length of Cylinder or Cone	SLEN	2000.0000 mm.
Diameter / Thickness Ratio	(D/T)	350.0000
Length / Diameter Ratio	LD	0.7143
Geometry Factor, A f(DT,LD)	A	0.0002827
Materials Factor, B, f(A, Chart)	B	28.2604 N./mm²
Maximum Allowable Working Pressure		0.11 N./sq.mm.

EMAWP = (4*B)/(3*(D/T)) = (4 * 28.2604)/(3 * 350.0000) = 0.1077

Results for Reqd Thickness for Ext. Pressure (Tca):

Corroded Thickness of Shell	TCA	7.8728 mm.
Outside Diameter of Shell	OD	2800.0000 mm.
Design Length of Cylinder or Cone	SLEN	2000.0000 mm.
Diameter / Thickness Ratio	(D/T)	355.6560
Length / Diameter Ratio	LD	0.7143
Geometry Factor, A f(DT,LD)	A	0.0002760
Materials Factor, B, f(A, Chart)	B	27.5889 N./mm²
Maximum Allowable Working Pressure		0.10 N./sq.mm.

EMAWP = (4*B)/(3*(D/T)) = (4 * 27.5889)/(3 * 355.6560) = 0.1034

Results for Maximum Length Between Stiffeners (Slen):

Corroded Thickness of Shell	TCA	8.0000	mm.
Outside Diameter of Shell	OD	2800.0000	mm.
Design Length of Cylinder or Cone	SLEN	2077.7944	mm.
Diameter / Thickness Ratio	(D/T)	350.0000	
Length / Diameter Ratio	LD	0.7421	
Geometry Factor, A f(DT,LD)	A	0.0002716	
Materials Factor, B, f(A, Chart)	B	27.1504	N./mm²
Maximum Allowable Working Pressure		0.10	N./sq.mm.

EMAWP = (4*B)/(3*(D/T)) = (4 * 27.1504)/(3 * 350.0000) = 0.1034

SUMMARY of EXTERNAL PRESSURE RESULTS:

Allowable Pressure at Corroded thickness	0.11	N./sq.mm.
Required Pressure as entered by User	0.10	N./sq.mm.
Required Thickness including Corrosion all.	7.8728	mm.
Actual Thickness as entered by User	8.0000	mm.
Maximum Length for Thickness and Pressure	2077.794	mm.
Actual Length as entered by User	2000.00	mm.

The CODECALC Program, (c) 1989-2000 by COADE Engineering Software
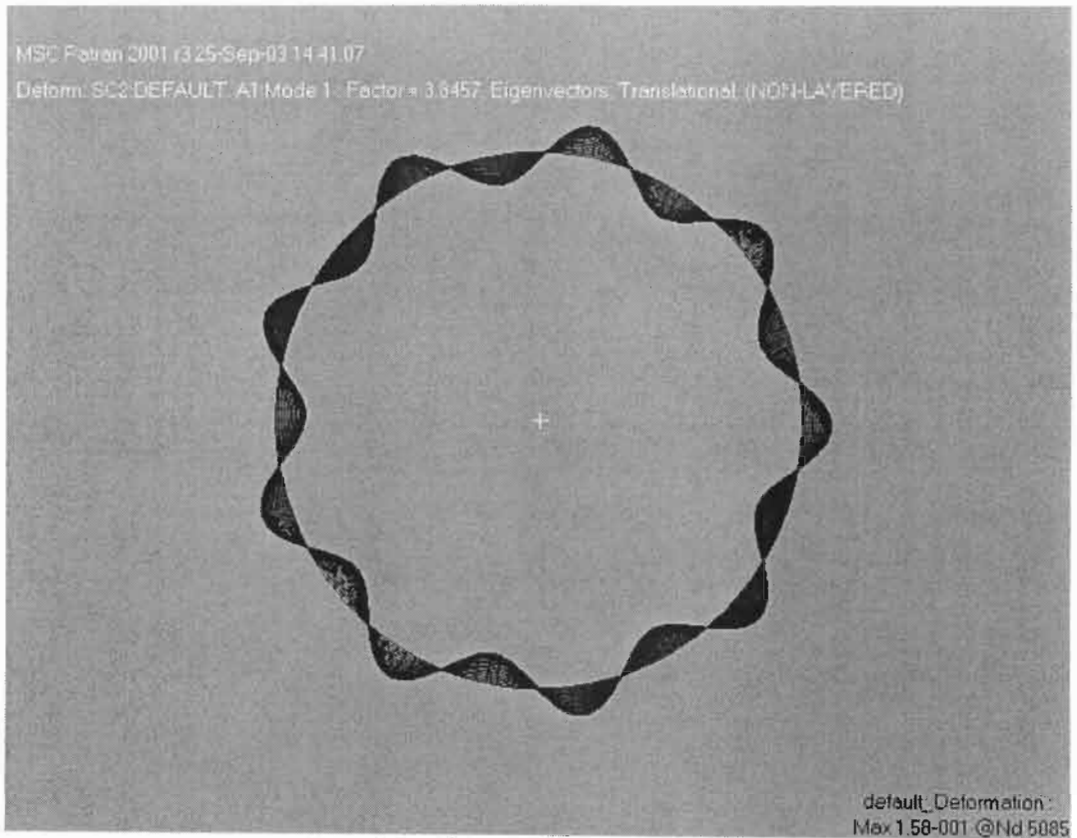
Vessel 1 – External Pressure 0.1MPa
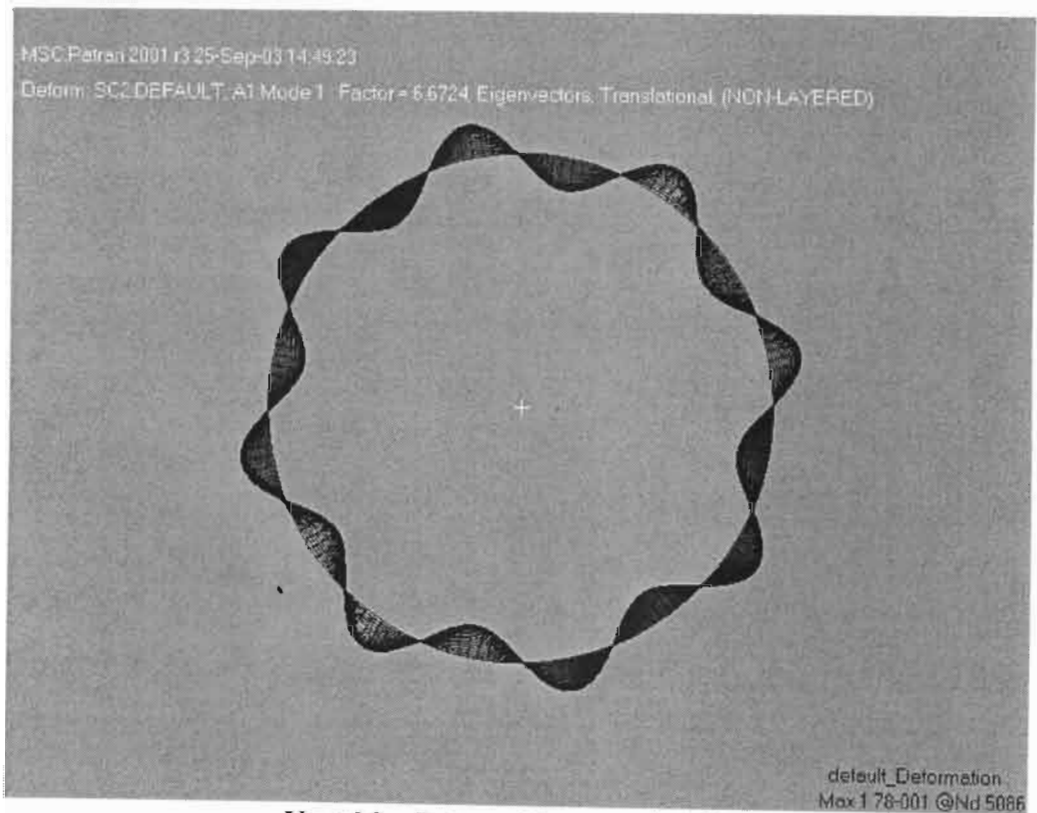
Vessel 2 – External Pressure 0.1MPa
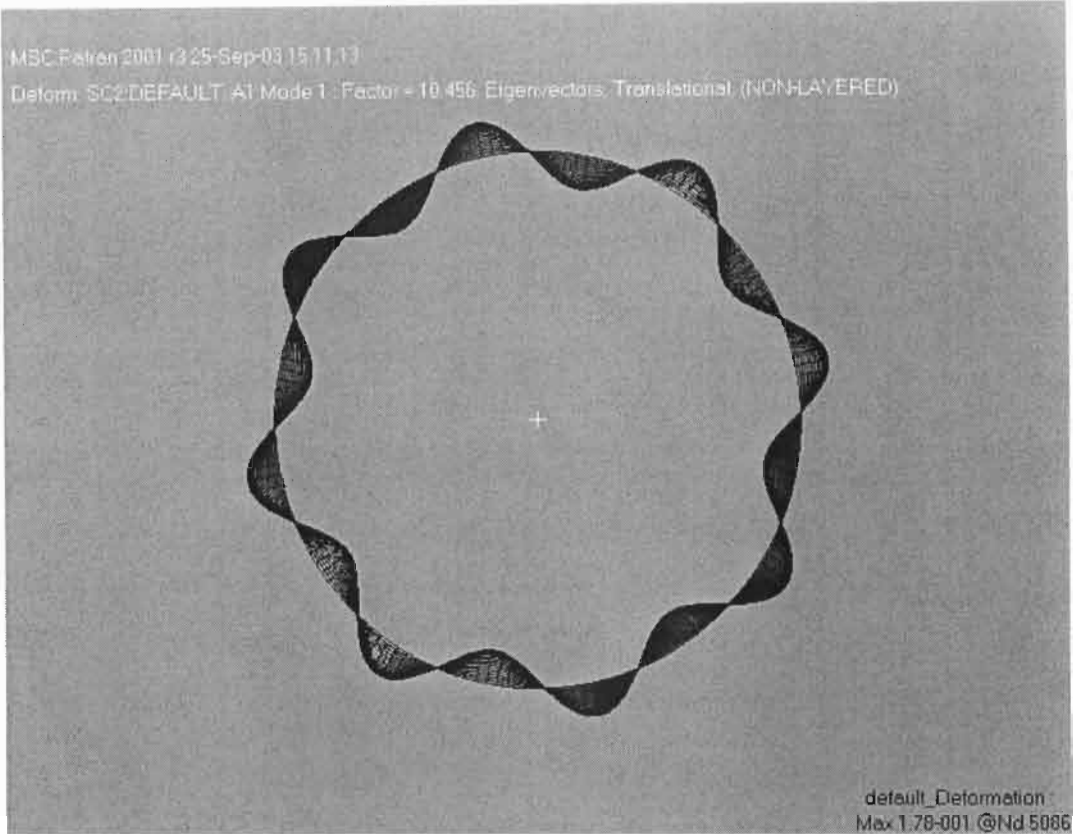
Vessel 3 – External Pressure 0.1MPa
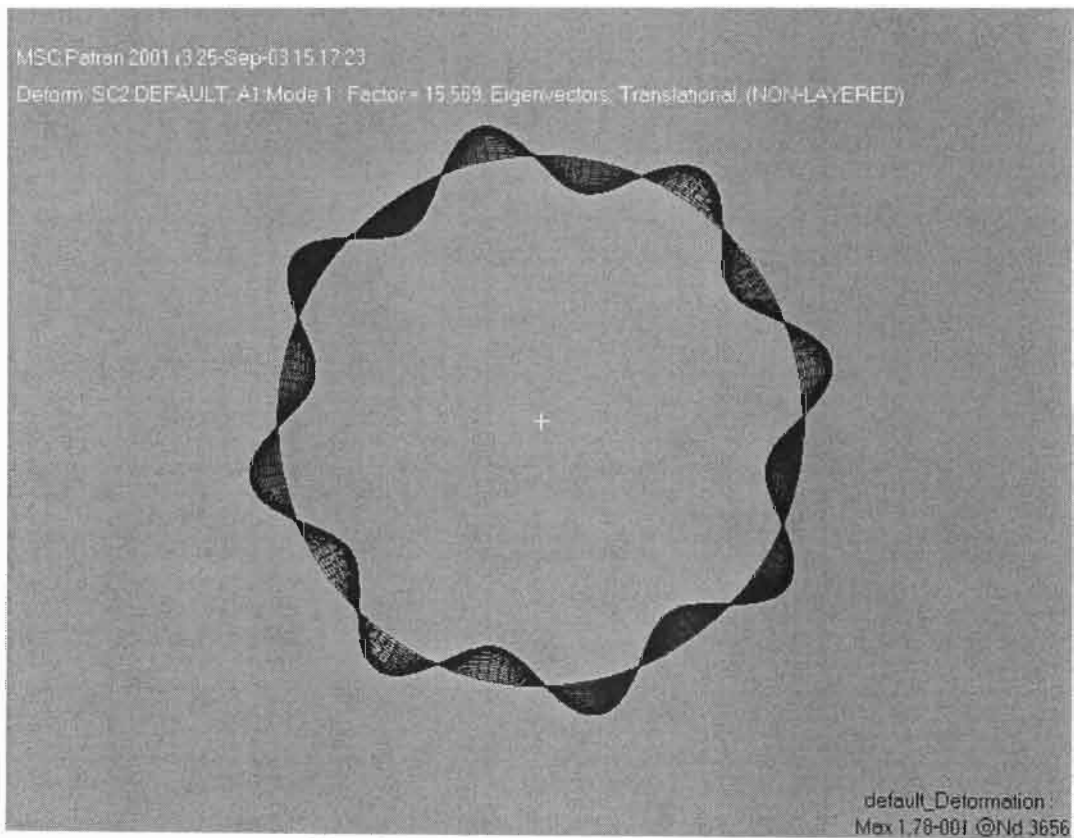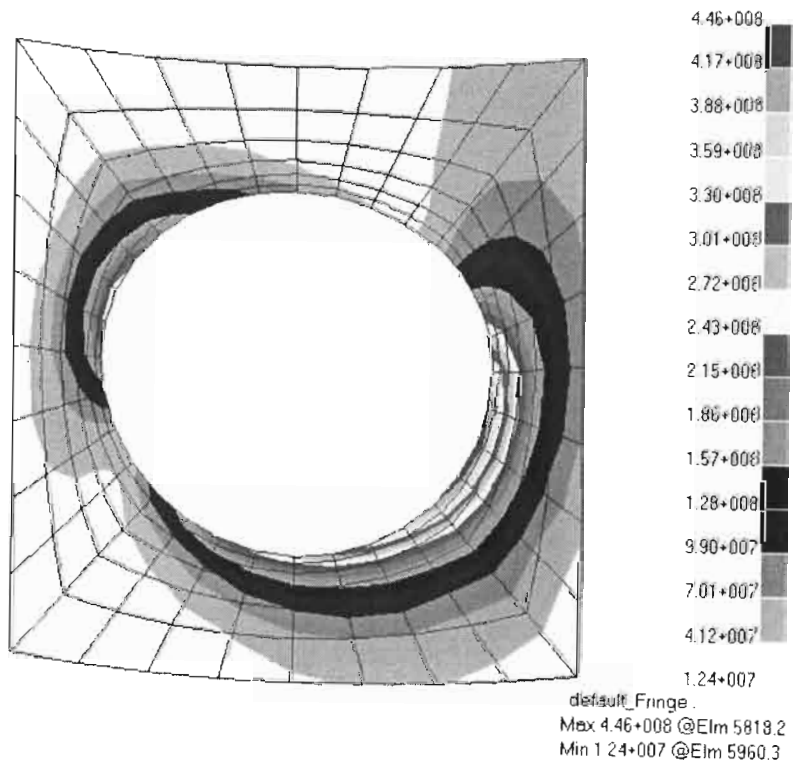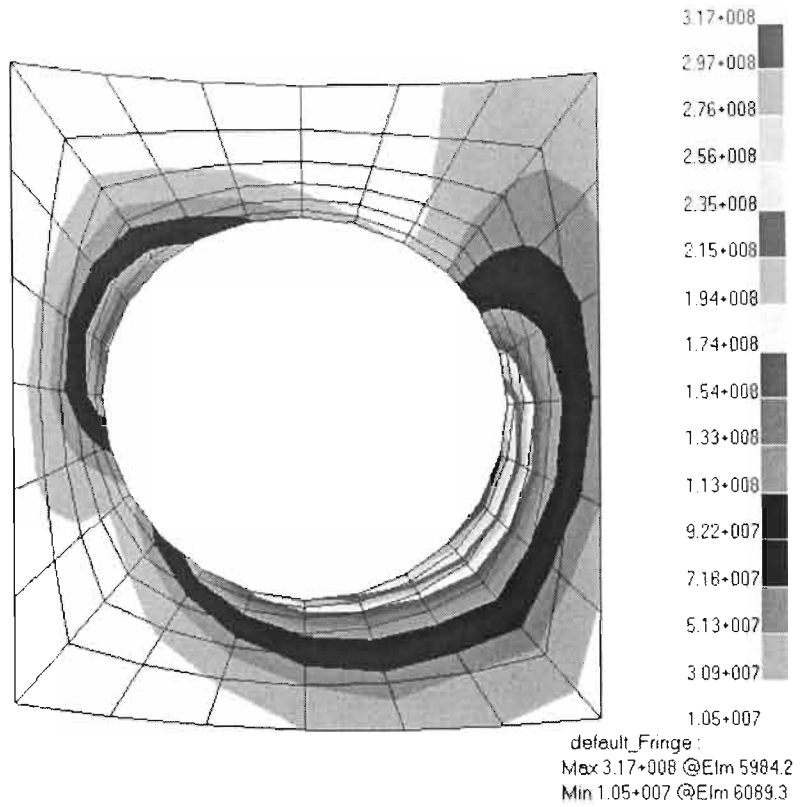

Vessel 4 – External Pressure 0.1MPa
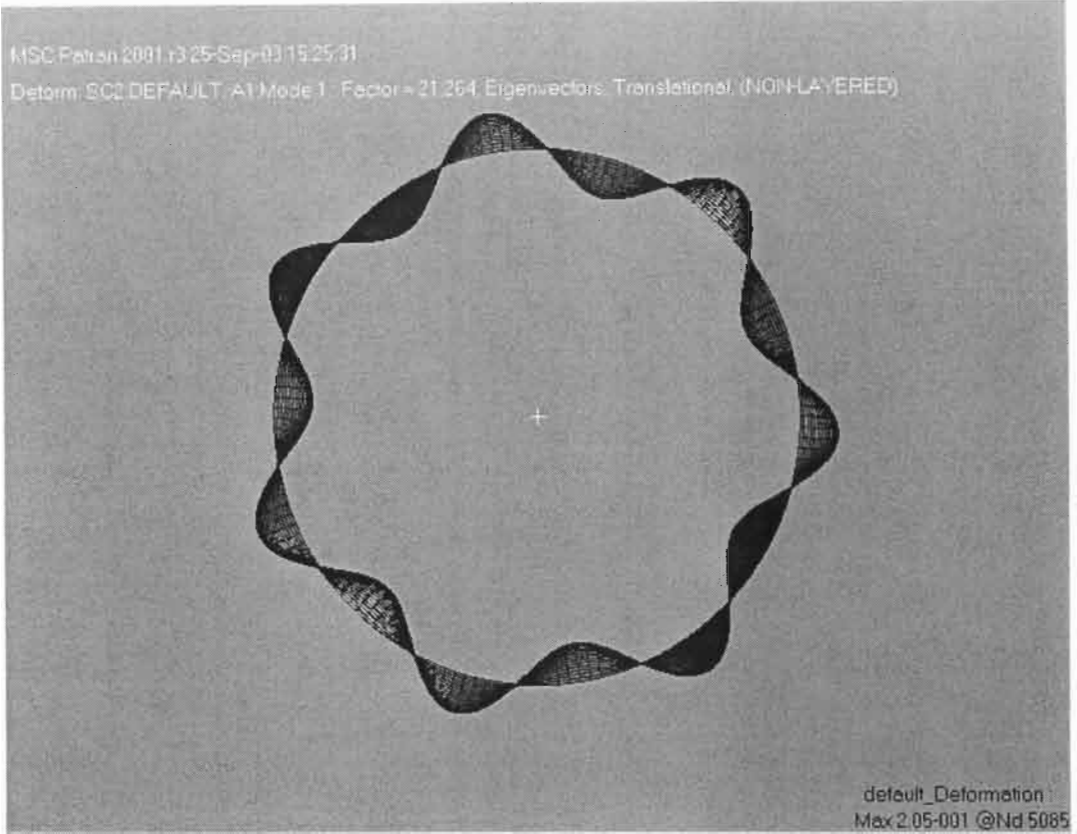
Vessel 5 – External Pressure 0.1MPa
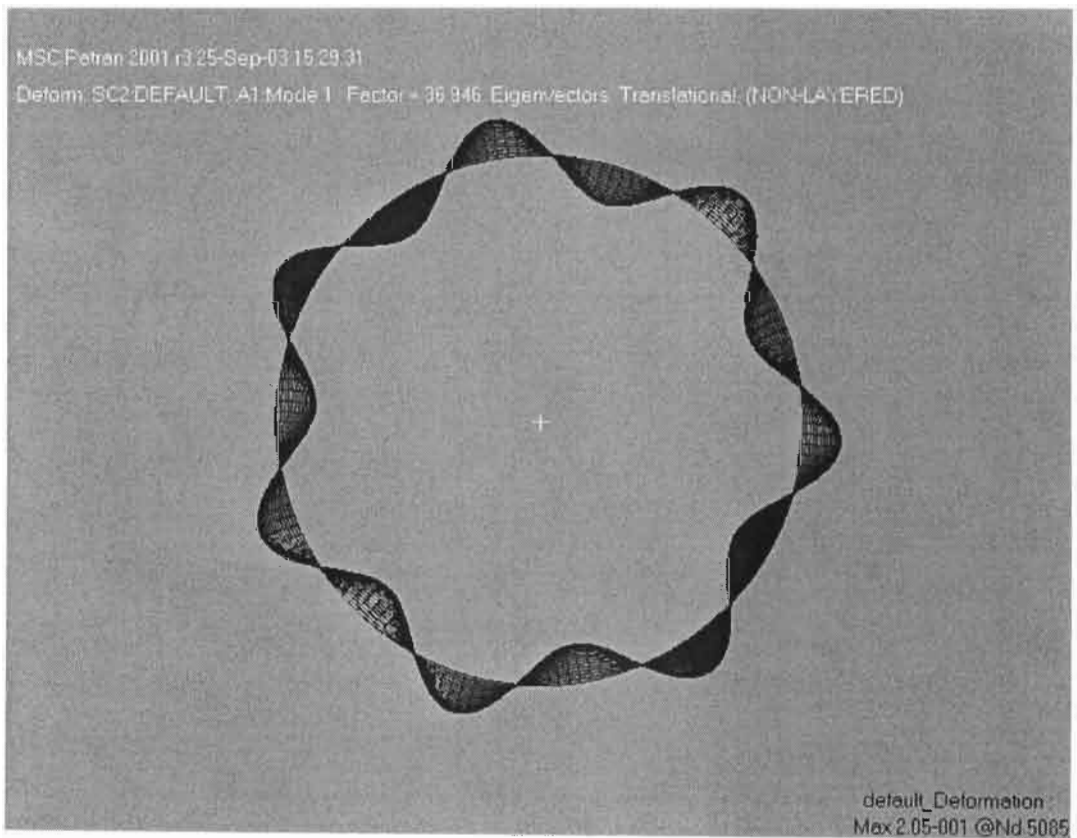
Vessel 6 – External Pressure 0.1MPa

165
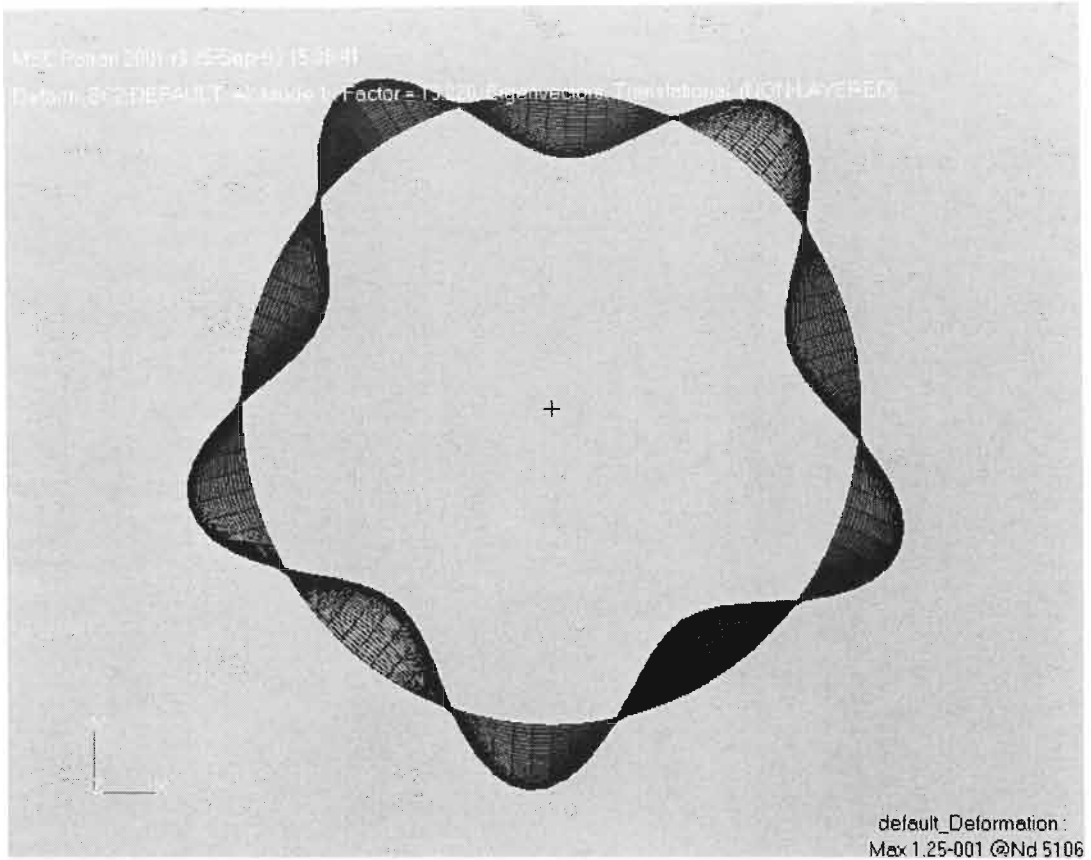
Vessel 7 – External Pressure 0.1MPa
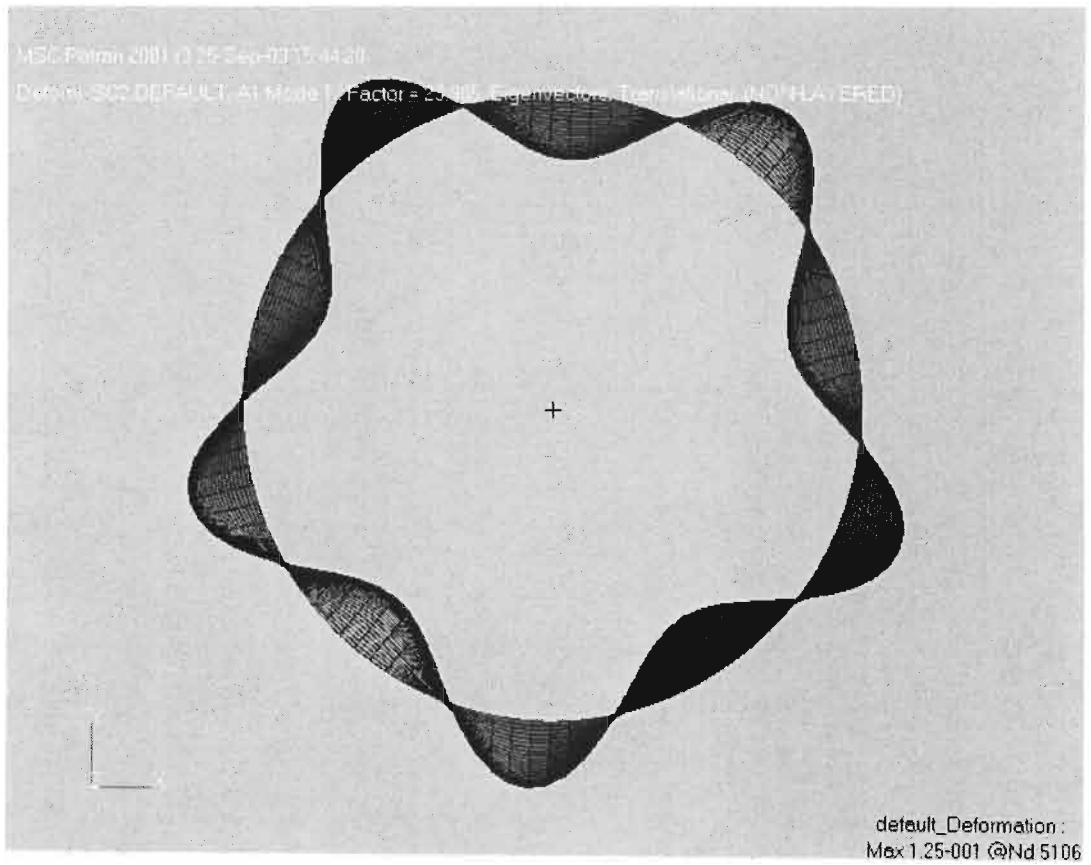
Vessel 8 – External Pressure 0.1MPa
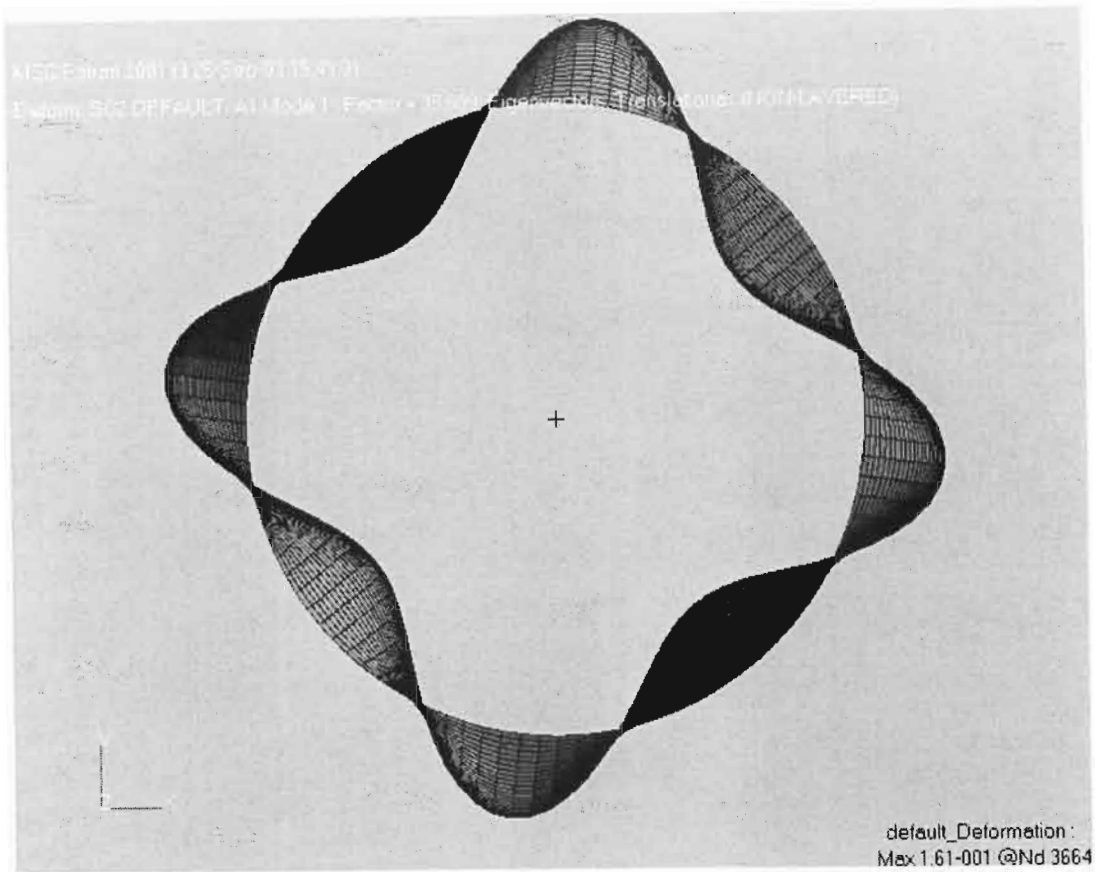
Vessel 9 – External Pressure 0.1MPa
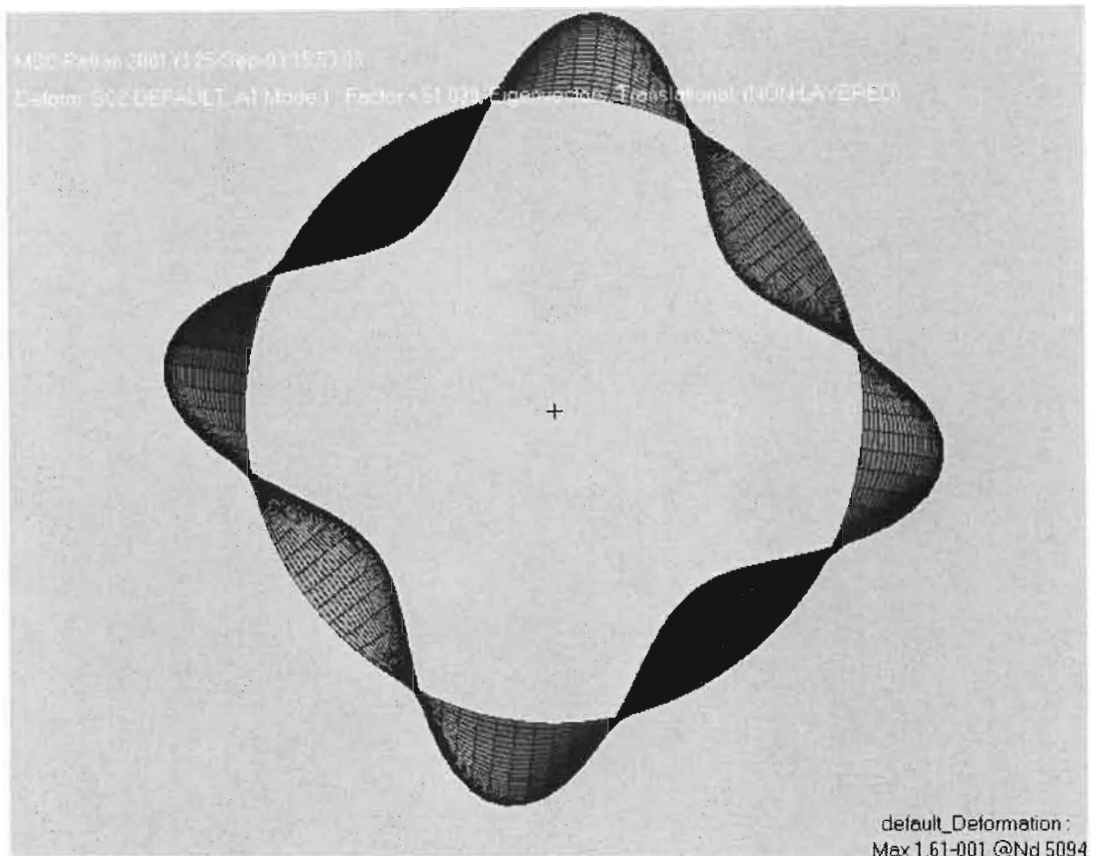
Vessel 10 – External Pressure 0.1MPa

167
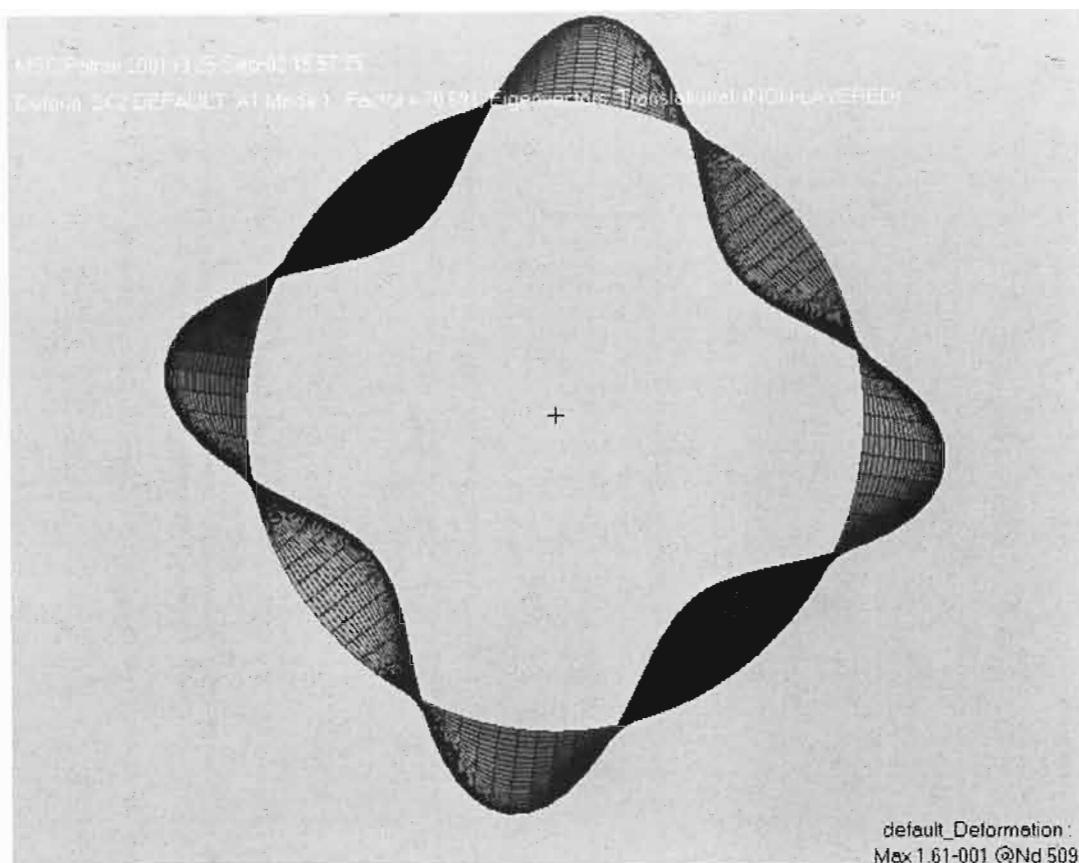
Vessel 11 – External Pressure 0.1MPa
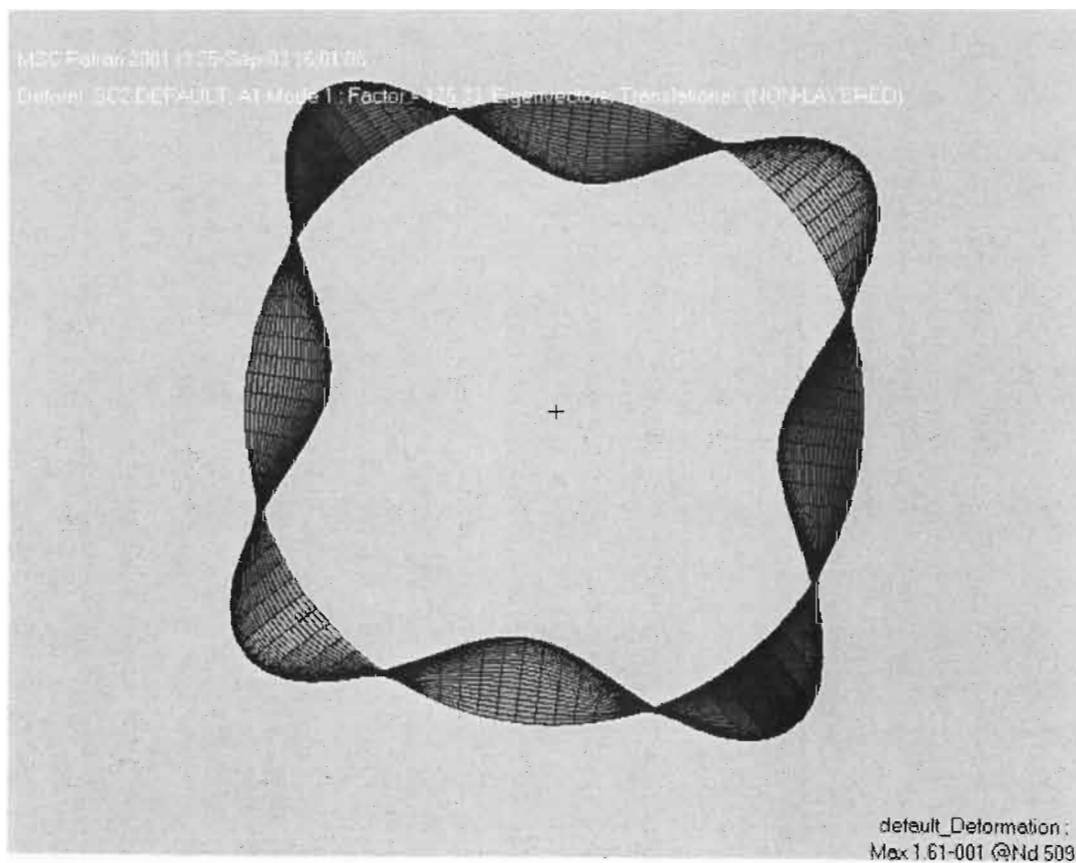
Vessel 12 – External Pressure 0.1MPa

168

FEM Stress Plots for Vessels 1-12 under external pressure and piping loads for a 24" Nozzle
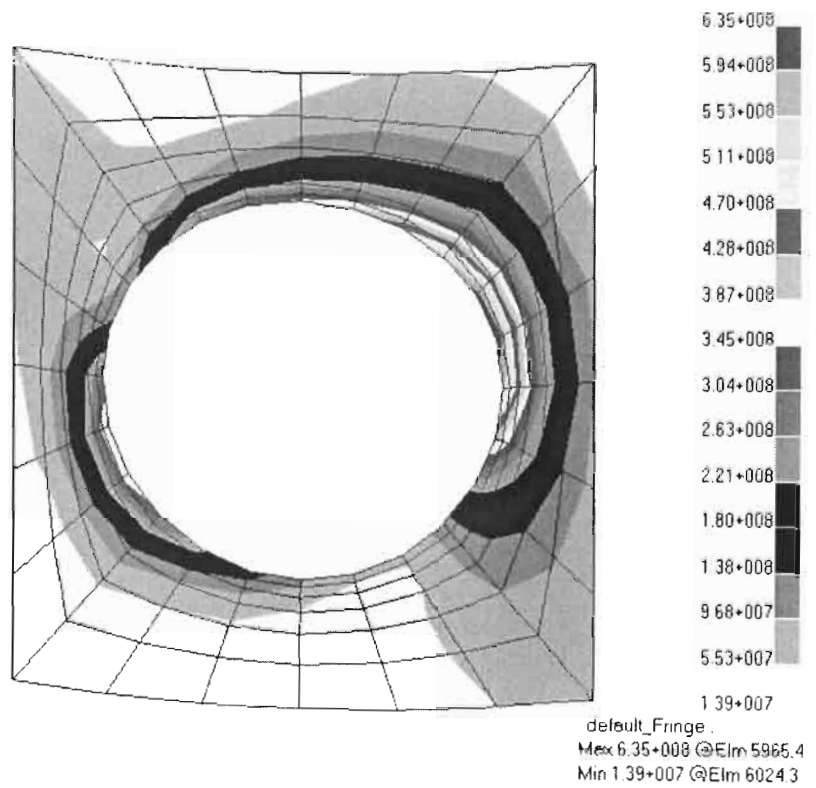
Vessel 1 – Combined Stress Intensity (24" Nozzle)

Vessel 2 – Combined Stress Intensity (24" Nozzle)

3.17+008
2.97+008
2.76+008
2.56+008
2.35+008
2.15+008
1.94+008
1.74+008
1.54+008
1.33+008
1.13+008
9.22+007
7.18+007
5.13+007
3.09+007
1.05+007

default_Fringe :
Max 3.17+008 @Elm 5984.2
Min 1.05+007 @Elm 6089.3

Vessel 3 – Combined Stress Intensity (24" Nozzle)

2.39+008
2.24+008
2.08+008
1.92+008
1.77+008
1.61+008
1.46+008
1.30+008
1.15+008
9.91+007
8.35+007
6.80+007
5.24+007
3.68+007
2.13+007
5.72+006

default_Fringe :
Max 2.39+008 @Elm 5819.2
Min 5.72+006 @Elm 5959.3
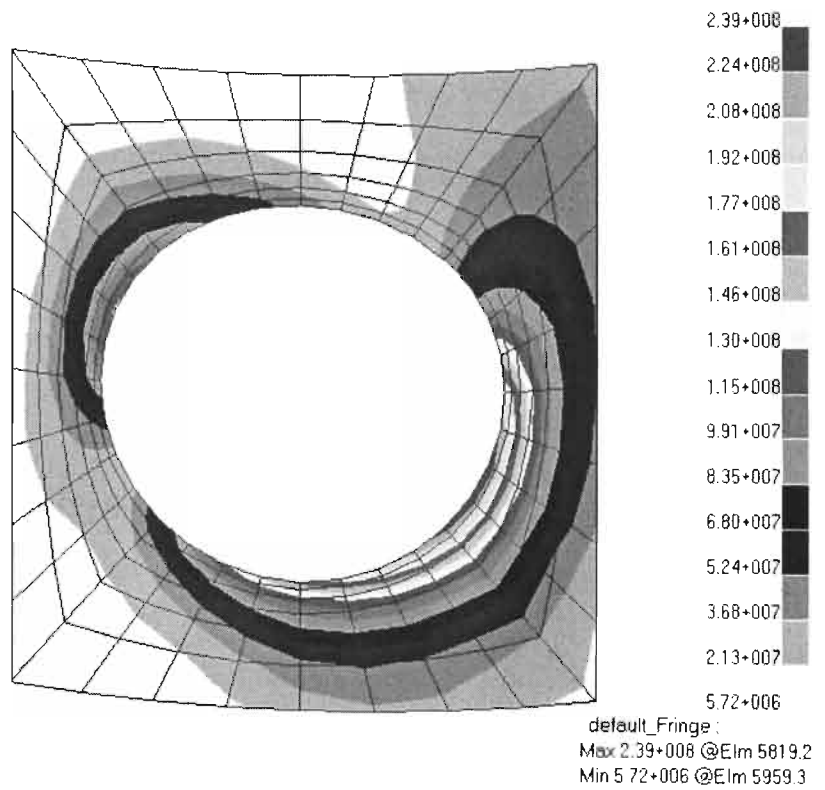
Vessel 4 – Combined Stress Intensity (24" Nozzle)

170

1.82+008
1.70+008
1.58+008
1.46+008
1.35+008
1.23+008
1.11+008
9.90+007
8.72+007
7.53+007
6.34+007
5.16+007
3.97+007
2.79+007
1.60+007
4.15+006
default_Fringe :
Max 1.82+008 @Elm 5715.2
Min 4.15+006 @Elm 5889.3
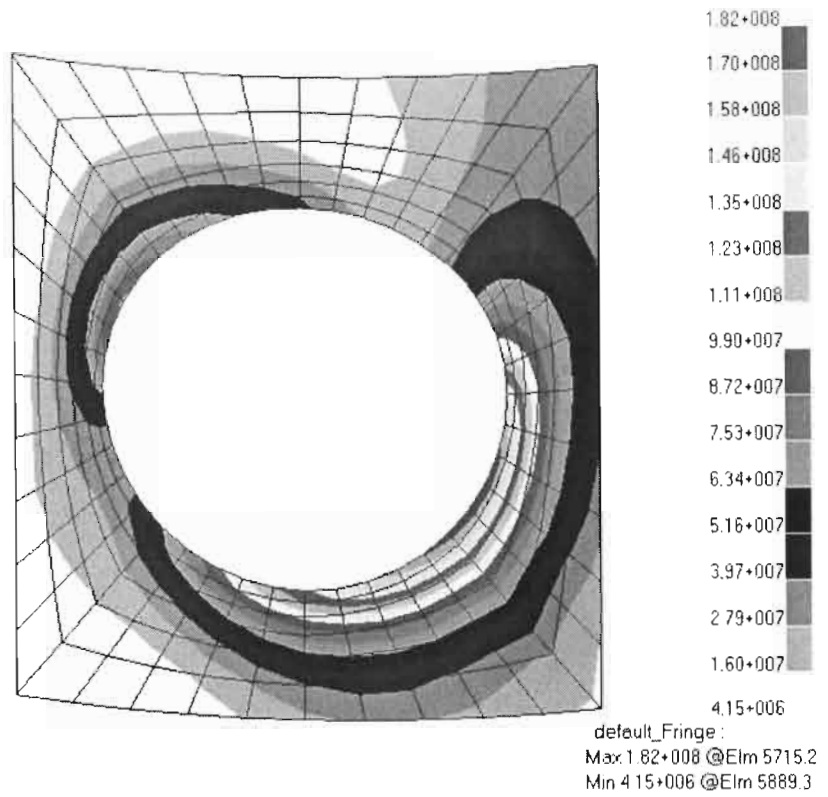
Vessel 5 – Combined Stress Intensity (24" Nozzle)

1.11+008
1.04+008
9.64+007
8.94+007
8.23+007
7.52+007
6.81+007
6.10+007
5.40+007
4.69+007
3.98+007
3.27+007
2.56+007
1.86+007
1.15+007
4.40+006
default_Fringe :
Max 1.11+008 @Elm 926.1
Min 4.40+006 @Elm 4052.3
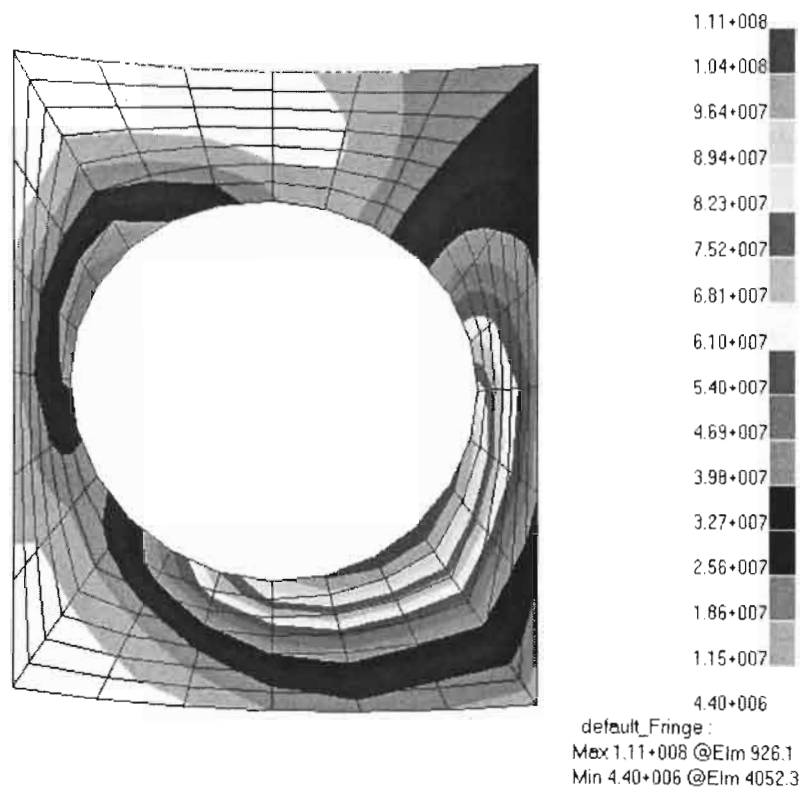
Vessel 6 – Combined Stress Intensity (24" Nozzle)

171
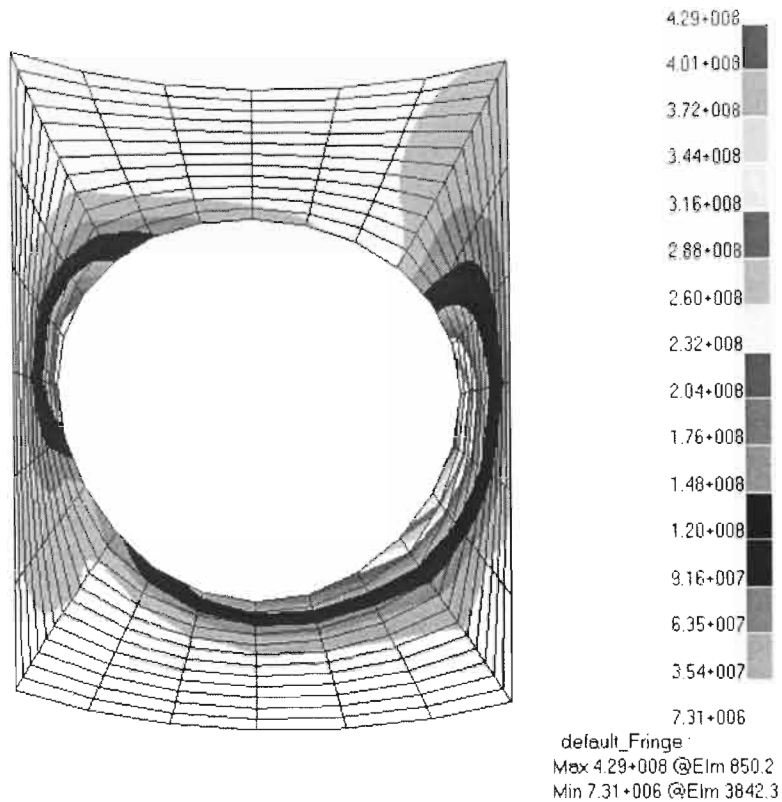
Vessel 7 – Combined Stress Intensity (24" Nozzle)
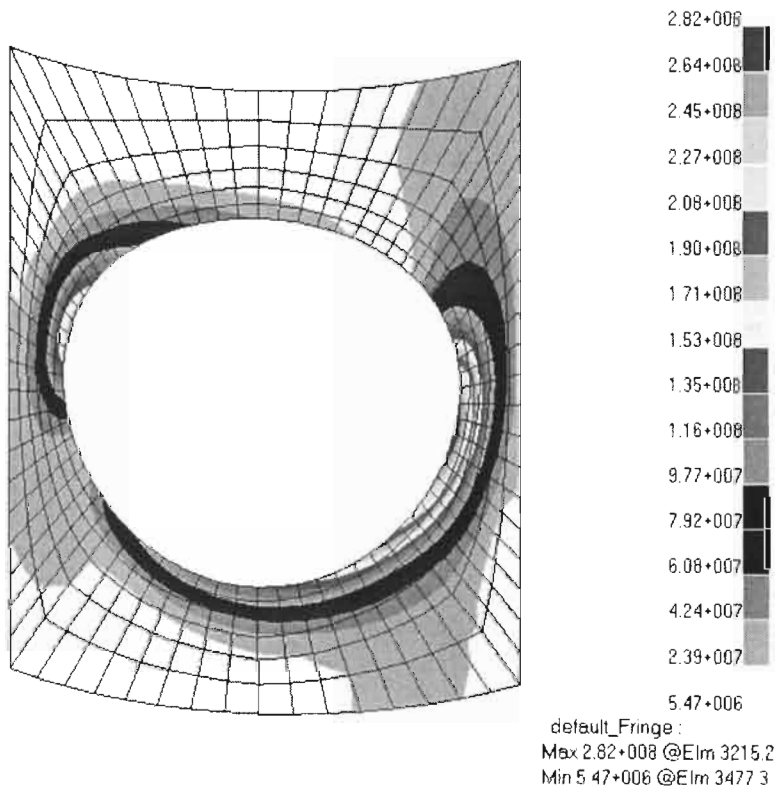
Vessel 8 – Combined Stress Intensity (24" Nozzle)

172
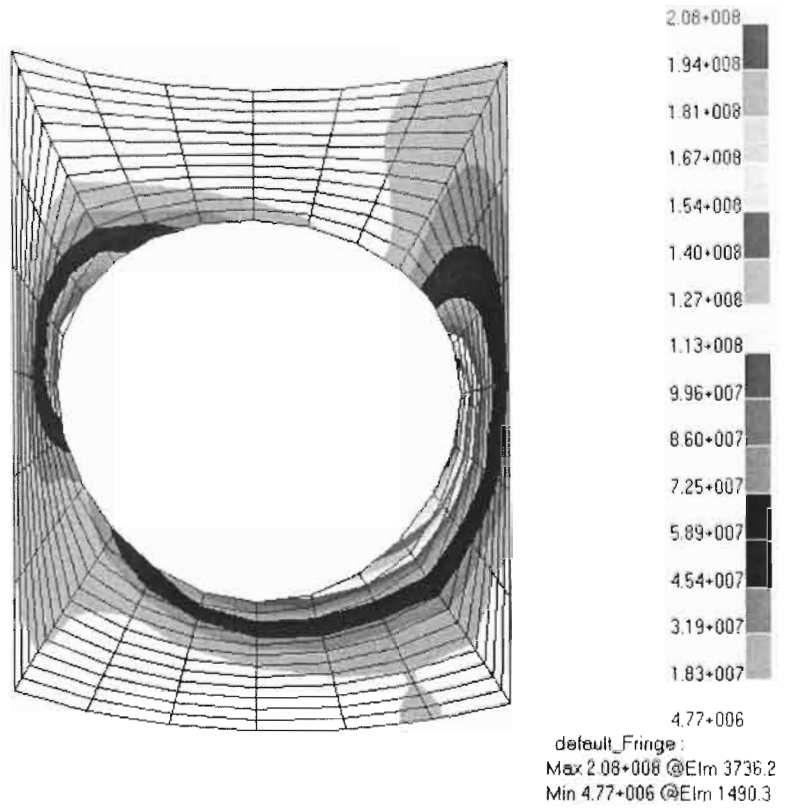
Vessel 9 – Combined Stress Intensity (24" Nozzle)
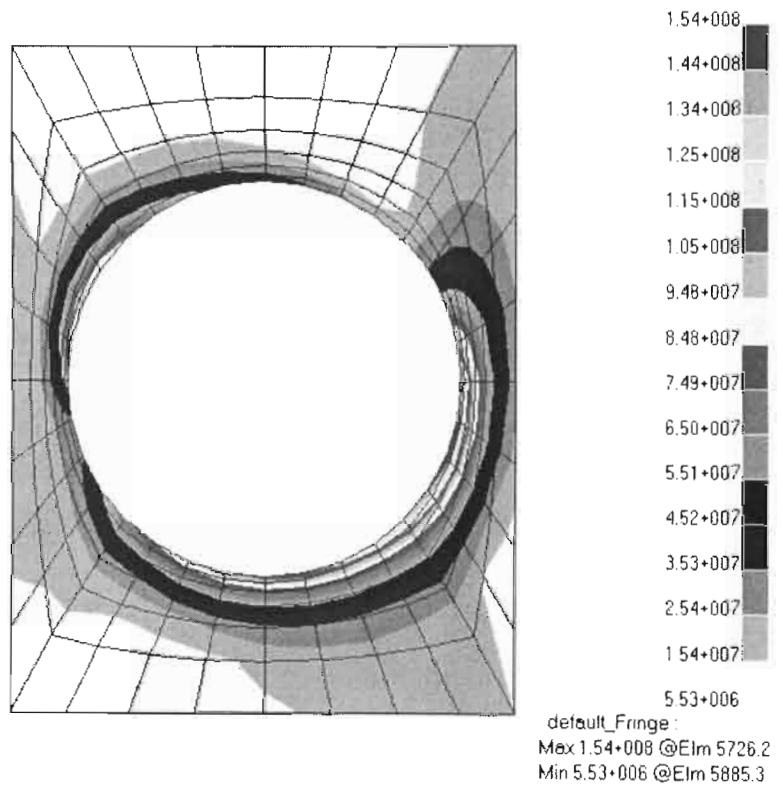
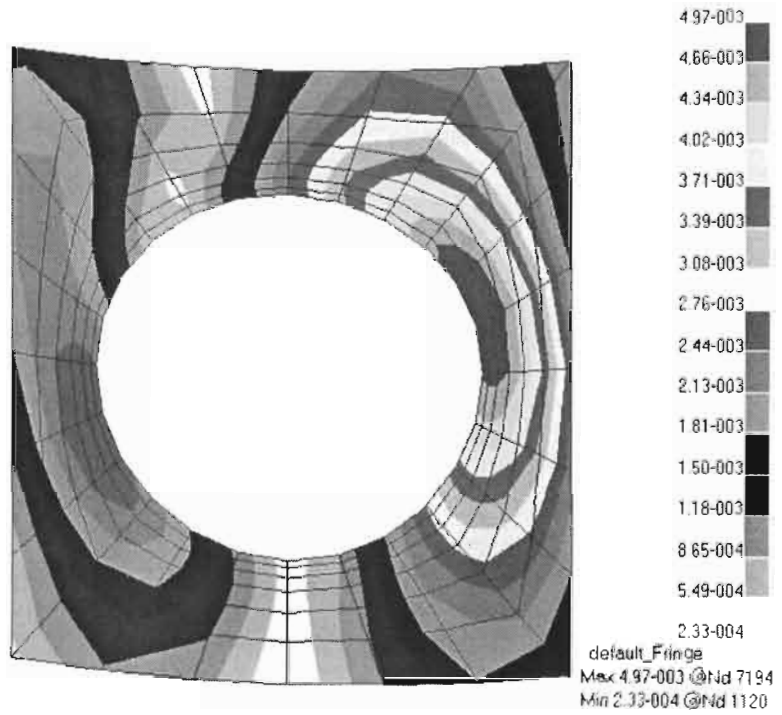**Vessel 10 – Combined Stress Intensity (24" Nozzle)**

173
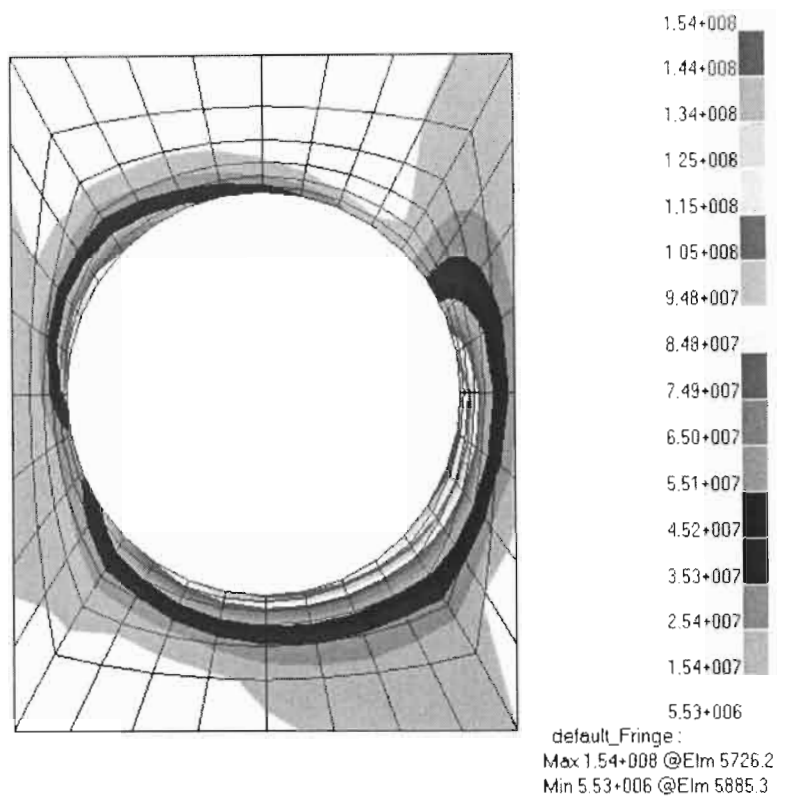
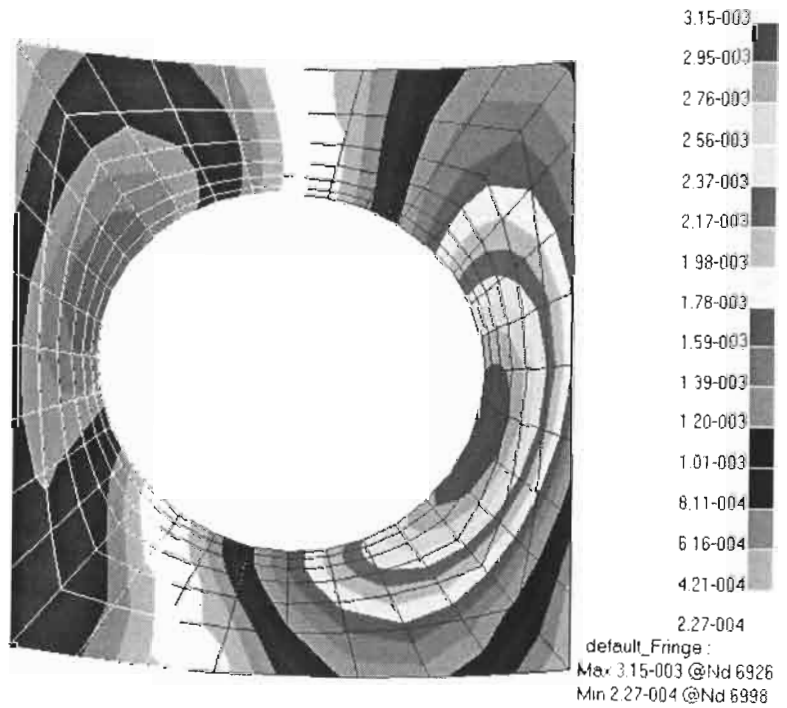**Vessel 11 – Combined Stress Intensity (24" Nozzle)**
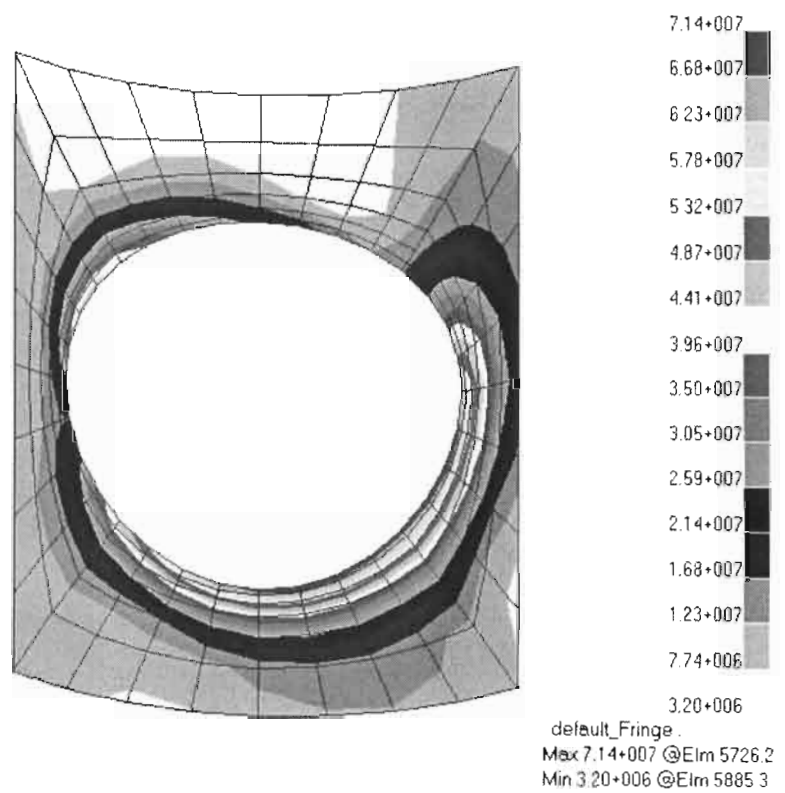
Vessel 12 – Combined Stress Intensity (24" Nozzle)
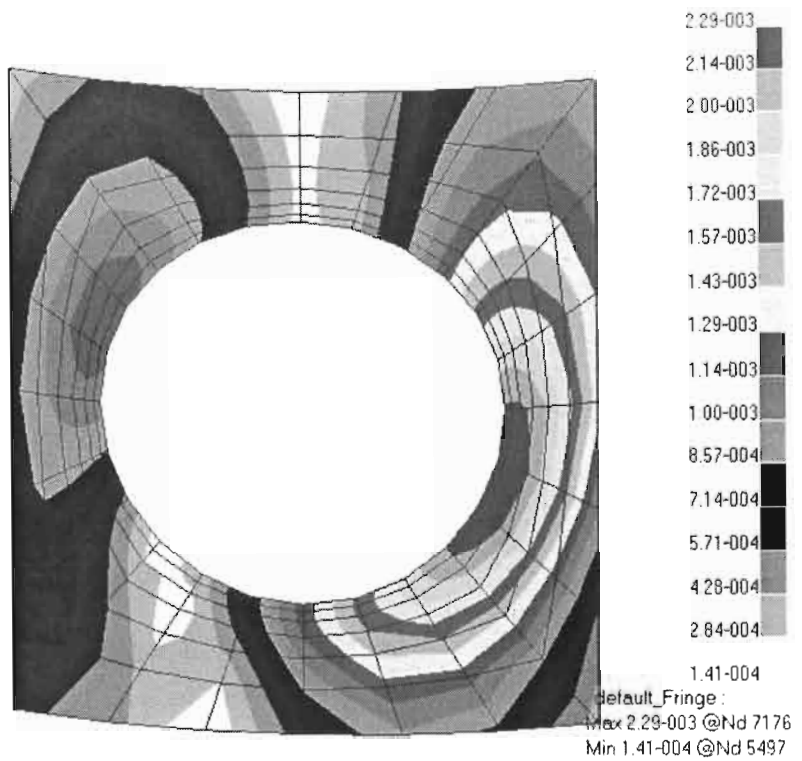
174

FEM Deflection Plots for Vessels 1-6 under external pressure and piping loads for a 24" Nozzle
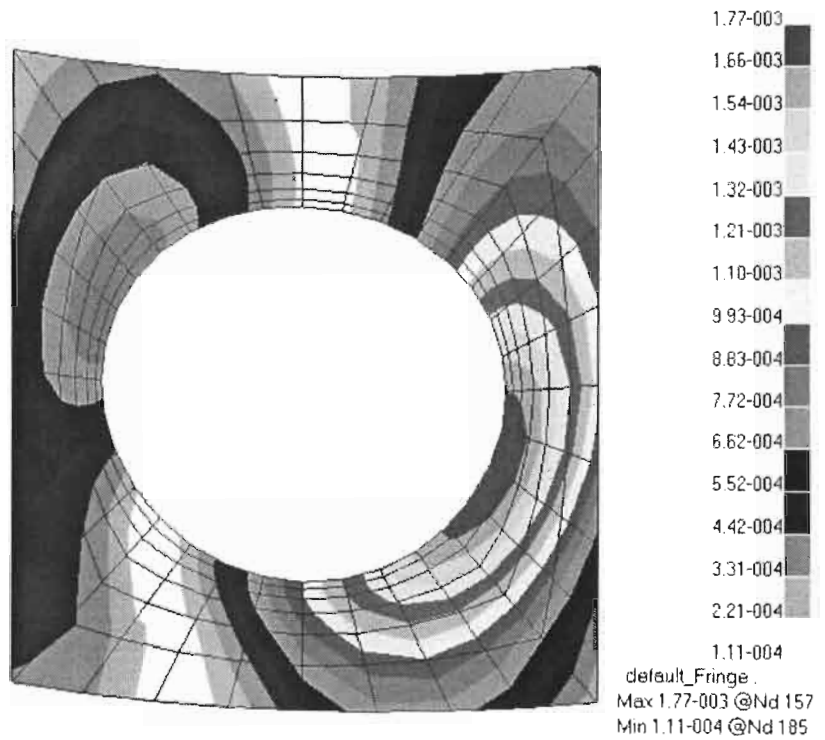

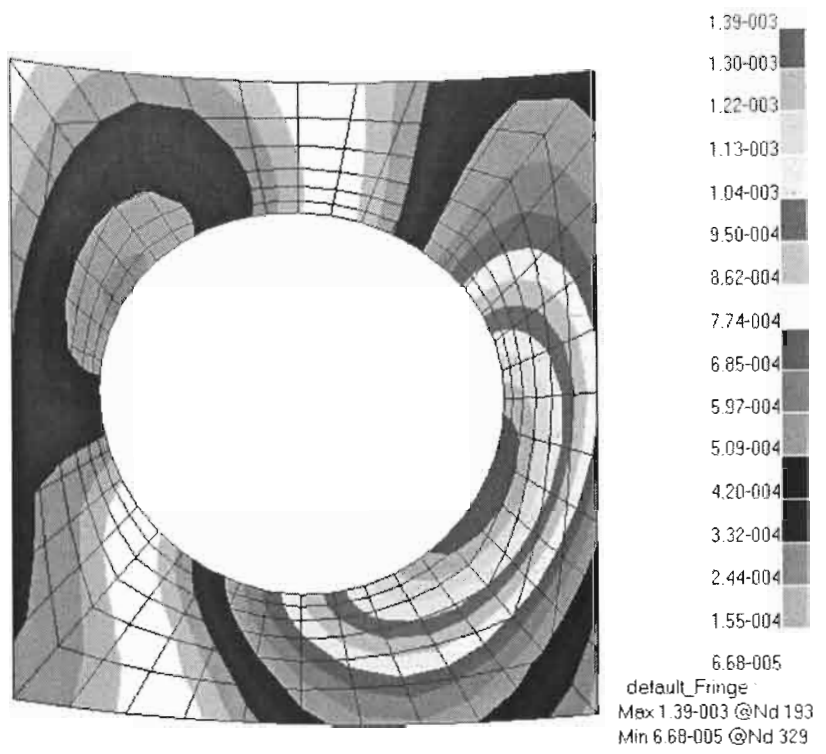**Vessel 1 – FEM Deflection (external pressure and 24" Nozzle)**
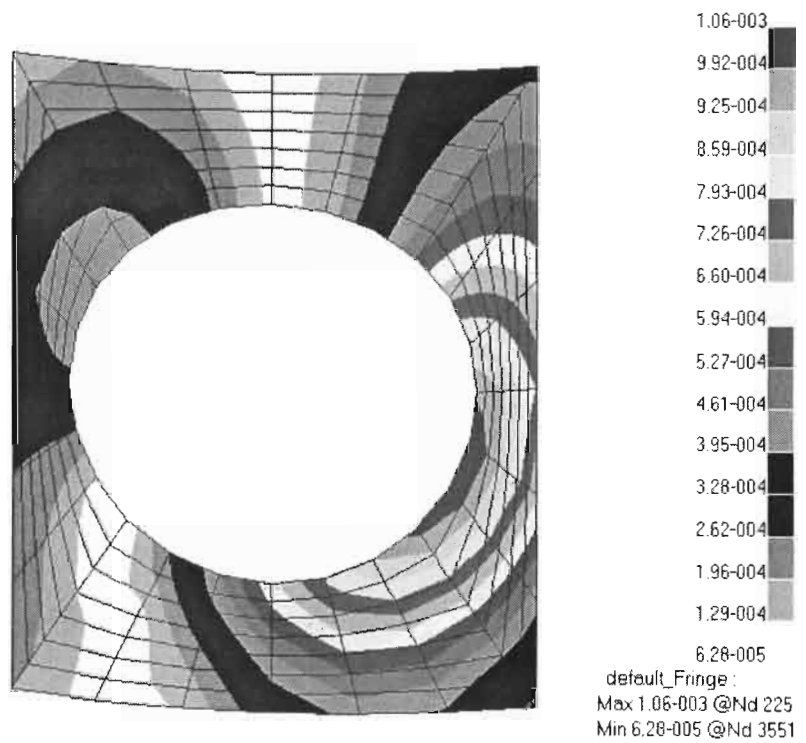

Vessel 2 – FEM Deflection (external pressure and 24" Nozzle)

Vessel 3 – FEM Deflection (external pressure and 24" Nozzle)

Vessel 4 – FEM Deflection (external pressure and 24" Nozzle)

176

**Vessel 5 – FEM Deflection (external pressure and 24" Nozzle)**

Vessel 6 – FEM Deflection (external pressure and 24" Nozzle)

177

Appendix D

| FEM Results for Vessels under External Pressure and Nozzle Piping Loads												
Vessels	1	2	3	4	5	6	7	8	9	10	11	12
Nozzles												
4"												
Pcr' (MPa)	0.362	0.640	1.014	1.500	2.080	3.626	1.023	1.926	3.156	4.700	6.617	11.853
8"												
Pcr' (MPa)	0.306	0.560	0.900	1.347	1.903	3.379	0.881	1.612	2.645	4.020	5.770	10.523
12"												
Pcr' (MPa)	0.279	0.504	0.818	1.228	1.743	3.116	0.789	1.490	2.452	3.709	5.291	9.560
16"												
Pcr' (MPa)	0.257	0.471	0.766	1.152	1.638	2.939	0.550	1.183	2.131	3.354	4.867	8.927
20"												
Pcr' (MPa)	0.225	0.436	0.725	1.102	1.575	2.838	0.394	0.830	1.520	2.519	3.868	7.705
24"												
Pcr' (MPa)	0.181	0.370	0.649	1.021	1.488	2.734	0.320	0.669	1.217	2.013	3.102	6.312

FEM Buckling Analyses for Vessel 6 and Vessel 12 under external pressure and piping loads for the six nozzles
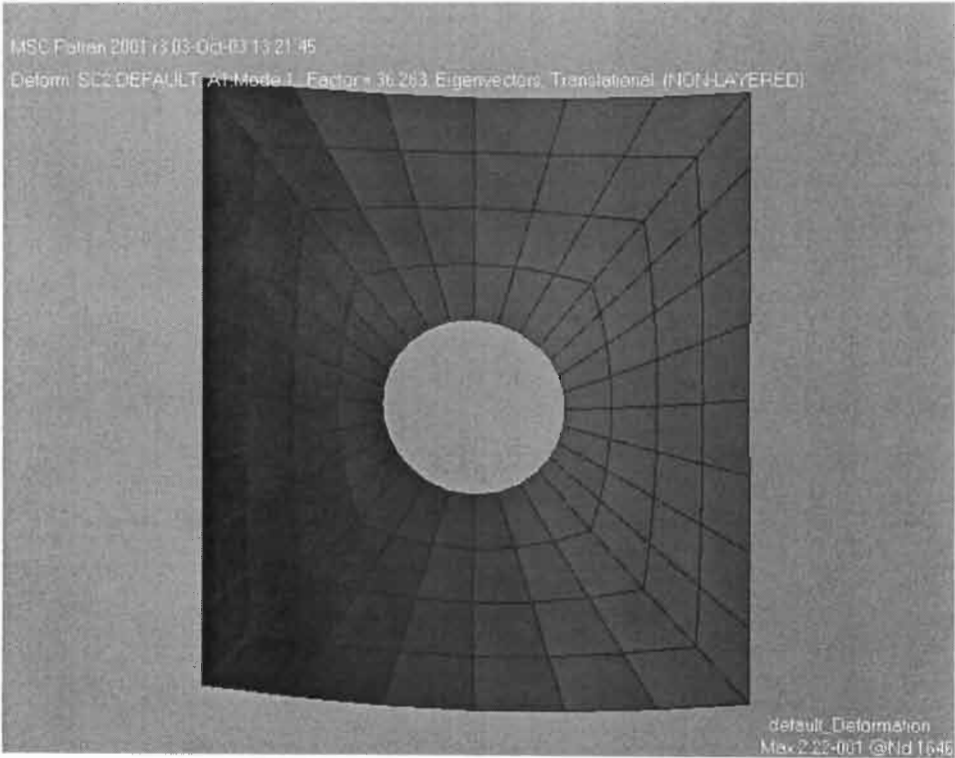
Vessel 6 – FEM Buckling Analysis 4" Nozzle
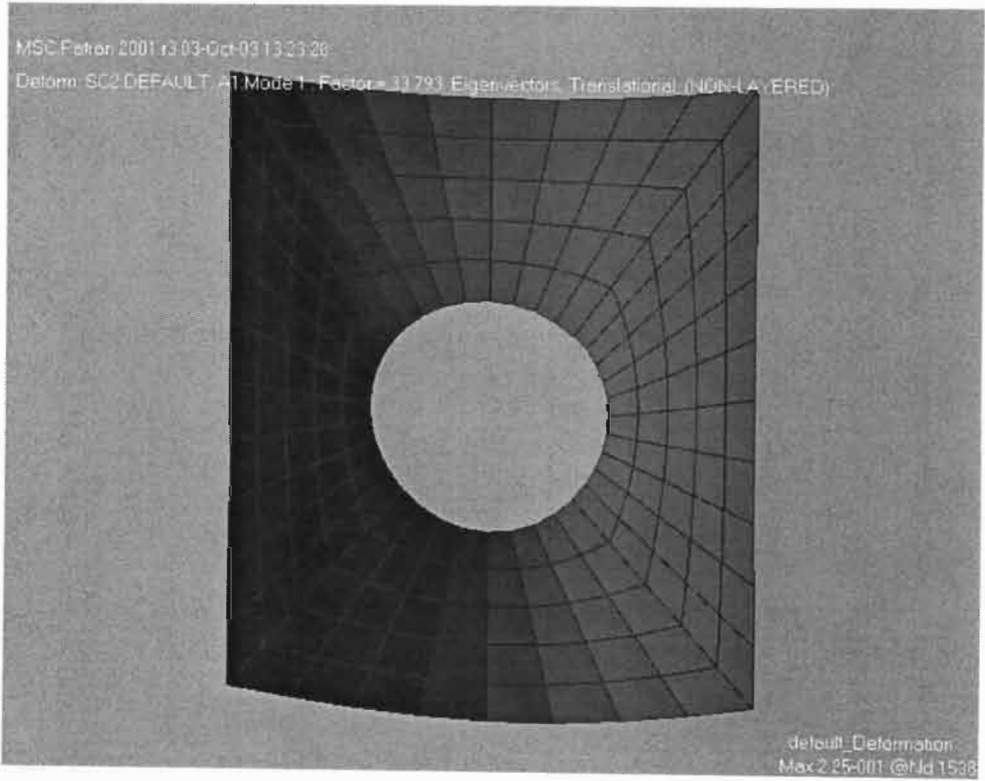
Vessel 6 – FEM Buckling Analysis 8" Nozzle
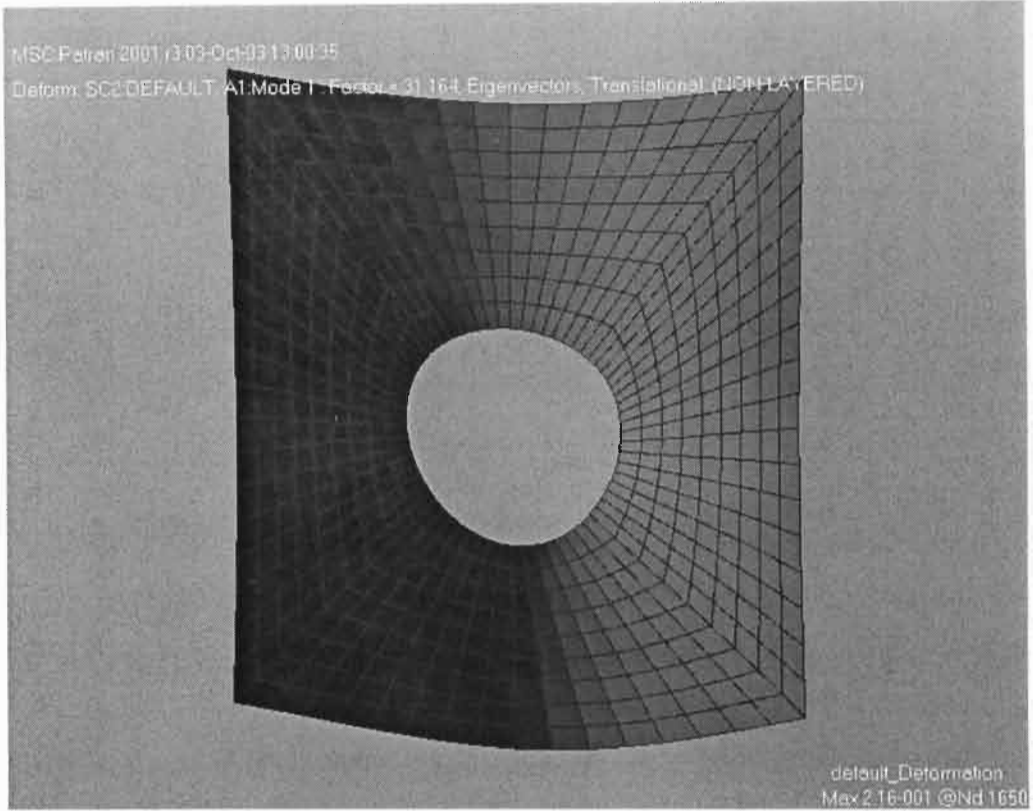
Vessel 6 – FEM Buckling Analysis 12" Nozzle

Vessel 6 – FEM Buckling Analysis 16" Nozzle

181

Vessel 6 – FEM Buckling Analysis 20" Nozzle

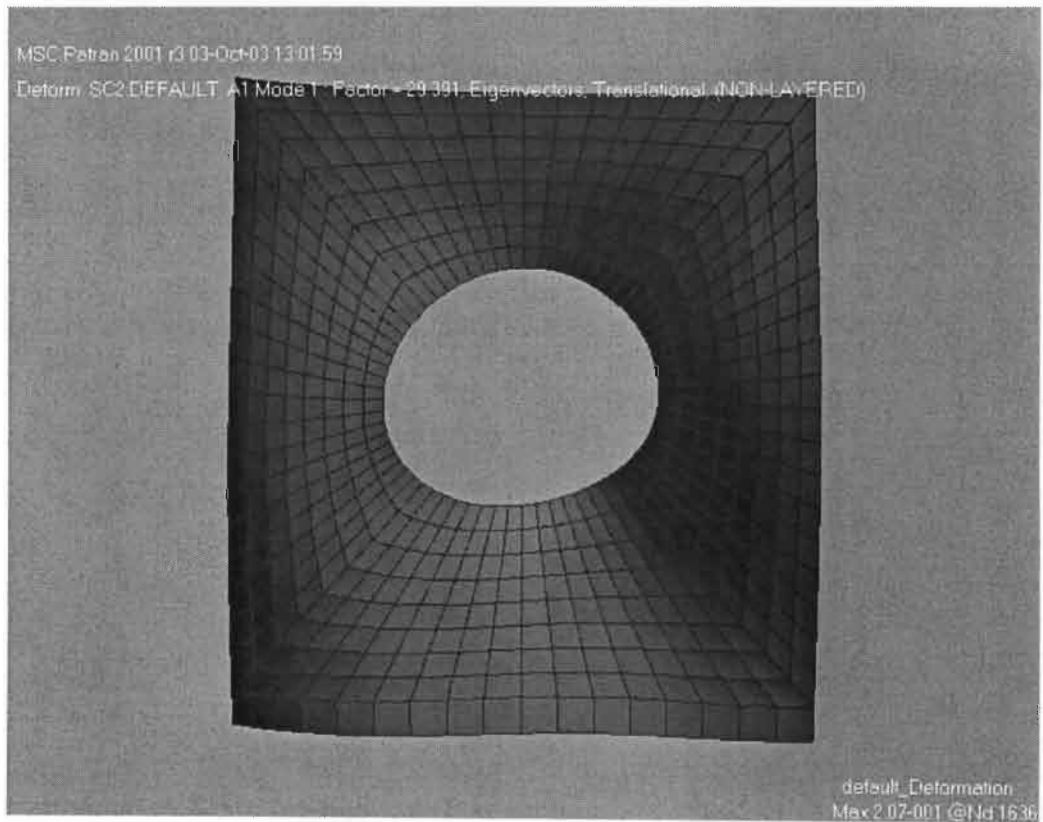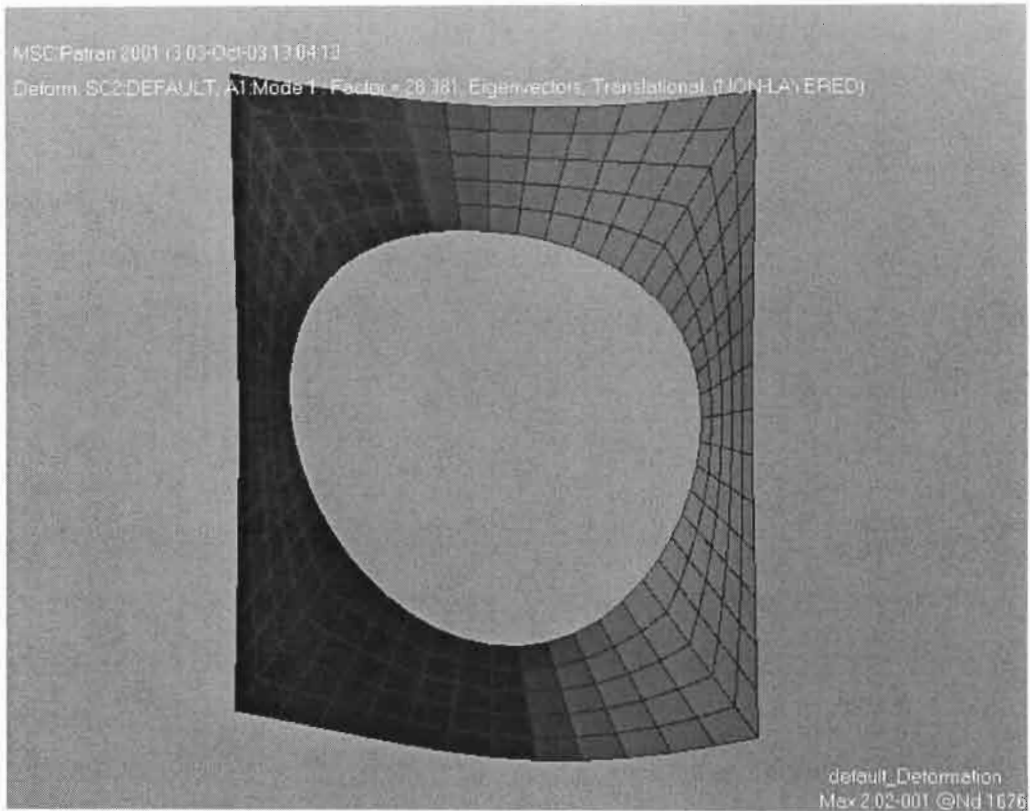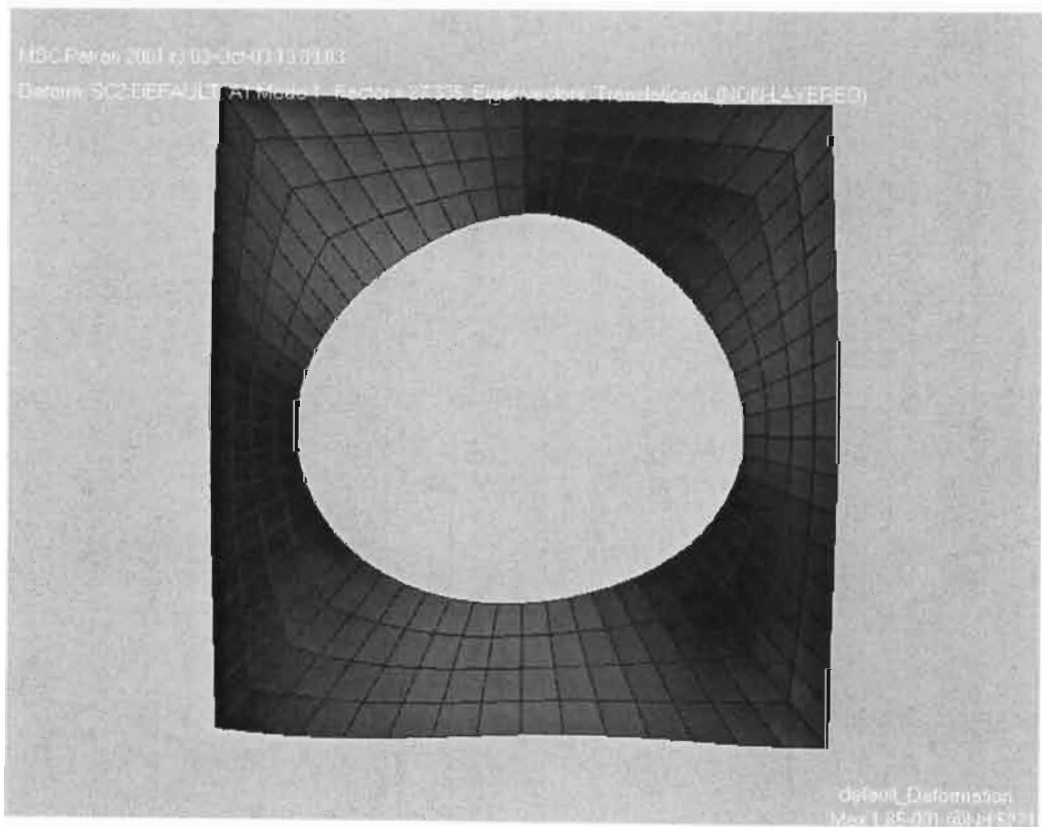**Vessel 6 – FEM Buckling Analysis 24" Nozzle**

Vessel 12 – FEM Buckling Analysis 4" Nozzle
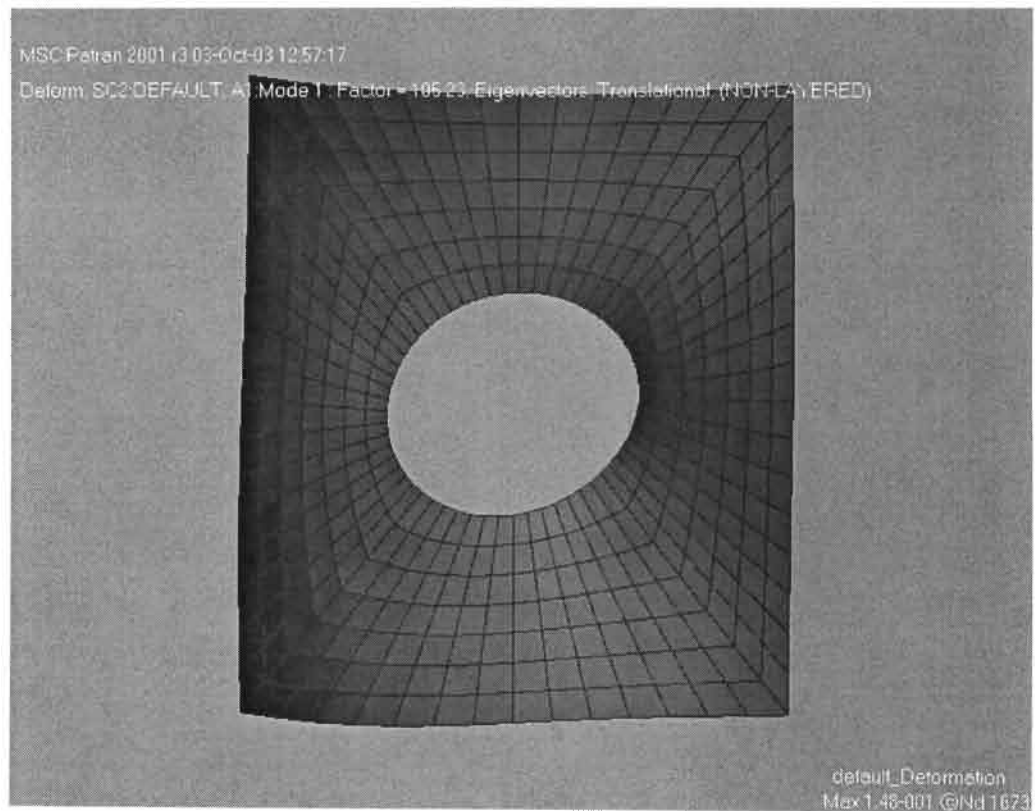
Vessel 12 – FEM Buckling Analysis 8" Nozzle
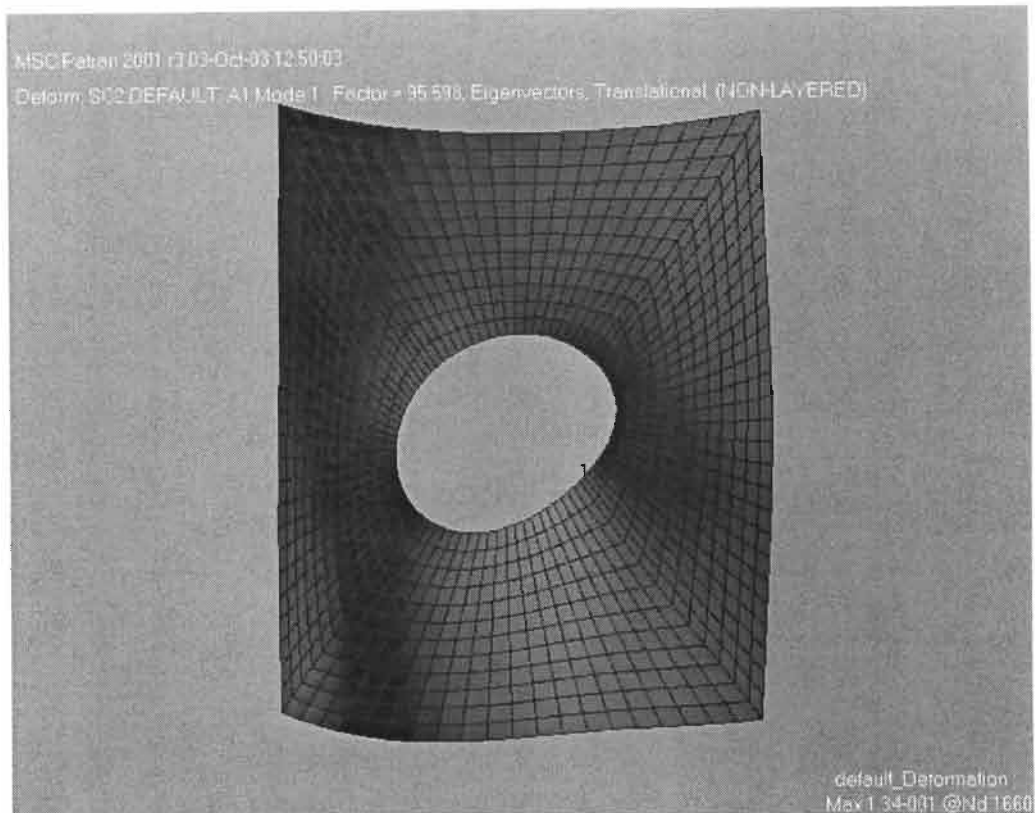
Vessel 12 – FEM Buckling Analysis 12" Nozzle
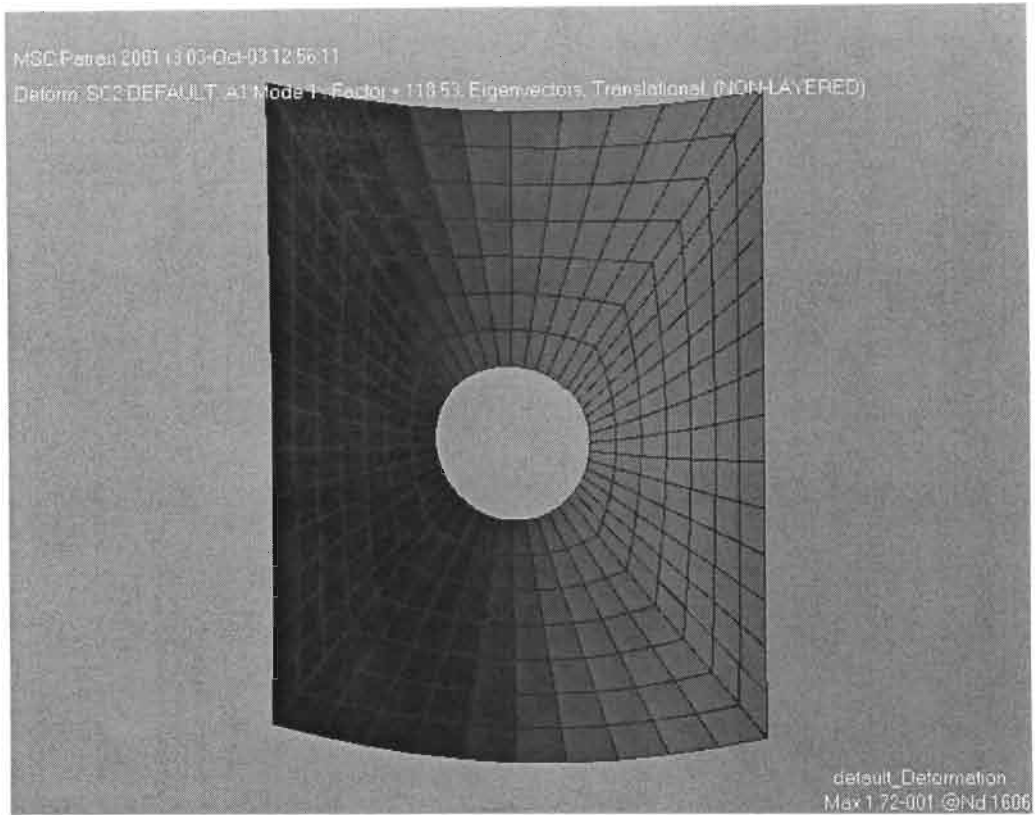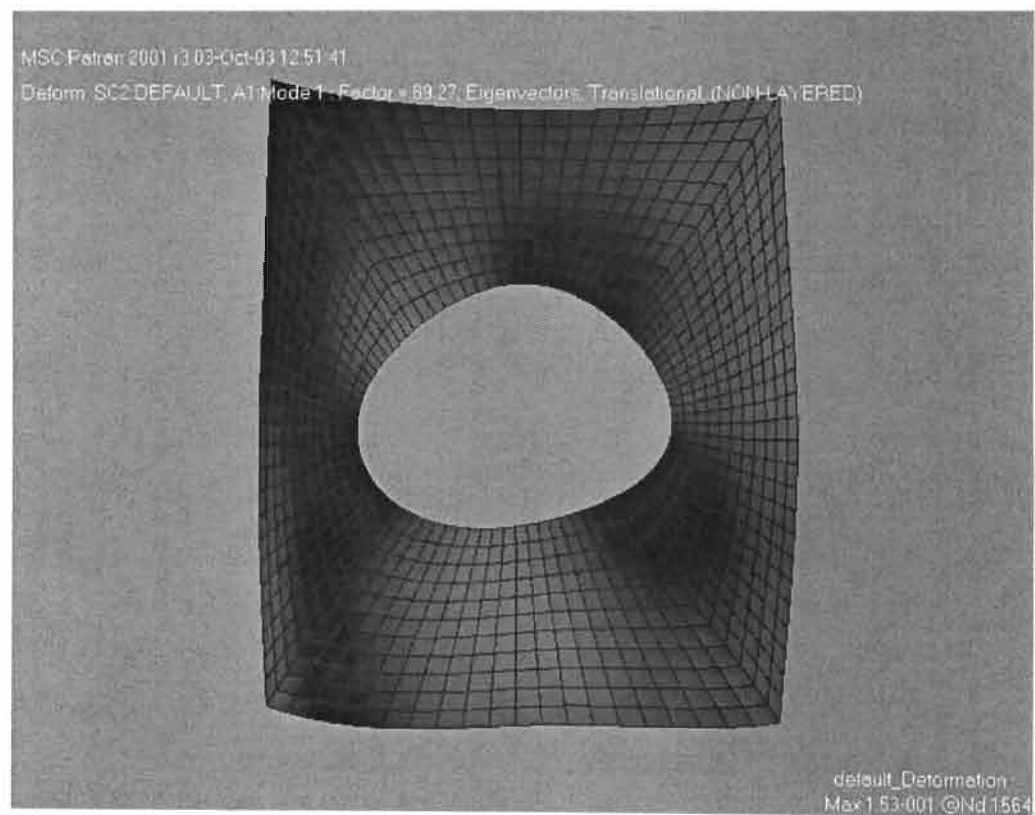

Vessel 12 – FEM Buckling Analysis 16" Nozzle

184
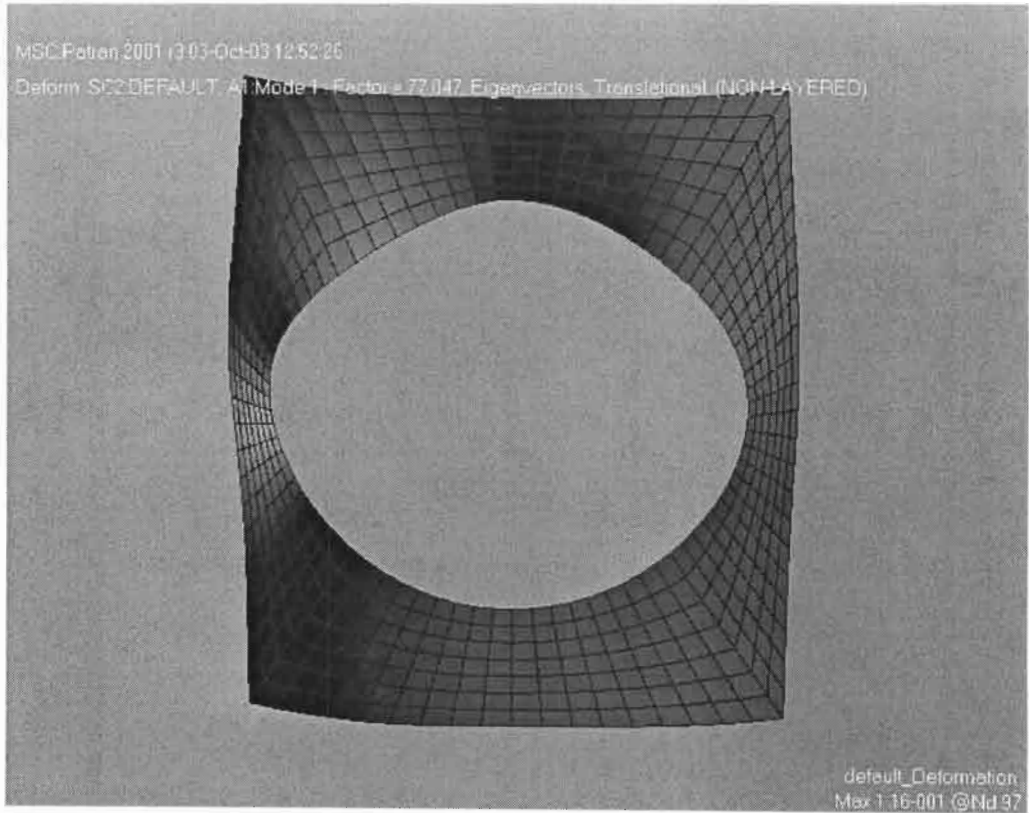
Vessel 12 – FEM Buckling Analysis 20" Nozzle

Vessel 12 – FEM Buckling Analysis 24" Nozzle

185
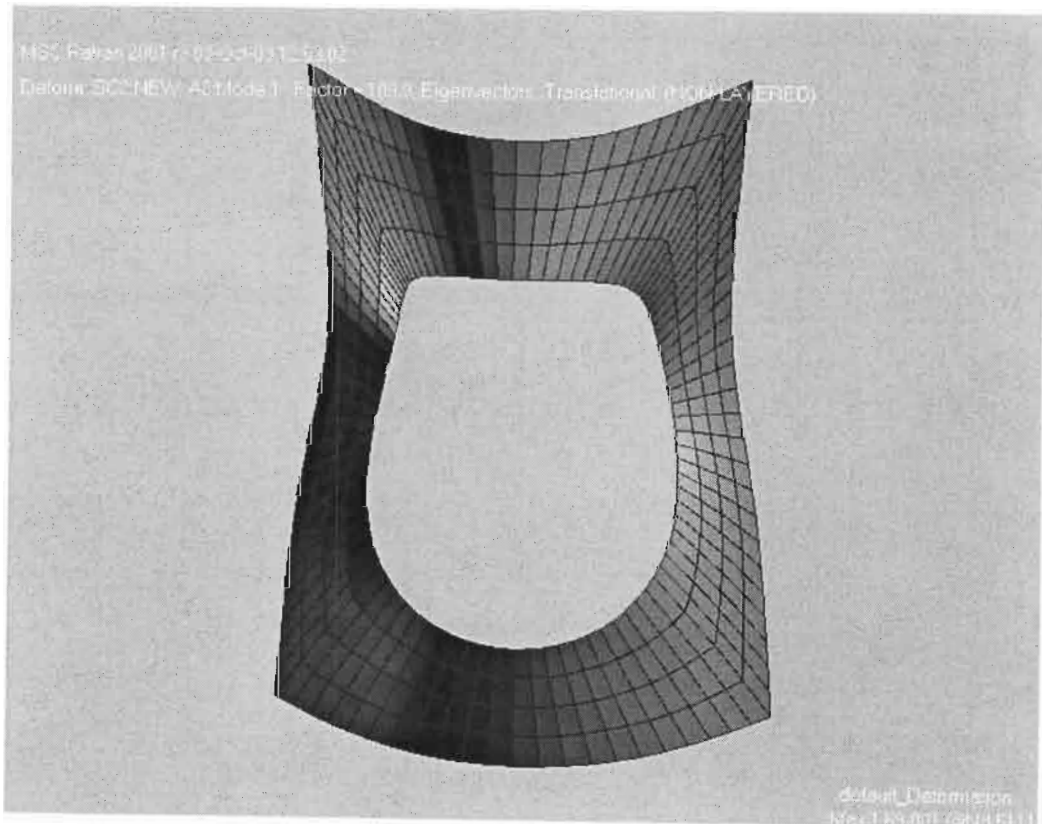
Relationships between the out-of-round stress and the WRC 107 maximum compressive stress for the 4", 8", 12", 16", 20" and 24" nozzles

$$y = 3\text{E-}08x^{3.414}$$

4" Nozzle

$$y = 4\text{E-}07x^{2.99}$$

8" Nozzle

$$y = 4E\text{-}06x^{2.755}$$

12" Nozzle

$$y = 4E\text{-}06x^{2.815}$$

16" Nozzle

$y = 1\text{E-}05x^{2.69}$

WRC 107 Maximum Compressive Stress (MPa)

20" Nozzle

$y = 3\text{E-}05x^{2.5356}$

WRC 107 Maximum Compressive Stress (MPa)
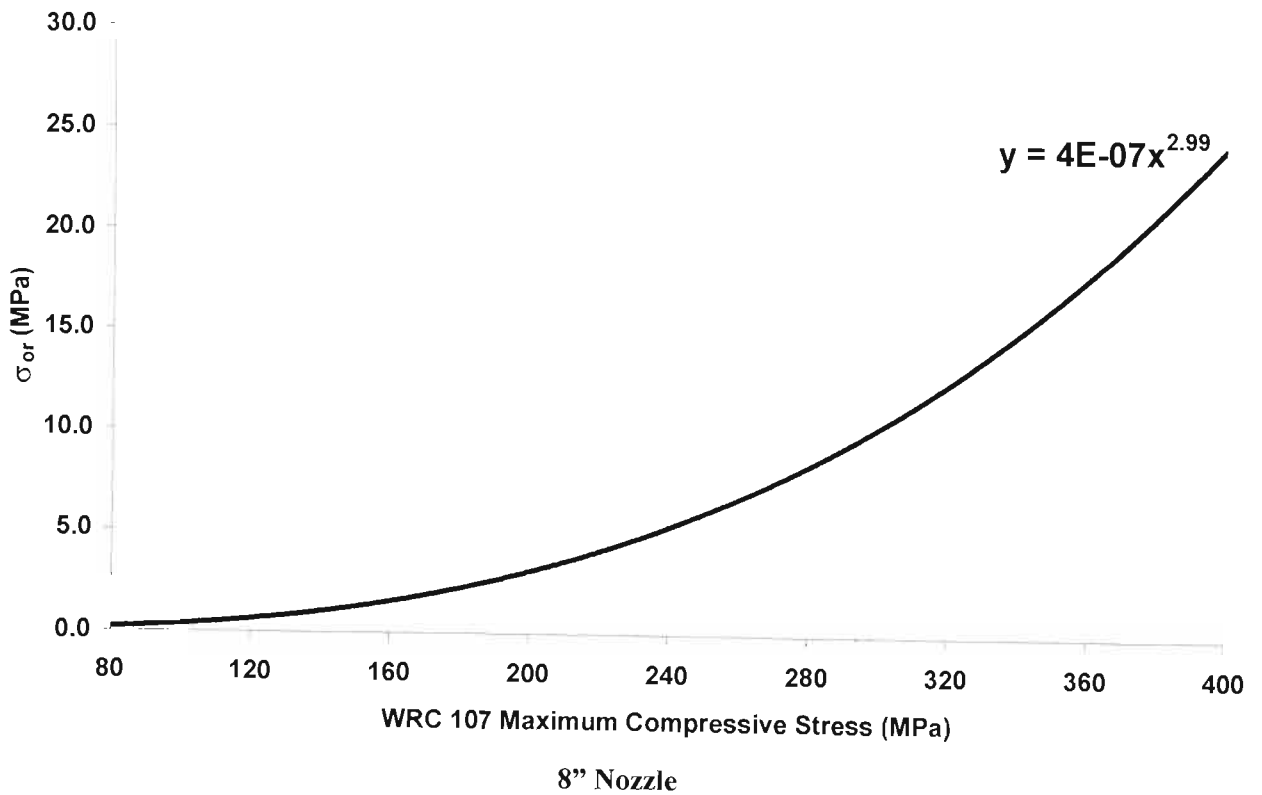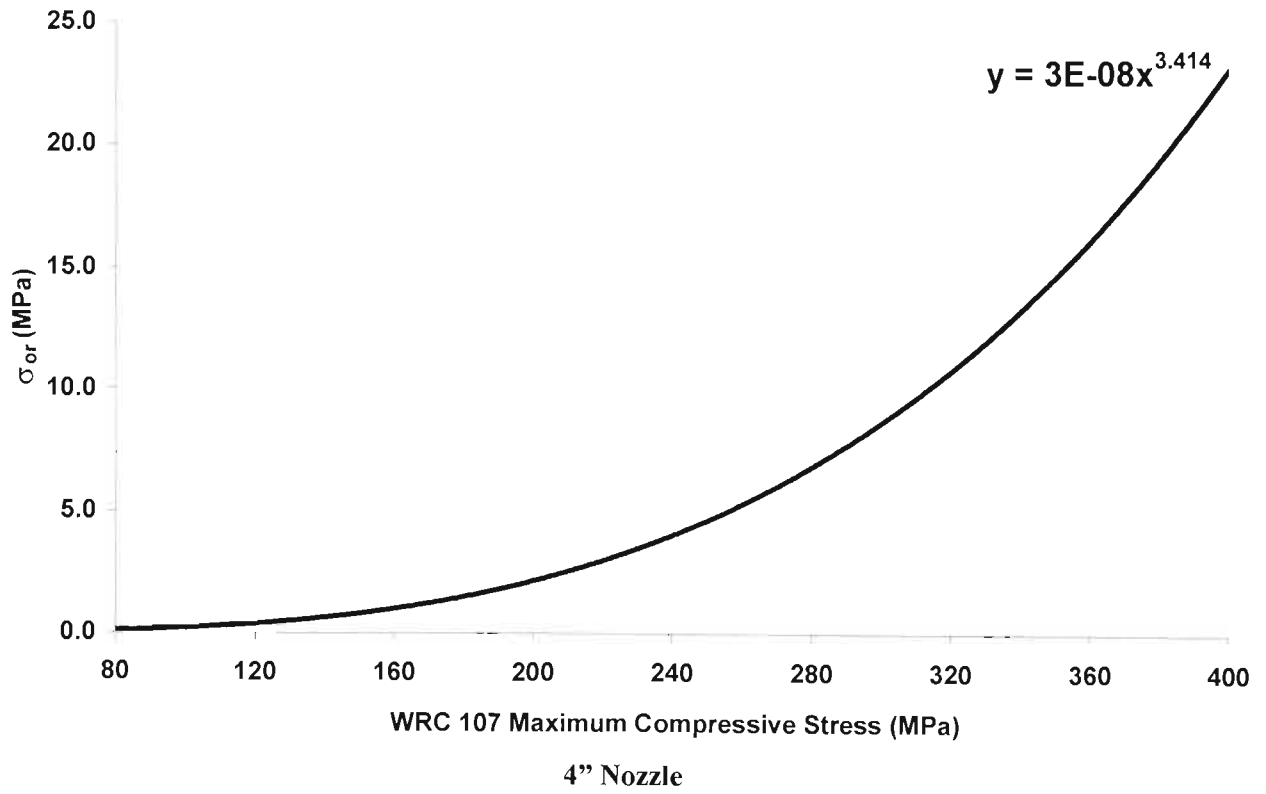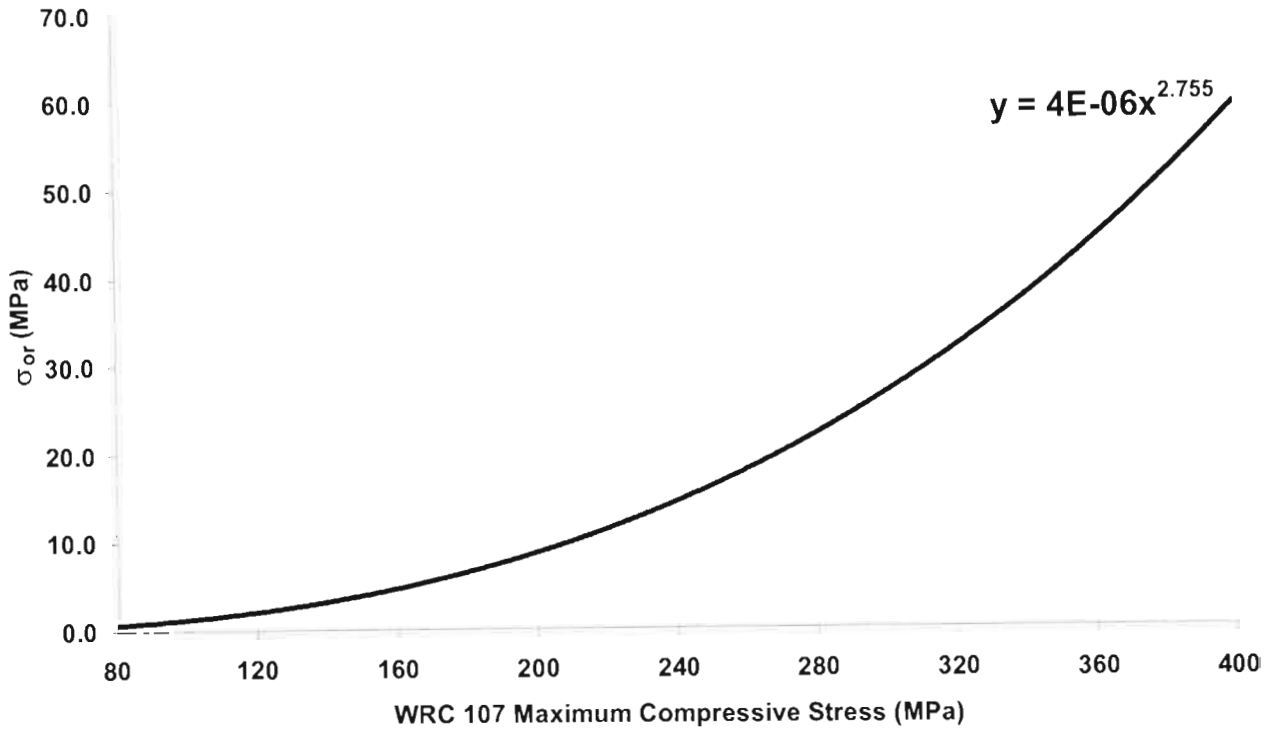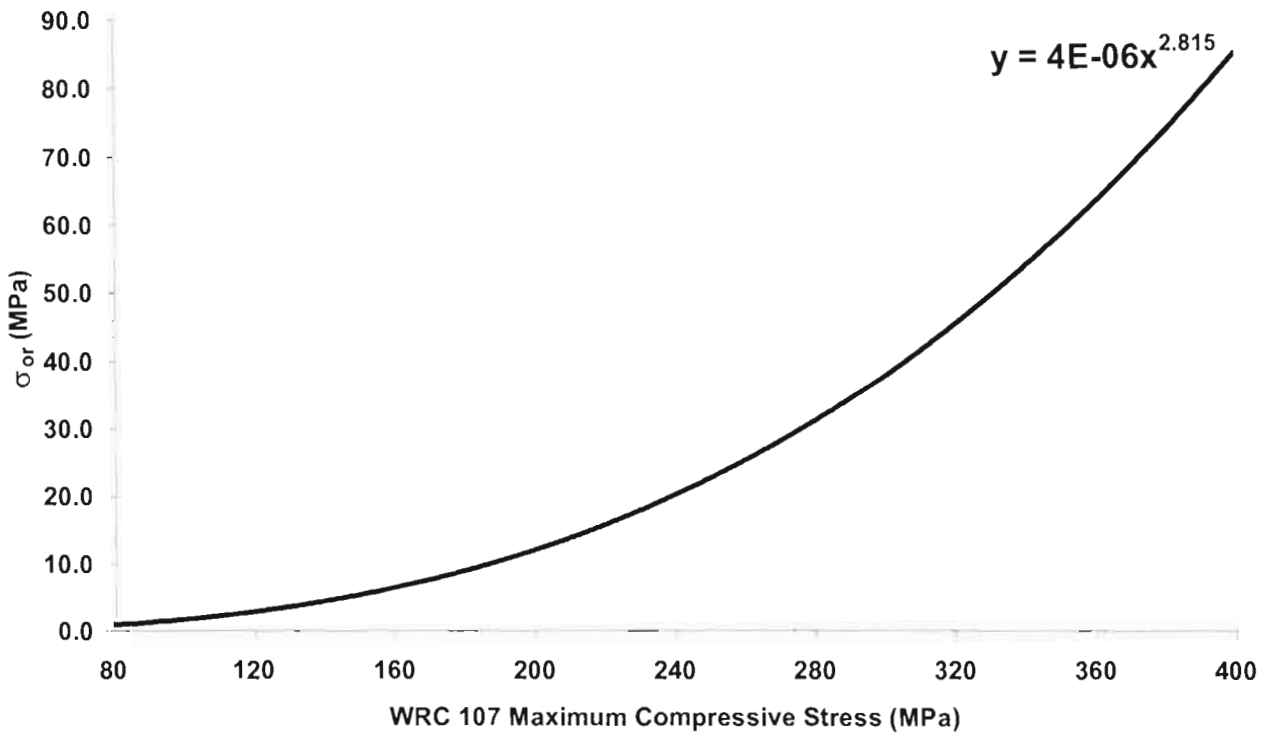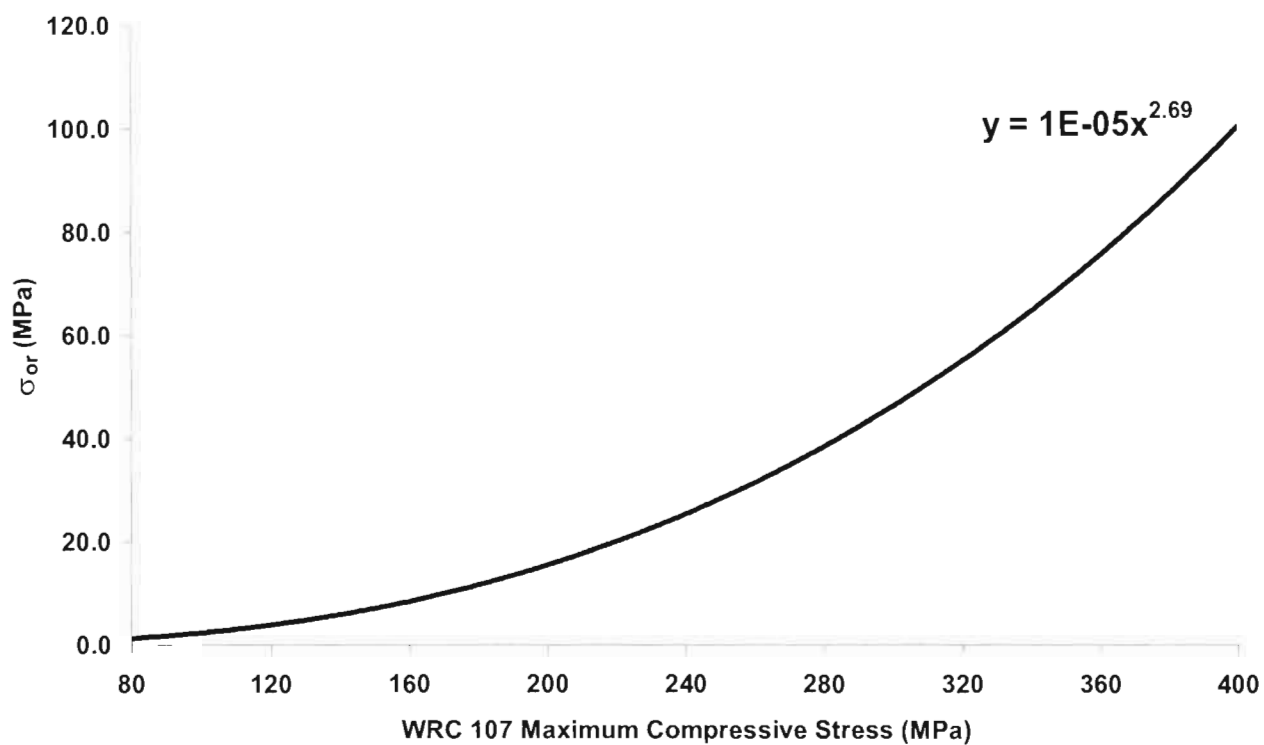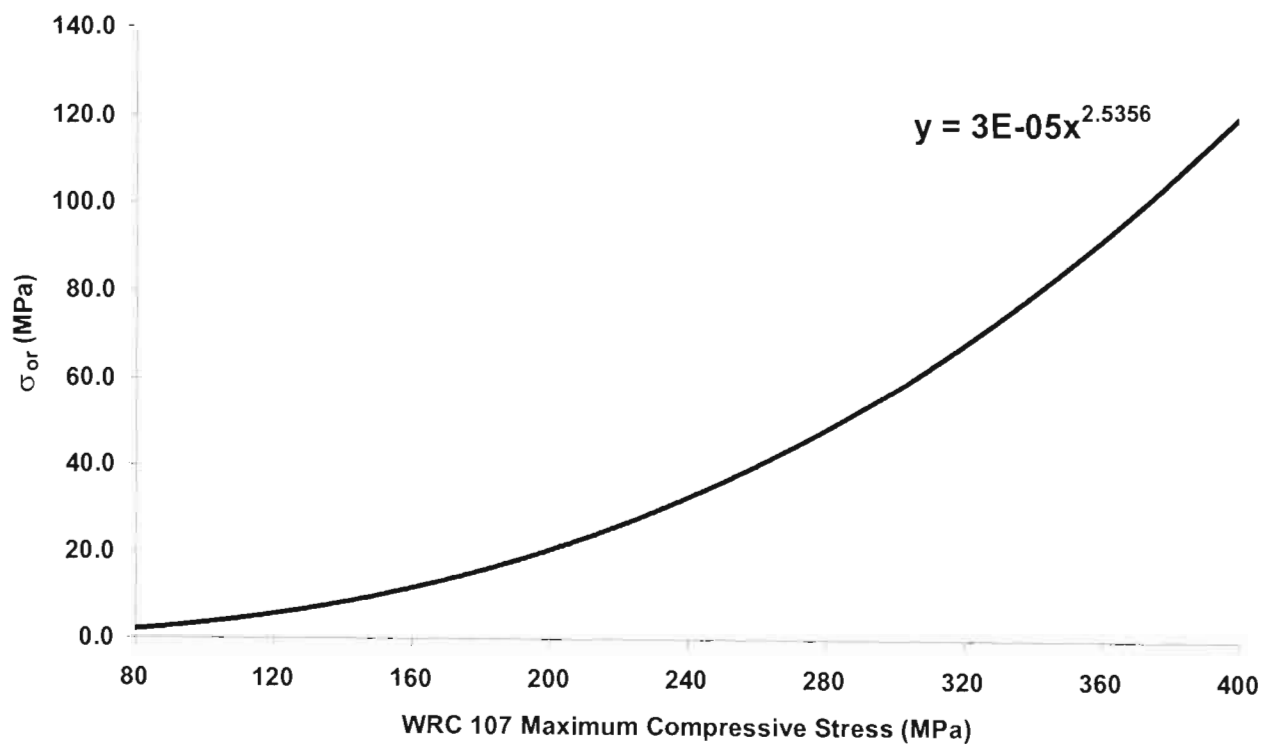
24" Nozzle

Appendix E

189

Vessel 1(Chapter 3) FEM Plots and design calculations for external pressure and piping loads
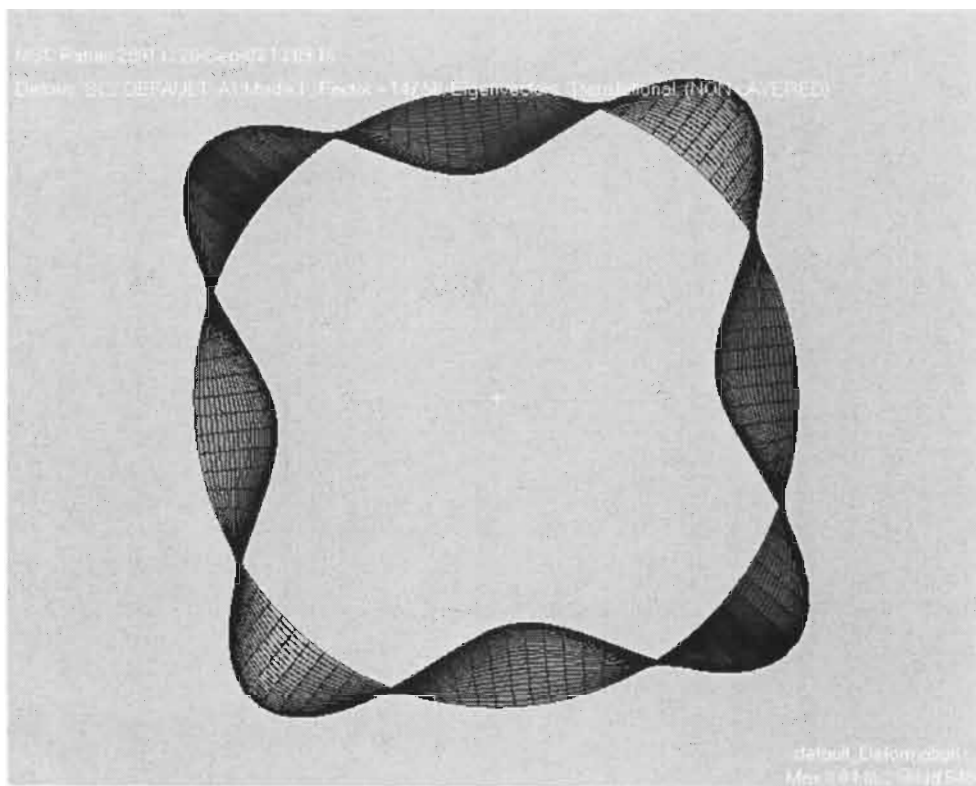
Vessel 1 (Table 3-4) – FEM Buckling Analysis (external pressure only)

Design of Pressure Vessels under External Pressure and Nozzle Piping Loads

: user fill in

ASME VIII Div 1 : UG-28

$D_o =$	598	mm
$t =$	14	mm
$CA =$	3	mm
$L =$	1000	mm
$E =$	200000	MPa
$n =$	3	

Critical Buckling Pressure Pcr = **14.270 MPa**

Nozzle

Nozzle : **6** inch

Calculation of Buckling Stress σ_{cr}'

$\sigma_{UTS} =$	**483** MPa
WRC 107 =	**287** MPa
Out of Roundness Stress =	**8** MPa
$A =$	**5.358** mm

$\sigma_{cr}' =$	**121.3 MPa**	**Holt**
$\sigma_{cr}' =$	**148.5 MPa**	**FEM**

Vessel 3(Chapter 3) FEM Plots and design calculations for external pressure and piping loads
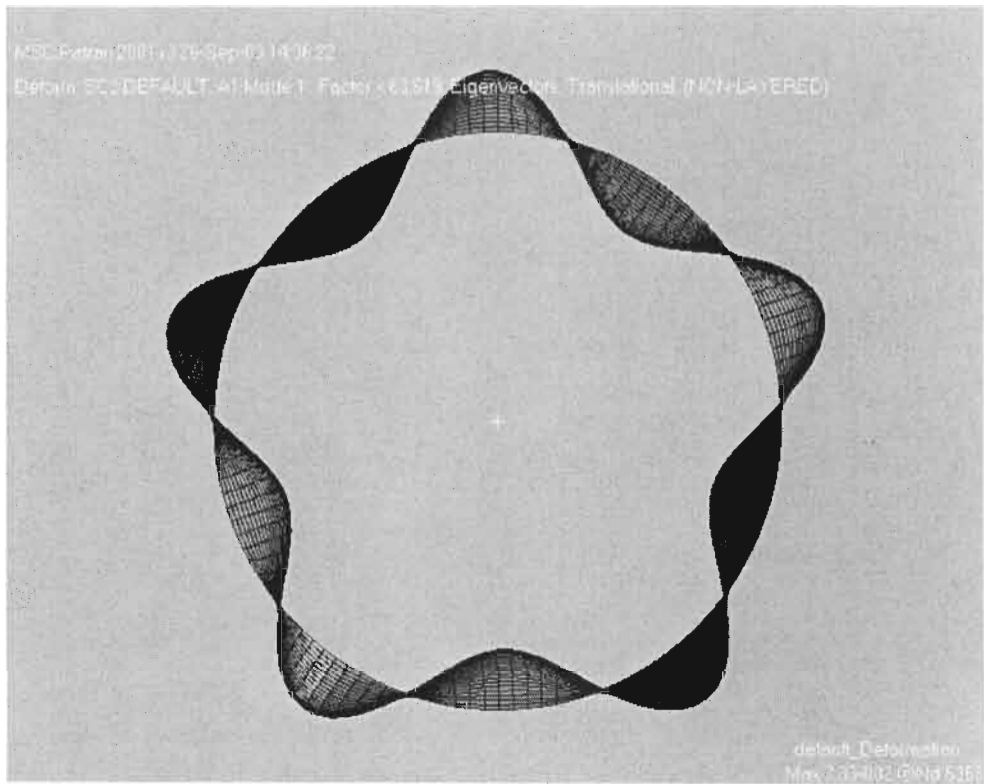
Vessel 3 (Table 3-4) – FEM Buckling Analysis (external pressure only)
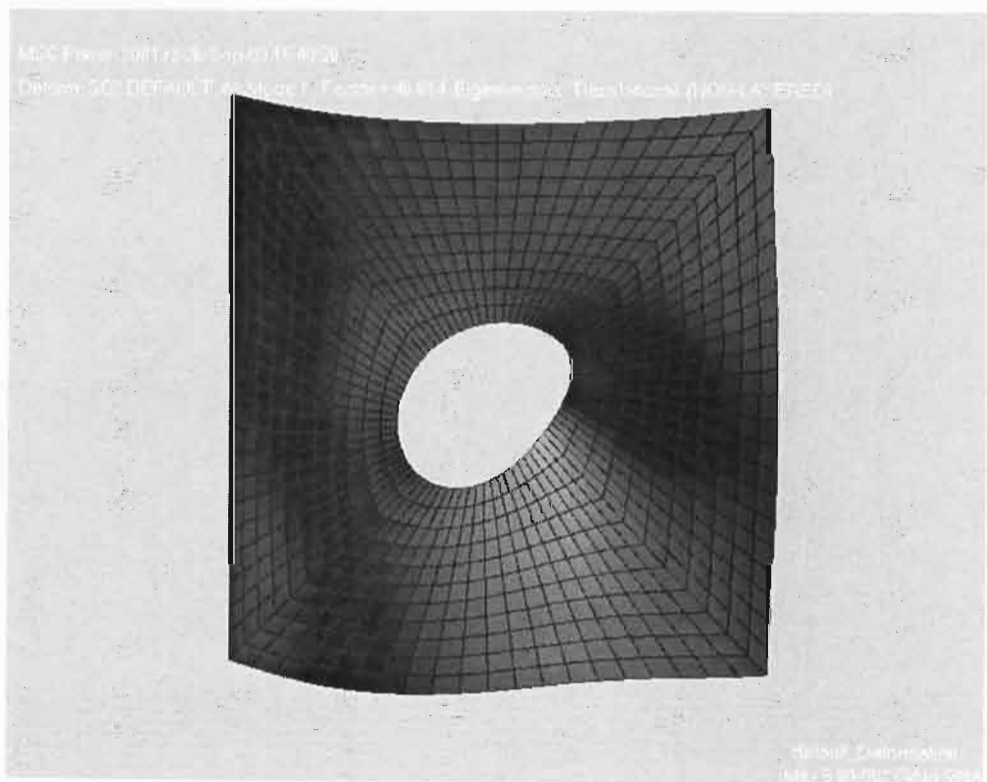
Vessel 3 (Table 3-4) – FEM Buckling Analysis (external pressure + 4" Nozzle)

Design of Pressure Vessels under External Pressure and Nozzle Piping Loads

: user fill in

ASME VIII Div 1 : UG-28

Do =   716 mm
t =   8 mm
CA =   0 mm
L =   800 mm
E =   200000 MPa
n =   5

Critical Buckling Pressure Pcr =   **6.141 MPa**

Nozzle

Nozzle :   **4** inch

Calculation of Buckling Stress σ_{cr}'

σ_{UTS} =   **483** MPa
WRC 107 =   **202.1** MPa
Out of Roundness Stress =   **2.3** MPa

A =   **0.674** mm

σ_{cr}' =	**201.6 MPa**	**Holt**
σ_{cr}' =	**202.2 MPa**	**FEM**

Appendix F

Effects of External Piping Loads on a Pressure Vessel under External Pressure

A Maharaj[a*], C J von Klemperer[a], S Adali[a]

[a]School of Mechanical Engineering, University of Natal, Durban, 4001, South Africa

Abstract

This paper deals with the effects of external piping loads at the nozzle on cylindrical pressure vessels under vacuum. It describes the various theoretical methods with regard to the design of pressure vessels under external atmospheric pressure. An approach to the design of pressure vessels, under the combined effect of external atmospheric pressure and piping loads at the nozzle, is then explored. Numerical models, validated by theory using the ASME (American Society of Mechanical Engineers) VIII Div 1 and 2 [1] Pressure Vessel Codes, are correlated with that of numerical models generated by the finite element analysis software MSC PATRAN [2].

Keywords: Piping loads; External atmospheric pressure; Finite element analysis

Nomenclature

σ_{cr}	critical buckling stress	P_{cr}'	reduced critical buckling pressure
σ_{max}	maximum local stress	K_{UTS}	ultimate tensile stress of material
σ_{cr}'	reduced critical buckling stress	A	out-of-roundness
P_{cr}	critical buckling pressure	u_o	initial radial deviation
L	unsupported length of vessel	M	total bending moment
D_o	outside diameter of vessel	r	cylinder outer radius
t	thickness of vessel	D	$= \dfrac{Et^3}{12(1-\mu^2)}$ flexural rigidity
μ	poison's ratio	M_{or}	out-of-round bending moment
n	lobes of buckling	σ_{or}	out-of-round stress
E	Young's Modulus of material	ϕ	angle

1. Introduction

There are currently several well-known and widely-used procedures for predicting the structural stability of pressure vessels under external pressure. However, effects of combined loads were not investigated fully. In the present paper the combined effects of the external atmospheric pressure and the piping loads at the nozzle are investigated.

195

*corresponding author (Tel: +27 31 260 1225, Fax: +27 31 260 3217; email: maharaja28@nu.ac.za)
These combined effects could be catastrophic if not addressed properly, especially when the stability of the structure is a crucial consideration, i.e. when buckling is a concern.

In unstable thin-walled vessels the imposition of an external force results in additional deformation, which may not vanish upon the removal of the force. Greater forces induced by piping loads at the nozzle cause greater deformations to occur [3,4], thereby rendering the vessel more unstable. The design of the vessel must therefore be modified to include also the effects of the piping loads at the nozzle. Expressions for the prediction of the critical buckling pressure under external pressure alone were first derived by von Mises and later improved by Windenburg and Trilling [3,5]. Currently, design engineers use the procedures provided in the ASME Pressure Vessel Design Code to predict the critical buckling pressure of a pressure vessel under external pressure. These expressions predict the general buckling behaviour of the entire vessel.

The combined effect of external pressure and piping loads will result in local buckling occurring at the shell-to-nozzle junction. The effects of nozzle loads cause increased stress concentrations to occur at the shell-to-nozzle junction. Stresses in this region are thus greater than the critical buckling stress for the vessel. This highly stressed region can result in local buckling [6-9]. Fig. 1 illustrates local stresses at the shell-to-nozzle junction, where the critical buckling stress σ_{cr} is exceeded. Since nozzle loads cause deviations in vessels [3,4], it can be assumed that this has the same effect on the stability of a vessel as does a vessel with geometric imperfections.

The collapse pressure of cylindrical vessels subjected to external pressure is dependent on the final fabricated shape. Imperfections or out-of-roundness in cylindrical vessels reduce the ability of these vessels to withstand buckling. Out-of-roundness (deflections caused by nozzle loads) at the shell-to-nozzle junction, reduces the buckling strength of the vessel. This results in stresses at this region, shown in Fig. 2, being much greater than the reduced buckling strength σ_{cr}', thus rendering the vessel more unstable.

2. Finite Element Models

The investigation of the theory and FEM (Finite Element Methods) critical buckling pressures are based on the 6 vessels (typical large diameter vessels commonly used in industry) shown in Table 1. Each of the above vessels (1 to 6) is analysed using a 24 inch (609.6mm outer diameter) nozzle together with its corresponding loads. Figure 3 gives a representation of nozzle loads with different orientations and typical values of these loads. The material properties are obtained from ASME VIII Div 2 Part D, as shown in Table 2.

196

In the present study, two FEM models of the pressure vessels, which are generated using MSC PATRAN, are considered. The first, Model A shown in Figure 4 [2], which is a circular cylinder with no nozzle loads is used to correlate the FEM buckling pressures with the calculated theoretical values. The second, Model B shown in Figure 5 [10,11], includes piping loads at the shell-to-nozzle junction, and is used to determine the critical buckling pressure of the 6 vessels mentioned above.

3. Design of Pressure Vessels under External Pressure

Several equations have been developed for the computation of the buckling pressure of vessels under external pressure. The first and most accurate equations were derived by von Mises [3,5]. Von Mises developed equations for vessels subjected to radial pressure only, as well as for vessels subjected to both radial and axial pressure. The design of vessels subjected to radial and axial pressure using the expression developed in Refs. [3,5], is deemed to be much safer, viz.,

$$P_{cr} = \left\{ \frac{1}{3} \left[n^2 + \left(\frac{\pi D_o}{2L} \right)^2 \right]^2 \frac{2E}{1-\mu^2} \left(\frac{t}{D_o} \right)^3 + \frac{2E \frac{t}{D_o}}{\left[n^2 \left(\frac{2L}{\pi D_o} \right)^2 + 1 \right]^2} \right\} \frac{1}{n^2 + \frac{1}{2} \left(\frac{\pi D_o}{2L} \right)^2} \tag{1}$$

Windenburg and Trilling [3,5] also derived an approximate equation given by

$$P_{cr} = \frac{2.42E}{\left(1-\mu^2\right)^{3/4}} \frac{\left(\frac{t}{D_o} \right)^{5/2}}{\frac{L}{D_o} - 0.45 \left(\frac{t}{D_o} \right)^{1/2}} \tag{2}$$

The number of lobes of buckling, *n*, is given by the equation.

$$n = \sqrt[4]{\frac{\frac{3}{4} \pi^2 \left(1-\mu^2\right)^{1/2}}{\left(L/D_o\right)^2 \left(t/D_o\right)}} \tag{3}$$

Due to its simplicity, the expression given in eq. 2, is recommended in the ASME Code for the design of vessels under external pressure. The ASME VIII Div 1 and 2 Code incorporates eq. 2

197

to create their procedures for the design of pressure vessels under external pressure. Table 3 shows the comparison between FEM critical buckling pressures and theoretical values using Model A. Von Mises critical buckling pressures provide the best correlation with the FEM values. The ASME values differ from the FEM values, due to safety factors included in the ASME Code [1] design procedures. The FEM model can be confirmed by determining the lobes of buckling for the vessels. Fig. 6 show the lobes of buckling for vessel 5, obtained from FEM analyses. For vessel 5, the theoretical value of n, using eq. 3, is calculated as $n = 7$. Figure 6 also shows 7 lobes confirming the FEM results.

4.   Design of Pressure Vessels under Eternal Pressure and Piping Loads

Results obtained using Model B are shown in Table 4. Critical buckling pressures for vessels 1 – 6, including nozzle loads, were determined by the FEM Model B. Table 4 indicates that nozzle loads reduce the critical buckling pressure. The critical buckling stress of a vessel, inclusive of nozzle loads, is calculated using the reduced buckling pressure given in Table 4. As stated earlier, local buckling at the shell-to-nozzle junction occurs when the stresses induced by both nozzle loads and external pressure exceed the critical buckling stress of the vessel. Table 5 gives a comparison of the theoretical stresses at the shell-to-nozzle junction, calculated using the WRC 107 [12] method and FEM, with the critical buckling stresses of the vessel. The critical buckling stress of a vessel with no nozzle loads is calculated using the buckling pressure generated by using eq. 2 given by Windenburg and Trilling [3,5].

It can be seen from Table 5 that the stresses generated by the combined loading of nozzle loads and external pressure (WRC 107 and FEM) exceed the critical buckling stresses for vessels 1 - 5. The inclusion of nozzle loads reduce the critical stress (Windenburg & Trilling) even further, which implies that severe local buckling will occur at the shell-to nozzle junction. The local stress calculated for vessel 6 is much lower than the critical buckling stress (inclusive of nozzle loads). The thickness of this vessel is 20mm, which implies that the vessel is much stronger and the stress is therefore much lower.

Reduced critical buckling stresses, for vessels 1 – 6 subjected to both external pressure and piping loads, have been achieved using FEM (Table 5). However, analytical results will also have to be generated. The design of pressure vessels under external pressure and piping loads at the nozzle requires the assumption that the piping loads cause deviations in the vessel, which implies that the vessel can be treated as an out-of-round cylinder [3]. Analytical methods have been developed to account for the effect of geometric imperfections in cylindrical shells subjected to external pressure. Holt [13] developed a formula for the buckling pressure of a vessel with an initial out-of-roundness, which is given by

$$P_{cr}^{'} = \cfrac{2K_{UTS}\cfrac{t}{D_o}}{1+\cfrac{4A}{t}\cfrac{E\left[n^2-1+v\left(\cfrac{\pi D_o}{2L}\right)^2\right]}{\left(1-v^2\right)\left(P_{cr}-P_{cr}^{'}\right)}\left(\cfrac{t}{D_o}\right)^3}$$ (4)

Eq. 4 was determined on the assumption that the initial out-of-roundness is similar in form to the assumed buckling mode shape. This is not the case for vessels under external pressure and external piping loads. A relationship between nozzle loads and eq. 4 has to be developed. To develop this relationship one needs to take into account the fact that nozzle loads increase the local stresses at the shell-to-nozzle junction. Geometric imperfections at localised areas also increase stress concentrations. Timoshenko [14] studied the effects of cylinders and tubes with initial noncircularity subjected to external pressure and developed a theory around this. The most common form of noncircularity is that of an elliptical or oval shape. Using this kind of imperfection the deviation caused by noncircularity could be shown to be [14],

$$u_1 = u_o \cos 2\phi$$ (5)

Fig. 7 shows an imperfect cylinder as given in [14,15]. When an external pressure is applied, an additional radial displacement u_2 will occur. Timoshenko [14] determined that the deflection caused by external pressure is given by the following higher order diferential equation :

$$\frac{d^2u_2}{d\phi^2} + u_2 = -\frac{r^2M}{D}$$ (6)

This equation also applies to Fig. 7. Considering an elemental ring of unit width the compressive force shown in Fig. 7 is given by $F = pr$. Thus the bending moment at any cross section is equal to the compressive force multiplied by the total radial deviation $u_1 + u_2$ at this cross section, viz.

$$M = pr\left(u_2 + u_o \cos 2\phi\right)$$ (7)

Substituting eq. 7 into eq. 6 and rearranging give :

$$\frac{d^2u_2}{d\phi^2} + u_2\left(1 + \frac{pr^3}{D}\right) = -\frac{pr^3 u_o \cos 2\phi}{D}$$ (8)

The solution of eq. 8 is given by

$$u_2 = \frac{u_o\, p \cos 2\phi}{P_{cr} - p} \tag{9}$$

Substituting eq. 9 into eq. 7 and taking the bending moment to be maximum at points ⊓ [and $\phi = \pi$, we obtain :

$$M_{or} = \frac{p u_o r}{1 - \left(p \middle/ P_{cr} \right)} \tag{10}$$

The compressive critical stress is obtained by converting M_{or} to a stress :

$$\sigma_{or} = \frac{3}{t^2} \cdot \frac{p D_o A}{1 - \left(p \middle/ P_{cr} \right)} \tag{11}$$

Where $D_o = 2r$ and $u_o = A$. The increased stress for an imperfect vessel can be determined using eq. 11. Substituting A from eq. 4 into eq. 11, one can determine a relationship between the maximum compressive stress (nozzle loads only) and the maximum out-of round stress (eq. 11). The differences between these stresses is shown in Table 6.

Table 6 gives the stresses, for vessels 1 to 6, for the maximum compressive stress generated by nozzle loads using WRC 107 and the maximum out-of-round stress calculated using eq. 11. The results indicate that out-of-round stresses and stresses generated by nozzle loads increase the stress concentration at localised regions. Therefore, a relationship between the two stresses can be developed. However, this relationship is for a 24" (609.6mm outer diameter) nozzle. Further relationships for various other nozzles can be developed.

5. Conclusion

The effects of piping loads on pressure vessels under external pressure have been investigated. Theoretical models have been generated and analysed and compared to results obtained by the finite element software MSC PATRAN. The theoretical results for vessels under external pressure alone coincide with the finite element values. For the effects of the piping loads further finite element analyses were generated and the results indicated that these vessels could be related to out-of-round cylinders. Out-of-roundness causes a reduction in the buckling strength of the vessel thus making it unstable.

Procedures will have to be developed for the design of these vessels under piping loads at the nozzle. This will involve the modification of the three major design parameters (diameter, length and thickness) to ensure a much stronger vessel under buckling. The design engineer will have to determine the critical buckling strength at the shell-to-nozzle junction. The research shows that this can be achieved by determining, for various types of nozzles, relationships between compressive stresses due to nozzle loads and stresses due to out-of-roundness. The out-of-round compressive stress will give an out-of-round value, which can be used in Holt's formula to calculate the critical buckling pressure at the shell-to-nozzle junction. To prevent local buckling from occurring, stresses induced in the shell due to external pressure and piping loads should be within the calculated critical buckling stress of the shell-to-nozzle junction.

6. References

1. ASME. ASME Boiler and Pressure Vessel Code. Section VIII Div 1 and 2, 1980.
2. MSC PATRAN – Reference Manual. The McNeal Schwendler Corporation, 2001.
3. Bickell M.B., Ruiz C. Pressure Vessel Design and Analysis. Macmillan, 1967.
4. Chapuliot S., Moulin D., Plancq D. Mechanical Behaviour of a Branch Pipe Subjected to Out-of-Plane Bending Load. Journal of Pressure Vessel Technology, 2002;124:7-13.
5. Allen H.G., Bulson P.S. Background to Buckling. 1st Edition, McGraw-Hill Book Company, USA, 1980.
6. Minjie C., Mark J., Holst F.G., Rotter J.M. Buckling Strength Of Thin Cylindrical Shells Under Localized Axial Compression. 15th ASCE Engineering Mechanics Conference, 2002.
7. Lagace P.A. Other Issues In Buckling/Structural Instability, 2001.
8. Walker P. Buckling of Cylinders With Local Loads Normal To The Shell. ABAQUS UK Users Group Conference, 2001.
9. Harvey J.F. Theory and Design of Pressure Vessels. P.E. van Nostrand Reinhold Company, 1985.
10. Schneider M.H., Feldes R.J., Halcomb J.R. and Hoff C.C. Stability Analysis of Perfect and Imperfect Cylinders using MSC Nastran Linear And Non-Linear Buckling. MSC World User's Conference Proceedings, Paper No. 27, 1995.
11. Dahlgren F. NCSX-Vacuum Vessel Stress Analysis. Princeto University, 2002.
12. Winchman K.R., Hopper A.G., Mershon J.L. Local Stresses in Spherical and Cylindrical Shells due to External Loadings. Welding Research Council Bulletin 107, 1979.
13. Holt M. A Procedure for Determining the Allowable Out-of-Roundness for Vessels Under External Pressure. Transactions of the ASME, 1952;74(7):1225-1230.
14. Timoshenko S.P., Gere J.M. Theory of Elastic Stability. Second Edition,McGraw-Hill Book Company, 1961.
15. Jawad M.H., Farr J.R. Structural Analysis and Design of Process Equipment. John-Wiley and Sons, 1989.

Figure Captions

Figure 1 : Local Stresses exceeding Critical Buckling Stress

Figure 2 : Local Stresses exceeding reduced Critical Buckling Stress

Figure 3 : Nozzle Loads with orientations

Figure 4 : Model A

Figure 5 : Model B

Figure 6 : Buckled Vessel 5 – Model A

Figure 7 : Cylinder with Initial Ellipticity under External Pressure

Tables

Table 1 : Vessels for Theoretical and FEM Analysis

Table 2 : Vessel Material Properties

Table 3 : Comparison of Buckling Pressures between Theory and FEM

Table 4 : FEM Analyses for Vessels with Nozzle Loads

Table 5 : Comparison of Local and Critical Buckling Stresses at the shell-to-nozzle junction

Table 6 : Stress relationship between nozzle loads and out-of-roundness
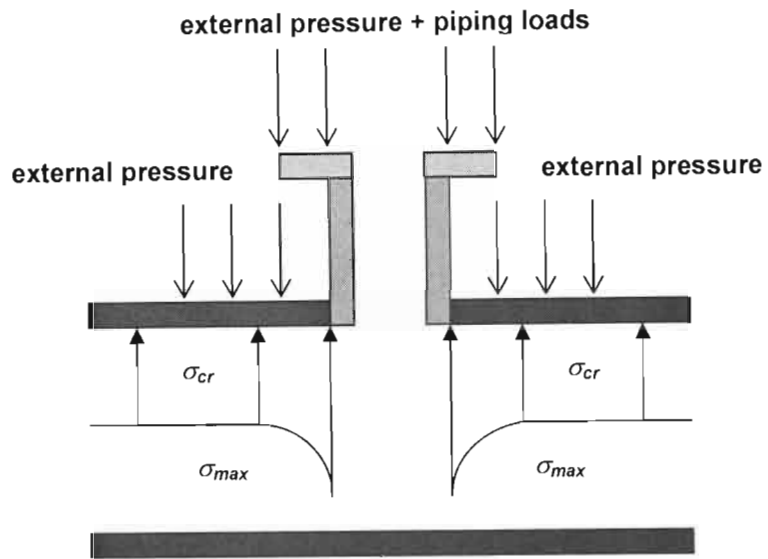
Figure 1 : Local Stresses exceeding Critical Buckling Stress
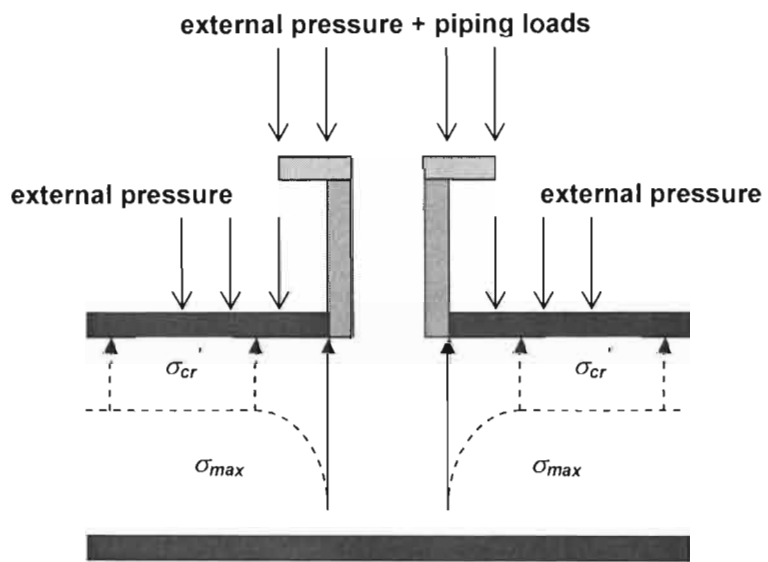
Figure 2 : Local Stresses exceeding reduced Critical Buckling Stress
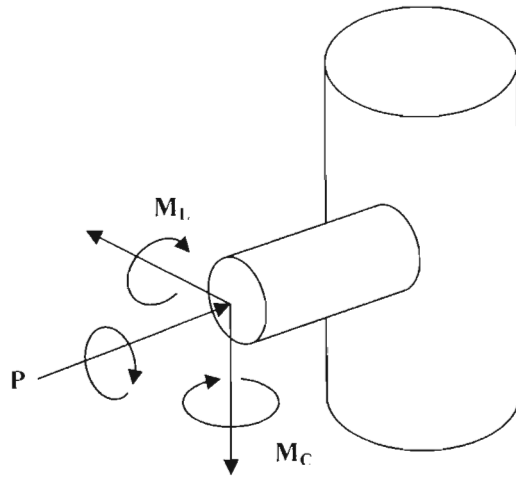
Nozzle Loads		
P	=	**35500N**
M_C	=	**16900Nmm**
M_L	=	**24800Nmm**

Figure 3 : Nozzle Loads with orientations

Figure 4 : Model A

Figure 5 : Model B

Isometric view
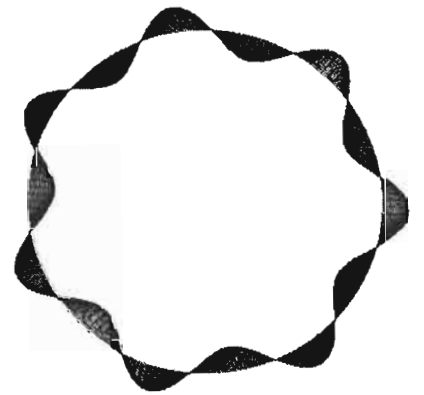
Top view

Figure 6 : Buckled Vessel 5 – Model A
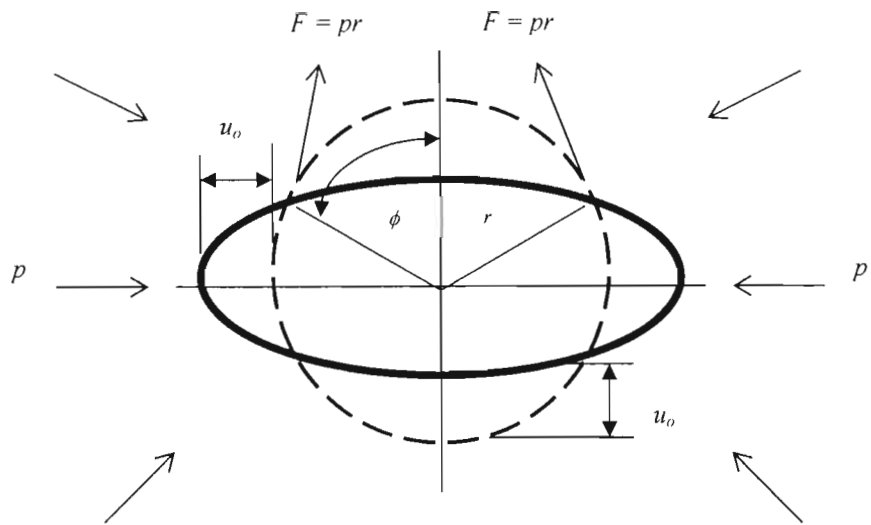
Figure 7 : Cylinder with Initial Ellipticity under External Pressure

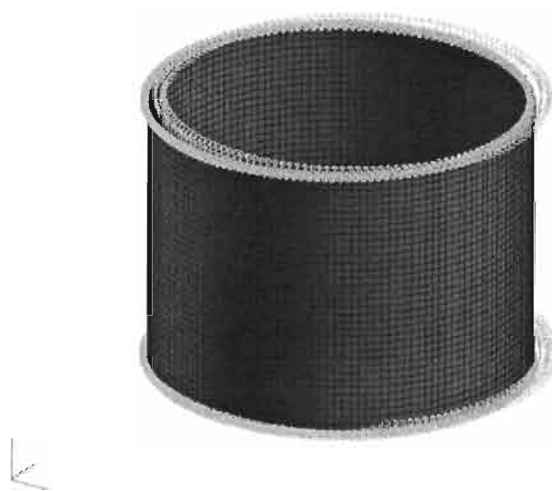| Vessel	Outer Diameter	Thickness	Corrosion Allowance	Length	External Pressure	Nozzle outer diameter (mm)
1	2800mm	8mm	0mm	2000mm	0.1 Mpa	609.6
2	2800mm	10mm	0mm	2000mm	0.1 Mpa	609.6
3	2800mm	12mm	0mm	2000mm	0.1 Mpa	609.6
4	2800mm	14mm	0mm	2000mm	0.1 MPa	609.6
5	2800mm	16mm	0mm	2000mm	0.1 MPa	609.6
6	2800mm	20mm	0mm	2000mm	0.1 MPa	609.6

Table 1 : Vessels for Theoretical and FEM Analysis

Material	K_{UTS} (MPa)	E (GPa)	
SA 516 Grade 70 (carbon steel)	483	200	0.3

Table 2 : Vessel Material Properties

Vessel	t/D_o	Buckling Pressure Mpa			
		ASME	Windenburg & Trilling	Von Mises	MSC PATRAN
1	0.0029	0.330	0.329	0.329	0.385
2	0.0036	0.570	0.577	0.583	0.667
3	0.0043	0.900	0.913	0.950	1.046
4	0.0050	1.320	1.347	1.347	1.557
5	0.0057	1.800	1.887	1.900	2.126
6	0.0071	2.532	3.316	3.459	3.695

Table 3 : Comparison of Buckling Pressures between Theory and FEM

Vessel	t/D_o	MSC PATRAN Buckling Pressure MPa – no nozzle	MSC PATRAN Buckling Pressure MPa – 24" Nozzle
1	0.0029	0.385	0.181
2	0.0036	0.667	0.370
3	0.0043	1.046	0.649
4	0.0050	1.557	1.021
5	0.0057	2.126	1.488
6	0.0071	3.695	2.734

Table 4 : FEM Analyses for Vessels with Nozzle Loads

Vessel	t/D_o	Local Stresses – Nozzle loads + External Pressure		Critical Buckling Stress	
		WRC 107	FEM	Windenburg & Trilling – no nozzle	Nozzle Loads + External Pressure
1	0.0029	612.6 MPa	635 MPa	57.6 MPa	31.7 MPa
2	0.0036	408.5 MPa	446 MPa	80.8 MPa	51.8 MPa
3	0.0043	289.8 MPa	317 MPa	106.5 MPa	75.7 MPa
4	0.0050	217.3 MPa	239 MPa	134.7 MPa	102.1 MPa
5	0.0057	173.8 MPa	182 MPa	165.1 MPa	130.2 MPa
6	0.0071	118.2 MPa	111 MPa	232.1 MPa	191.3 MPa

Table 5 : Comparison of Local and Critical Buckling Stresses at the shell-to-nozzle junction

Vessel	MSC PATRAN Buckling Pressure MPa – no nozzle	MSC PATRAN Buckling Pressure MPa – 24" Nozzle	A – German Code mm	Maximum Compressive Stress (WRC 107 – nozzle loads only) MPa	Maximum out-of-round stress (formula 11) MPa
1	0.385	0.181	13.731	595.2	258.6
2	0.667	0.370	9.729	394.7	99.1
3	1.046	0.649	7.223	278.2	47.4
4	1.557	1.021	5.568	207.4	25.8
5	2.126	1.488	4.316	165.2	15.0
6	3.695	2.734	3.167	111.3	6.9

Table 6 : Stress relationship between nozzle loads and out-of-roundness

BIBLIOGRAPHY

[1] Timoshenko S. (1936) *Theory of Elastic Stability*. 1st Edition. McGraw-Hill Book Company, USA.

[2] Siemon K. (1942) *Pressure Vessel Manual*. 5th Edition. Edwards Brothers Inc.

[3] Holt M. (1952) "A Procedure for Determining the Allowable Out-of-Roundness for Vessels Under External Pressure." *Transactions of the ASME*. v. 74(7), p1225-1230.

[4] Galletly G.D. and Bart R. (1956) "Effects of Boundary Conditions and Initial Out-of-Roundness on the Strength of Thin-Walled Cylinders Subjected to External Hydrostatic Pressure." *Journal of Applied Mechanics*, p351-358.

[5] Donnell L.H. (1956) "Effects of Imperfections on Buckling of Thin Cylinders Under External Pressure." *Journal of Applied Mechanics*. v. 23(4), p569-575.

[6] Lunchick M.E. and Short R.D.Jnr (1957) "Behaviour of Cylinders With Initial Shell Deflection." *Journal of Applied Mechanics*. v. 24(4), p559-564.

[7] Timoshenko S. (1958) *Strength of Materials Part II Advanced Theory and Problem*. 3rd Edition. VAN NOSTRAND REINHOLD COMPANY, New York.

[8] Flugge W. (1962) *Stresses in Shells*. 2nd Edition. Springer-Verlag, Germany.

[9] Bickel M.B. and Ruiz C. (1967) *Pressure Vessel Design and Analysis*. Macmillan.

[10] Arbocz J. (1974) "The Effects of Initial Imperfections on Shell Stability." *Thin Shell Structures : Theory, Experiment and Design*. Edited by Fung Y.C. and Sechler E.E. Prentice-Hall.

[11] Cook R.D. (1974) *Concepts and Applications of Finite Element Analysis*. John Wiley & Sons Inc.

[12] Fung Y.C. and Sechler E.E. (1974) *Thin Shell Structures : Theory, Experiment and Design*. Prentice-Hall, New Jersey.

[13] Kroenke W.C. (1974) "Classification of Finite Element Stresses According To ASME Section III Stress Categories." *Pressure Vessels and Piping Conference.* The Pressure Vessel and piping Division, ASME, p107-140.

[14] Gallagher R.H. (1975) *Finite Element Analysis Fundamentals.* Prentice-Hall Inc.

[15] Gwaltney R.C., Corum J.M., Bolt S.E. and Bryson J.W. (1976) "Experimental Stress Analysis of Cylinder-to-Cylinder Shell Models and Comparisons With Theoretical Predictions." *Journal of Pressure Vessel Technology Transactions of the ASME.* p283-290.

[16] Winchman K.R., Hopper A.G. and Mershon J.L. (1979) *Local Stresses in Spherical and Cylindrical Shells due to External Loadings WRC Bulletin 107.* Welding Research Council, New York.

[17] Allen H.G. and Bulson P.S. (1980) *Background to Buckling.* 1st Edition. McGraw-Hill Book Company, USA.

[18] Bednar H.H. (1981) *Pressure Vessel Design Handbook.* Van Nostrand Reinhold Company, New York.

[19] Ugural A.C. (1981) *Stresses in plates and shells.* McGraw-Hill Book Company, USA.

[20] Harvey J.F. (1985) *Theory and Design of Pressure Vessels.* P.E. van Nostrand Reinhold Company.

[21] Mershon J.L., Mokhtarian K., Ranjan G.V. and Rodabaugh E.C. (1987) *Local Stresses in Cylindrical Shells due to External Loadings WRC Bulletin 297.* Welding Research Council, New York.

[22] Jawad M.H. and Farr J.R. (1989) *Structural Analysis and Design of Process Equipment.* John-Wiley and Sons.

[23] Primm A.H. and Stoneking J.E. (1989) "Accuracy Of The Finite Element Method For Pressure Vessel/Nozzle Design." *The 1989 ASME Pressure Vessels and Piping Conferenc.* p3-9.

211

[24] Roche R.L. (1989) "Practical Procedure for Stress Classification." *International Journal of Pressure Vessels and Piping*. v. (37), p27-44.

[25] Hechmer J.L. and Hollinger G.L. (1989) "Code Evaluation of 3D Stresses on a Plane." *Pressure Vessels and Piping Conference*. p1-14.

[26] Ross C.T.F. (1990) *Pressure Vessels under External Pressure Statics and Dynamics*. Elsevier Science Publishers Ltd.

[27] Sanal Z. (1992) "Finite element analysis of discontinuity stresses at header-nozzle intersections of plate-fin heat exchangers." 7th *International Conference on Pressure Vessel Technology*. Reports on science and Technology, p1-6.

[28] Miller C.D. (1995) "The Effect of Initial Imperfections on the Buckling of Cylinders Subjected to External Pressure." *Pressure Vessel Research Council*. p1-18.

[29] Schneider M.H., Feldes R.J., Halcomb J.R. and Hoff C.C., (1995) "Stability Analysis of Perfect and Imperfect Cylinders using MSC Nastran Linear And Non-Linear Buckling." *MSC World User's Conference Proceedings*. Paper No. 27.

[30] Hechmer J.L. and Hollinger G.L. (1995) *Summary Report – PVRC Project Three Dimensional Stress Criteria*. Pressure Vessel and Research Council. p1-22.

[31] Benham P.P., Crawford R.J. and Armstrong C.G. (1996) *Mechanics of Engineering Materials*. 2nd Edition. Longman, UK.

[32] Chao R. (1996) *Local Stresses in Pressure Vessels Due to Internal Pressure and Nozzle Loadings*. Carmagen Engineering Report. Carmagen Engineering Inc.

[33] Gere J.M. and Timoshenko S.P. (1997) *Mechanics of Materials*. 4th Edition. PWS Publishing Company, New York.

[34] ASME (1998) *Rules for Construction of Pressure Vessels*. ASME Boiler and Pressure Vessel Code, Section VIII Div 1 and 2.

[35] MSC PATRAN – *Reference Manual* (2001). The McNeal Schwendler Corporation.

[36] Singh M. and Diehl D. (2001) *Modelling of Internal Pressure and Thrust Load on Nozzles using WRC 368.* COADE Mechanical Engineering News.

[37] Walker P. (2001) "Buckling of Cylinders With Local Loads Normal To The Shell." *ABAQUS UK Users Group Conference.* p1-11.

[38] Lagace P.A.(2001) *Other Issues In Buckling/Structural Instability.* Massachusetts Institute of Technology.

[39] Minjie C., Mark J., Holst F.G. and Rotter J.M. (2002) "Buckling Strength Of Thin Cylindrical Shells Under Localized Axial Compression." *15th ASCE Engineering Mechanics Conference.* p1-8.

[40] Chapuliot S., Moulin D. and Plancq D. (2002) "Mechanical Behaviour of a Branch Pipe Subjected to Out-of-Plane Bending Load." *Journal of Pressure Vessel Technology, Transactions of the ASME.* v. 124, p7-13.

[41] Dahlgren F. (2002) *NCSX-Vacuum Vessel Stress Analysis*, Princeton University.